MECHANISTIC UNDERSTANDING OF FATE AND TRANSPORT OF SELENIUM, ARSENIC, AND SULFUR IN A PILOT-SCALE CONSTRUCTED WETLAND TREATMENT SYSTEM DESIGNED FOR FLUE-GAS DESULFURIZATION WASTEWATER

by

MADHUBHASHINI BUDDHIKA GALKADUWA

B.S., University of Peradeniya, Sri Lanka, 2006
M.S., Post Graduate Institute of Science, University of Peradeniya, Sri Lanka, 2008

AN ABSTRACT OF A DISSERTATION

submitted in partial fulfillment of the requirements for the degree

DOCTOR OF PHILOSOPHY

Department of Agronomy
College of Agriculture

KANSAS STATE UNIVERSITY
Manhattan, Kansas

2015

Abstract

Constructed wetland treatment systems (CWTSs) are an alternative adaptation for flue-gas desulfurization (FGD) wastewater purification. A series of laboratory-based soil column studies mimicking a pilot-scale CWTS was carried out to evaluate the performance of the treatment system in detail. The main objectives of studies were to (1) understand the transport characteristics, retention capacity and transformation of selenium and other FGD constituents in the CWTS, (2) evaluate the effectiveness of soil treatments and influent flow rate on the performance of the CWTS, and (3) develop a mechanistic understanding of the CWTS performance through monitoring interrelationships of selenium (Se), arsenic (As), iron (Fe), and sulfur (S). Ferrihydrite (1% w/w), and labile organic carbon (OC) were used as soil treatments. Different influent flow rates, X (1.42 mL/hour), 2X, or 1/2X were used depending on the objectives of each study. Deoxygenated 1:1 mixture of FGD: raw water was the influent. It was delivered to the saturated columns with an upward flow. Effluent samples were collected continuously, and analyzed for constituents of concern. End of these experiments, soil from sectioned columns were used for total elemental analysis, sequential extraction procedure (SEP) for Se, and synchrotron-based X-ray spectroscopy analyses. Results indicated a complete Se retention by the columns. Boron, and fluorine partially retained whereas sodium, sulfur, and chlorine retention was weak, agreeing with field observations. Some of the initially-retained Se (~ 4 to 5%) was mobilized by changing redox conditions in the soil. Selenium fed with the wastewater accumulated in the bottom 1/3 (inlet) of the soil columns and was mainly sequestrated as stable forms revealed by SEP. Bulk-, and micro-XANES analyses suggested the retention mechanism of Se from the FGD wastewater was via the transformation of Se into reduced/stable forms [Se(IV), organic Se, and Se(0)]. Under wetland conditions, native soil As

was mobilized by reductive dissolution of As associated minerals. However, the ferrihydrite amendment suppressed the native soil As mobility. Micro-XRF mapping integrated with As, and Fe-XANES suggested that the mechanism of native soil As retention was the sequestration of released As with newly precipitated secondary Fe minerals. A long-term study carried out with X, 1/2X flow rates, and OC source indicated enhanced S retention by the slow flow rate (1/2X), most likely due to the time dependency of biogenic S reduction. Further, bulk S-, As-, and Fe-XANES revealed that long submergence period and the slow flow rate increased the formation of reduced and/or biogenic S, realgar-like, and greigite-like species. These observations indicated that modified flow rates could have a significant impact on the long-term trace element (such as As) sequestration in the CWTS. Our studies provide useful information to improve the performance, and longevity of a full-scale CWTS for FGD wastewaters.

MECHANISTIC UNDERSTANDING OF FATE AND TRANSPORT OF SELENIUM, ARSENIC, AND SULFUR IN A PILOT-SCALE CONSTRUCTED WETLAND TREATMENT SYSTEM DESIGNED FOR FLUE-GAS DESULFURIZATION WASTEWATER

by

MADHUBHASHINI BUDDHIKA GALKADUWA

B.S., University of Peradeniya, Sri Lanka, 2006
M.S., Post Graduate Institute of Science, University of Peradeniya, Sri Lanka, 2008

A DISSERTATION

submitted in partial fulfillment of the requirements for the degree

DOCTOR OF PHILOSOPHY

Department of Agronomy
College of Agriculture

KANSAS STATE UNIVERSITY
Manhattan, Kansas

2015

Approved by:

Major Professor
Ganga M. Hettiarachchi

Copyright

Abstract

Constructed wetland treatment systems (CWTSs) are an alternative adaptation for flue-gas desulfurization (FGD) wastewater purification. A series of laboratory-based soil column studies mimicking a pilot-scale CWTS was carried out to evaluate the performance of the treatment system in detail. The main objectives of studies were to (1) understand the transport characteristics, retention capacity and transformation of selenium and other FGD constituents in the CWTS, (2) evaluate the effectiveness of soil treatments and influent flow rate on the performance of the CWTS, and (3) develop a mechanistic understanding of the CWTS performance through monitoring interrelationships of selenium (Se), arsenic (As), iron (Fe), and sulfur (S). Ferrihydrite (1% w/w), and labile organic carbon (OC) were used as soil treatments. Different influent flow rates, X (1.42 mL/hour), 2X, or 1/2X were used depending on the objectives of each study. Deoxygenated 1:1 mixture of FGD: raw water was the influent. It was delivered to the saturated columns with an upward flow. Effluent samples were collected continuously, and analyzed for constituents of concern. End of these experiments, soil from sectioned columns were used for total elemental analysis, sequential extraction procedure (SEP) for Se, and synchrotron-based X-ray spectroscopy analyses. Results indicated a complete Se retention by the columns. Boron, and fluorine partially retained whereas sodium, sulfur, and chlorine retention was weak, agreeing with field observations. Some of the initially-retained Se (~ 4 to 5%) was mobilized by changing redox conditions in the soil. Selenium fed with the wastewater accumulated in the bottom 1/3 (inlet) of the soil columns and was mainly sequestrated as stable forms revealed by SEP. Bulk-, and micro-XANES analyses suggested the retention mechanism of Se from the FGD wastewater was via the transformation of Se into reduced/stable forms [Se(IV), organic Se, and Se(0)]. Under wetland conditions, native soil As

was mobilized by reductive dissolution of As associated minerals. However, the ferrihydrite amendment suppressed the native soil As mobility. Micro-XRF mapping integrated with As, and Fe-XANES suggested that the mechanism of native soil As retention was the sequestration of released As with newly precipitated secondary Fe minerals. A long-term study carried out with X, 1/2X flow rates, and OC source indicated enhanced S retention by the slow flow rate (1/2X), most likely due to the time dependency of biogenic S reduction. Further, bulk S-, As-, and Fe-XANES revealed that long submergence period and the slow flow rate increased the formation of reduced and/or biogenic S, realgar-like, and greigite-like species. These observations indicated that modified flow rates could have a significant impact on the long-term trace element (such as As) sequestration in the CWTS. Our studies provide useful information to improve the performance, and longevity of a full-scale CWTS for FGD wastewaters.

Table of Contents

List of Figures

List of Tables

Abbreviations

Abbreviation	Explanation
CWTS	Constructed Wetland Treatment System
ES	Engineered soil
FGD	Flue-gas Desulfurization
Fh	Ferrihydrite
FWS	Free Water Surface
HSSF	Horizontal Subsurface Flow
JEC	Jeffrey Energy Center
OC	Organic Carbon
SEP	Sequential Extraction Procedure
TS	Topsoil
XAS	X-ray Absorption Spectroscopy
XRF	X-ray Fluorescence
XANES	X-ray Absorption Near Edge Structure
VF	Vertical Flow

Acknowledgements

I would like to express my heartiest gratitude to my major supervisor, Dr. Ganga M. Hettiarachchi, for giving fullest support, guidance, and encouragement throughout my project as well as paving the way to tackle future endeavors successfully. I would also like to acknowledge Dr. Gerard J. Kluitenberg for helping me tremendously in various ways with the soil column experiments. I extend my thankfulness to the Ph.D. committee members, Dr. Gerard J. Kluitenberg, Dr. Michel D. Ransom, Dr. Stacy Hutchinson, Dr. Larry Erickson, and Dr. Larry Davis. I also highly acknowledge the Graduate School Chairperson, Dr. Charles W. Martin. I want to thank the Department of Agronomy, the faculty, and the staff members who helped me during the past four and half years, and surely the funding sources; Westar Energy Center and Burns & McDonnell, Kansas Agricultural Experimental Station, and KSU Electrical Power Affiliate Program. I really thank my Soil Chemistry group members including former members; Dr. Chammi Attanayake, Dr. Ranju Karna, Dr. Phillip Defoe, Vindhya Gudichuttu, and present members; Pavithra Pitumpe Arachchige, Joy Pierzynski, Jay Weeks, Dorothy Menefee, and Zafer Alasmary. Also, I would greatly appreciate student helpers who contributed their help to my research project. I would like to specially thank Dr. Deon Van der Merwe, and Lori Blevins at the Veterinary Diagnostic Lab for assisting with ICP-MS. I would acknowledge the Advanced Photon Source (APS) at Argonne National Lab, Chicago, IL, for providing me the great opportunity to perform synchrotron-based X-ray techniques. I thank all scientists at sectors 5-BM-D, 9-BM-B, 10-ID-B, and 13-ID-E at the APS. I would like to thank all my friends who supported me throughout the doctoral degree. Finally, I am very grateful to my husband, Sadish Karunaweera, for his love, support, and encouragement, and my family members for supporting and encouraging me with their best wishes from thousands of miles away.

Dedication

To my loving parents, brother and sister who always pave the way for my success:

Tikiri Banda Galkauwa

Bandara Manike Galkaduwa

Anuradha Bandara Galkaduwa

Thakshila Kumari Galkaduwa

To my ever loving husband:

Sadish Karunaweera

To my parents-in-law for giving me strength, and love:

Rajendra Karunaweera

Shriyani Karunaweere

Chapter 1 - Introduction

Coal is one of the main energy sources to generate 39% of the total electricity in the United States (USEIA, 2014). Coal-fired power plants emit air pollutants such as carbon dioxide (CO_2), sulfur dioxide (SO_2), nitrous oxides (NOx), mercury (Hg), and particulate matter to the atmosphere. Out of all, SO_2 is considered as the major pollutant that impacts human health and ecosystems (Srivastava and Jozewicz, 2001; USEPA, 2015a). To minimize SO_2 emissions from coal-fired power plants, the United States Environmental Protection Agency (USEPA) has imposed rules and regulations through the Acid Rain SO_2 Reduction Program established under Title IV of the Clean Air Act Amendments of 1990 (USEPA, 2015b). As a consequence, flue-gas desulfurization (FGD) technologies are being installed in coal-fired power plants to decrease potentially toxic gas emissions, mainly the SO_2 concentration in the flue gas.

Wet scrubber FGD systems are 90% efficient in removing SO_2 from the flue gas through the reaction with an alkaline aqueous slurry consisting of either lime [$Ca(OH)_2$] or limestone ($CaCO_3$) (Srivastava et al., 2001; Taylor et al., 2005). Upon the dewatering process of FGD systems, pollutants may partition between the solid phase, and the liquid phase (scrubber purge waste stream) (USEPA, 2009), ultimately entering to water. Generally, FGD wastewater is enriched in trace elements such as selenium (Se), arsenic (As), Hg as well as other constituents including boron (B), sulfur (S), fluorine (F), chlorine (Cl), total solids, and total dissolved solids (EPRI, 2006; EPRI, 2007). However, depending on coal type, and treatment methodologies used in power plants, the concentrations of constituents may vary from site to site (EPRI, 2006). Because of elevated concentrations of constituents, in general, FGD wastewater fails to comply with surface water quality standards established by National Pollutant Discharge Elimination System (NPDES) permit program, and Clean Water Act (EPRI, 2007). So, although FGD

technology is efficient in minimizing air pollution, these systems generate wastewater capable of water or land pollution if discharged without further treatments.

Constructed wetland treatment systems (CWTSs) are being considered as an economically, and environmentally effective alteration to treat various kinds of wastewaters such as, municipal, agricultural, and industrial wastewater (such as FGD, electronic, steel, chemical, and food-processing), and inorganic and organic contaminated water by physical, chemical, and biological means (Kadlec and Wallace, 2008; Khan et al., 2009; Schwindaman et al., 2014; Vymazal, 2010; Xu et al., 2014). Feasibility of CWTSs designed for FGD wastewater treatment is not widely documented (Eggert et al., 2008; Mooney and Murray-Gulde, 2008). The CWTSs have been identified as a potential option for treating Se, As and Hg in FGD wastewater (Eggert et al., 2008). Sundberg-Jones and Hassan (2007) identified the main species of Se, Hg, and As associated with sediment in this CWTS by sequential chemical extraction procedures. However, to our knowledge, the mechanistic understanding on trace element retention in a CWTS designed for FGD wastewater is not addressed in detail.

Selenium is one of the problematic constituents present in FGD wastewater at elevated level. The chemistry of Se is complicated as it is an element with multiple oxidation states. Biogeochemical behavior of Se in soils/sediments depends on its oxidation states which alter with pH, redox potential, soil mineralogy, microbial activities, and other soil conditions. Selenium in water mainly exists as more mobile and bioavailable form of Se(VI), and Se(IV). Under wetland conditions, oxidized Se species [Se(VI)] are reduced into most stable species [Se(IV), Se(0), and Se(-II)] (Masscheleyn and Patrick, 1993), thereby hindering the mobility and the bioavailability due to adsorption, precipitation/co-precipitation reactions with oxy(hydr)oxy soil minerals or the association with organic matter (Fernández-Martínez and Charlet, 2009;

Goldberg et al., 2007; Peak et al., 2006; Peak, 2006). Previous studies have revealed that CWTSs are a viable sink for Se contaminated wastewater (Gao et al., 2000; Gao et al., 2003a; Gao et al., 2003b; Zhang and Moore, 1996; Zhang and Moore, 1997).

Since the behavior of As is different to that of Se under wetland conditions, CWTSs may not be efficient for As removal from FGD wastewater (Masscheleyn et al., 1991a; Masscheleyn et al., 1991b). The speciation and the biogeochemical behavior of As are also controlled by altering pH, and redox potential, along with adsorption/desorption and precipitation reactions (Cherry et al., 1979; Sadiq, 1997). At neutral pH, arsenate [As(V)], and arsenite [AS(III)] are the major oxidation states of inorganic As species that predominant in soil solution (Sadiq, 1997; Smedley and Kinniburgh, 2002). Under anoxic conditions, the fate and transport of As in soils/sediments is controlled by the coupling of S, and Fe biogeochemical cycles (Moore et al., 1988; Sadiq, 1997; Smedley and Kinniburgh, 2002). Although FGD wastewater does not have high levels of As concentration, reductive dissolution of native soil (used as the CWTS material) Fe minerals and concomitant release of As to the soil solution may influence the performance efficiency of the CWTS. Since the CWTSs are being used for treating FGD wastewater constituents, understanding the mechanisms of As mobility, and possible treatments to minimize As mobility in the CWTS designed for treating FGD wastewater are essential. Ferrihydrite has been identified as a "scavenger" for As removal from contaminated water because of its amorphous nature, and high surface reactive area for adsorption reactions (Carlson et al., 2002; Lizama et al., 2011; Michel et al., 2007; Mohan and Pittman, 2007; Riveros et al., 2001). In this dissertation work, it was hypothesized that the secondary transformation of added ferrihydrite enhances sequestration of released As from native soil upon the reductive dissolution of Fe minerals under wetland conditions.

Microbially-mediated sulfate reduction to sulfide, and subsequent formation of stable metal sulfide phases is a critical mechanism for trace metal sequestration in the environment through chemical stabilization (Buddhawong et al., 2005; Stein et al., 2007; White et al., 1997). This process is stimulated by labile organic carbon (OC) acting as an electron donor (Rahman et al., 2011). Results from a pilot-scale CWTS at Westar Energy's Jeffrey Energy Center (JEC), St. Marys, KS designed for FGD wastewater treatment revealed that the efficiency of S removal or sulfate reduction, and the retention of As in the CWTS was weak. The FGD wastewater is typically enriched with sulfate (SO_4^{2-}) and supersaturated with respect to calcium sulfate. Hydraulic retention time (HRT), and hydraulic loading rate (HLR) have been identified as crucial factors that determine the performance of a CWTS (Kadlec and Wallace, 2008; Marchand et al., 2010; USEPA, 1995). It is hypothesized here that reduction of SO_4^{2-} to sulfide is accelerated by the presence of sulfate reducing bacteria (SRB) and OC. Sulfate reduction may significantly impact the efficiency of the CWTS for S retention and subsequent trace element retention. Similarly, due to time dependency of this bioreduction, the flow rate of the FGD wastewater may also have a significant effect on the efficiency of the CWTS.

The fate and transport of trace elements, such as Se and As, depend upon their chemical speciation. Total elemental analysis and an operationally defined sequential extraction procedure (SEP) provide indirect information about the elemental distribution and the possible speciation within the CWTS soil materials (Gao et al., 2000; Martens and Suarez, 1997; Wenzel et al., 2001; Wright et al., 2003; Zimmerman and Weindorf, 2010). However, direct speciation, and/or understanding the mechanisms of trace elements retention is not possible by these conventional methods alone. Synchrotron based X-ray spectroscopy analyses such as X-ray absorption near edge structure (XANES) spectroscopy provide detailed chemical and structural information

about an element in a heterogeneous system like soil (Fendorf et al., 1994; Gräfe et al., 2014; Luo and Zhang, 2010; Pickering et al., 1995; Wiramanaden et al., 2010). Additionally, micro-focused X-ray fluorescence (XRF) mapping in conjunction with micro-XANES can be used to investigate the spatial distribution, elemental correlations, and the chemical speciation of Se, As, and other elements of interest in soils (Lombi et al., 2011; Peak et al., 2006; Pickering et al., 1995). However, micro-scale X-ray absorption spectroscopy (XAS) techniques are not sufficient enough to glean average speciation of an element because of the limited area being investigated. Therefore, microscale investigations can be integrated with bulk-scale XAS techniques to elucidate the underlying mechanisms of Se, and As mobility or retention in the CWTS (Lombi et al., 2006; Majumdar et al., 2012). Since the biogeochemical cycles of trace elements are often coupled with Fe, and S cycling in a wetland system, bulk-XANES analysis of Fe, and S will be useful to gain relatively more complete understanding of the mechanisms on trace element retention in the CWTS.

A series of continuous flow through laboratory-based soil column experiments mimicking a pilot-scale CWTS was designed, and performed to assess the following general objectives. The first main objective was to understand the transport characteristics, and retention capacity of FGD wastewater constituents in the CWTS, and the second objective was to evaluate the effectiveness of soil treatments, and the influent flow rate on the performance of the CWTS for the retention of FGD constituents. This dissertation consists of three studies, and their specific objectives are given below:

1. The objectives of the first study, Transport and transformation of selenium, and other constituents of flue-gas desulfurization wastewater in a pilot-scale constructed wetland treatment system (Chapter 3), were to evaluate the transport characteristics, retention

capacity, and transformation of Se and other FGD wastewater constituents in a CWTS, and to gather mechanistic information of Se retention in the CWTS.

2. The objectives of the second study, Minimizing arsenic mobility using ferrihydrite in a pilot-scale constructed wetland treatment system designed for flue-gas desulfurization wastewater (Chapter 4), were to minimize native soil As mobility in a CWTS using ferrihydrite (Fh) as an amendment, and to understand underlying mechanisms for native soil As mobility or retention in non-treated and ferrihydrite-treated wetland materials using synchrotron-based X-ray spectroscopy techniques.
3. The objectives of the third study, Understanding of the retention of trace elements by sulfate reduction in a pilot-scale constructed wetland treatment system designed for flue-gas desulfurization wastewater (Chapter 5), were to assess the effect of flow rate and soil treatments (ferrihydrite, and labile OC) on S, and As retention, and to gather mechanistic information of interrelationships between S, As, and Fe cycling.

References

Buddhawong, S., P. Kuschk, J. Mattusch, A. Wiessner and U. Stottmeister. 2005. Removal of arsenic and zinc using different laboratory model wetland systems. Engineering in Life Sciences 5:247-252.

Carlson, L., J. Bigham, U. Schwertmann, A. Kyek and F. Wagner. 2002. Scavenging of as from acid mine drainage by schwertmannite and ferrihydrite: A comparison with synthetic analogues. Environ. Sci. Technol. 36:1712-1719.

Cherry, J., A. Shaikh, D. Tallman and R. Nicholson. 1979. Arsenic species as an indicator of redox conditions in groundwater. Journal of Hydrology 43:373-392.

Eggert, D.A., J.H. Rodgers Jr, G.M. Huddleston and C.E. Hensman. 2008. Performance of pilot-scale constructed wetland treatment systems for flue gas desulfurization waters. Environmental Geosciences 15:115-129.

EPRI. 2007. Treatment technology summary for critical pollutants of concern in power plant wastewaters. Rep. 1012549. Electric Power Research Institute, Palo Alto, CA:.

EPRI. 2006. EPRI technical manual: Guidance for assessing wastewater impacts of FGD scrubbers. Rep. 1013313. Electric Power Research Institute, Palo Alto, CA, USA.

Fendorf, S., D. Sparks, G. Lamble and M. Kelley. 1994. Applications of X-ray absorption fine structure spectroscopy to soils. Soil Sci. Soc. Am. J. 58:1583-1595.

Fernández-Martínez, A. and L. Charlet. 2009. Selenium environmental cycling and bioavailability: A structural chemist point of view. Reviews in Environmental Science and Bio/Technology 8:81-110.

Gao, S., K. Tanji, D. Peters and M. Herbel. 2000. Water selenium speciation and sediment fractionation in a california flow-through wetland system. J. Environ. Qual. 29:1275-1283.

Gao, S., K. Tanji, Z. Lin, N. Terry and D. Peters. 2003a. Selenium removal and mass balance in a constructed flow-through wetland system. J. Environ. Qual. 32:1557-1570.

Gao, S., K.K. Tanji, D.W. Peters, Z. Lin and N. Terry. 2003b. Selenium removal from irrigation drainage water flowing through constructed wetland cells with special attention to accumulation in sediments. Water Air Soil Pollut. 144:263-284.

Goldberg, S., S.M. Lesch and D.L. Suarez. 2007. Predicting selenite adsorption by soils using soil chemical parameters in the constant capacitance model. Geochim. Cosmochim. Acta 71:5750-5762.

Gräfe, M., E. Donner, R.N. Collins and E. Lombi. 2014. Speciation of metal (loid) s in environmental samples by X-ray absorption spectroscopy: A critical review. Anal. Chim. Acta 822:1-22.

Kadlec, R.H. and S. Wallace. 2008. Treatment wetlands. CRC press, Boca Raton, Florida.

Khan, S., I. Ahmad, M.T. Shah, S. Rehman and A. Khaliq. 2009. Use of constructed wetland for the removal of heavy metals from industrial wastewater. J. Environ. Manage. 90:3451-3457.

Lizama, K., T.D. Fletcher and G. Sun. 2011. Removal processes for arsenic in constructed wetlands. Chemosphere 84:1032-1043.

Lombi, E., G.M. Hettiarachchi and K.G. Scheckel. 2011. Advanced in situ spectroscopic techniques and their applications in environmental biogeochemistry: Introduction to the special section. J. Environ. Qual. 40:659-666.

Lombi, E., K. Scheckel, R. Armstrong, S. Forrester, J. Cutler and D. Paterson. 2006. Speciation and distribution of phosphorus in a fertilized soil. Soil Sci. Soc. Am. J. 70:2038-2048.

Luo, L. and S. Zhang. 2010. Applications of synchrotron-based X-ray techniques in environmental science. Science China Chemistry 53:2529-2538.

Majumdar, S., J.R. Peralta-Videa, H. Castillo-Michel, J. Hong, C.M. Rico and J.L. Gardea-Torresdey. 2012. Applications of synchrotron μ-XRF to study the distribution of biologically important elements in different environmental matrices: A review. Anal. Chim. Acta 755:1-16.

Marchand, L., M. Mench, D. Jacob and M. Otte. 2010. Metal and metalloid removal in constructed wetlands, with emphasis on the importance of plants and standardized measurements: A review. Environmental Pollution 158:3447-3461.

Masscheleyn, P.H. and W.H. Patrick. 1993. Biogeochemical processes affecting selenium cycling in wetlands. Environmental Toxicology and Chemistry 12:2235-2243.

Masscheleyn, P.H., R.D. Delaune and W. Patrick. 1991a. Arsenic and selenium chemistry as affected by sediment redox potential and pH. J. Environ. Qual. 20:522-527.

Masscheleyn, P.H., R.D. Delaune and W.H. Patrick Jr. 1991b. Effect of redox potential and pH on arsenic speciation and solubility in a contaminated soil. Environ. Sci. Technol. 25:1414-1419.

Michel, F.M., L. Ehm, S.M. Antao, P.L. Lee, P.J. Chupas, G. Liu, D.R. Strongin, M.A. Schoonen, B.L. Phillips and J.B. Parise. 2007. The structure of ferrihydrite, a nanocrystalline material. Science 316:1726-1729.

Mohan, D. and C.U. Pittman. 2007. Arsenic removal from water/wastewater using adsorbents—a critical review. J. Hazard. Mater. 142:1-53.

Mooney, F.D. and C. Murray-Gulde. 2008. Constructed treatment wetlands for flue gas desulfurization waters: Full-scale design, construction issues, and performance. Environmental Geosciences 15:131-141.

Moore, J.N., W.H. Ficklin and C. Johns. 1988. Partitioning of arsenic and metals in reducing sulfidic sediments. Environ. Sci. Technol. 22:432-437.

Peak, D. 2006. Adsorption mechanisms of selenium oxyanions at the aluminum oxide/water interface. J. Colloid Interface Sci. 303:337-345.

Peak, D., U. Saha and P. Huang. 2006. Selenite adsorption mechanisms on pure and coated montmorillonite: An EXAFS and XANES spectroscopic study. Soil Sci. Soc. Am. J. 70:192-203.

Pickering, I.J., G.E. Brown and T.K. Tokunaga. 1995. Quantitative speciation of selenium in soils using X-ray absorption spectroscopy. Environ. Sci. Technol. 29:2456-2459.

Rahman, K.Z., A. Wiessner, P. Kuschk, M. van Afferden, J. Mattusch and R.A. Müller. 2011. Fate and distribution of arsenic in laboratory-scale subsurface horizontal-flow constructed wetlands treating an artificial wastewater. Ecol. Eng. 37:1214-1224.

Riveros, P., J. Dutrizac and P. Spencer. 2001. Arsenic disposal practices in the metallurgical industry. Can. Metall. Q. 40:395-420.

Sadiq, M. 1997. Arsenic chemistry in soils: An overview of thermodynamic predictions and field observations. Water Air Soil Pollut. 93:117-136.

Schwindaman, J.P., J.W. Castle and J.H. Rodgers. 2014. Fate and distribution of arsenic in a process-designed pilot-scale constructed wetland treatment system. Ecol. Eng. 68:251-259.

Smedley, P. and D. Kinniburgh. 2002. A review of the source, behaviour and distribution of arsenic in natural waters. Appl. Geochem. 17:517-568.

Srivastava, R.K. and W. Jozewicz. 2001. Flue gas desulfurization: The state of the art. J. Air Waste Manage. Assoc. 51:1676-1688.

Srivastava, R.K., W. Jozewicz and C. Singer. 2001. SO_2 scrubbing technologies: A review. Environ. Prog. 20:219-228.

Stein, O.R., D.J. Borden-Stewart, P.B. Hook and W.L. Jones. 2007. Seasonal influence on sulfate reduction and zinc sequestration in subsurface treatment wetlands. Water Res. 41:3440-3448.

Sundberg-Jones, S.E. and S.M. Hassan. 2007. Sediment-associated elements in a constructed wetland treatment system: Distribution, characterization, and toxicity. Bioremediation, Biodiversity and Bioavailability 1:41-55.

Buddhawong, S., P. Kuschk, J. Mattusch, A. Wiessner and U. Stottmeister. 2005. Removal of arsenic and zinc using different laboratory model wetland systems. Engineering in Life Sciences 5:247-252.

Carlson, L., J. Bigham, U. Schwertmann, A. Kyek and F. Wagner. 2002. Scavenging of as from acid mine drainage by schwertmannite and ferrihydrite: A comparison with synthetic analogues. Environ. Sci. Technol. 36:1712-1719.

Cherry, J., A. Shaikh, D. Tallman and R. Nicholson. 1979. Arsenic species as an indicator of redox conditions in groundwater. Journal of Hydrology 43:373-392.

Eggert, D.A., J.H. Rodgers Jr, G.M. Huddleston and C.E. Hensman. 2008. Performance of pilot-scale constructed wetland treatment systems for flue gas desulfurization waters. Environmental Geosciences 15:115-129.

EPRI. 2007. Treatment technology summary for critical pollutants of concern in power plant wastewaters. Rep. 1012549. Electric Power Research Institute, Palo Alto, CA:.

EPRI. 2006. EPRI technical manual: Guidance for assessing wastewater impacts of FGD scrubbers. Rep. 1013313. Electric Power Research Institute, Palo Alto, CA, USA.

Fendorf, S., D. Sparks, G. Lamble and M. Kelley. 1994. Applications of X-ray absorption fine structure spectroscopy to soils. Soil Sci. Soc. Am. J. 58:1583-1595.

Fernández-Martínez, A. and L. Charlet. 2009. Selenium environmental cycling and bioavailability: A structural chemist point of view. Reviews in Environmental Science and Bio/Technology 8:81-110.

Gao, S., K. Tanji, D. Peters and M. Herbel. 2000. Water selenium speciation and sediment fractionation in a california flow-through wetland system. J. Environ. Qual. 29:1275-1283.

Gao, S., K. Tanji, Z. Lin, N. Terry and D. Peters. 2003a. Selenium removal and mass balance in a constructed flow-through wetland system. J. Environ. Qual. 32:1557-1570.

Gao, S., K.K. Tanji, D.W. Peters, Z. Lin and N. Terry. 2003b. Selenium removal from irrigation drainage water flowing through constructed wetland cells with special attention to accumulation in sediments. Water Air Soil Pollut. 144:263-284.

Goldberg, S., S.M. Lesch and D.L. Suarez. 2007. Predicting selenite adsorption by soils using soil chemical parameters in the constant capacitance model. Geochim. Cosmochim. Acta 71:5750-5762.

Gräfe, M., E. Donner, R.N. Collins and E. Lombi. 2014. Speciation of metal (loid) s in environmental samples by X-ray absorption spectroscopy: A critical review. Anal. Chim. Acta 822:1-22.

Kadlec, R.H. and S. Wallace. 2008. Treatment wetlands. CRC press, Boca Raton, Florida.

Khan, S., I. Ahmad, M.T. Shah, S. Rehman and A. Khaliq. 2009. Use of constructed wetland for the removal of heavy metals from industrial wastewater. J. Environ. Manage. 90:3451-3457.

Lizama, K., T.D. Fletcher and G. Sun. 2011. Removal processes for arsenic in constructed wetlands. Chemosphere 84:1032-1043.

Lombi, E., G.M. Hettiarachchi and K.G. Scheckel. 2011. Advanced in situ spectroscopic techniques and their applications in environmental biogeochemistry: Introduction to the special section. J. Environ. Qual. 40:659-666.

Lombi, E., K. Scheckel, R. Armstrong, S. Forrester, J. Cutler and D. Paterson. 2006. Speciation and distribution of phosphorus in a fertilized soil. Soil Sci. Soc. Am. J. 70:2038-2048.

Luo, L. and S. Zhang. 2010. Applications of synchrotron-based X-ray techniques in environmental science. Science China Chemistry 53:2529-2538.

Majumdar, S., J.R. Peralta-Videa, H. Castillo-Michel, J. Hong, C.M. Rico and J.L. Gardea-Torresdey. 2012. Applications of synchrotron μ-XRF to study the distribution of biologically important elements in different environmental matrices: A review. Anal. Chim. Acta 755:1-16.

Marchand, L., M. Mench, D. Jacob and M. Otte. 2010. Metal and metalloid removal in constructed wetlands, with emphasis on the importance of plants and standardized measurements: A review. Environmental Pollution 158:3447-3461.

Masscheleyn, P.H. and W.H. Patrick. 1993. Biogeochemical processes affecting selenium cycling in wetlands. Environmental Toxicology and Chemistry 12:2235-2243.

Masscheleyn, P.H., R.D. Delaune and W. Patrick. 1991a. Arsenic and selenium chemistry as affected by sediment redox potential and pH. J. Environ. Qual. 20:522-527.

Masscheleyn, P.H., R.D. Delaune and W.H. Patrick Jr. 1991b. Effect of redox potential and pH on arsenic speciation and solubility in a contaminated soil. Environ. Sci. Technol. 25:1414-1419.

Michel, F.M., L. Ehm, S.M. Antao, P.L. Lee, P.J. Chupas, G. Liu, D.R. Strongin, M.A. Schoonen, B.L. Phillips and J.B. Parise. 2007. The structure of ferrihydrite, a nanocrystalline material. Science 316:1726-1729.

Mohan, D. and C.U. Pittman. 2007. Arsenic removal from water/wastewater using adsorbents—a critical review. J. Hazard. Mater. 142:1-53.

Mooney, F.D. and C. Murray-Gulde. 2008. Constructed treatment wetlands for flue gas desulfurization waters: Full-scale design, construction issues, and performance. Environmental Geosciences 15:131-141.

Moore, J.N., W.H. Ficklin and C. Johns. 1988. Partitioning of arsenic and metals in reducing sulfidic sediments. Environ. Sci. Technol. 22:432-437.

Peak, D. 2006. Adsorption mechanisms of selenium oxyanions at the aluminum oxide/water interface. J. Colloid Interface Sci. 303:337-345.

Peak, D., U. Saha and P. Huang. 2006. Selenite adsorption mechanisms on pure and coated montmorillonite: An EXAFS and XANES spectroscopic study. Soil Sci. Soc. Am. J. 70:192-203.

Pickering, I.J., G.E. Brown and T.K. Tokunaga. 1995. Quantitative speciation of selenium in soils using X-ray absorption spectroscopy. Environ. Sci. Technol. 29:2456-2459.

Rahman, K.Z., A. Wiessner, P. Kuschk, M. van Afferden, J. Mattusch and R.A. Müller. 2011. Fate and distribution of arsenic in laboratory-scale subsurface horizontal-flow constructed wetlands treating an artificial wastewater. Ecol. Eng. 37:1214-1224.

Riveros, P., J. Dutrizac and P. Spencer. 2001. Arsenic disposal practices in the metallurgical industry. Can. Metall. Q. 40:395-420.

Sadiq, M. 1997. Arsenic chemistry in soils: An overview of thermodynamic predictions and field observations. Water Air Soil Pollut. 93:117-136.

Schwindaman, J.P., J.W. Castle and J.H. Rodgers. 2014. Fate and distribution of arsenic in a process-designed pilot-scale constructed wetland treatment system. Ecol. Eng. 68:251-259.

Smedley, P. and D. Kinniburgh. 2002. A review of the source, behaviour and distribution of arsenic in natural waters. Appl. Geochem. 17:517-568.

Srivastava, R.K. and W. Jozewicz. 2001. Flue gas desulfurization: The state of the art. J. Air Waste Manage. Assoc. 51:1676-1688.

Srivastava, R.K., W. Jozewicz and C. Singer. 2001. SO_2 scrubbing technologies: A review. Environ. Prog. 20:219-228.

Stein, O.R., D.J. Borden-Stewart, P.B. Hook and W.L. Jones. 2007. Seasonal influence on sulfate reduction and zinc sequestration in subsurface treatment wetlands. Water Res. 41:3440-3448.

Sundberg-Jones, S.E. and S.M. Hassan. 2007. Sediment-associated elements in a constructed wetland treatment system: Distribution, characterization, and toxicity. Bioremediation, Biodiversity and Bioavailability 1:41-55.

Taylor, M.R., E.S. Rubin and D.A. Hounshell. 2005. Control of SO_2 emissions from power plants: A case of induced technological innovation in the US. Technological Forecasting and Social Change 72:697-718.

USEIA. 2014. Coal - U.S. energy information administration (EIA). http://www.eia.gov/coal/ (accessed July 13, 2015).

USEPA. 2015a. Six common air pollutants. http://www.epa.gov/airquality/urbanair/ (accessed July 13, 2015).

USEPA. 2015b. Acid rain program. http://www.epa.gov/airmarkets/programs/arp/index.html. (accessed June 30, 2015).

USEPA. 2009. Steam electric power generating point source category: Final detailed study report (EPA 821-R-09-008). U.S. Environmental Protection Agency.

USEPA. 1995. A handbook of constructed wetlands. U.S. Environmental Protection Agency, Washington, D.C, USA.

Vymazal, J. 2010. Constructed wetlands for wastewater treatment. Water 2:530-549.

Wenzel, W.W., N. Kirchbaumer, T. Prohaska, G. Stingeder, E. Lombi and D.C. Adriano. 2001. Arsenic fractionation in soils using an improved sequential extraction procedure. Anal. Chim. Acta 436:309-323.

White, C., J.A. Sayer and G.M. Gadd. 1997. Microbial solubilization and immobilization of toxic metals: Key biogeochemical processes for treatment of contamination. FEMS Microbiol. Rev. 20:503-516.

Wiramanaden, C.I., K. Liber and I.J. Pickering. 2010. Selenium speciation in whole sediment using X-ray absorption spectroscopy and micro X-ray fluorescence imaging. Environ. Sci. Technol. 44:5389-5394.

Wright, M.T., D.R. Parker and C. Amrhein. 2003. Critical evaluation of the ability of sequential extraction procedures to quantify discrete forms of selenium in sediments and soils. Environ. Sci. Technol. 37:4709-4716.

Xu, J., Y. Shi, G. Zhang, J. Liu and Y. Zhu. 2014. Effect of hydraulic loading rate on the efficiency of effluent treatment in a recirculating puffer aquaculture system coupled with constructed wetlands. Journal of Ocean University of China 13:146-152.

Zhang, Y. and J.N. Moore. 1997. Reduction potential of selenate in wetland sediment. J. Environ. Qual. 26:910-916.

Zhang, Y. and J.N. Moore. 1996. Selenium fractionation and speciation in a wetland system. Environ. Sci. Technol. 30:2613-2619.

Zimmerman, A.J. and D.C. Weindorf. 2010. Heavy metal and trace metal analysis in soil by sequential extraction: A review of procedures. Int. J. Anal. Chem. 2010:387803.

Chapter 2 - Literature review

Coal-fired power plants

According to the information provided by U.S. Energy Information Administration in 2014, about 39% of the total electricity in the United States was generated by coal. Coal is a non-renewable energy source and will be depleted with time. Coal is one of the energy sources that are used for electricity generation because of its affordable price, readily availability, high energy production upon combustion, and the easiness to burn. Coal-fired power plants emit environmentally harmful gases, including carbon dioxide (CO_2), sulfur dioxide (SO_2), nitrous oxides (NO_x), mercury (Hg), and particulate matter to the atmosphere. Among these constituents, SO_2 is the major pollutant that influences human health, and environmental ecosystems due to acid rain precipitation. The United States Environmental Protection Agency (USEPA) has identified fossil fuel-fired power plants as being responsible for 73% of the SO_2 emission nationwide (USEPA, 2015a).

Humans exposure to high ambient levels of air contaminated with SO_2 may cause health issues such as bronchoconstriction and asthma symptoms (Rubin et al., 2004; Srivastava and Jozewicz, 2001; Srivastava et al., 2001; Taylor et al., 2005). Besides SO_2 emission, NO_x from coal-fired power plants also leads to environmental concerns such as depletion of the ozone layer (USEPA, 2015a). As an effort to mitigate these potentially toxic gas emissions, and their dramatic effect on humans and the ecological environment, coal-fired power plants have been taking necessary precautions. Those rules are regulated by Clean Air Act. To minimize SO_2 emissions from the flue-gas generated from coal-fired power plants, the USEPA established regulations from the Acid Rain SO_2 Reduction Program, established under Title IV of the Clean Air Act Amendments of 1990 (USEPA, 2015b). After Phase II of the Acid Rain SO_2 Reduction

Program began in 2000, flue-gas desulfurization (FGD) technologies started being installed in coal-fired power plants to decrease SO_2 concentration in the flue gas.

Flue-gas desulfurization (FGD) systems

Among various techniques to control SO_2 emissions from electricity generation power plants by coal combustion, implementation of FGD technology on sites can decrease SO_2 emission significantly. In 2010, power plants with the FGD systems generated 58% of the total electricity by burning coal, while producing only 27% of total SO_2 emissions (USEIA, 2011). Power plants are expected to continue installing new FGD systems in substantial numbers until at least 2025, further minimizing SO_2 emission. The efficiency of SO_2 removal from FGD systems depends upon the characteristics such as type of specific equipment, age, and sulfur content of coal (USEIA, 2011). Among three main types of coal used for electricity generation, bituminous coal, and lignite coal generally have higher sulfur content than subbituminous coal, which also varies by regions (USEIA, 2011).

In general, there are two types of FGD systems; dry scrubber FGD, and wet scrubber FGD (Srivastava et al., 2001). Of these technologies, the wet scrubber FGD systems are more commonly implemented in coal-fired power plants. This type of FGD systems are capable of decreasing the SO_2 concentration in the flue-gas by more than 90% (Srivastava and Jozewicz, 2001; Srivastava et al., 2001; Taylor et al., 2005). Figure 2.1shows the main pathways of the wet scrubber FGD systems. In these systems, SO_2 enriched flue-gas is contacted with an alkaline slurry that is generally made from either lime [$Ca(OH)_2$] or limestone ($CaCO_3$) in an absorber reaction tank. The wet FGD scrubber systems that use limestone as the source of Ca are cost effective for the removal of SO_2.

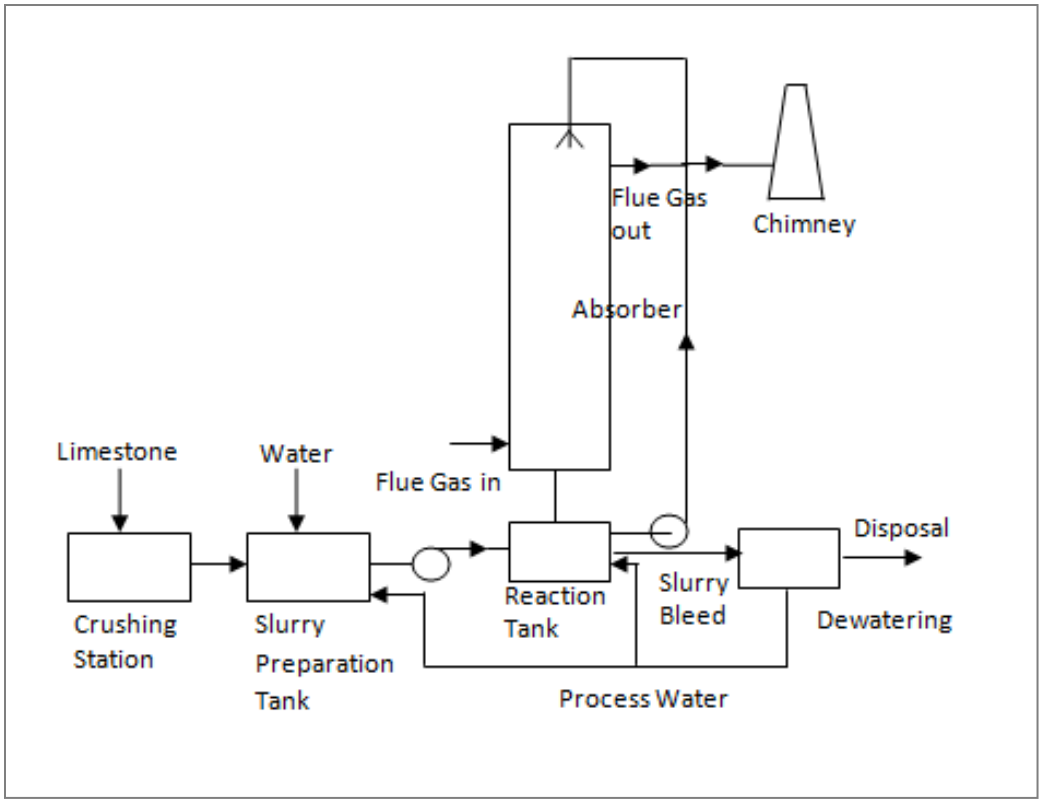

Figure 2.1 A schematic diagram of a wet flue-gas desulfurization process (redrawn from Srivastava and Jozewicz, 2001).

The overall reactions that take place in the absorber, and the reaction tank are expressed as follows.

$CaCO_3(s) + SO_2(g) + \frac{1}{2}O_2(g) + 2H_2O(l) \rightarrow CaSO4 \bullet 2H_2O(s) + CO_2(g)$ (Moretti et al., 2012)

In the SO_2 removal process, first cooled flue gas is saturated with the slurry and forms calcium sulfite ($CaSO_3$.1/2 H_2O). Then, under the forced oxidization system (by injecting air into the slurry) $CaSO_3$ is converted to calcium sulfate ($CaSO_4.2H_2O$) or gypsum. This process contributes to approximately 98% of SO_2 removal efficiency in coal-fired power plants (Moretti et al., 2012; Srivastava and Jozewicz, 2001; Srivastava et al., 2001). The efficacy of SO_2 removal of the wet scrubber FGD systems using limestone can be improved by physical, and chemical

parameters, such as the liquid-to-gas (L/G) ratio, the absorber gas velocity, pH of the reaction tank, temperature of the scrubber, HCl, HF, and the use of additives (organic acids) (Córdoba, 2015). These wet FGD treatments are also effective for the emission control of highly volatile trace elements, such as Hg (Ito et al., 2006). The precipitated form of $CaSO_4$ tends to capture emitted As, Se, and Hg from the coal combustion process (Diaz-Somoano and Martinez-Tarazona, 2004; Ochoa-González et al., 2013). Córdoba (2015) reviewed that about 60 to 70% of Hg removed by the FGD technology was found to be in the by-product of the FGD process (gypsum).

Flue-gas desulfurization wastewater

The pollutants in the flue-gas which absorbed to the slurry may partition between the solid phase, and the liquid phase (scrubber purge waste stream) upon dewatering process of the FGD system (USEPA, 2009). Although FGD scrubber systems are efficient in reducing the SO_2 concentration in the flue-gas, they create water pollution due to high levels of contaminants such as trace elements (e.g., Se, As, and Hg), total solids, salts as well as many other constituents including fluorine, chlorine, sulfate, and boron (EPRI, 2006; EPRI, 2007; USEPA, 2009). The Electric Power Research Institute (EPRI) conducted a screening evaluation of FGD wastewater at eight plants, and the characterization of constituents is presented Table 2.1.

The wastewater generated from FGD systems is supersaturated with respect to calcium sulfate, and highly buffered with bicarbonate (EPRI, 2006). The pH of FGD wastewater ranges from 4.5 to 9.0 (Higgins et al., 2009). The total suspended solid concentration may range from 33 mg/L to 140,000 mg/L, depending on coal, and limestone used, as well as layout of the scrubber. As shown in Table 2.1, the concentration of some of the constituents varies significantly among sites. The variability of the composition of FGD wastewater from site to site

depends upon the coal type, type of scrubber, materials of construction in the FGD system, FGD system operation, and the dewatering of gypsum system (Eggert, 2009; EPRI, 2006; USEPA, 2009). Higgins et al. (2009) also found that the FGD wastewaters have high concentrations of total suspended solids, chloride, sulfate, bicarbonate, sodium, potassium, and magnesium. Also, FGD wastewater contained trace elements including As, Hg, Se, and boron (B), which may also vary with the coal type.

Discharging of the pollutants or the contaminants in FGD wastewater can potentially be a threat to local wildlife, and human health. Generally, FGD wastewater fails to meet Clean Water Act, and National Pollution Discharge Elimination System (NPDES) requirements due to the concentrations of constituents present at evaluated levels. Under the authorization of the Clean Water Act, the NPDES permit program controls water pollution by regulating point sources that discharge pollutants from industrial, municipal, and other facilities to surface waters. Sites must obtain NPDES permits if polluted water is directly discharged to surface waters (USEPA, 2014).

The bioavailability of trace elements in wastewater depends on their speciation which is determined by the characteristics of both the metal, and surrounding environment (e.g., temperature, pH, salinity, oxidation-reduction (redox) potential, total organic content, suspended particulate content, and water velocity) (USEPA, 2013). It has been reported that Se is a common element present in combustion wastewater, which impacts the environment, and the ecology (USEPA, 2013). Because of the toxicity of constituents failing to comply with surface water quality standards, FGD wastewater should not be discharged to surface water bodies without being treated.

Table 2.1Characteristics of flue-gas desulfurization wastewater from eight coal-fired power plants (reproduced from EPRI, 2009).

		EPRI Screening Study			
		Dissolved		Total	
Parameter ID	**Units**	**Median**	**Range**	**Median**	**Range**
Aluminum	µg/L	1,000	260 -18,000	39,000	9,700 -170,000
Antimony	µg/L	50	10 - 50	280	12 - 500
Arsenic	µg/L	16	4.1 - 110	260	10 - 380
Barium	µg/L	250	97 - 840	2,000	180 - 3,000
Beryllium	µg/L	40	5.2 - 40	220	3.2 - 400
Boron	mg/L	260	15 - 480	200	16 - 450
Cadmium	µg/L	50	13 - 83	280	9.3 - 500
Calcium	mg/L	750	670 - 4,000	2,900	700 - 33,000
Chromium	µg/L	100	14 - 100	600	30 - 1,000
Cobalt	µg/L	78	22 - 100	1,000	22 - 1,000
Copper	µg/L	100	63 - 270	650	100 - 3,300
Iron	µg/L	1,000	130 - 1,000	62,000	1,500 - 280,000
Lead	µg/L	50	6.5 - 50	280	6.8 - 500
Magnesium	mg/L	1,100	390 - 4,400	1,500	440 - 4,300
Manganese	µg/L	6,400	1,700 - 52,000	11,000	1,900 - 52,000
Mercury	µg/L	0.6	0.1 - 8.5	61	8.2 - 99
Molybdenum	µg/L	170	40 - 700	2,500	52 - 2,500
Nickel	µg/L	260	120 - 1,200	1,700	130 - 2,000
Potassium	mg/L	115	21- 880	99	27 - 577
Selenium	µg/L	1,100	70 - 1,800	1,700	86 - 2,600
Selenium IV	µg/L	410	110 - 430		
Selenium VI	µg/L	6.0	4.2 - 1,207		
Silver	µg/L	100	13 - 100	550	4 - 1,000
Sodium	mg/L	670	72 - 4,800	320	66 - 45,000
Thallium	µg/L	100	13 - 100	550	5.6 - 1,000
Titanium	µg/L	600	125 - 1,000	10,000	170 - 10,000
Vanadium	µg/L	150	31 - 250	2,500	33 - 2,500
Zinc	µg/L	1,000	100 - 2,800	1,700	180 - 7,100
Acidity	mg $CaCO_3$/L	270	46 - 11,000	370	53 - 10,000
Alkalinity	mg $CaCO_3$/L	180	23 - 520	250	26 - 4,500
Chloride	mg/L	2,400	690 - 23,000	2,400	460 - 25,000
Conductivity	µhos/cm	10,000	4,300 - 63,000	9,500	4,200 - 67,000
Fluoride	mg/L	15	6.5 - 51		
Hardness as $CaCO_3$	mg/L	4,100	3,000 - 5,300	4,300	3,000 - 5,600
pH	pH units	7.3	6.2 - 7.3	6.9	6.1 - 7.3
Sulfate	mg/L	3,200	1,700 - 5,700	9,500	9,500 - 9,500
TDS	mg/l	14,000	6,000 - 50,000	14,000	1,400 - 45,000
TKN	mg N/L	24	2.4 - 58	24	2.1 - 84
TSS	mg/L	4.2	2.2 - 7.6	13,000	33 - 140,000
Flow	mgd	0.19	0.17 - 0.21	0.19	0.17 - 0.21

FGD wastewater treatment strategies

The USEPA has identified a variety of FGD wastewater treatment technologies operated by coal-fired power plants. Those options are described in "Steam Electric Power Generating Point Source Category: Final Detailed Study Report "(EPRI, 2006). These strategies include settling ponds, chemical precipitation, biological treatment, constructed wetlands, design/operation of zero discharge, and vapor-compression evaporation system.

Settling ponds can reduce the amount of total suspended solids in wastewater, as well as specific pollutants that are in particulate form. Solid particles or suspended solids from wastewater can be removed by gravity. In a chemical precipitation wastewater treatment system, chemicals are added to the wastewater to facilitate settling and removal of the solids by changing the physical state of dissolved and suspended solids. There are three main types of precipitation systems used to precipitate metals from FGD wastewater. They are hydroxide precipitation, Fe precipitation, and S precipitation. The precipitation with hydroxides to form coagulation, and co-precipitation with Fe(II) or Fe(III) can increase the removal of dissolved metals via forming stable phases (EPRI, 2006). The addition of sulfide chemicals can be used to remove heavy metals such as Hg from FGD wastewater (Hanlon, 2010). The removal of metals as sulfide precipitates is more effective than hydroxide precipitates because metal sulfides are more stable. The alkali-sulfide process has been widely utilized for treating from wastewater from wet scrubber FGD (Chapman and Layman, 2007). Pleasant Prairie Power Plant in Wisconsin used alkali-sulfide process to precipitate very low levels of Hg, and other heavy metals in FGD scrubber wastewater (EPRI, 2006).

Biological wastewater treatment systems use microorganisms to remove organic pollutants (chemical oxygen demand (COD)/biological oxygen demand (BOD)), and inorganic

pollutants (Riffe et al., 2008). There are two main types of biological treatment systems that are being used to treat wastewater; they are aerobic systems, and anoxic/anaerobic systems (USEPA, 2009). The aerobic biological treatment system can be effectively used to reduce BOD from the wastewater. The anoxic zone is designed for denitrification, and better reduction of certain pollutants such as Se, and Hg. Further, in the anoxic region, sulfate reducing bacteria are added to biological reduction of selenates and selenites to elemental selenium, thereby enhancing the removal efficiency (EPRI, 2006). The GE Water & Process Technologies have used ABMet® biological technology (to enhance bioreduction) in two power plants at Duke Energy, and Progress Energy in North Carolina to remove As, Hg, and other solubilized heavy metals from FGD wastewater (Pickett et al., 2006). Using this method, they were able to reduce Se concentration by more than 99% (Pickett et al., 2006). These biological systems are used in Chesapeake Bay watershed to reduce nitrogen, and COD/BOD while fixed film biological treatment systems are used for Se reduction at power plants in North Carolina (Riffe et al., 2008). About 1360 megawatt (MW) power plant in the eastern U.S used a biological reactor system for heavy metals, and nitrate reduction (Riffe et al., 2008). A two-unit 1,120 MW coal-fired generating facility in the eastern U.S. used microbially-mediated bioreactors (microbial activities promoted by carbon addition) to remove Se from FGD wastewater (EPRI, 2006). Zero-liquid discharge is usually the last option for treating FGD wastewater for disposal purposes. High capital cost is needed to install and there are high costs for operation and maintenance. Zero-liquid discharge with deep well injection is also fairly high cost. More detail about this method is given in (EPRI, 2006).

Moreover, there are several treatment strategies reported in the literature for FGD wastewater purification before discharging into surface water bodies. Nielsen et al. (1997) tested

a fluidized-bed technique to remove heavy metals from the FGD wastewater. They found greater reduction for nickel, cadmium, and zinc. An optimum pH 9.0 to 9.1 showed enhanced heavy metal removal efficiency from FGD wastewater because of the formation of metal hydroxides in a fluidized bed reactor (Zhou et al., 1999). To decrease trace elements concentration to parts per billion levels is a challenge due to the complex matrix of FGD wastewater (EPRI, 2006; USEPA, 2009). An innovation treatment method for wastewater treatment using hybrid zero-valent Fe was an effective strategy for Se, and Hg removal from FGD wastewater (Huang et al., 2013).

Most of the treatment strategies for FGD wastewater are associated with many disadvantages. Those include high costs for construction, operation and maintenance, solid handling and disposal (EPRI, 2006). Constructed wetland treatment systems (CWTSs) have considerable potential for treating FGD wastewater constituents (EPRI, 2006). Also, these systems are an environmentally and economically effective option to treat FGD wastewater via combination of chemical, physical, and biological mechanisms.

Constructed wetland treatment systems (CWTSs)

Constructed wetlands treatment systems (CWTSs) are engineered systems that have been designed and constructed to utilize the natural processes such as wetland vegetation, soils, and their associated microbial functionality to treat wastewater (Vymazal, 2010). The experiments conducted using wetland macrophytes for wastewater treatment were first reported in Germany in the early 1950s (Vymazal, 2010). The removal mechanisms of constituents in a CWTS include sedimentation, filtration, precipitation, volatilization, adsorption, and plant uptake (Kadlec and Wallace, 2008). These mechanisms are responsible for chemical, physical, and biological processes (Peterson, 1998; Sundaravadivel and Vigneswaran, 2001). The advantages of the CWTSs are low operational and maintenance costs, capability of removing various pollutants

such as heavy metals, nutrients, and organic compounds from various contaminated waters (Vymazal, 2010; Yeh, 2008).

There are special characteristics of wetland ecosystems which make them suitable for wastewater purification; (1) wetland systems are semi-aquatic systems which contain large quantities of water, (2) wetland consist of partly oxic, partly anoxic soils where organic matter breakdown is involved in redox reactions, and (3) wetlands support a highly productive vegetation which is capable of taking up large amounts of nutrients (Verhoeven and Meuleman, 1999). The performance of the wetlands used for wastewater treatment depends strongly upon the loading rate and their hydrological and ecological characteristics (Kadlec and Wallace, 2008; Verhoeven and Meuleman, 1999). The constructed wetlands are effective at treating wastewater compared to natural wetland because they can be designed in order to achieve the maximum performance (Verhoeven and Meuleman, 1999). Faulwetter et al. (2009) reviewed the microbial mechanisms responsible for removal of carbon, nitrogen, and sulfur compounds in treatment wetlands. The removal efficiency of a pollutant is usually associated with a specific microbial functional group. Thus, design and operational methodologies that enhance the activity of specific microbial functional group can improve the performance of the treatment wetlands.

There are three main types of CWTS that are commonly used for wastewater treatments; (1) free water surface (FWS), (2) horizontal subsurface flow (HSSF), and (3) vertical flow (VF) (Kadlec and Wallace, 2008). The FWS wetlands contain areas exposed to the atmosphere, and they are more or less similar to natural wetlands (Figure 2.2). More than 50% of the area is densely covered by vegetation. Evaporation, and seepage processes are common in the FWS wetlands. This type of constructed wetlands is effective in removing suspended solids, organic pollutants, and nitrogen (Vymazal, 2010). However, phosphorous removal efficiency is low

because of limited contact of wastewater with soil particles where adsorption and or precipitation reactions are common (Vymazal, 2010). This type of wetland is suitable for municipal wastewater, urban, agricultural, industrial stormwater treatment, and many other types of wastewater (Kadlec and Wallace, 2008; Vymazal, 2010). Free water surface constructed wetlands are often used in North America, Australia, and Europe.

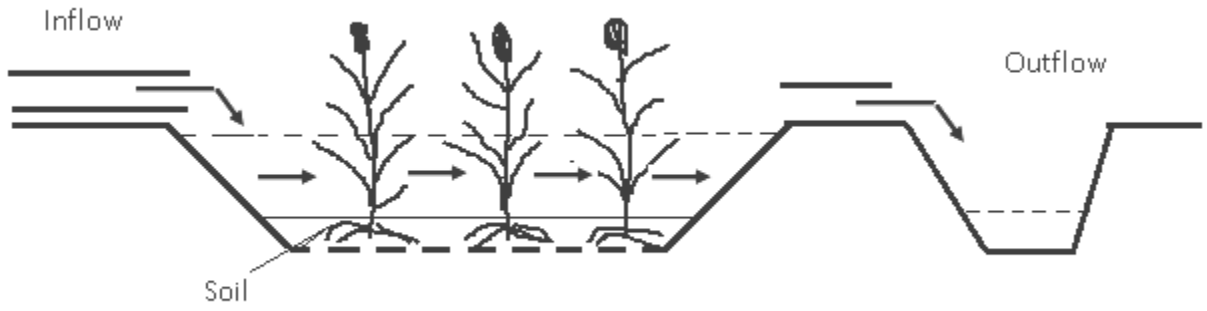

Figure 2.2 Schematic representation of a free water surface (FWS) wetland (redrawn from Kadlec and Wallace, 2008).

The HSSF wetlands (Figure 2.3) consist of gravel or soil beds planted with wetland vegetation. In this design, a rectangular bed is planted with common reed (*Phragmites australis*) and lined with an impermeable membrane (Vymazal et al., 2006). Mechanically pre-treated wastewater enters into the HSSF wetland, and passes slowly under the surface of the bed. Finally, the treated wastewater is collected back from the outlet. These wetland systems are designed in order for water to stay adjacent to the roots of the plants (Kadlec and Wallace, 2008). Pollutants are removed by microbial degradation, chemical, and physical processes. This wetland technology is often used for domestic, municipal, industrial, agricultural, landfill leachate, and runoff water treatment (Vymazal, 2010).

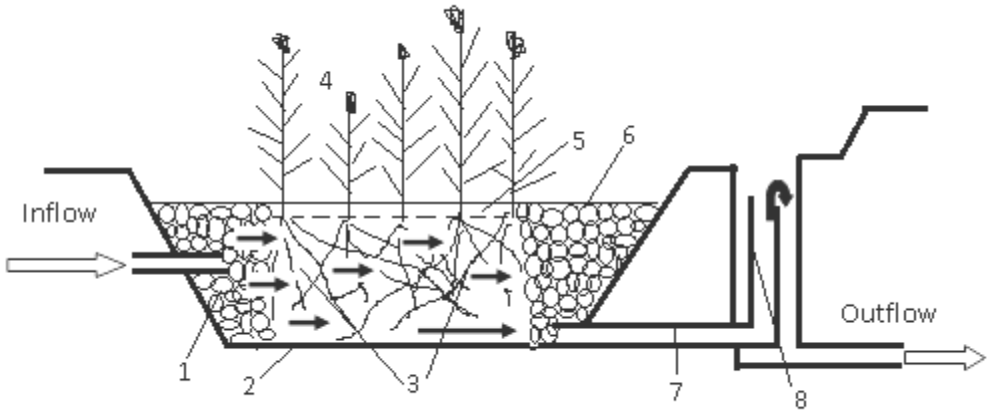

Figure 2.3 Schematic representation of a constructed wetland with horizontal sub-surface flow (HSSF) (redrawn from Vymazal et al., 2006). 1. Distribution zone filled with large stones, 2. impermeable liner, 3. filtration medium (gravel, crushed rock), 4. vegetation, 5. water level in the bed, 6. collection zone filled with large stones, 7. collection drainage pipe, and 8. outlet structure for maintaining the water level in the bed. The arrows indicate only a general flow pattern.

The VF constructed wetlands (Figure 2.4) consist of a flat bed of graded gravel topped with sand. These wetlands are planted with macrophytes. It has been suggested in the VF wetlands to use an upflow system in order to minimize oxygen transfer and to promote reductive dehalogenation (Kadlec and Wallace, 2008). This type of constructed wetland is efficient for nitrogen, and BOD removal, but not for phosphorus (Vymazal et al., 2006). The subsurface type wetlands are more beneficial over FWS wetlands for metals reduction, and their stabilization. The VF sub-surface CWTSs are used to treat domestic, municipal wastewater, and various other types of wastewater (Vymazal, 2010).

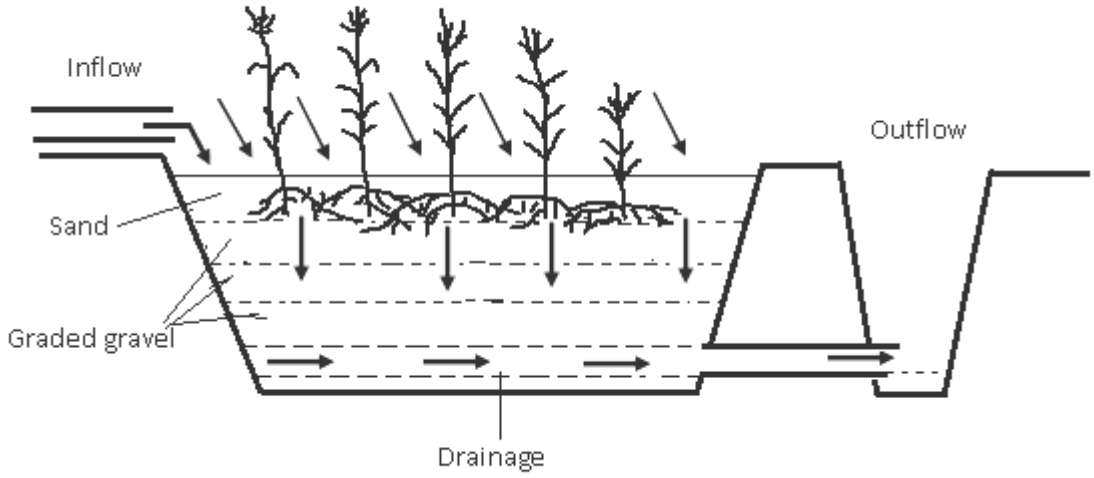

Figure 2.4 Schematic representation of a constructed wetland with vertical sub-surface flow (redrawn from Vymazal et al. 2006).

In the literature, the usability of CWTSs for treating a wide variety of wastewater is reported in detail. Ye et al. (2003) studied the possibility of using a CWTS for electricity utility wastewater. They found that wetland microcosms significantly reduced Se, As, B, as well as cyanide concentration in the wastewater. Generally, microcosm studies should be carried out in a pilot-scale level before testing in real field conditions because microcosms are cheap to construct and provide mass balance predictions for each contaminant (Ye et al., 2003). The CWTSs vegetated with cattail (*Typha latifolia L.*), and soft rush (*Juncus effusus L.*) were very effective at mitigating iron, and cadmium from metal-contaminated leachate from a coal ash pile at the Widows Creek electric utility, Alabama (Ye et al., 2001). Here, they concluded that wetland sediments were the primary sink for metal contaminants and effective in long-term remediation purposes. Machemer and Wildeman, (1992) showed that copper and zinc of acid mine drainage are completely removed by sulfide generation mediated by microbial reduction of sulfate in a CWTS. Previous studies have found that one of the dominant mechanisms of metal removal

from acid mine drainage is with sulfide precipitation (Faulwetter et al., 2009; Johnson and Hallberg, 2005; Mays and Edwards, 2001; Sheoran and Sheoran, 2006).

Schwindaman et al. (2014) designed and build a pilot-scale CWTS to remove As from simulated groundwater. They found that As retention in the oxidized zone which was amended with zero-valent iron (ZVI) was significantly greater than in the reduced zone. The addition of ZVI enhanced As retention in the oxidized zone by co-precipitation or sorption reactions. Also, the rate of As removal was enhanced by co-precipitation reactions with iron sulfide in the reduced zone. From this study, they suggested that a CWTS can be successfully used to treat As contaminated groundwater.

The respiration process coupled with electron acceptors, and the reactions associated with pollutants removal depend upon the oxidation-reduction (redox) conditions existing in wetland conditions (Faulwetter et al., 2009). Fluctuation in redox potential and pH in the wetland sediments influence transformations of metals between chemical forms, thereby affecting their mobility, and plant availability (Gambrell, 1994). Upon flooding, the pH of oxidized soils tend to be neutral (pH 7), regardless of soil being acidic or alkaline. The pH remains near neutral favors metals immobilization in wetlands (Gambrell, 1994; Ponnamperuma, 1972).

The main mechanisms of the metal removal in CWTSs occur through plant uptake, soil adsorption, and precipitation (Sheoran and Sheoran, 2006). Metal contaminants in wastewater adsorb to soil particles containing Fe, Al, and Mn oxy(hydr)oxides via forming ligand exchange or chemisorption reactions. The removal of P from agricultural nutrient water generally involves rapid adsorption, and precipitation reactions in the constructed wetlands (Vymazal, 2007; Vymazal, 2010). The reduction of selenate to selenite is an important mechanism of Se retention

in the CWTS because selenite is strongly adsorbed by soil mineral phases (Gao et al., 2003a; Gao et al., 2003b).

One of the most important pathways of removing some specific trace elements by a CWTS is the biological removal through wetland plant species (Sheoran and Sheoran, 2006). Rhizosphere bacterial activity can stimulate Se, and Hg phytoremediation by promoting their accumulation in the tissues of wetland plants such as bulrush (*Scirpus robustus* Pursh), and rabbitfoot grass (*Polypogon monspeliensis* (L.) Desf.) (De Souza et al., 1999). Lin and Terry (2003) found that rabbitfoot grass (*Polypogon monspeliensis* (L.) Desf), and its associated microbes enhance the Se(VI) reduction to organic Se forms which are readily volatilized.

Dissimilatory SO_4^{2-} reduction enhanced by sulfate reducing bacteria (SRB) in anoxic soils of CWTSs facilitates metals retention due to the formation of stable sulfide mineral phases (Sheoran and Sheoran, 2006; Wu et al., 2013). The retention of As in CWTSs can be enhanced by forming As sulfide compounds such as orpiment (As_2S_3), and arseno pyrite in the presence of S and Fe (Buddhawong et al., 2005; Lizama et al., 2011). It has been suggested that the FWS wetlands are more effective for Fe removal because of enhanced Fe precipitation under aerobic conditions (Kröpfelová et al., 2009). The retention of As, and manganese (Mn) under anoxic condition is poor because reduced As, and Mn compounds are soluble and may be washed out under anaerobic conditions. This is a common occurrence in natural wetlands (Kröpfelová et al., 2009).

Spacil et al. (2011) designed a CWTS to evaluate the removal of Se, As, and low-molecular weight organics (LMWO) from produced water from petroleum extraction. In this study they used simulated fresh produced water. The treatment goals of this study were to decrease Se concentration by microbial reduction, decrease As concentration by Fe co-

precipitation, and decrease LMWO concentration by biodegradation. Results indicated that rate, and removal efficiency of As was less than those of Se, and LMWO. They suggested that if aqueous Fe is in colloidal form, As will not co-precipitate. Therefore, a series of pilot-scale CWTS cells with oxidizing conditions, and treated with Fe should be designed in order to target the co-precipitation pathway to remove As. In addition, a series of reducing cells with organic carbon amendment is needed to promote microbially reducing pathways to remove Se.

Selenium is a challenging constituent in FGD wastewater. It is difficult to treat using conventional treatment strategies (EPRI, 2006). Therefore, CWTSs have been proposed as an environmentally, and economically effective solution to polish Se in FGD wastewater. However, limited studies have been published regarding the feasibility of CWTSs specifically designed for FGD wastewater. Pilot-scale CWTSs were designed at Clemson University, SC for the remediation of constituents of concern in FGD wastewater (Eggert et al., 2008). Results of this study indicated that CWTSs are efficient in decreasing the concentrations of Se, and Hg in the FGD wastewater.

In this study, they designed equalization basins as the initial component of the system to remove suspended solids, and to homogenize concentrations of constituents before introduction into the treatment system. Three different types of FGD wastewater were used to determine the performance of Se, Hg, and As. Those are formulated FGD water, four actual-amended FGD water, and pilot-scale scrubber FGD water. The formulated FGD wastewater was synthesized based on analyses results from actual FGD wastewater. In the formulation process, municipal wastewater was amended with high-purity salts of targeted constituents of concern (Se, Hg, and As), technical grade salts for chloride and sulfate, fly ash at 1000 mg/L, and dibasic acid at an equivalent COD concentration of 250 mg/L. Additional constituents such as nitrate, boron,

copper, zinc, chromium, and other elements or compounds were not amended for this formulated FGD wastewater. Because of low concentrations of Se, and Hg in the diluted actual FGD wastewater, those two trace elements were amended to achieve a total concentration of Se, and Hg approximately 2 mg/L, and 0.2 mg/L, respectively.

There were two treatment reactors reducing reactors, and oxidizing reactors, used for their study. The redox potential of the reducing reactors was -100 to -250 mV, and the pH was between 5 and 7 in hydrosoil. Plant species was bulrush, which helped to maintain reducing conditions. Double chip pine mulch (5%) was used as organic matter to promote microbial activities for dissimilatory SO_4^{2-} reduction. In the oxidizing reactors, redox potential was -50 to +200 mV, which was accomplished by selecting a porous hydrosoil with low organic carbon. Selected wetland plants had a high rate of radial oxygen loss. Because of the variation of the concentrations of constituents of three different FGD wastewaters, they suggested that the coal source can influence the chemical composition of FGD wastewater (Eggert et al., 2008). Based on the results from this study, they concluded that CWTSs can decrease the concentrations of targeted constituents (Se, and Hg) in FGD water complying with NPDES requirements. Selenium removal for formulated FGD, actual-amended FGD, and pilot-scrubber FGD wastewaters was 84.5%, 80.1%, and 29.5% to 89.7%, respectively. For the pilot-scale scrubber FGD waters, the efficiency of Se removal decreased with each scrubber FGD water. This could most likely due to the inhibition of removal mechanism by constituents in these FGD wasters because of decreasing binding sites or reactants, or the differences in Se forms (Eggert et al., 2008). The mean removal rates for As were 64.4% was for formulated FGD water, but no removal for actual-amended FGD water, and pilot-scale scrubbers. From these results, they concluded that CWTS can be a viable treatment strategy for FGD wastewater, but continuous

research is needed to understand the mechanisms of biogeochemical cycling of constituents of concern.

Based on the results gained from the pilot-scale CWTS designed at Clemson University, a full-scale CWTS for FGD wastewater was designed at power plants in North Carolina (Mooney and Murray-Gulde, 2008). In this study, they explained the importance of testing the treatment performance of the CWTS at a pilot-scale design first. The results of the pilot study provided the design criteria for each component (Mooney and Murray-Gulde, 2008). Also, these results are useful for engineers to perform preliminary design, and cost estimation of full-scale design (Mooney and Murray-Gulde, 2008). The full-scale CWTS was designed and constructed to remove Se and Hg from FGD wastewater. The overall hydraulic retention time of the CWTS system was 7 days. Results indicated that the average removal rate of Hg was 91%, and Se removal in the full-scale CWTS was variable (0-72%). Mooney and Murray-Gulde (2008) concluded that the performance of the full-scale CWTS achieved Hg and Se concentrations that are acceptable for NPDES discharge criteria. However, since the removal efficiency of Se was low and it had been variable in the CWTS, additional research was being conducted to improve Se removal. They suggested that some factors such as Se speciation and additives including polymers and dibasic acid may influence Se removal.

Sundberg et al. (2006) found that Hg, Se, and As from FGD wastewater was enriched in detritus collected from the pilot-scale CWTS. As a follow-up study of the pilot-scale CWTS, Sundberg-Jones and Hassan (2007b) employed an operationally-defined sequential extraction procedures to get information about mobility, bioavailability, biogeochemical processes of Se, Hg, and As in sediment and their potential impact on the aquatic system. Results indicated that Hg was mainly in its elemental fraction in the sediment. The Hg associated with sulfide was also

extracted in the residual fraction. In addition, the results from this study indicated that As was primarily in the residual fraction which may include As bound to silicate and mineral phases as well as organically-bound As. These results suggested that Hg and As were stable, immobile, and non-bioavailable, if the pH, and the redox potential of the sediment remained stable because the mobility and the bio-availability of these trace elements can alter with these soil conditions (Sundberg-Jones and Hassan, 2007b). The sequential extraction procedure for Se identified that about half of the total Se in the sediment was in mobile and bioavailable, while the rest of the total Se was stable and not bioavailable to plants and organisms (Sundberg-Jones and Hassan, 2007b). The plant species such as bulrush (*Schoenoplectus californicus*) and cattail (*Typha angustifolia*) in the pilot-scale CWTS were effective in bioconcentrating Hg, As, and Se from the FGD wastewater (Sundberg-Jones and Hassan, 2007a).

Selenium

Selenium in the environment

Selenium (Se) is a naturally occurring element which lies between metalloids, and non-metals in the periodic table (Fordyce, 2013). The atomic number of Se is 34, and its atomic weight is 78.96 with $[Ar]3d^{10}4s^{2}4p^{4}$ electron configuration. Selenium belongs to Group VIA of the periodic table, below S. Therefore, Se has similar chemical characteristics to S. Selenium is essential for humans, and other animals at trace levels. However, it becomes toxic at elevated concentrations. This element is difficult to control in the environment because of its narrow range between deficiency (<40 $\mu g day^{-1}$) and toxicity (>400 $\mu g day^{-1}$) (Fernández-Martínez and Charlet, 2009; Fordyce, 2013).

Fordyce (2007) reported that the Se content of most soils is very low (0.01 to 2 mg kg^{-1}). The mean concentration of world soils is 0.4 mg kg^{-1} while the high concentration of Se (1200

mg/kg) is reported in seleniferous areas (Fordyce, 2007). The normal background soil concentration of Se is 0.1-2 mg kg^{-1} (Lindsay, 1979). The typical range of Se concentration in water is 0.1 µg/L to100 µg/L. According to the USEPA drinking water standards, the maximum contaminant level (MCL) of Se is 50 µg/L. Kansas surface water quality standards for aquatic life is 20 µg Se/L (acute), and 5 µg Se/L (chronic) (Tate, 2005). For agricultural purposes, Se concentration of livestock is 50 µg/L, and that of irrigation water is 20 µg/L. Anthropogenic activities such as mining, fossil fuel combustion, oil refining, and agricultural irrigation affect Se released into the environment (CH2M Hill, 2010). The main release of Se into the environment as a consequence of human activities is from the combustion of coal. Wastewater generated from forced FGD systems predominantly contains elevated levels of Se (EPRI, 2006; CH2M Hill, 2010).

The mobility and the bioavailability of Se are determined by the physical and chemical factors such as pH, redox conditions, Se chemical speciation, soil texture, mineralogy, organic matter content, and the presence of competitive ions (Fernández-Martínez and Charlet, 2009; Fordyce, 2007). The chemistry of Se is complex because it has multi oxidation states. Those are selenate [Se(VI)], selenite [Se(VI)], elemental Se [Se(0)], and selenide [Se(-II)]. The fully oxidized form, Se(VI), exists as an oxyanion in solution as biselenate ($HSeO_4^-$) or selenate (SeO_4^{2-}) with a $pK_a = 1.8$ whereas selenite is a weak acid that can exist as H_2SeO_3, $HSeO_3^-$, or SeO_3^{2-} (depending on the solution pH) with $pK_{a1} = 2.70$ and $pK_{a2} = 8.54$ (Fernández-Martínez and Charlet, 2009). The pe-pH diagram of Se species is shown in Figure 2.5.

Redox potential is the measurement of oxidized or reduced conditions in soil. Oxidation is the loss of electrons whereas reduction is the gain of electrons. The oxidized component is the electron accepter or the oxidant, and the reduced component is the electron donor or the

reductant. The redox conditions in soil systems can be expressed using two parameters; pe, which is the negative log value of electron activity, and/or Eh, the voltage difference between the platinum and a hydrogen electrode in the standard state. Large positive values for pe and Eh indicate oxidized conditions, and negative values indicate reduced conditions. Upon flooding, the redox potential of soils decreases and remains near zero to negative values depending on the submergence time, organic matter content, and soil microbial activities (Sahrawat, 2005). Depending on the redox potential, soils can be categorized into well drained (+700 to +500 millivolts (mV)), moderately reduced (+400 to +200 mV), reduced (+100 mV to -100 mV), and highly reduced (-100 mV to -300 mV). At pH 7, the pe of highly oxidized, moderately reduced, reduced, and highly reduced soil ranged between +12 to +8, +7 to +3, and +2 to -2, and -2 to -5, respectively.

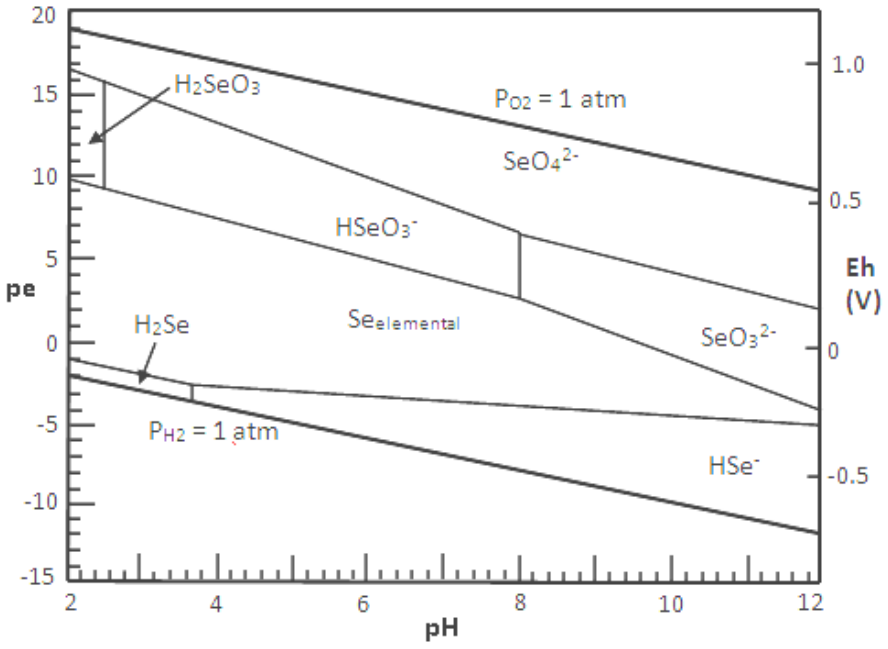

Figure 2.5 pe-pH diagram for selenium (Se) (redrawn from McNeal and Balistrieri 1989).

Under oxic conditions or at high redox potential and in alkaline soils (pe + pH > 15.0), Se(VI) is the dominant species. Selenate is soluble, and it has low adsorption and low precipitation capacities (Fernández-Martínez and Charlet, 2009; Fordyce, 2007; Nakamaru and Altansuvd, 2014). In the moderate redox potential range (pe + pH < 15.0 and >7.5), Se(IV) is the dominant species, and its mobility is primarily governed by sorption/desorption processes on various mineral surfaces of oxy(hydr)oxide minerals (Fernández-Martínez and Charlet, 2009; Nakamaru and Altansuvd, 2014). Inner-sphere or irreversible complexes formed by Se(IV) are strongly adsorbed by soil surfaces whereas Se(VI) is weakly adsorbed by non-specifically outer-sphere complexes (Peak, 2006a; Su and Suarez, 2000). Elemental Se, and Se(-II) tend to be available in strongly reduced conditions (pe + pH < 7.5) in a variety of Se(-II) precipitates and organic-rich environments, and these forms are unavailable to plants and animals (Fordyce, 2007; Nakamaru and Altansuvd, 2014). Selenao-amino acids (e.g., selenomethionine and selenocysteine), methyl selenide, and methyl selenones are organic Se forms that are often found in the environment (Masscheleyn and Patrick, 1993).

The oxidation-reduction reactions of Se, and its biogeochemical cycling are important to understand its transformation reactions in wetland soils/sediments. The transformation of Se(VI) to Se(IV) takes place at the Eh between +200 to +300 mV where nitrate reduction starts. When the Eh drops below +50 mV, Se(IV) is transformed to Se(0) where Fe reduction starts (Masscheleyn and Patrick, 1993). As soil Eh decreases further, Se(0) is reduced to Se(-II). Reduction of Se(IV) to Se(0) is catalyzed by green rust (Myneni et al., 1997). Under oxidized and moderately reduced conditions, methylated and dimethylselenide compounds are present. The solubility, toxicity, and fate and transport of Se in the wetland conditions are tremendously influenced by the alteration of its oxidation state (Masscheleyn and Patrick, 1993).

Selenium and health

The essentiality of Se as a trace element was identified in the late 1950s and early 1960s (Fordyce, 2007). Around 35 selenoproteins have been identified, and some of selenoproteins perform important enzymatic functions for human biology (Rayman, 2000). Selenium enters to the food chain via plant uptake from soils. The Se deficiency is commonly seen in regions where soils are low in Se concentration (Rayman, 2000). Soil chemical properties such as acidity, and complexation with Fe and Al reduces Se uptake by plants. Selenium has been identified as an essential component of enzyme glutathione peroxidase (GSH-Px), which helps protecting tissues against oxidative damage (Fordyce, 2007). The daily dietary need of Se for adults ranges between 50 to 200µg day^{-1} as recommended by the U.S. National Research Council (NRC), but this range depends on physiological status (Fordyce, 2013). The recommended daily allowances of dietary Se in women, men, and infants are approximately 55µg day^{-1}, 75µg day^{-1}, and 8.7–10µg day^{-1}, respectively (Fordyce, 2013). A deficiency of Se affects oxidative damage to red blood cells and reduces the activity of glutathione peroxidase enzyme (Watts, 1994). Due to the interaction of Se with Vitamin E and fatty acids, all Se deficiency diseases in animals might be associated with vitamin E deficiency. Selenium causes white muscle diseases of animals. Those diseases include reduced appetite, growth, production and reproductive fertility, unthriftyness, and muscle weakness (Fordyce, 2007). Selenium deficiency in animals is prevalent around the world and commonly found in South America, North America, Africa, Europe, Asia, Australia, and New Zealand (Fordyce, 2007).

The Se dietary intake of humans varies from region to region depending on the Se concentration of soil. The most common Se deficiency diseases reported in humans are keshan disease, an endemic cardiomyopathy (heart disease) that mainly affects children and women;

kashin-beck disease, an endemic osteoarthropathy causing deformity of the affected joints; iodine deficiency disorders, role of seleno-enzymes in thyroid function; and cancer (Fordyce, 2007). Selenium deficiency can link to other diseases such as immune function, viral infection, reproduction, depressed mood and more hostile behavior, thyroid function, cardiovascular disease, oxidative-stress or inflammatory conditions (Rayman, 2000).

Fordyce (2013) has reviewed the effect of Se toxicity in animals. Experiments carried out with laboratory animals have found that hydrogen selenide can cause lover tumors in rats. Selenium sulfide was proven to be carcinogenic for rats. Selenosis was reported in aquatic species and birds. For example, birds at the Kesterson Reservoir in California, US, were affected by high Se concentration (300 mg Se/L) of agricultural drainage water (Fordyce, 2007). Methylation of Se is a detoxification mechanism performed by animals. Mono-, di-, or trimethylated Se are formed by metabolizing organic and inorganic Se. Among these, monomethylated forms are more toxic. Selenium toxicity to humans is less common than Se deficiency. An endemic human selenosis was reported in seleniferous areas of China in 1960s (Yang et al., 1983). The reason for Se toxicity in this case was the consumption of high-Se crops grown on soils derived from coal. Selenium concentration of soil in these regions was reported up to 6000 mg kg^{-1}. The primary symptoms of selenosis are hair and nail loss (Fordyce, 2013). Disorders of the nervous system, skin, poor dental heath, garlic breath, and paralysis are also the symptoms of selenosis (Fordyce, 2013; Yang et al., 1983).

Selenium adsorption in soil

Since selenate and selenite are the two most common Se species found in soil solution, their adsorption behavior in soil has been extensively studied. Selenite, and reduced species are immobile compared to the selenate because of adsorption, co-precipitation or surface

precipitation reactions with soil mineral components, and complexation with organic matter (Fernández-Martínez and Charlet, 2009; Peak, 2006; Su and Suarez, 2000). Selenium oxyanions have a great tendency to bind with Fe and Al oxy(hydr)oxide minerals because of their surface chemical properties such as high point of zero charge, high surface area, and high density of surface functional groups for ligand exchange reactions (Peak, 2006). Selenate adsorbs onto solid surfaces as non-specifically adsorbing ions by forming outer-sphere complexation (Peak et al., 2006; Peak, 2006), whereas selenite is absorbed by specifically formed inner-sphere complexation (Peak et al., 2006; Su and Suarez, 2000). In inner-sphere complexation, soluble metal(loids) ion species and a free ligand (or a surface functional group) are directly linked without any water molecule involvement whereas soluble species and a ligand are attached outside the hydration sphere to form outer-sphere complexes (Essington, 2004; Jordan et al., 2013). The ligand replaces a water molecule from hydration sphere when inner-sphere complexes are formed, but the ligand does not displace water when forming outer-sphere complexes.

Spectroscopic techniques are extensively being used to determine surface complexation of Se with oxy(hydr)oxy mineral surfaces. Peak (2006) determined the bonding mechanisms of selenate, and selenite on hydrous aluminum oxide (HAO) over a wide range of reaction pH using extended X-ray absorption fine structure (EXAFS) spectroscopy. It was found that selenate solely forms outer-sphere complexes co-occurring with a very small amount of inner-sphere complexes. Selenite is adsorbed to HAO by forming inner-sphere bidentate-binuclear (corner-sharing) surface complexes, and some outer-sphere complexes. Peak et al. (2006) also investigated the bonding mechanisms of selenite on Al hydroxide, and aluminosilicate-coated

minerals which represent the minerals in natural environment. In this study, they used EXAFS, and X-ray absorption near-edge structure (XANES) spectroscopy techniques.

Selenate adsorption to maghemite (γ-Fe_2O_3) was studied by Jordan et al. (2013) for the first time both on the macroscopic and the molecular level. At the molecular level, Attenuated total reflection Fourier-transform infrared (ATR FT-IR) and EXAFS spectroscopy techniques were used to reveal the structure of the sorbed surface species. The ATR FT-IR analysis found that selenate is sorbed onto maghemite as bidentate outer-sphere surface complexes over the pH range of 3.5–8.0 via electrostatic interaction. However, the EXAFS results revealed that selenate forms a small portion of inner-sphere complexes together with outer-sphere surface complexes, especially at acidic pH. Jordan et al. (2014) investigated the mechanism of selenite adsorption as well to maghemite (γ-Fe_2O_3) on both the macroscopic and the molecular level. In this study, they used EXAFS techniques at the molecular level. The EXAF results revealed that selenite is adsorbed to maghemite via bidentate-binuclear corner-sharing and bidentate mononuclear edge-sharing inner-sphere complexes. The shift of isoelectric point and zeta potential towards lower values upon anion adsorption is an indication of inner-sphere coordination or surface precipitation (Jordan et al., 2014).

Inner-sphere selenite adsorption to hematite was determined by Catalano et al. (2006). The adsorption of selenate and selenite was predicted by a triple-layer model. The selenate adsorption occurs via electrostatic attraction to form outer-sphere complexes with goethite while selenite is adsorbed on the goethite surface by forming monovalent and bivalent selenite-Fe complexes (Zhang and Sparks, 1990). In this study, they used a pressure jump chemical relaxation technique to identify the kinetics of selenite adsorption to the goethite. The adsorption of selenite to the goethite was a two-step reaction. The fast step attributes the formation of an

outer-sphere surface complex, and the slower step represents an inner-sphere surface complex (Zhang and Sparks, 1990).

Foster et al. (2003) studied the selenite sorption complexes on synthesized hydrous manganese oxides using X-ray absorption fine structure (XAFS) spectroscopic analysis. The results depicted that selenite ion can form a mixture of inner-sphere complexes of bidentate (mononuclear) edge-sharing complexes and monodentate corner-sharing complexes with the hydrous manganese oxides. The ATR FT-IR spectroscopy and EXAFS techniques revealed that selenate forms only inner-sphere surface complexes on hematite (Peak and Sparks, 2002). In this study, it was learned also that selenate forms outer-sphere complexes on goethite and amorphous Fe hydroxide at pH 6 and above, but it forms a mixture of outer- and inner-sphere surface complexes at pH between 3.5 and 6.0 (Peak and Sparks, 2002).

The capacity of Se adsorption in soils depends on environmental factors such as pH, redox potential, and competitive ions (Goh and Lim, 2004). Goldberg (2013) studied the adsorption behavior of selenite on Al, Fe oxides and clay minerals, such as illite. The adsorption of selenite to Al, and Fe oxides decreased rapidly with increasing solution pH beyond 8. The low pH favored maximum adsorption of seleneite. In general, the adsorption of selenite decreases with increasing solution pH (Goldberg and Glaubig, 1988; Goldberg et al., 2007). Previous studies have found that the adsorption of selenite to soils was more favorable over a wide range of pH compared to the adsorption of selenate (Goh and Lim, 2004; Martinez et al., 2006). The sorption of selenite to hematite was favorable over the pH ranges from acidic to pH 9 (Duc et al., 2006) while that of selenate was from 3.5 to 6 (Peak and Sparks, 2002).

The adsorption mechanism of Se (selenate or selenite) is strongly controlled by the ionic strength of the solution (Zhang and Sparks, 1990). As described by previous studies, Su and

Suarez (2000) found that the adsorption of selenite onto amorphous Fe hydroxide was not influenced by increasing ionic strength, but the adsorption strength of selenate significantly decreased as the ionic strength increased. Since the outer-sphere complexation is weaker than inner-sphere complexation it is influenced by the ionic strength changes (Su and Suarez, 2000). The occurrence of outer-sphere surface complexation can be identified by the changes of adsorption envelop with pH and ionic strength (Duc et al., 2006; Peak, 2006). Several studies have reported that the ionic strength did not influence the sorption of selenite, but the sorption of selenate to maghemite, magnetite, hematite, goethite, amorphous Fe oxy(hydr)oxides, and γ-Al_2O_3 was affected by changing the ionic strength of the solution. This confirmed that selenite was more likely to form inner-sphere surface complexes with different soil minerals (Duc et al., 2006; Elzinga et al., 2009; Jordan et al., 2013; Jordan et al., 2014; Martinez et al., 2006; Su and Suarez, 2000).

The mobility and the bioavailability of Se is greatly affected by competitive anions such as SO_4^{2-}, PO_4^{3-}, CO_3^{2-}, and Cl^-, which tend to compete for sorption sites (Goh and Lim, 2004). Dhillon and Dhillon (2000) found that greater amount of sorbed selenite at acidic pH was desorbed by PO_4^{3-} through ligand-exchange reactions. Japanese soil under high phosphate concentration inhibited the selenite sorption capacity (Nakamaru and Sekine, 2008; Nakamaru and Altansuvd, 2014). Goh and Lim (2004) attempted to compare the effect of competitive anions such as SO_4^{2-}, and PO_4^{3-} on a tropical soil found in Singapore. The results indicated that PO_4^{3-} had a strong effect than SO_4^{2-} on the adsorption of selenite. It was also revealed in this study that SO_4^{2-} can compete for selenate sorption sites, but not for the selenite sorption sites because of strong inner-sphere binding mechanism of selenite Goh and Lim (2004).

Selenium precipitation

Equilibrium thermodynamic reactions have been used to identify Se solubility and mineral precipitation in soils and sediments (Elrashidi et al., 1987; Seby et al., 2001). At a neutral pH, $BaSeO_4^0$ is the most stable selenate mineral in soil, and selenate minerals are too soluble to persist in aerobic soil (Elrashidi et al., 1987). In near neutral and acid soils, $MnSeO_3$ is the most stable selenite mineral whereas $PbSeO_3$ is the most stable mineral in alkaline soil (Elrashidi et al., 1987). The solubility of $PbSeO_3$ tends to increase below and above pH 7.8. Based on thermodynamics, $Fe_2(SeO_3)_3$ or $Fe_2(OH)_4SeO_3$ are not expected to be formed in acidic soils (Elrashidi et al., 1987). Under highly reducing soil, solubilities of selenide minerals are extremely low, and Cu_2Se was predicted to be the least soluble mineral in acidic soil (Elrashidi et al., 1987). In both neutral and alkaline soils, PbSe, and Sn selenide minerals are most stable. According to thermodynamic prediction, elemental Se is not as stable as selenides. Hence, it is not expected to be stable in soil (Elrashidi et al., 1987). However, Masscheleyn et al. (1991b) indicated that under reduced conditions elemental Se is stable over a wide range of pH. The recipitation of metal selenides under anaerobic conditions is a sink for Se in solution (Masscheleyn et al., 1991b). Under reducing conditions, Se solubility is governed by precipitation reactions of metal selenides such as FeSe and $FeSe_2$, and elemental Se (Seby et al., 2001).

Selenium in wetlands

Constructed wetland treatments systems (CWTSs) are an alternative treatment technology for Se removal from contaminated water. During the microbial assimilation process oxidized Se species are transformed to volatile organically bound selenide components such as dimethyl selenide (DMSe) and dimethyl diselenide (DMDSe) (Masscheleyn and Patrick, 1993).

Volatilization from CWTS is one of the main mechanisms for Se removal from contaminated water such as Se-laden effluents from oil refineries, and agricultural drainage water (Hansen et al., 1998; Lin and Terry, 2003). The microbial processes responsible for Se volatilization are influenced by the Se concentration in water, sediment, and plants; flooding-drying of ponds, temperature, air flow, decomposition of plants, and organic materials in wetlands (Zhang and Moore, 1997). Pilon-Smits et al. (1999) studied twenty aquatic plants to investigate Se removal efficiency from selenate- or selenite-treated water. The results showed two aquatic species, salt marsh bulrush and mare's tail, had high rate of Se volatilization. The selenite-treated water enhanced the rate of volatilization because it can be rapidly transformed into organic Se forms.

In addition to Se volatilization, chemical reduction and immobilization in the sediment is one of the fates of soluble Se entering into wetlands. Previous studies have found that wetland sediment is an effective sink for removing selenate from aqueous phases (Tokunaga et al., 1996; Tokunaga et al., 1997; Zhang and Moore, 1996). Organic carbon is an important factor which affects the selenate reduction in wetland sediment (Zhang and Moore, 1997). The formation of Se(0) and metal selenide species such as FeSe at low redox potential or wetland conditions governs the Se solubility (Masscheleyn and Patrick, 1993). The complex biogeochemical mechanisms in CWTSs influence the efficiency of Se removal from contaminated wastewater streams. Eggert et al. (2008) suggested that the mechanism of Se removal from FGD wastewater was rapid complexation of selenite with Fe oxy(hydr)oxides or direct adsorption of selenate to Fe oxy(hydr)oxides. Upon flooding, sequential reduction of Se(VI) to Se(IV) and Se(0) is fast (as early as 3.8 days) and suppresses Se mobility (Tokunaga et al., 1997).

Aquatic plants which dominate the major portion of organic matter in wetlands may play an important role in taking up Se from contaminated water (Frankenberger and Engberg, 1998).

The oxidized forms of Se [Se(VI), and Se(IV)] are more readily available for plants because of their solubility. In contrast, reduced forms [Se(0), and Se(-II)] are unavailable for plants because they are relatively insoluble. Cattail, parrot's feather, and iris leaved rush are the most effective species that can accumulate Se(VI) in shoot tissues. They are a logical selection for cleaning selenate-contaminated water in CWTSs (Pilon-Smits et al., 1999). Aquatic plant species response to Se(VI) and Se(IV) in a different way. Selenate is translocated readily to shoot while selenite mostly accumulates in the root. Thus, Pilon-Smits et al. (1999) concluded that phytoextraction of selenate-contaminated water from wetland species is five times greater than selenite-contaminated water. Factors such as salinity, pH, temperature, levels of other pollutants, and competitive strength affect the performance of the wetland plant species (Pilon-Smits et al., 1999). It is important to mention that Se accumulation in plant tissues (shoot and root) is a threat to wildlife. Thus, their disposal in an appropriate way is important (Pilon-Smits et al., 1999).

Arsenic

Arsenic in the environment

Arsenic (As) is a naturally occurring element listed as a metalloid in the periodic table (Smith et al., 1998). The atomic number of As is 33, and its atomic weigh is 74.92 with $[Ar]3d^{10}4s^{2}4p^{3}$ electron configuration. Arsenic belongs to Group VA of the periodic table. It is ranked as the twentieth most abundant element in the earth's crust (Bissen and Frimmel, 2003). In aerated soils, the behavior of As is similar to that of phosphorous (P) (Smith et al., 1998). The main source of As in soils is derived from the parent materials. The average As concentration in world soil is 7.2 mg/kg (McCarty et al., 2011), and the average As concentration of US surface soil is 6.6 mg/kg (Smith et al., 2013). Acid sulfate soils developed from pyritic parent materials usually show high As concentration ranging between 8 to 40 mg/kg (Smith et al., 1998). In the

environment, As is primarily associated with sulfide minerals such as orpiment (As_2S_3), realgar (AsS), mispickel (FeAsS), loellingite ($FeAs_2$), niccolite (NiAs), cobaltite (CoAsS), tennantite ($Cu_{12}As_4S_{13}$), and enargite (Cu_3AsS_4) (Bissen and Frimmel, 2003). Coal may have the As concentration up to 1500 mg/kg with an average of 12 mg/kg (Bissen and Frimmel, 2003).

In fresh water, the concentration of As ranges between 0.15 µg/L and 0.45 µg/L. The As concentration in river waters is reported to be as low as 0.1 to 0.8 µg/L. The As concentrations in river waters in south-eastern USA is recorded in the range 0.15 to 0.45 µg/L (Smedley and Kinniburgh, 2002). The measured As concentration in contaminated water from Ganges alluvial deposits in Bangladesh and West Bengal reached up to 1000 µg/L (Nickson et al., 1998). The maximum contaminant level in drinking water established for As by the World Health Organization is 10 µg/L (Goh and Lim, 2004). In 2001, USEPA lowered the As permissible level in drinking water from 50 µg/L to 10 µg/L. Arsenic contamination in the environment often results from anthropogenic activities such as industries, mining and/or smelting processes, burning of fossil fuels, tannery waste, arsenical fungicides, herbicides, fertilizers, and insecticides in agriculture, and wood industry (Bissen and Frimmel, 2003; Smith et al., 1998).

In nature, As mainly exists in four oxidation states; arsenate [As(V)], arsenite [As(III)], elemental As [As(0)], and arsine [As(-III)]. The major As species in solution is As(V) as arsenate and As(III) as arsenite, and they primarily exist as oxyanionic acids (Bhattacharya et al., 2007; Smedley and Kinniburgh, 2002). Additionally, inorganic As species are methylated by plants and microbial (bacteria, yeasts, algae) activities forming monomethylarsonic acid (MMA), dimethylarsinic acid (DMA), and gaseous forms of arsine (Bentley and Chasteen, 2002; Bissen and Frimmel, 2003; Smith et al., 1998). The speciation and the biogeochemical behavior of As is controlled by altering pH, and redox potential along with adsorption/desorption, and

precipitation reactions (Cherry et al., 1979; Sadiq, 1997; Smedley and Kinniburgh, 2002). The Eh-pH diagram for aqueous As species is shown in Figure 2.6. Arsenic (III) is the most abundant species in an anoxic (pe+pH<6) condition whereas in an oxic environment (pe+pH>10), As(V) is more dominant. Both As(III) and As(V) can be found in suboxic soil solution where pe+pH ranges between 6 and 8 (Sadiq, 1997). At near neutral pH, $H_2AsO_4^-$, $HAsO_4^{2-}$, and $H_3AsO_3^o$ species become predominant (Sadiq, 1997; Smedley and Kinniburgh, 2002).

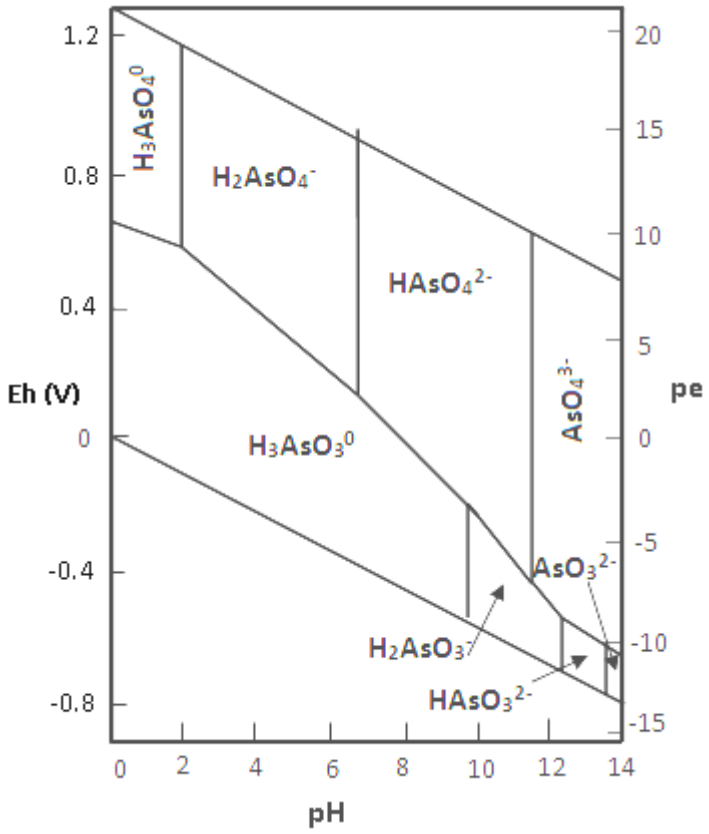

Figure 2.6 Eh-pH diagram for aqueous As species in the system As–O_2–H_2O at 25 ^{0}C and 1bar total pressure (redrawn from Smedley and Kinniburgh 2002).

Masscheleyn et al. (1991b) studied the effect of soil redox potential and pH on the speciation and solubility of As in a contaminated soil. At redox potential between +200 and +500 mV, As(V) was the main species that contributed to total soluble As concentration. In contrast, As(III) was the dominant soluble As species upon reduction (0 to -200 mV). Under oxidizing

conditions, they observed enhanced soluble As concentration at alkaline pH (pH 8) compared to acidic pH. As pH increases, desorption of arsenate also increases because sorption sites become negatively charged. The transformation of As(V) to As(III) is a slow process. Therefore, thermodynamically unstable As(V) species can also be observed under reduced conditions (Masscheleyn et al., 1991a).

Arsenic and health

Arsenic is thought to be one of the most toxic elements to humans, animals, and plants. The toxicity of As depends on its speciation. Usually, arsenite [As(III)] is more toxic than arsenate [As(V)] (Hughes, 2002; Ratnaike, 2003; Jomova et al., 2011). Inorganic As forms are more toxic than organic forms to living organisms, including humans, and other animals (Sharma and Sohn, 2009). Arsenic(III) compounds are known to be re-adsorbed faster by biological systems. These compound have high affinity to sulfhydryl groups in proteins, and cause deactivation of enzymes which are involved in cellular energy pathways, and DNA replication and repair (Bissen and Frimmel, 2003; Ratnaike, 2003). Arsenic(V) is substituted for phosphate in high energy compounds such as adenosine triphosphate (ATP) and uncouples oxidative phosphorylation (Bissen and Frimmel, 2003; Ratnaike, 2003). Arsenic(III) tends to bind thiol or sulfhydryl groups in tissue proteins of the liver, lungs, kidney, spleen, gastrointestinal mucosa, and keratin-rich tissues such as skin, hair, and nails (Ratnaike, 2003). Arsenic exposure pathways are inhalation, absorption through the skin, and mainly ingestion of contaminated drinking water. The organic and inorganic As compounds may enter the plant food chain via agricultural products or from soil irrigated with water contaminated by As (Ratnaike, 2003).

Bangladesh and West Bengal, India have been reported as the two worst As affected areas in the world (WHO, 1999). Acute effects of As poisoning include vomiting, abdominal

pain, and diarrhoea (Ratnaike, 2003; WHO, 1999). The long-term exposure effects (chronic) to high As levels of inorganic As in drinking water are changes in skin pigmentation, skin lesions, hard patches on the palms, and soles of the feet. In addition, cardiovascular disease, neurological effects, changes in behavior, confusion, and memory loss, bladder, kidney, ureter and all urethral cancers, and lung disease have been reported as chronic effects of As exposure (Ratnaike, 2003; WHO, 1999).

The human body has the capability of detoxifying the inorganic As compounds As(III) and As(V) by methylation, to a certain amount. However, the possibility of As methylation is limited when As uptake exceeds 400 to 500 μg/d (Bissen and Frimmel, 2003). Certain organisms (fungi and bacteria) have the capability of methylating inorganic As species by first converting As(V) to As(III), then converting methylate to form less toxic species, such as MMA, DMA or trimethylarsine (TMA) (Bissen and Frimmel, 2003; Bissen and Frimmel, 2003).

Arsenic adsorption in soils

Adsorption/desorption reactions can significantly influence the As mobility in the environment. The partitioning of As between the solution, and the solid phase is determined by its oxidation state. In general, As(V) is more prone to bind strongly and irreversibly to soil/sediment mineral constituents than As(III). Consequently, As(V) is potentially less mobile, and less bioavailable (Dixit and Hering, 2003; Goldberg and Johnston, 2001). Sorption efficiency of As in the soil solution depends upon pH, redox conditions, clay percentage or composition of soil minerals, and the presence or absence of competing ions (Dixit and Hering, 2003; Manning and Goldberg, 1996a; Manning and Goldberg, 1996b; Sadiq, 1997). The effectiveness of adsorption of arsenite and arsenate on minerals and clay surfaces strongly correlated with pH (Goldberg, 2002; Raven et al., 1998). Manning and Goldberg (1996b)

investigated the adsorption of arsenate on kaolinite, illite, and montmorillonite as a function of pH and in the presence of competing anions (such as phosphate and molybdate). The maximum adsorption of arsenate occurred at pH 6.0 on montmorillonite, pH 6.5 on illite, and approximately at pH 5.0 for kaolinite. The results of this study also indicated that as the pH increases (pH >6.5), the adsorption of arsenate to the clay minerals decreased. In addition, the adsorption of arsenate on clay minerals significantly decreased in the presence of phosphate, but it was not greatly decreased by molybdate when the pH was greater than 6. Goldberg (2002) investigated the effect of pH on As adsorption to clay minerals and amorphous Al, and Fe oxides. The results indicated that arsenate adsorption to oxides, and clay minerals reached a maximum at low pH and decreased with increasing pH. This study found that the adsorption of arsenite reached a maximum around at pH 8.5 for all clay minerals and amorphous oxides. Arsenate adsorption on Fe, Al oxy(hydr)oxides, and aluminosilicates is maximum at pH below 8.0 whereas high pH is favorable for As(III) adsorption (Sadiq, 1997). In general, Fe oxy(hydr)oxides are involved in the adsorption of As in both acidic and alkaline soils whereas the surface of Al oxy(hydr)oxides and clay minerals are important in As adsorption only in acidic soils (Sadiq, 1997). Raven et al. (1998) studied the kinetics and equilibria of the adsorption of arsenite and arsenate on ferrihydrite, at pH 4.6 and pH 9.2. It was concluded from the study that both arsenite and arsenate showed greater affinity for ferrihydrite. In addition, a high pH or high As solution concentration favored the retention of larger amount of arsenite than arsenate.

For surface complexation, arsenite forms both inner- and outer-sphere complexes on amorphous Fe oxide and outer-sphere surface complexes on amorphous Al oxide. Arsenate adsorbs solely via strong inner-sphere complexation on both amorphous Fe and Al oxides

(Goldberg and Johnston, 2001; Jain et al., 1999; Randall et al., 2001). However, X-ray scattering study has revealed that arsenate could also form inner- and outer-sphere complexes simultaneously with Fe and Al oxides (Catalano et al., 2008). The surface complexation of arsenate sorbed on goethite has been deduced from EXAFS spectroscopy. It was a bidentate-binuclear interaction (Fendorf et al., 1997). Manning et al. (2002) used a conventional stirred reaction apparatus and extended EXAFS technique to study the reactions of arsenite and arsenate with synthetic birnessite (MnO_2). The results showed that arsenite was oxidized to arsenate by MnO_2. As revealed by the EXAFS analysis, then arsenate can be adsorbed onto MnO_2 solid phase through a bidentate-binuclear corner sharing (bridged) complex. Non-specifically or outer-sphere surface bound As might be more susceptible for desorption from Fe (hydr)oxides under anoxic soil conditions (Kocar et al., 2006; Manning and Goldberg, 1997).

Adsorption of As via chemisorptions or ligand exchange reactions depend on competitive anions, such as phosphate, sulfate, silicate, and organic anions in the soil solution (Dixit and Hering, 2003; Guan et al., 2009; Jain and Loeppert, 2000; Manning and Goldberg, 1996; Mohan and Pittman, 2007). Additionally, Manning and Goldberg (1996) investigated the effects of pH and competing anions such as phosphate, and molybdate on the adsorption of arsenate on goethite and gibbsite. The adsorption of arsenate on both goethite and gibbsite was decreased with an equal concentration of phosphate at a pH range of 2 to 11 whereas molybdate influenced in decreasing the arsenate adsorption only below pH 6 (Manning and Goldberg, 1996). The affinity of As for inner- and outer-sphere complexation on Fe/Al amorphous oxides depends on ionic strength of the solution (Arai et al., 2001; Goldberg and Johnston, 2001; Manning and Goldberg, 1997; Renkou et al., 2009). Antelo et al. (2005) found that the salt effect of As(V)

adsorption on goethite was negligible. This is an indication of specifically bound or inner-sphere complexation between As(V) and the goethite.

Organic matter can have a profound impact on As mobility in the environment because the presence of organic matter can form insoluble and soluble complexes with As. Organic matter may have a greater potential for As sorption due to formation of organo-As complex (Pikaray et al., 2005). Ko et al. (2004) studied the kinetics of adsorption and desorption of As onto humic-coated hematite or arsenic-presorbed hematite. They found that humic acids form complexes with arsenite and arsenate in the presence of bridging metals such as Al^{3+}, and Fe^{3+}. Also, the humic acid favored oxidation of arsenite to arsenate, thereby controlling its mobility. On the contrary, dissolved organic matter can enhance As mobility in soil due to competition between As and organic molecules for sorption sites on soil minerals (Bauer and Blodau, 2006; Bauer and Blodau, 2009; Ko et al., 2004). Some humic acids (amine groups) carrying the positive charge at pH 7 may form humic-clay complexes that have the capacity to retain As role in adsorbing As(V) to organic matter (Saada et al., 2003).

Arsenic precipitation

Precipitation as a solid phase is another mechanism that governs removal of As from solution phase (Sadiq, 1997). For soils under oxic and suboxic conditions, As solubility is controlled by $Fe_3(AsO_4)_2$. In contrast, in anoxic soils, sulfides of As(III) minerals control the As solution concentration (Sadiq, 1997). As the system gets more reduced, As(III) forms comparatively stable As-sulfur mineral phases with sulfides which are formed by microbially mediated sulfate reduction (Moore et al., 1988; Sadiq, 1997; Smedley and Kinniburgh, 2002). The mobility of As in natural systems is often coupled with the biogeochemical cycling of Fe, and S most likely due to the precipitation/co-precipitation reactions with poorly crystalline Fe

oxy(hydr)oxides, Fe monosulfides (FeS), and pyrite (FeS_2) (Moore et al., 1988; Schwindaman et al., 2014; Smedley and Kinniburgh, 2002). The rate of As removal by precipitation reactions is controlled by the ratio of reactive Fe to S in the system (O'Day et al., 2004). The stability of co-precipitated or adsorbed As to sulfides minerals is intermediate for As(V) and As(III) because they prone to be solubilized upon oxidation of soils/sediments (Moore et al., 1988; Smedley and Kinniburgh, 2002). Both As(V) and As(III) can precipitate with soil constituents under certain conditions. The affinity of As(III) for sulfide minerals and the formation of FeAsS-like phases in slightly acidic solutions and As_2S_3 in highly sulfidic zones can control the As solution concentration (Bostick and Fendorf, 2003). The X-ray absorption spectroscopy analysis has revealed the surface precipitation of As with FeS and FeS_2 (Bostick and Fendorf, 2003). The precipitation of Fe(III)-arsenate at neutral to mildly acidic conditions has significantly decreased the As concentration in mining contaminated water (Wang and Mulligan, 2006). A recent study carried out by Fan et al. (2014) revealed that formation of Fe(II)/Fe(III)-arsenate precipitates enhanced the adsorption capacity of arsenate at anoxic soil conditions.

Reductive dissolution of arsenic

The fate and transport of As in the environment and its toxicity are substantially controlled by the biogeochemical transformations of As associated phases (Kocar et al., 2008; Polizzotto et al., 2005). Iron oxides play a major role in attenuating the concentration of As in solution via adsorption and co-precipitation (Smedley and Kinniburgh, 2002). Iron mineral phases such as ferrihydrite, lepidocrocite, goethite and hematite have strong sorbent strength for the immobilization of As in natural waters because of their greater abundance and binding affinities for As (Manning et al., 1998; Raven et al., 1998). However, microbially-driven reductive dissolution of Fe oxy(hydr)oxides can result in a significant release of As to solution

(Horneman et al., 2004; Nickson et al., 2000). In reduced conditions, As-rich oxy(hydr)oxy minerals undergo reductive dissolution and release As(III) and As(V) to solution (Nickson et al., 1998; Nickson et al., 2000). Previous studies have revealed that reductive dissolution of Fe minerals and concomitant release of As processes are stimulated by Fe reducing bacteria in the presence of organic matter as a substrate (Bauer and Blodau, 2006; Borch et al., 2009; Mladenov et al., 2009).

Takahashi et al. (2004) investigated the As behavior in paddy fields during the cycle of flooded and non-flooded periods. They found that As in irrigation waters was bound to Fe oxy(hydr)oxide in the soil during non-flooded periods. Upon flooding, the As was easily released from the soil to water because of the reductive dissolution of the Fe phase. Yamaguchi et al. (2011) studied the factors that control the partitioning of As among soil-to-solution under anaerobic conditions. The results indicated that the partitioning of As between the soil-to-solution is strongly controlled by the redox potential, pH, organic carbon, and dissolved amounts of Fe-bearing phases in soils.

Congruent dissolution and the strong correlation between Fe and As have indicated that As is released to solution by the reductive dissolution of Fe minerals (Kneebone et al., 2002; Masscheleyn et al., 1991b). Previous studies have found that unstable Fe minerals phases are transformed to secondary minerals during their reductive dissolution. The subsequent incorporation of As on newly formed Fe phases can significantly influence As sequestration rather than dissolution (Kocar et al., 2006; Pedersen et al., 2006; Tufano and Fendorf, 2008). Zachara et al. (2002) reported that dissimilatory metal-reducing bacteria can transform ferrihydrite to crystalline ferric (goethite, hematite, lepidocrocite), ferrous (siderite, vivianite), and mixed valence (magnetite, green rust) solids in anoxic conditions. The primary factor of

controlling the formation of secondary Fe phases is Fe(II) flux (Zachara et al., 2002). Benner et al. (2002) found that the reductive dissolution of ferrihydrite, and the secondary precipitation of goethite and magnetite was predominantly controlled by Fe(II) concentration and its supply rate.

Biogeochemical cycling of sulfur, and iron

Biogeochemical cycles are by which essential elements move through both biotic (the biosphere), and abiotic compartments (the atmosphere, hydrosphere, and lithosphere) on earth. The transfer of element involves biological, geological, and chemical processes. Hence, the name biogeochemical cycles is used for the overall process. The biogeochemical cycles link all organisms and abiotic features on earth, and these cycles differ in their pathways. The most ecologically important and well known element cycles are carbon, nitrogen, oxygen, phosphorus, sulfur, water, and iron.

Sulfur cycling

Sulfur is the tenth most abundant element in the universe. It is brittle, yellow, tasteless, and odorless. It is a non-metallic element. The atomic number of S is 16, and its atomic weight is 32.07. The electron configuration of is $1s^2 2s^2 2p^6 3s^2 3p^4$. This element is located in the VIA of the periodic table. Sulfur is an essential macronutrient for plants and animals. There are five main oxidation states of S, including -2, -1, 0, +4, and +6. Within oxic soils and surface waters, most inorganic S occurs as sulfate. Elemental S and sulfides (reduced S) are uncommon in well-drained soils because they are oxidized rapidly to sulfate. Organic S in soil occurs in two primary forms: ester sulfates that have C-O-SO_3 linkages; and carbon-bonded S that mainly consists with C-S linkages. The main transformations involved in the S cycle are immobilization, mobilization, and mineralization of S compounds (Edwards, 1998).

The immobilization or assimilation of S into microbial cells is completely dependent upon the metabolism of microorganisms. During the immobilization process, inorganic forms of S such as sulfate (SO_4^{2-}), sulfite (SO_3^{2-}), sulfide (S^{2-}), thiosulfate ($S_2O_3^{2-}$), and trithionite compounds convert to organic S. The mobilization is the process by which large organic S molecules are microbially reduced to smaller S molecules. In contrast to the immobilization, the mobilization increases the mobility of organic S compounds. There are two possible mechanisms offered for rapid mobilization. Those are direct oxidation of C-S linkages, and conversion of C-S linkages to ester sulfate linkages. The mineralization of S is the microbially-driven decomposition of organic S compounds. This process depends on the S supply, and microbial demand. During the oxidation, mineralized S is transformed to SO_4^{2-} and inorganic S species are converted to SO_4^{2-}. Under reducing environments, SO_4^{2-} is reduced to S^{2-} by microorganisms. Dissimilatory SO_4^{2-} reduction is more favorable under anaerobic and alkaline conditions by *Desulfovibrio, Desulfotomaculum, and Desulfomas* microorganisms. The rate of SO_4^{2-} reduction is determined by the reactivity of organic matter (Stein et al., 2007; Sturman et al., 2008).

Iron cycling

Iron is the most abundant element on earth. The atomic number of Fe is 26, and its atomic weight is 55.84. It is a transition element that belongs to Group VIIIA and block d of the periodic table. Iron is a silvery-white or grayish metal having ductile, and malleable physical properties. Its compounds can exist in the oxidation states of -2, 0, +2, +3, +4. However, the bivalent Fe(II) (Fe^{2+}) or ferrous, and the trivalent Fe(III) (Fe^{3+}) or ferric are the two main species abundant in soils. The divalent state of Fe is associated with phyllosilicates, and pyrite (FeS_2) minerals. Upon aerobic weathering, they are readily oxidized into trivalent ion, forming sparingly soluble Fe-oxide minerals at neutral to alkaline soil pH environment (Schwertmann,

2008). Amorphous-Fe [$Fe(OH)_3$], maghemite (γ-Fe_2O_3), lepidocrocite (γ-FeOOH), hematite (α-Fe_2O_3), goethite (α-FeOOH), molysite ($FeCl_3$), jarosite ($KFe_3(SO_4)_2(OH)_6$), and ferrihydrite ($Fe_{10}O_{14}(OH)_2$) are Fe(III) minerals while FeO, lawrencite ($FeCl_2$), siderite ($FeCO_3$), fayalite (Fe_2SiO_4), $FeSO_4$ are Fe(II) minerals. Magnetite (Fe_3O_4), and ferrosic oxide ($Fe_3(OH)_6$) are consisted of both Fe(II) and Fe(III) forms (Lindsay, 1979). Because of their unique characteristics including mineral-specific color, large specific surface area (50-300 m^2/g), substantially high adsorption capacity, very low solubility, isomorphous substitution of Al, and poor crystallinity, Fe minerals play an important role in the soil environment.

Soil pH has the greatest effect on the mobility, and the bioavailability of Fe. Under acidic pH conditions Fe(III) is soluble, whereas under neutral pH conditions Fe(III) is precipitated as hydroxides. The solubility of Fe(III) oxy(hydr)oxside minerals depends on their specific surface area, crystallinity, and impurity content (Bonneville et al., 2004). The redox potential determines the valence change of Fe. The reduction of Fe(III) to Fe(II) takes place at a redox potential between 0 to +200 mV at neutral pH. For soils with oxic conditions, Fe(III) species are dominant whereas highly soluble Fe(II) species are readily available at reduced conditions (Gambrell, 1994; Ponnamperuma, 1972).

Under anoxic conditions, Fe(III) oxy(hydr)oxide minerals undergo reductive dissolution reactions through biotic, and abiotic pathways (Lovley and Phillips, 1987). Oxidation of organic matter and its coupling to the Fe reduction is one of the most important reactions in aquatic sediments, soils, and groundwater (Lovley et al., 2004). Caccavo et al. (1992) showed that the rate of microbially-mediated reduction of Fe oxy(hydr)oxides is influenced by different factors such as the microbial community structure and biomass, the type and abundance of Fe(III) oxy(hydr)oxides, and the sorption affinity between the oxide phases and bacteria. Dissimilatory

Fe reducing bacteria oxidize soil organic matter or H_2 and promote the reduction of various Fe(III) oxide phases.

Ferrihydrite [$Fe_{10}O_{14}$ $(OH)_2$] is an amorphous meta-stable Fe mineral that has a high surface reactive area (Jambor and Dutrizac, 1998). Because of its unique structure, ferrihydrite has been extensively used as a "scavenger" for trace elements such as As removal from contaminated water through surface adsorption reactions (Carlson et al., 2002; Lizama et al., 2011; Michel et al., 2007; Mohan and Pittman, 2007; Riveros et al., 2001). However, due to its poor crystallinity, ferrihydrite is transformed to stable crystalline Fe(III) phases under the reaction of reductive dissolution which depends on pH, temperature, redox potential, and carbonate concentration (Cudennec and Lecerf, 2006; Das et al., 2010; Schwertmann and Murad, 1983). Microbially-mediated reduction of ferrihydrite results in dissolution, and re-precipitation to stable mineral phases such as goethite and magnetite in the presence of Fe(II) (Benner et al., 2002; Berthelin et al., 2006; Hansel et al., 2003; Pedersen et al., 2006). The biogenic transformation of Fe(III) phases is controlled by supply rate and magnitude of Fe(II) (Hansel et al., 2003; Zachara et al., 2002). In reduced soil conditions, Fe cycling is often coupled with S cycling. Iron(II) produced by dissimilatory Fe reducing bacteria and subsequent reaction with sulfide result the formation of biogenic ferrous sulfide such as Fe monosulfides (FeS), greigite and pyrite (FeS_2) (Kwon et al., 2014; Neal et al., 2001; Saalfield and Bostick, 2009).

References

Antelo, J., M. Avena, S. Fiol, R. López and F. Arce. 2005. Effects of pH and ionic strength on the adsorption of phosphate and arsenate at the goethite–water interface. J. Colloid Interface Sci. 285:476-486.

Arai, Y., E.J. Elzinga and D.L. Sparks. 2001. X-ray absorption spectroscopic investigation of arsenite and arsenate adsorption at the aluminum oxide–water interface. J. Colloid Interface Sci. 235:80-88.

Bauer, M. and C. Blodau. 2009. Arsenic distribution in the dissolved, colloidal and particulate size fraction of experimental solutions rich in dissolved organic matter and ferric iron. Geochim. Cosmochim. Acta 73:529-542.

Bauer, M. and C. Blodau. 2006. Mobilization of arsenic by dissolved organic matter from iron oxides, soils and sediments. Sci. Total Environ. 354:179-190.

Benner, S.G., C.M. Hansel, B.W. Wielinga, T.M. Barber and S. Fendorf. 2002. Reductive dissolution and biomineralization of iron hydroxide under dynamic flow conditions. Environ. Sci. Technol. 36:1705-1711.

Bentley, R. and T.G. Chasteen. 2002. Microbial methylation of metalloids: Arsenic, antimony, and bismuth. Microbiol. Mol. Biol. Rev. 66:250-271.

Berthelin, J., G. Ona-Nguema, S. Stemmler, C. Quantin, M. Abdelmoula and F. Jorand. 2006. Bioreduction of ferric species and biogenesis of green rusts in soils. Comptes Rendus Geoscience 338:447-455.

Bhattacharya, P., A.H. Welch, K.G. Stollenwerk, M.J. McLaughlin, J. Bundschuh and G. Panaullah. 2007. Arsenic in the environment: Biology and chemistry. Sci. Total Environ. 379:109-120.

Bissen, M. and F.H. Frimmel. 2003. Arsenic—a review. part I: Occurrence, toxicity, speciation, mobility. Acta Hydrochim. Hydrobiol. 31:9-18.

Bonneville, S., P. Van Cappellen and T. Behrends. 2004. Microbial reduction of iron (III) oxyhydroxides: Effects of mineral solubility and availability. Chem. Geol. 212:255-268.

Borch, T., R. Kretzschmar, A. Kappler, P.V. Cappellen, M. Ginder-Vogel, A. Voegelin and K. Campbell. 2009. Biogeochemical redox processes and their impact on contaminant dynamics. Environ. Sci. Technol. 44:15-23.

Bostick, B.C. and S. Fendorf. 2003. Arsenite sorption on troilite (FeS) and pyrite (FeS_2). Geochim. Cosmochim. Acta 67:909-921.

Buddhawong, S., P. Kuschk, J. Mattusch, A. Wiessner and U. Stottmeister. 2005. Removal of arsenic and zinc using different laboratory model wetland systems. Engineering in Life Sciences 5:247-252.

Caccavo, F., R.P. Blakemore and D.R. Lovley. 1992. A hydrogen-oxidizing, Fe(III)-reducing microorganism from the great bay estuary, new hampshire. Appl. Environ. Microbiol. 58:3211-3216.

Carlson, L., J. Bigham, U. Schwertmann, A. Kyek and F. Wagner. 2002. Scavenging of As from acid mine drainage by schwertmannite and ferrihydrite: A comparison with synthetic analogues. Environ. Sci. Technol. 36:1712-1719.

Catalano, J.G., C. Park, P. Fenter and Z. Zhang. 2008. Simultaneous inner-and outer-sphere arsenate adsorption on corundum and hematite. Geochim. Cosmochim. Acta 72:1986-2004.

Catalano, J.G., Z. Zhang, P. Fenter and M.J. Bedzyk. 2006. Inner-sphere adsorption geometry of Se (IV) at the hematite (100)–water interface. J. Colloid Interface Sci. 297:665-671.

Chapman, C.A. and C.M. Layman. 2007. Considerations impacting the technology selection process for FGD purge stream wastewater treatment systems. Rep. IWC 07-38. Bechtel Power Corporation, Frederick, MD USA, IWC-68th Annual meeting.

Cherry, J., A. Shaikh, D. Tallman and R. Nicholson. 1979. Arsenic species as an indicator of redox conditions in groundwater. Journal of Hydrology 43:373-392.

Córdoba, P. 2015. Status of flue gas desulphurisation (FGD) systems from coal-fired power plants: Overview of the physic-chemical control processes of wet limestone FGDs. Fuel 144:274-286.

Cudennec, Y. and A. Lecerf. 2006. The transformation of ferrihydrite into goethite or hematite, revisited. Journal of Solid State Chemistry 179:716-722.

Das, S., M.J. Hendry and J. Essilfie-Dughan. 2010. Transformation of two-line ferrihydrite to goethite and hematite as a function of pH and temperature. Environ. Sci. Technol. 45:268-275.

De Souza, M., C. Huang, N. Chee and N. Terry. 1999. Rhizosphere bacteria enhance the accumulation of selenium and mercury in wetland plants. Planta 209:259-263.

Dhillon, K. and S. Dhillon. 2000. Dhillon, S.K. and K.S. Dhillon. 2000. Selenium adsorption in soils as influenced by different anions. Journal of Plant Nutrition and Soil Science 163:577-582.

Diaz-Somoano, M. and M.R. Martinez-Tarazona. 2004. Retention of arsenic and selenium compounds using limestone in a coal gasification flue gas. Environ. Sci. Technol. 38:899-903.

Dixit, S. and J.G. Hering. 2003. Comparison of arsenic (V) and arsenic (III) sorption onto iron oxide minerals: Implications for arsenic mobility. Environ. Sci. Technol. 37:4182-4189.

Duc, M., G. Lefevre and M. Fédoroff. 2006. Sorption of selenite ions on hematite. J. Colloid Interface Sci. 298:556-563.

Eggert, D.A., J.H. Rodgers Jr, G.M. Huddleston and C.E. Hensman. 2008. Performance of pilot-scale constructed wetland treatment systems for flue gas desulfurization waters. Environmental Geosciences 15:115-129.

Eggert, D.A. 2009. Constructed wetland treatment system: An approach for mitigating risks of flue gas desulfurization waters. Ph.D. Diss. Clemson University, Clemson , SC.

Elrashidi, M., D. Adriano, S. Workman and W. Lindsay. 1987. Chemical equilibria of selenium in soils: A theoretical Development1. Soil Sci. 144:141-152.

Elzinga, E.J., Y. Tang, J. McDonald, S. DeSisto and R.J. Reeder. 2009. Macroscopic and spectroscopic characterization of selenate, selenite, and chromate adsorption at the solid–water interface of γ-al 2 O 3. J. Colloid Interface Sci. 340:153-159.

EPRI. 2006. Guidance for assessing wastewater impacts of FGD scrubbers. Technical manual. Rep. 1013313. Electric Power Research Institute, Palo Alto, CA.

EPRI. 2007. Treatment technology summary for critical pollutants of concern in power plant wastewaters. Rep. 1012549. Electric Power Research Institute, Palo Alto, CA.

Essington, M.E. 2004. Soil and water chemistry: An integrative approach. CRC press, Boca Raton, FL.

Fan, J., Y. Wang, C. Liu, L. Wang, K. Yang, D. Zhou, W. Li and D.L. Sparks. 2014. Effect of iron oxide reductive dissolution on the transformation and immobilization of arsenic in soils: New insights from X-ray photoelectron and X-ray absorption spectroscopy. J. Hazard. Mater. 279:212-219.

Faulwetter, J.L., V. Gagnon, C. Sundberg, F. Chazarenc, M.D. Burr, J. Brisson, A.K. Camper and O.R. Stein. 2009. Microbial processes influencing performance of treatment wetlands: A review. Ecol. Eng. 35:987-1004.

Fendorf, S., M.J. Eick, P. Grossl and D.L. Sparks. 1997. Arsenate and chromate retention mechanisms on goethite. 1. Surface structure. Environ. Sci. Technol. 31:315-320.

Fernández-Martínez, A. and L. Charlet. 2009. Selenium environmental cycling and bioavailability: A structural chemist point of view. Reviews in Environmental Science and Bio/Technology 8:81-110.

Fordyce, F. 2007. Selenium geochemistry and health. Ambio. 36:94-97.

Fordyce, F.M. 2013. Selenium deficiency and toxicity in the environment. p.375-416. *In* O. Selinus (ed.) Essentials of medical geology. Springer. Netherlands.

Foster, A.L., G.E. Brown and G.A. Parks. 2003. X-ray absorption fine structure study of As (V) and Se (IV) sorption complexes on hydrous Mn oxides. Geochim. Cosmochim. Acta 67:1937-1953.

Frankenberger, W.T. and R.A. Engberg. 1998. Environmental chemistry of selenium. CRC Press.

Gambrell, R. 1994. Trace and toxic metals in wetlands—a review. J. Environ. Qual. 23:883-891.

Gao, S., K. Tanji, D. Peters and M. Herbel. 2000. Water selenium speciation and sediment fractionation in a california flow-through wetland system. J. Environ. Qual. 29:1275-1283.

Gao, S., K. Tanji, Z. Lin, N. Terry and D. Peters. 2003a. Selenium removal and mass balance in a constructed flow-through wetland system. J. Environ. Qual. 32:1557-1570.

Gao, S., K.K. Tanji, D.W. Peters, Z. Lin and N. Terry. 2003b. Selenium removal from irrigation drainage water flowing through constructed wetland cells with special attention to accumulation in sediments. Water Air Soil Pollut. 144:263-284.

Goh, K. and T. Lim. 2004. Geochemistry of inorganic arsenic and selenium in a tropical soil: Effect of reaction time, pH, and competitive anions on arsenic and selenium adsorption. Chemosphere 55:849-859.

Goldberg, S. 2013. Modeling selenite adsorption envelopes on oxides, clay minerals, and soils using the triple layer model. Soil Sci. Soc. Am. J. 77:64-71.

Goldberg, S. 2002. Competitive adsorption of arsenate and arsenite on oxides and clay minerals. Soil Sci. Soc. Am. J. 66:413-421.

Goldberg, S. and C.T. Johnston. 2001. Mechanisms of arsenic adsorption on amorphous oxides evaluated using macroscopic measurements, vibrational spectroscopy, and surface complexation modeling. J. Colloid Interface Sci. 234:204-216.

Goldberg, S. and R. Glaubig. 1988. Anion sorption on a calcareous, montmorillonitic soil-selenium. Soil Sci. Soc. Am. J. 52:954-958.

Goldberg, S., S.M. Lesch and D.L. Suarez. 2007. Predicting selenite adsorption by soils using soil chemical parameters in the constant capacitance model. Geochim. Cosmochim. Acta 71:5750-5762.

Guan, X., H. Dong, J. Ma and L. Jiang. 2009. Removal of arsenic from water: Effects of competing anions on As (III) removal in $KMnO_4$–Fe (II) process. Water Res. 43:3891-3899.

Hanlon, J.A. 2010. National pollutant discharge elimination system (NPDES) permitting of wastewater discharges from flue gas desulfurization (FGD) and coal combustion residuals (CCR) impoundments at steam electric power plants. Rep. 44. USEPA, Office of water, Washington, D.C., USA.

Hansel, C.M., S.G. Benner, J. Neiss, A. Dohnalkova, R.K. Kukkadapu and S. Fendorf. 2003. Secondary mineralization pathways induced by dissimilatory iron reduction of ferrihydrite under advective flow. Geochim. Cosmochim. Acta 67:2977-2992.

Hansen, D., P.J. Duda, A. Zayed and N. Terry. 1998. Selenium removal by constructed wetlands: Role of biological volatilization. Environ. Sci. Technol. 32:591-597.

Higgins, T., T. Sandy and S.W. Givens. 2009. Flue gas desulfurization wastewater treatment primer. Power (New York).

Hill, CH2M. 2010. Review of available technologies for the removal of selenium from water. Final Report, Prepared for North American Metals Council (NAMC).

Horneman, A., A. van Geen, D.V. Kent, P. Mathe, Y. Zheng, R. Dhar, S. O'connell, M. Hoque, Z. Aziz and M. Shamsudduha. 2004. Decoupling of As and Fe release to Bangladesh groundwater under reducing conditions. part I: Evidence from sediment profiles. Geochim. Cosmochim. Acta 68:3459-3473.

Huang, Y.H., P.K. Peddi, C. Tang, H. Zeng and X. Teng. 2013. Hybrid zero-valent iron process for removing heavy metals and nitrate from flue-gas-desulfurization wastewater. Separation and Purification Technology 118:690-698.

Hughes, M.F. 2002. Arsenic toxicity and potential mechanisms of action. Toxicol. Lett. 133:1-16.

Ito, S., T. Yokoyama and K. Asakura. 2006. Emissions of mercury and other trace elements from coal-fired power plants in japan. Sci. Total Environ. 368:397-402.

Jain, A. and R.H. Loeppert. 2000. Effect of competing anions on the adsorption of arsenate and arsenite by ferrihydrite. J. Environ. Qual. 29:1422-1430.

Jain, A., K.P. Raven and R.H. Loeppert. 1999. Arsenite and arsenate adsorption on ferrihydrite: Surface charge reduction and net OH^- release stoichiometry. Environ. Sci. Technol. 33:1179-1184.

Jambor, J.L. and J.E. Dutrizac. 1998. Occurrence and constitution of natural and synthetic ferrihydrite, a widespread iron oxyhydroxide. Chem. Rev. 98:2549-2586.

Johnson, D.B. and K.B. Hallberg. 2005. Acid mine drainage remediation options: A review. Sci. Total Environ. 338:3-14.

Jomova, K., Z. Jenisova, M. Feszterova, S. Baros, J. Liska, D. Hudecova, C. Rhodes and M. Valko. 2011. Arsenic: Toxicity, oxidative stress and human disease. Journal of Applied Toxicology 31:95-107.

Jordan, N., A. Ritter, H. Foerstendorf, A. Scheinost, S. Weiß, K. Heim, J. Grenzer, A. Mücklich and H. Reuther. 2013. Adsorption mechanism of selenium (VI) onto maghemite. Geochim. Cosmochim. Acta 103:63-75.

Jordan, N., A. Ritter, A.C. Scheinost, S. Weiss, S. Dieter and H. René. 2014. Selenium (IV) uptake by maghemite (γ-Fe_2O_3). Environ. Sci. Technol. 48: 1665–1674.

Kadlec, R.H. and S. Wallace. 2008. Treatment wetlands. CRC press. Florida, USA.

Kneebone, P., P. O'Day, N. Jones and J. Hering. 2002. Deposition and fate of arsenic in iron-and arsenic-enriched reservoir sediments. Environ. Sci. Technol. 36:381-386.

Ko, I., J. Kim and K. Kim. 2004. Arsenic speciation and sorption kinetics in the As–hematite–humic acid system. Colloids Surf. Physicochem. Eng. Aspects 234:43-50.

Kocar, B.D., M.J. Herbel, K.J. Tufano and S. Fendorf. 2006. Contrasting effects of dissimilatory iron (III) and arsenic (V) reduction on arsenic retention and transport. Environ. Sci. Technol. 40:6715-6721.

Kocar, B.D., M.L. Polizzotto, S.G. Benner, S.C. Ying, M. Ung, K. Ouch, S. Samreth, B. Suy, K. Phan and M. Sampson. 2008. Integrated biogeochemical and hydrologic processes driving arsenic release from shallow sediments to groundwaters of the mekong delta. Appl. Geochem. 23:3059-3071.

Kröpfelová, L., J. Vymazal, J. Švehla and J. Štíchová. 2009. Removal of trace elements in three horizontal sub-surface flow constructed wetlands in the Czech Republic. Environmental Pollution 157:1186-1194.

Kwon, M.J., M.I. Boyanov, D.A. Antonopoulos, J.M. Brulc, E.R. Johnston, K.A. Skinner, K.M. Kemner and E.J. O'Loughlin. 2014. Effects of dissimilatory sulfate reduction on Fe III (hydr)oxide reduction and microbial community development. Geochim. Cosmochim. Acta 129:177-190.

Lin, Z. and N. Terry. 2003. Selenium removal by constructed wetlands: Quantitative importance of biological volatilization in the treatment of selenium-laden agricultural drainage water. Environ. Sci. Technol. 37:606-615.

Lindsay, W.L. 1979. Chemical equilibria in soils. Wiley, NY.

Lizama, K., T.D. Fletcher and G. Sun. 2011. Removal processes for arsenic in constructed wetlands. Chemosphere 84:1032-1043.

Lovley, D.R., D.E. Holmes and K.P. Nevin. 2004. Dissimilatory Fe (III) and Mn (IV) reduction. Adv. Microb. Physiol. 49:219-286.

Lovley, D.R. and E.J. Phillips. 1987. Competitive mechanisms for inhibition of sulfate reduction and methane production in the zone of ferric iron reduction in sediments. Appl. Environ. Microbiol. 53:2636-2641.

Machemer, S.D. and T.R. Wildeman. 1992. Adsorption compared with sulfide precipitation as metal removal processes from acid mine drainage in a constructed wetland. J. Contam. Hydrol. 9:115-131.

Manning, B.A. and S. Goldberg. 1997. Adsorption and stability of arsenic (III) at the clay mineral-water interface. Environ. Sci. Technol. 31:2005-2011.

Manning, B.A. and S. Goldberg. 1996a. Modeling competitive adsorption of arsenate with phosphate and molybdate on oxide minerals. Soil Sci. Soc. Am. J. 60:121-131.

Manning, B.A. and S. Goldberg. 1996b. Modeling arsenate competitive adsorption on kaolinite, montmorillonite and illite. Clays Clay Miner. 44:609-623.

Manning, B.A., S.E. Fendorf, B. Bostick and D.L. Suarez. 2002. Arsenic (III) oxidation and arsenic (V) adsorption reactions on synthetic birnessite. Environ. Sci. Technol. 36:976-981.

Martinez, M., J. Gimenez, J. De Pablo, M. Rovira and L. Duro. 2006. Sorption of selenium (IV) and selenium (VI) onto magnetite. Appl. Surf. Sci. 252:3767-3773.

Masscheleyn, P.H. and W.H. Patrick. 1993. Biogeochemical processes affecting selenium cycling in wetlands. Environmental Toxicology and Chemistry 12:2235-2243.

Masscheleyn, P.H., R.D. Delaune and W. Patrick. 1991a. Arsenic and selenium chemistry as affected by sediment redox potential and pH. J. Environ. Qual. 20:522-527.

Masscheleyn, P.H., R.D. Delaune and W.H. Patrick Jr. 1991b. Effect of redox potential and pH on arsenic speciation and solubility in a contaminated soil. Environ. Sci. Technol. 25:1414-1419.

Mays, P. and G. Edwards. 2001. Comparison of heavy metal accumulation in a natural wetland and constructed wetlands receiving acid mine drainage. Ecol. Eng. 16:487-500.

McCarty, K.M., H.T. Hanh and K. Kim. 2011. Arsenic geochemistry and human health in south east asia. Rev. Environ. Health 26:71-78.

McNeal, J.M. and L.S. Balistrieri. 1989. Geochemistry and occurrence of selenium: An overview. Selenium in Agriculture and the Environment. Soil Science Society of America Special Publication No. 23, Madison, WI, USA.

Michel, F.M., L. Ehm, S.M. Antao, P.L. Lee, P.J. Chupas, G. Liu, D.R. Strongin, M.A. Schoonen, B.L. Phillips and J.B. Parise. 2007. The structure of ferrihydrite, a nanocrystalline material. Science 316:1726-1729.

Mladenov, N., Y. Zheng, M.P. Miller, D.R. Nemergut, T. Legg, B. Simone, C. Hageman, M.M. Rahman, K.M. Ahmed and D.M. McKnight. 2009. Dissolved organic matter sources and consequences for iron and arsenic mobilization in Bangladesh aquifers. Environ. Sci. Technol. 44:123-128.

Mohan, D. and C.U. Pittman. 2007. Arsenic removal from water/wastewater using adsorbents—a critical review. J. Hazard. Mater. 142:1-53.

Mooney, F.D. and C. Murray-Gulde. 2008. Constructed treatment wetlands for flue gas desulfurization waters: Full-scale design, construction issues, and performance. Environmental Geosciences 15:131-141.

Moore, J.N., W.H. Ficklin and C. Johns. 1988. Partitioning of arsenic and metals in reducing sulfidic sediments. Environ. Sci. Technol. 22:432-437.

Moretti, A., C. Jones and P. Asia. 2012. Advanced emissions control technologies for coal-fired power plants. BR -1886. Power-Gen Asia. Bangkok, Thailand

Myneni, S., T.K. Tokunaga and G. Brown. 1997. Abiotic selenium redox transformations in the presence of Fe(II, III) oxides. Science 278:1106-1109.

Nakamaru, Y.M. and J. Altansuvd. 2014. Speciation and bioavailability of selenium and antimony in non-flooded and wetland soils: A review. Chemosphere 111:366-371.

Nakamaru, Y.M. and K. Sekine. 2008. Sorption behavior of selenium and antimony in soils as a function of phosphate ion concentration. Soil Sci. Plant Nutr. 54:332-341.

Neal, A.L., S. Techkarnjanaruk, A. Dohnalkova, D. McCready, B.M. Peyton and G.G. Geesey. 2001. Iron sulfides and sulfur species produced at hematite surfaces in the presence of sulfate-reducing bacteria. Geochim. Cosmochim. Acta 65:223-235.

Nickson, R., J. McArthur, W. Burgess, K.M. Ahmed, P. Ravenscroft and M. Rahmann. 1998. Arsenic poisoning of Bangladesh groundwater. Nature 395:338-338.

Nickson, R., J. McArthur, P. Ravenscroft, W. Burgess and K. Ahmed. 2000. Mechanism of arsenic release to groundwater, Bangladesh and west Bengal. Appl. Geochem. 15:403-413.

Nielsen, P., T. Christensen and M. Vendrup. 1997. Continuous removal of heavy metals from FGD wastewater in a fluidised bed without sludge generation. Water Science and Technology 36:391-397.

Ochoa-González, R., M. Díaz-Somoano and M.R. Martínez-Tarazona. 2013. Influence of limestone characteristics on mercury re-emission in WFGD systems. Environ. Sci. Technol. 47:2974-2981.

O'Day, P.A., D. Vlassopoulos, R. Root and N. Rivera. 2004. The influence of sulfur and iron on dissolved arsenic concentrations in the shallow subsurface under changing redox conditions. Proc. Natl. Acad. Sci. U. S. A. 101:13703-13708.

Peak, D. 2006. Adsorption mechanisms of selenium oxyanions at the aluminum oxide/water interface. J. Colloid Interface Sci. 303:337-345. .

Peak, D. and D. Sparks. 2002. Mechanisms of selenate adsorption on iron oxides and hydroxides. Environ. Sci. Technol. 36:1460-1466.

Peak, D., U. Saha and P. Huang. 2006. Selenite adsorption mechanisms on pure and coated montmorillonite: An EXAFS and XANES spectroscopic study. Soil Sci. Soc. Am. J. 70:192-203.

Pedersen, H.D., D. Postma and R. Jakobsen. 2006. Release of arsenic associated with the reduction and transformation of iron oxides. Geochim. Cosmochim. Acta 70:4116-4129.

Peterson, H.G. 1998. Use of constructed wetlands to process agricultural wastewater. Canadian Journal of Plant Science 78:199-210.

Pickett, T., J. Sonstegard and B. Bonkoski. 2006. Using biology to treat selenium: Biologically treating scrubber wastewater can be an alternative to physical-chemical treatment. Power Engineering. http://www3.epa.gov/region1/npdes/merrimackstation/ (accessed on June 26, 2015).

Pikaray, S.; Banerjee, S.; Mukherji, S. Sorption of arsenic onto Vindhyan shales: role of pyrite and organic carbon. *Curr. Sci.* **2005**, *88*, 1580-1585.

Pilon-Smits, E., M. De Souza, G. Hong, A. Amini, R. Bravo, S. Payabyab and N. Terry. 1999. Selenium volatilization and accumulation by twenty aquatic plant species. J. Environ. Qual. 28:1011-1018.

Polizzotto, M.L., C.F. Harvey, S.R. Sutton and S. Fendorf. 2005. Processes conducive to the release and transport of arsenic into aquifers of Bangladesh. Proc. Natl. Acad. Sci. U. S. A. 102:18819-18823.

Ponnamperuma, F. 1972. The chemistry of submerged soils. Adv. Agron. 24:29-96.

Randall, S.R., D.M. Sherman and K.V. Ragnarsdottir. 2001. Sorption of As (V) on green rust (Fe_4 (II) Fe_2(III)$(OH)_{12}$ $SO_4 \cdot$ $3H_2O$) and lepidocrocite (γ-FeOOH): Surface complexes from EXAFS spectroscopy. Geochim. Cosmochim. Acta 65:1015-1023.

Ratnaike, R.N. 2003. Acute and chronic arsenic toxicity. Postgrad. Med. J. 79:391-396.

Raven, K.P., A. Jain and R.H. Loeppert. 1998. Arsenite and arsenate adsorption on ferrihydrite: Kinetics, equilibrium, and adsorption envelopes. Environ. Sci. Technol. 32:344-349.

Rayman, M.P. 2000. The importance of selenium to human health. The Lancet. 356:233-241.

Renkou, X., W. Yong, D. Tiwari and W. Houyan. 2009. Effect of ionic strength on adsorption of As (III) and As (V) on variable charge soils. Journal of Environmental Sciences 21:927-932.

Riffe, M.R., B.E. Heimbigner, P.G. Kutzora and K.A. Braunstein. 2008. Wastewater treatment for FGD purge streams. Rep. 2015. Siemens Water Technologies Corp., MEGA Symposium, Baltimore, MD.

Riveros, P., J. Dutrizac and P. Spencer. 2001. Arsenic disposal practices in the metallurgical industry. Can. Metall. Q. 40:395-420.

Rubin, E.S., D. Hounshell, S. Yeh, M. Taylor, L. Schrattenholzer, K. Riahi, L. Barreto and S. Rao. 2004. The effect of government actions on environmental technology innovation: Applications to the integrated assessment of carbon sequestration technologies.

Saada, A., D. Breeze, C. Crouzet, S. Cornu and P. Baranger. 2003. Adsorption of arsenic (V) on kaolinite and on kaolinite–humic acid complexes: Role of humic acid nitrogen groups. Chemosphere 51:757-763.

Saalfield, S.L. and B.C. Bostick. 2009. Changes in iron, sulfur, and arsenic speciation associated with bacterial sulfate reduction in ferrihydrite-rich systems. Environ. Sci. Technol. 43:8787-8793.

Sadiq, M. 1997. Arsenic chemistry in soils: An overview of thermodynamic predictions and field observations. Water Air Soil Pollut. 93:117-136.

Sahrawat, K. 2005. Fertility and organic matter in submerged rice soils. Curr. Sci. 88:735-739.

Schwertmann, U. and E. Murad. 1983. Effect of pH on the formation of goethite and hematite from ferrihydrite. Clays Clay Miner. 31:277-284.

Schwertmann, U. 2008. Iron oxides. p. 363-369. Ward Chesworth (ed.) *In* Encyclopedia of soil science. Springer. New York, USA .

Schwindaman, J.P., J.W. Castle and J.H. Rodgers. 2014. Fate and distribution of arsenic in a process-designed pilot-scale constructed wetland treatment system. Ecol. Eng. 68:251-259.

Seby, F., M. Potin-Gautier, E. Giffaut, G. Borge and O. Donard. 2001. A critical review of thermodynamic data for selenium species at 25 C. Chem. Geol. 171:173-194.

Sharma, V.K. and M. Sohn. 2009. Aquatic arsenic: Toxicity, speciation, transformations, and remediation. Environ. Int. 35:743-759.

Sheoran, A. and V. Sheoran. 2006. Heavy metal removal mechanism of acid mine drainage in wetlands: A critical review. Minerals Eng 19:105-116.

Smedley, P. and D. Kinniburgh. 2002. A review of the source, behaviour and distribution of arsenic in natural waters. Appl. Geochem. 17:517-568.

Smith, D.B., W.F. Cannon, L.G. Woodruff, F. Solano, J.E. Kilburn and D.L. Fey. 2013. Geochemical and mineralogical data for soils of the conterminous united states. US Geological Survey Data Series 801:19.

Smith, E., R. Naidu and A.M. Alston. 1998. Arsenic in the soil environment. Adv. Agron. 64:149-195.

Spacil, M.M., J.H. Rodgers Jr, J.W. Castle and W.Y. Chao. 2011. Performance of a pilot-scale constructed wetland treatment system for selenium, arsenic, and low-molecular-weight organics in simulated fresh produced water. Environmental Geosciences 18:145-156.

Srivastava, R.K. and W. Jozewicz. 2001. Flue gas desulfurization: The state of the art. J. Air Waste Manage. Assoc. 51:1676-1688.

Srivastava, R.K., W. Jozewicz and C. Singer. 2001. SO_2 scrubbing technologies: A review. Environ. Prog. 20:219-228.

Stein, O.R., D.J. Borden-Stewart, P.B. Hook and W.L. Jones. 2007. Seasonal influence on sulfate reduction and zinc sequestration in subsurface treatment wetlands. Water Res. 41:3440-3448.

Sturman, P.J., O.R. Stein, J. Vymazal and L. Kröpfelová. 2008. Sulfur cycling in constructed wetlands. p. 329-344. *In* Jan Vymazal (ed.) Wastewater treatment, plant dynamics and management in constructed and natural wetlands. Springer.

Su, C. and D.L. Suarez. 2000. Selenate and selenite sorption on iron oxides an infrared and electrophoretic study. Soil Sci. Soc. Am. J. 64:101-111.

Sundaravadivel, M. and S. Vigneswaran. 2001. Constructed wetlands for wastewater treatment. Crit. Rev. Environ. Sci. Technol. 31:351-409.

Sundberg, S.E., S.M. Hassan and J.H. Rodgers. 2006. Enrichment of elements in detritus from a constructed wetland and consequent toxicity to *hyalella azteca*. Ecotoxicol. Environ. Saf. 64:264-272.

Sundberg-Jones, S.E. and S.M. Hassan. 2007a. Macrophyte sorption and bioconcentration of elements in a pilot constructed wetland for flue gas desulfurization wastewater treatment. Water Air Soil Pollut. 183:187-200.

Sundberg-Jones, S.E. and S.M. Hassan. 2007b. Sediment-associated elements in a constructed wetland treatment system: Distribution, characterization, and toxicity. Bioremediation, Biodiversity and Bioavailability 1:41-55.

Takahashi, Y., R. Minamikawa, K.H. Hattori, K. Kurishima, N. Kihou and K. Yuita. 2004. Arsenic behavior in paddy fields during the cycle of flooded and non-flooded periods. Environ. Sci. Technol. 38:1038-1044.

Tate, M. 2005. Kansas water quality standards and supporting documents. Kansas Department of Health and Environment, Topeka, Kansas.

Taylor, M.R., E.S. Rubin and D.A. Hounshell. 2005. Control of SO_2 emissions from power plants: A case of induced technological innovation in the US. Technological Forecasting and Social Change 72:697-718.

Tokunaga, T.K., I.J. Pickering and G.E. Brown. 1996. Selenium transformations in ponded sediments. Soil Sci. Soc. Am. J. 60:781-790.

Tokunaga, T.K., G.E. Brown, I.J. Pickering, S.R. Sutton and S. Bajt. 1997. Selenium redox reactions and transport between ponded waters and sediments. Environ. Sci. Technol. 31:1419-1425.

Tufano, K.J. and S. Fendorf. 2008. Confounding impacts of iron reduction on arsenic retention. Environ. Sci. Technol. 42:4777-4783.

USEIA. 2011. Coal plants without scrubbers account for a majority of U.S. SO_2 emissions - today in energy. http://www.eia.gov/todayinenergy/detail.cfm?id=4410. (accessed June 10, 2015).

USEPA. 2015a. Six common air pollutants. http://www.epa.gov/airquality/urbanair/ (accessed July 13, 2015).

USEPA. 2015b. Acid rain program. http://www.epa.gov/airmarkets/programs/arp/index.html. (accessed June 30, 2015).

USEPA. 2014. National pollutant discharge elimination system (NPDES) permit program. http://water.epa.gov/polwaste/npdes/ (accessed July 16, 2015).

USEPA. 2013. Environmental assessment for the proposed effluent limitations guidelines and standards for the steam electric power generating point source category. Rep. EPA-821-R-13-003. U.S.Environmental Protection Agency, Office of Water, Washington , DC, USA.

USEPA. 2009. Steam electric power generatin point source category: Final detailed study report. Rep. EPA 821-R-09-008. U.S. Environmental Protection Agency.

Verhoeven, J.T. and A.F. Meuleman. 1999. Wetlands for wastewater treatment: Opportunities and limitations. Ecol. Eng. 12:5-12.

Vymazal,J. M. Greenway, K. Tonderski, H. Brix, and U. Mander. 2006. Constructed Wetlands for Wastewater Treatment. p. 69-91. *In* Verhoeven, J.T., B. Beltman, R. Bobbink and D.F. Whigham (eds.) Wetlands and natural resource management. Springer, NY.

Vymazal, J. 2010. Constructed wetlands for wastewater treatment. Water 2:530-549.

Vymazal, J. 2007. Removal of nutrients in various types of constructed wetlands. Sci. Total Environ. 380:48-65.

Wang, S. and C.N. Mulligan. 2006. Natural attenuation processes for remediation of arsenic contaminated soils and groundwater. J. Hazard. Mater. 138:459-470.

Watts, D.L. 1994. The nutritional relationships of selenium. Journal of Orthomolecular Medicine 9:111-111.

WHO. 1999. Preventing disease through healthy environments. Fact sheet no. 210. World Health Organization, Geneva, Switzerland.

Wu, S., P. Kuschk, A. Wiessner, J. Müller, R.A. Saad and R. Dong. 2013. Sulphur transformations in constructed wetlands for wastewater treatment: A review. Ecol. Eng. 52:278-289.

Yamaguchi, N., T. Nakamura, D. Dong, Y. Takahashi, S. Amachi and T. Makino. 2011. Arsenic release from flooded paddy soils is influenced by speciation, eh, pH, and iron dissolution. Chemosphere 83:925-932.

Yang, G.Q., S.Z. Wang, R.H. Zhou and S.Z. Sun. 1983. Endemic selenium intoxication of humans in china. Am. J. Clin. Nutr. 37:872-881.

Ye, Z., Z. Lin, S. Whiting, M. De Souza and N. Terry. 2003. Possible use of constructed wetland to remove selenocyanate, arsenic, and boron from electric utility wastewater. Chemosphere 52:1571-1579.

Ye, Z., S. Whiting, J. Qian, C. Lytle, Z. Lin and N. Terry. 2001. Trace element removal from coal ash leachate by a 10-year-old constructed wetland. J. Environ. Qual. 30:1710-1719.

Yeh, T. 2008. Removal of metals in constructed wetlands: Review. Pract. Periodical Hazard. , Toxic, Radioact. Waste Manage. 12:96-101.

Zachara, J.M., R.K. Kukkadapu, J.K. Fredrickson, Y.A. Gorby and S.C. Smith. 2002. Biomineralization of poorly crystalline Fe (III) oxides by dissimilatory metal reducing bacteria (DMRB). Geomicrobiol. J. 19:179-207.

Zhang, P. and D.L. Sparks. 1990. Kinetics of selenate and selenite adsorption/desorption at the goethite/water interface. Environ. Sci. Technol. 24:1848-1856.

Zhang, Y. and J.N. Moore. 1997a. Reduction potential of selenate in wetland sediment. J. Environ. Qual. 26:910-916.

Zhang, Y. and J.N. Moore. 1997b. Environmental conditions controlling selenium volatilization from a wetland system. Environ. Sci. Technol. 31:511-517.

Zhang, Y. and J.N. Moore. 1996. Selenium fractionation and speciation in a wetland system. Environ. Sci. Technol. 30:2613-2619.

Zhou, P., J. Huang, A.W. Li and S. Wei. 1999. Heavy metal removal from wastewater in fluidized bed reactor. Water Res. 33:1918-1924.

Chapter 3 - Transport and transformation of selenium and other constituents of flue-gas desulfurization wastewater in a constructed wetland treatment system

Abstract

Constructed wetland treatment systems (CWTSs) are an adopted option for Se removal from flue-gas desulfurization (FGD) wastewater, but the mechanism of Se retention in these systems is not well understood. A laboratory-based soil column study, mimicking a pilot-scale CWTS, was carried out to understand the behavior and the retention capacity of FGD wastewater constituents, and to develop a mechanistic understanding of Se retention. Deoxygenated 1:1 mixture of FGD wastewater: raw water was delivered to the saturated soil columns with an upward flow at a rate of 1.42 mL/hour for 100 days. The columns were then flushed with the raw water at the same flow rate for an additional 100 days. Effluent was analyzed for constituents of concern. Soil from the sectioned columns were used for total elemental analysis, sequential extraction procedure (SEP), and synchrotron-based X-ray spectroscopy techniques. Effluent analysis indicated complete retention of Se in the soil. Boron and fluorine partially retained in the soil, but sulfur, sodium and chlorine did not retain, agreeing with field observations. Selenium in the influent accumulated in the bottom (inlet) of the soil columns. The SEP revealed

that Se was mainly sequestered as stable/residual forms. Bulk- and micro- X-ray absorption near edge spectroscopy (XANES) indicated that Se mainly existed as reduced/stable species [Se(IV), organic Se and Se(0)] and long submergence period reduced Se further. The retention mechanism of Se from the FGD wastewater was the transformation of Se into reduced/stable forms.

Introduction

Coal combustion for generating electricity detrimentally affect environment and human health due to the emission of pollutants, such as carbon dioxide (CO_2), sulfur dioxide (SO_2), nitrogen oxides (NO_x), mercury, and particulate matter. Sulfur dioxide emission from coal-fired power plants is a main source of air pollution. Scrubbing flue-gas desulfurization (FGD) systems have been installed in many coal-fired power plants to decrease the concentration of SO_2 in the flue gas, thereby complying with Clean Air Act standards. Wet scrubber FGD systems are 90% efficient in reducing SO_2 emission (Srivastava et al., 2001; Taylor et al., 2005) through the reaction of limestone. However, water generated by the dewatering process of these systems is generally enriched with elevated levels of trace elements, such as selenium (Se), arsenic (As), and mercury (Hg), as well as many other constituents (sulfur, boron, sodium, bromine, fluorine, chlorine, nitrate, etc.) (EPRI, 2006). Thus, FGD wastewater generally fails to meet surface water quality standards, and therefore has the potential to cause surface water pollution (EPRI, 2006; EPRI, 2007).

The wastewater generated by wet scrubber FGD systems must be treated before discharging into aquatic systems, if it is to meet water quality standards. Selenium is one of the challenging pollutants in FGD wastewater and it can potentially influence animals and human health (EPRI, 2006). Although Se is an essential micronutrient for animals and humans, it

becomes toxic easily due to the narrow range between deficiency and toxicity (Fordyce, 2013). Long-term exposure to elevated levels of Se becomes toxic to humans (Fordyce, 2007). The chemistry of Se is complicated because of it has different oxidation states, which are influenced by redox potential (Eh), pH, and other soil conditions (Fordyce, 2007; Masscheleyn et al., 1990; Masscheleyn et al., 1991; Zhang and Moore, 1997). Selenate [Se(VI)], selenite [Se(IV)], elemental selenium [Se(0)], selenide [Se(-II)], and organic Se complexes are the predominant species in soils and sediments (Fernández-Martínez and Charlet, 2009). Selenate and selenite mainly exists in water, and they are more likely to be mobile, toxic, and bioavailable (Fordyce, 2007; Nakamaru and Altansuvd, 2014). Upon flooding, Se(VI) is transformed to Se(IV) at moderate Eh conditions (i.e., +200 to +300 mV) and eventually forms more reduced species, depending on submergence time and the redox potential (Masscheleyn and Patrick, 1993; Nakamaru and Altansuvd, 2014; Sahrawat, 2005). Selenite and reduced Se species are immobile compared to Se(VI) because of adsorption, co-precipitation, surface precipitation reactions with soil mineral components, and sorption to soil organic matter (Fernández-Martínez and Charlet, 2009; Peak, 2006; Su and Suarez, 2000). Selenite is strongly adsorbed on soil colloidal surface by forming strong inner-sphere complexes whereas selenate is weakly adsorbed by outer-sphere complexes (Peak, 2006; Su and Suarez, 2000).

Constructed wetland treatment systems (CWTSs) are an economically and environmentally feasible option to treat variety of wastewaters such as municipal, agricultural, industrial wastewater, FGD wastewater, and inorganic and organic contaminated water (Budd et al., 2009; Díaz et al., 2012; Eggert et al., 2008; Hammer, 1989; Hansen et al., 1998; Kadlec and Wallace, 2008; Lin and Terry, 2003; Mooney and Murray-Gulde, 2008; Rahman et al., 2011; Ye et al., 2003; Ye et al., 2001; Yeh, 2008). Nevertheless, only a limited number of studies have

been conducted on CTWSs specifically designed for treating FGD wastewater. It has been found that Se and Hg in FGD wastewater were effectively removed by CWTSs (Eggert et al., 2008). Full-scale CWTSs implemented at power plants in North Carolina also highlighted their efficiency for FGD wastewater treatment (Mooney and Murray-Gulde, 2008). Duke Energy identified that CWTSs are an innovative technology to treat constituents of FGD wastewater (Wylie et al., 2008). However, to our knowledge, the mechanistic understanding of retention of FGD constituents in a CTWS was not addressed in detail. Eggert et al., 2008 also pointed out that elucidating the mechanisms of biogeochemical cycling of FGD wastewater constituents is needed to enhance their sequestration in the CWTS. Using sequential extraction procedures, previous studies have assessed the speciation characteristics of Hg, Se, and As in wetland sediments treated with FGD wastewater (Sundberg-Jones and Hassan, 2007), but information regarding the direct speciation is not reported. Since the changes of the oxidation state of Se significantly influence its solubility, mobility, and fate and transport, an improved understanding of chemical speciation and biogeochemical cycling is essential. Ultimately, this will provide better insights recognizing optimization techniques/conditions to enhance the long-term treatment efficiency of the CWTS.

Although operationally defined SEP provides indirect information about Se speciation in soils and wetland sediments (Gao et al., 2000; Martens and Suarez, 1997; Wright et al., 2003; Zhang and Moore, 1996; Zhang et al., 1999), phases identified by these conventional procedures are not completely phase-specific or phase-selective. Either definitive information of retention mechanism or true Se speciation in soils is not possible to provide by the SEP. X-ray absorption near edge structure (XANES) spectroscopy is a well-established technique to identify different oxidation states of Se because of spectral energy shift in the absorption edge of each species

(Pickering et al., 1995). Bulk-XANES gives the average speciation information of a system whereas microfocused specially resolved X-ray fluorescence (micro-XRF) mapping coupled with micro-XANES techniques are capable of probing the underlying mechanisms at microscale. Therefore, SEP, bulk- and micro-scale XANES techniques should be integrated to fully understand the mechanism of Se retention in the CWTS used for FGD wastewater treatment.

In this study, a laboratory-based soil column experiment, mimicking a pilot-scale CWTS, was designed and performed to (1) understand the transport characteristics, retention capacity and transformation of Se and other constituents of FGD wastewater in a CWTS, and (2) to elucidate the mechanistic interactions and/or relationships of FGD wastewater Se with the CWTS using SEP and synchrotron-based X-ray spectroscopy techniques.

Materials and Methods

Collection of soil and FGD wastewater

Topsoil (TS) and engineered soil (ES), wetland construction materials, were obtained from Westar Energy's Jeffrey Energy Center (JEC) in St. Marys, KS. The JEC is located in Emmett Township, Pottawatomie County, approximately 100 miles northwest of Kansas City, Kansas (39°17'10"N, 96°07'01"W). The engineered soil (ES) consisted of 25% topsoil, 10% subsoil, 40% sand, and 25% leafy-based compost, by volume. The collected soil materials were individually mixed well for homogeneity. They were then gently ground using a ceramic mortar and pestle, sieved through 2 mm-screen, and air-dried. Samples of both materials were analyzed for basic soil properties, such as texture, pH, cation exchange capacity (CEC), and organic matter (OM) content (Combs and Nathan, 1998) using established methodologies (Table 3.1).

The FGD wastewater and Kansas river water (i.e., raw water) used in this experiment were also collected from the JEC power plant on 13th of May, 2011. Basic chemical properties

such as pH, electrical conductivity, total solids, and total dissolved solids were measured by following standard protocols (Greenberg, et al., 1992). The concentrations of constituents (total elements and some selected anions) in the FGD wastewater and the raw water were determined using the methodology described in influent and effluent analysis section below.

Set-up of column study

The experiments were conducted using flow cells (Soil Measurement Systems LLC., Arizona, USA) that each consisted of an acrylic tube (5.08 cm diameter, 30.5 cm length) and two acrylic end-plate assemblies. Three tubes were packed with the TS and three were packed with the ES. To minimize variations in bulk density over the length of the tubes, each was packed in eight 3.81 cm lifts using a wet packing procedure (Skaggs et al., 2002). The mass of moist soil material required for each lift was determined using target bulk densities of 1.2 Mg/m^3 and 1.35 Mg/m^3 for the TS and ES materials, respectively. After the six tubes were fitted with end-plate assemblies, they were saturated from below with the raw water by incrementally raising the water level over a period of 24 hours. Syringe pumps (Legato 210 Syringe Pump, KD Scientific Inc., USA) were then used to introduce deoxygenated (bubbled with N_2) raw water, with flow in upward direction at a rate of 1.42 mL/hour (Figure A.1). The set-up of the soil column experiment is shown in Figure A.2. After steady-state flow was achieved (approximately one pore volume delivered), the flow experiment was initiated by switching the influent solution to a deoxygenated 1:1 mixture of FGD wastewater and raw water. This influent was delivered for 100 days with upward constant flow. Effluent was collected in increments of 0.5 pore volume (PV) from the outlet at top of each column (Figure A.3) and pH was measured immediately. After recording their weight and volume, the effluent samples were immediately filtered and stored as non-acidified or acidified samples at 4 ^0C depending on the targeted analysis. The

collection increment of 0.5 PV corresponded to a time interval of approximately 5 days for the TS columns and approximately 4.5 days for the columns filled with ES material. At the end of the experiment (after 100 days of FGD wastewater feeding), two selected columns, one from TS (TS-2) and the other from ES (ES-2), were flushed with the raw water for an additional 100 days. Effluent samples were collected every day and analyzed for constituents of concern.

Breakthrough curves (BTCs) were constructed by plotting the relative effluent solute concentration (C/C_0) against the number of pore volumes to understand the behavior of the constituents of FGD wastewater. In a BTC, the concentration of a constituent of interest in an effluent solution is denoted as C whereas C_0 is the concentration of that same constituent in the influent FGD wastewater solution.

Analysis of influent and effluent

The FGD wastewater, the raw water, and all column effluent samples were immediately filtered through 0.45 µm syringe filters (Environmental Express Inc., South Carolina, USA) and acidified with 2 to 3 drops of 6 M HCl. The concentrations of dissolved elements were analyzed using a Varian 720-ES Inductive couple plasma-optical emission spectrometer (ICP-OES). An Agilent 7500 series inductively coupled plasma-mass spectrometer equipped with a dynamic reaction cell (ICP-MS-DRC) was used to measure the concentrations of Se, As, and Hg. Unacidified samples were filtered through 0.2 µm syringe filters (Environmental Express Inc., South Carolina, USA) and analyzed using an ion chromatograph (ICS-1000, Dionex Corporation) to determine the concentrations of anions. Details about the analyses of influent and effluent are given in supporting information (SI) of Appendix A.

Soil sampling and analysis

Following completion of the flow experiments, the end-plate assemblies were removed and the columns were cut into six sections (each ~5.08 cm in length) (Figure A.4) that were numbered 1 through 6 from bottom to top. Immediately after they were cut, the column sections were tightly covered with saran wrap to avoid exposure to oxygen. The column sections were then weighed and immediately transferred into a glove box filled with N_2 gas. Inside the glove box, soil was scooped out from cylindrical parts, and homogenized. Soil samples from the bottom, middle, and top sections of the columns were frozen at -20 ^{0}C for future analyses. The total Se analysis, SEP and synchrotron-based X-ray spectroscopy analyses were performed to evaluate Se distribution as well as indirect and direct speciation of sequestered Se in the soil.

The total elemental concentration in the soil was determined using a 30% H_2O_2 and aqua regia digestion procedure (Premarathna et al., 2010) (more details in the SI of Appendix A). The digested soil samples were analyzed for Se and As using the ICP-MS-DRC while the concentrations of other elements (B, S, Fe, and Mn) were measured using the ICP-OES.

Sequential extractions procedure

Soil samples collected from the six sections of each soil column were used to extract Se using a seven-step sequential extraction procedure (Wright et al., 2003). First, air-dried soils were finely ground with an agate mortar and pestle. Then, 2.5 g of soil sample was added into a pre-weighed 50 mL polypropylene centrifuge tube. Prior to each extraction step, the weight of the residue remaining in the centrifuge tube was recorded and solid losses were minimized (see Table 6.1for more detail). The Se fractionation (%) was calculated by subtracting the original concentration of Se in each fraction from the Se extracted for each column section. The

difference was then divided by the total Se accumulated from FGD wastewater in each section as shown in the following equation.

$$Selenium\ fraction\ (\%) = \left(\frac{Extracted\ Se\ from\ a\ column\ section\ (\mu g/kg) - Extracted\ Se\ from\ original\ soil(\mu g/kg)}{Concentration\ of\ accumulated\ Se\ from\ FGD\ wastewater\ (\mu g/kg)}\right) \times 100$$

Selenium bulk-XANES analysis

According to the results for total Se analysis (discussed below), Se only accumulated in the bottom 1/3 (inlet) of the soil columns. Therefore, homogeneously mixed sub samples from the bottom sections were used for bulk-XANES analysis to assess the direct solid phase Se speciation. Detail steps for sample preparation are given in SI of Appendix A. Selenium bulk-XANES analysis was performed at beamline 10 ID-B, MRCAT (Materials Research Collaborative Access Team), at the APS. The MRCAT is an insertion device beam line equipped with Si (111) double-crystal monochromator. The Se K-edge was calibrated to 12658.5 eV using a Se foil. All XANES spectra for soil samples were collected in fluorescence mode. Multiple scans (8 to 12 scans) were gathered for each sample to get better signal-to-noise ratio. The XANES spectra of a series of Se standards were collected in transmission mode (3-5 scans for each standard). Data processing, aligning, smoothing, normalization and merging of collected scans were done following the standard procedures of ATHENA software (Ravel and Newville, 2005). The Se speciation was obtained by linear combination fitting (LCF) in the ATHENA within an energy range of −20 eV below to +30 eV above the edge. The LCF procedure of each soil sample was attempted to reconstruct all the spectral combinations of Se standards used for the analysis. The set of Se standards used for the LCF included sodium selenate (Na_2SeO_4), sodium selenite (Na_2SeO_3), selenium sulfide (SeS_2), iron (II) selenide (FeSe), seleno-DL-

cystine, Se minerals, and elemental Se. The combination which had lowest reduced χ^2 and R-factor was selected as the best fitting. The accuracy of LCF relies on how well the spectra of selected standards represent the components of actual samples.

Selenium micro-XRF and micro-XANES analysis

The micro-XRF mapping and micro-XANES were conducted at sector 13 ID-E, GSECARS (GeoSoilEnviro Consortium of Advanced Radiation Sources), at the APS. Micro-XRF maps followed by micro-XANES spectra were collected in fluorescence mode with a solid-state 13-element solid state Ge detector and a double crystal monochromator; Si (111) and Si (311). The Se K-edge was calibrated to 12688.5 eV with sodium selenate. Prior to the analysis, soil samples were finely ground using an agate mortar and pestle in a N_2 filled glove box. To make thin sections, a tiny amount of powdered sample was homogeneously spread on a scotch tape. Unattached soil particles were carefully removed from the surface. Before taking samples out from the glove box, a piece of tape was used to cover and seal the thin section completely. Since the Se concentration was low (< 2 mg/kg) even after 100 days of feeding with the FGD wastewater, micro-XRF coarse mapping followed by sub mapping was performed to find where Se was exactly located. Two coarse maps per sample were generated over an area of 200 μm x 200 μm with 1 μm steps. Using the coarse XRF maps, area of interests (AOIs) (relatively high Se concentration) were used for micro-XRF sub maps. Selenium hotspots (brightest points) were selected on sub maps and micro-XANES spectra at the fluorescence mode were collected for more detailed information.

Results and Discussion

Characterization of FGD influent

Concentrations of constituents of FGD wastewater and raw water were measured to identify major components of the influent (Table 3.2). The 1:1 mixture of FGD wastewater: raw water was used as the influent throughout the experiment. The concentrations of As and Hg in the FGD wastewater used for this study was negligible as compared to those were recorded in previous studies (Eggert et al., 2008; EPRI, 2006; EPRI, 2007). The reason might be the differences in the coal materials, and the treatment processes used at the JEC to remove some constituents in the FGD wastewater. The composition of the FGD wastewater could significantly vary with power plants, batch, and source of coal utilized for energy generation. Among the trace elements, the concentration of Se was higher (255.3 µg/L) than As (3.1 µg/L), and Hg (8.2 µg/L). Also, the Se concentration in the FGD wastewater was greater than the acute level of Kansas surface water quality parameters (20 µg Se/L) (Tate, 2005). The B concentration of FGD wastewater was 6.4 mg/L. A high concentration of B (>0.2 mg/L) could potentially cause plant toxicity (Nable et al., 1997). The B concentration in the FGD wastewater exceeded the Kansas water quality parameter recommended for irrigation (0.75 mg/L). The F^- concentration of the wastewater was 20.5 mg/L and it was ten times greater than the Kansas irrigation water quality standard (2 mg/L). The concentrations of other constituents including total-S, Ca, Na, Cl^-, electrical conductivity and total dissolved solids were also at high levels. It can be expected that high salinity (EC>3 dS/m) of the FGD wastewater could change soil chemical properties over time (Essington, 2004). Water availability to plants and crops may decrease due to increased osmotic pressure caused by high salinity. Visual MINTEQ (Gustafsson, 2004) calculations

performed for water analysis data from the JEC (Table 6.2). The results indicated that FGD wastewater was supersaturated with respect to gypsum.

pH of effluents and soils

The pH of the original FGD wastewater and the raw water solutions was 8.4 and 8.6, respectively. When columns were initially fed with the FGD influent, the pH of effluent samples collected from the TS and the ES columns was 8.0 and 8.2, respectively. After around 0.5 PVs, the pH of effluent mostly remained alkaline for both TS (7.3-7.7) and ES (7.5-7.9) throughout the experiment. The original TS, and ES materials had pH 7.1, and 6.8, respectively, indicating that originally both soils were near neutral. Feeding with the FGD wastewater over 100 days resulted in changes of the soil pH (Table 6.3). The pH measurements indicated a slightly higher pH at the bottom section (inlet) of soil columns as compared to the top sections. This could most likely due to non-acidic salt accumulation (Essington, 2004) and/or on-going reductive dissolution reactions that consume protons (Ponnamperuma, 1972). An additional 100 days of flushing with the raw water affected slight changes of the soil pH. Overall, the soil pH of both TS and ES column systems was at around 8 over the study period. Maintaining near neutral to somewhat alkaline pH is a favorable factor for trace metal immobilization in wetlands (Gambrell, 1994).

Breakthrough curves (BTCs)

In this study, BTCs were generated to assess the behavior of the FGD wastewater constituents in the CWTS. The BTCs of Se, B, F^-, and Na are discussed here because of their dissimilar behavior in the soil columns. The concentration of Se in the influent wastewater that delivered into the soil columns was 128 µg/L. The concentration remained almost constant over the experimental period. The BTCs generated for Se (Figure 3.1a) indicated that Se in the

effluent water released from the both types of soil columns was below the detection limit (<0.2 µg/L). The results of the flushing experiment also showed that there was no detectable level of initially-retained Se came out from the columns, over an additional 100 days (Figure 3.2). These results implied that, regardless of the soil type, Se in the FGD wastewater was strongly (i.e., more or less irreversibly) retained by soil materials under reduced conditions. More than 90% efficient in removing Se from FGD wastewater was also reported by previous studies (Eggert et al., 2008; Wylie et al., 2008). The Se speciation of FGD wastewater (carried out by a commercial lab for JEC) showed higher concentration of Se(VI) (88.4%) than that of Se(IV) (10.7%). Under submerged conditions, Se(VI) is reduced into Se(IV) which leads to form irreversible inner-sphere complexes with oxy(hydr)oxy soil minerals and associates with organic phase, ultimately enhancing the stability (Peak et al., 2006; Peak, 2006). As the system gets further reduced, Se(IV) is transformed into Se(0) and Se(-II) (Masscheleyn and Patrick, 1993; Nakamaru and Altansuvd, 2014). Since the mobility of these species are relatively low, the reduction of Se promoted by microbially-mediated processes is an effective bioremediation technique for Se contaminated water (Fernández-Martínez and Charlet, 2009; Tang et al., 2015).

Partial retention of B and F^- occurred in the soil columns over the experimental period (Figure 3.1b). A mass balance calculation showed that TS and ES removed about 82.0 ± 1.3%, and 68.4 ±1.4% of B in the FGD wastewater, respectively. In this study, the alkaline pH should have facilitated B retention in the soils. Previous studies have found that B adsorption highly correlates with pH. An enhanced adsorption of B to soils was observed at pH 5.5 to 8.5 (Chen et al., 2009; Goldberg and Glaubig, 1986). In the current study, a significant amount of the initially-retained B, 81% from TS-2, and 85% from ES-2, came out by flushing with the raw water for an additional 100 days. Hence, the TS was able to retain only 19% and the ES were able to retain

only 15% of B in the FGD wastewater. Weakly adsorbed B, most likely due to the formation of outer-sphere complexes with soil can easily be leached out (i.e., exchanged by other ions) from sorption sites. (Peak et al., 2003). In this study, the TS showed greater capacity in retaining B from the FGD wastewater compared to the ES material. This could be explained by the compositional differences of the two materials. Previous studies have shown that sorption of B to soil is highly dependent upon the soil texture, pH, amount of clay, specific surface area, organic matter content of soils, and the complexation between humic acid (Elrashidi and O'connor, 1982; Goldberg et al., 2005; Gu and Lowe, 1990). Thus, high OM content and the CEC of the TS material may have influenced to a greater adsorption capacity for B.

The BTC generated for F^- (Figure 3.1c) indicated that at the beginning of the experiment (between 0 to 2 PVs) some of F^- in the FGD wastewater came out from the soil columns. After 2 PVs, the concentration of F^- of the effluent samples was not detectable (<0.1 mg/L). The mass balance calculation showed that about 92% of F^- in the FGD solution was removed by both TS and ES columns. The mobility of F^- depends upon the sorption capacity of soil which varies with pH, clay, and oxy(hydr)oxide minerals (Ozsvath, 2009). Weakly bound and exchangeable F^- ions to soil surfaces can easily be released by water flow. This could most likely be the reason for releasing F^- at the beginning of the study. Since there was no F^- released after 2 PVs, we presume here that fluorite (CaF_2) precipitation might have controlled the F^- concentration in the solution (Chae et al., 2006). Continuous-dissolution of Ca-bearing minerals and F^- supply with FGD wastewater can induce the formation of fluorite. The Visual MINTEQ calculation for effluent showed that solution was supersaturated with respect to fluorite at pH 8.0. Other studies have found that precipitation of fluorite is a main pathway of removing F^- from an aqueous phase (Fan et al., 2003; Turner et al., 2005). Thus, the mechanism of F^- retention in the CWTS may most

likely be due to the precipitation of fluorite. However, some of initially retained F^- was flushed out over an additional 100 days with the raw water; 22% and 33% from TS and ES, respectively. This could presumably be due to the solubility of precipitated fluorite upon the introduction of the raw water (Apambire et al., 1997). Therefore, the efficiency of F^- removal from the FGD influent solution was 78% by the TS and 67% by the ES. These results imply that some of the initially-retained FGD wastewater constituents such as B, and F^- can potentially be mobilized by flushing situations in the CWTS (i.e., feeding non-FGD weak salt solutions) in the CWTS.

As expected, the effluent BTC of Na had an early breakthrough (Figure 3.1d) in the both soils, indicating that Na retention in the CWTS was weak. After 1.8 PV of the ES and 2.7 PV of the TS, the relative concentration of Na was greater than one, most likely due to the release of exchangeable Na from soils. Once exchangeable Na leached out completely, the relative concentration of Na reached the level closer to one. The characteristics and the behavior of total-S, SO_4^{2-}-S, and Cl^- were also similar to the Na. Thus, the retention efficiency of these FGD wastewater constituents in the CWTS is expected to be low.

A pilot-scale CWTS at the JEC provided a unique opportunity to assess the behavior of FGD wastewater constituents under real field conditions (Talley, 2012). The removal efficiency of each constituent by the soil column system and the pilot-scale CWTS are presented in Table 3.3. The removal efficiencies of the flushed columns (TS-2 and ES-2) were used to compare the performance efficacy of the pilot-scale CWTS as those were more realistic for the field situation. The effectiveness of removing Se from the FGD wastewater by the soil columns was 100% whereas that of by the CWTS was 80%. We presume here that variations of field conditions may have influenced the Se removal. Since Se is a redox-sensitive element, drying and wetting conditions of soil at the field situation could potentially alter its behavior (Jayaweera and Biggar,

1996). From a follow up study, we observed that some of the initially-retained Se (~5%) was mobilized by changing oxidation/reduction conditions of soil (results not presented here). The efficiency of the B removal by the soil columns and by the CWTS was same. The soil columns showed a 67 to 78% effectiveness for F^- removal and the CWTS was 72% efficient for F^- removal from the FGD wastewater. These two systems were inefficient in removing relatively non-reactive constituents such as Cl^-, and SO_4^{2-}. Some of these constituents showed negative removal efficiency, indicating washing off of native soil constituents. In general, the results obtained from the soil column study were in good agreement with the CWTS, implying that continuous flow-through soil column system was able to successfully mimic the pilot-scale CWTS designed for the FGD wastewater treatment.

Distribution of Se in the soil columns

The total Se concentration of the TS and the ES materials was 298.3 µg/kg and 317.8 µg/kg, respectively. These concentrations are in the range of normal background soil concentration of Se (0.1 to 2 mg/kg) (Lindsay, 1979). According to the soil analysis results for the 100 days of FGD fed TS columns, most of Se fed with FGD wastewater accumulated in the bottom parts (inlet) of the soil columns (Figure 3.3). The total amount of Se retained in the sections of 1, 2, and 3 was 143.1±60.1 µg, 208.8±30.7 µg, and 7.2±10.3 µg, respectively and decreased from bottom to top. Retention of Se in the top sections was negligible, and it was more or less similar to the Se concentrations in the original soils. Thus, the mobility of Se within the CWTS is limited under reduced conditions. In the 100 days of FGD fed followed by 100 days of flushed TS column (Figure 3.3), the total amount of Se retention was 141.6 µg for section 1 (inlet), 203.3 µg for section 2, and 20.8 µg for section 3. Flushing with the raw water for an

additional 100 days did not significantly mobilize the initially-retained Se, which could support the evidence that Se sorbed onto soil surfaces in a manner that it was not easily exchangeable.

The Se distribution within the ES columns was slightly different compared to the TS columns. Most of the Se from the FGD wastewater primarily accumulated in the sections closed to the inlet, but there was a slight mobility to middle and upper sections (Figure 3.6). Sections 1, 2, and 3 of the ES columns yielded the highest Se accumulation and it was 76.7±0.8 µg, 131.0±39.6 µg, and 112.5±18.4 µg, respectively. Flushing with the raw water tended to mobilize some of the initially-retained Se to the middle portion of the ES column. This implies that the stability of retained Se in the ES material was not as strong as in the TS.

Selenium fractionation

As discussed above, the Se retention from the FGD influent was negligible in the upper sections of the columns. Furthermore, the total Se accumulated in section 3 of the TS columns was < 5%. Thus, SEP results of only sections 1 and 2 of the TS, and all three bottom sections of the ES columns are presented in Table 3.4 and Table 3.5. The Se phase of each fraction < 5% is also not included in the results. Selenium extracted by water (water soluble), exchangeable (KCl extractable), and P-buffer (ligand-exchangeable) fractions represents relatively mobile and bioavailable forms of Se whereas organically associated, elemental, recalcitrant organic and the residual fractions are the most stable Se forms (Kulp and Pratt, 2004; Oram et al., 2008; Sundberg-Jones and Hassan, 2007; Wright et al., 2003).

The results of SEP of the TS original material (Figure A.7) showed that less stable exchangeable and adsorbed Se constituted 58.3% of the total Se (Table 3.4). The more stable Se was in the range of 7.6 to 55.5%. Among the stable phases, the organically associated Se fraction was dominant. This implies that most of inherent Se is preferentially incorporated into the OM

(5.1% OM content) of the TS material. The greater amount of Se (78%) was extracted from the less stable phases in the ES original material (Figure A.7) whereas the most stable Se was 9.3 to 27.7% of the total Se (Table 3.5). It should be noted here that the ES is a mixture of topsoil, subsoil, sand, leafy-based compost.

According to the SEP results of the 100 days of FGD fed TS (Figure 3.5), the total amount of extracted Se in the soluble fraction was 30.1% and 21.0% for section 1 and section 2, respectively (Table 3.4). The exchangeable fraction of both sections was negligible, which could imply that there was no easily exchangeable Se accumulated from the FGD wastewater. From the total amount of Se retained in sections 1 and 2, respectively 43.8% and 47.3% represented the most stable residual fraction, clearly indicating as the dominant fraction (Figure 3.5). The rest of accumulated Se (40.2 to 45.2%) in each section was distributed among the other stable fractions. The Se phase associated with the soil OM can be extracted by NaOH whereas NaOCl oxidizing agent can be used to extract recalcitrant organic forms. Thus, 13.8% (section 1), and 15.8% (section 2) constituted to the total amount of organically-bound Se (Table 3.4). In addition to the recalcitrant organic Se forms, stable selenide phase can also possible to be recovered by the NaOCl extraction step (Wright et al., 2003). The total amount of mobile phases of Se extracted from the 100 days of FGD fed followed by 100 days of flushed TS was 28.6% and 31.5% in sections 1 and 2, respectively (Table 3.4). The sequestration of accumulated Se in the residual fraction of these sections was considerably decreased (about 27%) upon flushing with the raw water. Although yet showing the stability, this implies that some of initially-sequestered Se in the most stable fraction was redistributed among the other stable fractions (Figure 3.3).

The Se fractionation of the ES columns was different from that of the TS columns (Figure 3.4). The total amount of less stable Se fractions were considerably high and they were

44.4%, 45%, and 50.6%, respectively in sections 1, 2, and 3 of the ES columns fed with the FGD wastewater for 100 days (Table 3.5). The greater amount of the accumulated Se dominant in the less stable fractions shows the instability of Se retention in the ES compared to the TS. The rest of the accumulated Se (49.4 to 55.6%) was distributed among the other stable phases. Among those, the organically-bound Se forms were dominated. The combination of the organically associated and the recalcitrant organic fractions was 66.7% for section 1, 45.0% for section 2, and 50.0% for section 3 (Table 3.5). The organic matter added as leafy compost to the ES starting material may have contributed to retaining Se from the FGD wastewater. Neither of these sections did indicate that Se was sequestered in the residual fraction. Although the accumulated Se was slightly mobilized upon flushing with the raw water, the remaining portion of Se in section 1 was strongly sequestered in the residual fraction (Table 3.5). The Se which was mobilized to sections 2 and 3 was further transported to the upper sections, most likely due to the instability of retained Se in the ES material (Figure 3.6).

Selenium solid state speciation using synchrotron-based XANES

The bulk-XANES spectra of Se standards clearly showed that Se K-edge energy shifts with changing the oxidation state (Figure 3.7). The edge energy of Se compounds varies in the following order: sodium selenate> sodium selenite> seleno-DL-cystine > elemental Se> Se sulfide, Fe(II) selenide (Table 3.6). The LCF results of the TS original material showed that Se was present in the forms of Se(IV) (48.5%), and organic Se (51.5%) (Figure 3.8). This is in accordance with the results of SEP. The presence of reduced Se species in the inherent material suggests that Se is stable even prior to the submergence. After 100 days of feeding with the FGD wastewater, Se was mainly present as Se(IV) (68%), and Se(0) (32%) (Table 3.7). Thus, Se fed with the FGD wastewater was transformed to reduced and stable forms under reduced soil

conditions. Both Se-XANES and SEP data were in good agreement and showed accumulated Se existed as most stable forms. The Se speciation of the soil which was under the submergence for 200 days (FGD fed followed by 100 days of flushing) also predominated by Se(IV) (40%) and Se(0) (60%) (Figure 3.8). The amount of Se(0) significantly increased as opposed to the soil which was under 100 days of submergence. This suggests that a long submergence period or a long residence time of the CWTS would enhance further reduction of Se, ultimately hindering its mobility and bioavailability. The bulk-XANES speciation of sulfur also showed reduced S species (53%), intermediate S (8%), and oxidized S (39%) represented in the flushed TS whereas larger proportion (95%) dominated as oxidized S in the 100 days of submerged soil. Thus, a prolong period of submergence could eventually enhance the Se sequestration due to the coupling with biogeochemical cycling of S (Hockin and Gadd, 2003; Nakamaru and Altansuvd, 2014). Previous studies on Se speciation in constructed wetland systems used for treating agricultural drainage water also showed that Se(VI) was transformed to a mixture of Se(IV), Se(0), and organic Se (Lin and Terry, 2003). Myneni et al. (1997) predicted that Se(VI) is reduced to Se(0) in the presence of green rust. In the current study, green rust was identified in the TS columns by Fe bulk-XANES analysis. Green rust is a mixture of Fe(II), and Fe(III) minerals that predominately occurs in suboxic soil environments (Myneni et al., 1997; Refait et al., 2000). The LCF results of the ES (Figure 3.9) showed that Se in the original material was present as Se(IV) (67%) and organic Se (33%). After 100 days of feeding with the FGD wastewater, the speciation of accumulated Se in the ES did not significantly change and it mainly remained as Se(IV) and organic Se (Table 3.7). The SEP data also showed organically associated Se was the dominant form in the ES. The accumulated Se in the 100 days of FGD fed followed by 100 days of flushed ES also existed as Se(IV) (49%) and organic Se (51%). This indicates

that prolonged submergence enhances the association of Se with organic substances in the CWTS added with compost.

X-ray microprobe techniques are well-suited for identifying the spatial distribution of Se and its chemical speciation in a spatially resolved manner. Micro-XRF mapping (Figure 3.10) can provide better detection limits, high sensitivity, and indirect evidence of the presence and distribution of specific minerals and their correlations at microscale (Lombi and Susini, 2009; Lombi et al., 2011). Additionally, integration of micro-XANES with micro-XRF elemental maps is a powerful approach to recognize minor species which may not have identified by the bulk-XANES. In the current study, micro-XRF fallowed by micro-XANES analyses were performed only for soil samples collected from TS columns due to limited beam time availability.

The spatial distribution of Fe, and Mn along with Se was investigated to assess their interrelationships (Figure 3.11and Figure 3.12). The Se micro-XRF maps of both scenarios indicated that sequestered Se in soil was heterogeneously distributed within the sample area selected for mapping. The distribution of high intense Se spots was limited to a very few locations in the images. This could most likely be due to the relatively low concentration of Se in the soil. On the other hand, several hotspots of Fe were scattered throughout the micro-XRF maps because the concentration of Fe was high compared to Se, and Mn in the soil (Figure 3.11and Figure 3.12). The correlations between Se, Fe, and Mn ranged from nonexistent to weak although they were significant ($p<0.05$), in some cases (Figure A.8). The weaker correlation could partly be due to the low concentration of Se and Se was sparsely distributed within the area chosen for mapping. The highest Se-Fe correlation was found in the AOI-1, and AOI-4 (Figure A.9). In these areas, Se was appeared to be associated with Fe and S (Figure 3.13), which

indirectly implies that Se might be precipitated/co-precipitated with Fe minerals (such as oxides/sulfides).

The speciation of Se analyzed by micro-XANES also revealed that Se(IV) and Se(0) were the dominant species, which further confirms the results from bulk-XANES. In the P1 and P2 hotspots on the 100 days of FGD fed TS, the Se(IV) was 77.6 to 81.3% and the Se(0) was 22.4 to 18.7% (Figure 3.14). The micro-XANES speciation of P3 and P4 on the 100 days of FGD fed followed by 100 days of flushed TS (Figure 3.15) also constituted the reduced and stable Se(IV) (64.5 to 91%), and Se(0) (9 to 35.5%). Additionally, more reduced features on the Se K-edge can visually be seen on the XANES spectra of P3 and P4 in which soil was under 200 days of submergence (Figure 3.15). This is further confirming that long submergence will enhance the reduction of Se accumulated further, resulting in strong retention in the CWTS.

The integration of bulk-, and micro-XANES results provided direct evidence for the presence of stable Se(IV), Se(0), and organic Se species in the soils treated with the FGD wastewater. These observations are beneficial to better understand the retention mechanism of Se in the CWTS. Since the mobility, and the bioavailability of reduced Se forms are low compared to the oxidized forms [i.e., Se(VI)], the transport of Se within the CWTS is minimum. Therefore, the transformation of oxidized Se in the FGD wastewater to reduced/stable forms under the wetland conditions can retard the mobility and its detrimental effects on humans and the environment.

Conclusions

There was no detectable level of the Se in the FGD wastewater released over the study period. This suggests us that Se had a strong retention in the soils under reduced/wetland conditions. Some of the constituents of FGD wastewater such as B and F^- partially retained in the

CWTS whereas the retention capacity of S, Na and Cl^- was weak. This confirms the fact that CWTSs are highly effective for removing Se from FGD wastewater. The Se delivered to the soils accumulated in the bottom parts (inlet) of the soil columns, indicating that the mobility of Se within the CWTS is minimum and the wetland cells are not fully "saturated with Se". The results from the SEP, bulk-XANES, and micro-XRF fallowed by micro-XANES analyses were in good agreement. The integration of these data suggested that the mechanism of Se retention in the CWTS was mainly via the transformation of oxidized Se into reduced/stable forms. Our results also showed that prolong period of submergence of the CWTS would enhance the stability of retained Se. Understanding the behavior of the FGD wastewater constituents and their retention mechanisms using a laboratory-scale soil column study was beneficial to enhance the performance efficiency of a full-scale CWTS.

Acknowledgements

We acknowledge the funding support of this study by Westar Energy, Burns & McDonnell, and Kansas Agricultural Experimental Station. We want to thank MRCAT operations which are supported by the Department of Energy and the MRCAT member institutions. GeoSoilEnviroCARS is supported by the National Science Foundation - Earth Sciences (EAR-1128799) and Department of Energy- GeoSciences (DE-FG02-94ER14466). This research used resources of the Advanced Photon Source, a U.S. Department of Energy (DOE) Office of Science User Facility operated for the DOE Office of Science by Argonne National Laboratory under Contract No. DE-AC02-06CH11357.We would like to thank to Dr. Deon Van der Merwe and Lori Blevins at Veterinary Diagnostic Laboratory, Kansas State University for providing assistance with the ICP-MS analysis, and Ranju R. Karna for helping with the XAS data collection.

References

Apambire, W., D. Boyle and F. Michel. 1997. Geochemistry, genesis, and health implications of fluoriferous groundwaters in the upper regions of Ghana. Environ. Geol. 33:13-24.

Budd, R., A. O'Geen, K.S. Goh, S. Bondarenko and J. Gan. 2009. Efficacy of constructed wetlands in pesticide removal from tailwaters in the central valley, California. Environ. Sci. Technol. 43:2925-2930.

Chae, G., S. Yun, M. Kwon, Y. Kim and B. Mayer. 2006. Batch dissolution of granite and biotite in water: Implication for fluorine geochemistry in groundwater. Geochem. J. 40:95-102.

Chen, W., S. Ho and D. Lee. 2009. Effect of pH on boron adsorption-desorption hysteresis of soils. Soil Sci. 174:330-338.

Combs, S.M. and M.V. Nathan. 1998. Soil organic matter. p. 53-58. *In* Recommended chemical soil test procedures for the north central region. Missouri Ag. Exp. Stn. SB 1001, Colombia, MO.

Dean A. Martens and Donald L. Suarez. 1997. Selenium speciation of soil/ sediment determined with sequential extractions and hydride generation atomic absorption spectrophotometry. 31:133.

Díaz, F.J., A.T. O′Geen and R.A. Dahlgren. 2012. Agricultural pollutant removal by constructed wetlands: Implications for water management and design. Agric. Water Manage. 104:171-183.

Eggert, D.A., J.H. Rodgers Jr, G.M. Huddleston and C.E. Hensman. 2008. Performance of pilot-scale constructed wetland treatment systems for flue gas desulfurization waters. Environmental Geosciences 15:115-129.

Elrashidi, M. and G. O'connor. 1982. Boron sorption and desorption in soils. Soil Sci. Soc. Am. J. 46:27-31.

EPRI. 2006. Guidance for assessing wastewater impacts of FGD scrubbers. Technical manual. Rep. 1013313. Electric Power Research Institute, Palo Alto, CA.

EPRI. 2007. Treatment technology summary for critical pollutants of concern in power plant wastewaters. Rep. 1012549. Electric Power Research Institute, Palo Alto, CA.

Essington, M.E. 2004. Soil and water chemistry: An integrative approach. CRC press, Boca Raton, FL.

Fan, X., D.J. Parker and M.D. Smith. 2003. Adsorption kinetics of fluoride on low cost materials. Water Res. 37:4929-4937.

Fernández-Martínez, A. and L. Charlet. 2009. Selenium environmental cycling and bioavailability: A structural chemist point of view. Reviews in Environmental Science and Bio/Technology 8:81-110.

Fordyce, F. 2007. Selenium geochemistry and health. Ambio. 36:94-97.

Fordyce, F.M. 2013. Selenium deficiency and toxicity in the environment. p.375-416. *In* O. Selinus (ed.) Essentials of medical geology. Springer. Netherlands.

Gambrell, R. 1994. Trace and toxic metals in wetlands—a review. J. Environ. Qual. 23:883-891.

Gao, S., K. Tanji, D. Peters and M. Herbel. 2000. Water selenium speciation and sediment fractionation in a california flow-through wetland system. J. Environ. Qual. 29:1275-1283.

Goldberg, S. and R. Glaubig. 1986. Boron adsorption on California soils. Soil Sci. Soc. Am. J. 50:1173-1176.

Goldberg, S., D. Corwin, P. Shouse and D. Suarez. 2005. Prediction of boron adsorption by field samples of diverse textures. Soil Sci. Soc. Am. J. 69:1379-1388.

Greenberg, A.E., Clesceri, L.S., and Eaton, A.D. 1992. Solids. p. 2-53-2-55. *In* Eugene W. Rice (ed.) Standard methods for the examination of water and wastewater. 18th ed. APHA, Washington, DC.

Gu, B. and L. Lowe. 1990. Studies on the adsorption of boron on humic acids. Can. J. Soil Sci. 70:305-311.

Gustafsson, J.P. 2004. Visual MINTEQ. Ver. 3.1. Royal Institute of Technolog, KTH, Sweden.

Hammer, D.A. 1989. Constructed wetlands for wastewater treatment: Municipal, industrial and agricultural. CRC Press, FL .

Hansen, D., P.J. Duda, A. Zayed and N. Terry. 1998. Selenium removal by constructed wetlands: Role of biological volatilization. Environ. Sci. Technol. 32:591-597.

Hockin, S.L. and G.M. Gadd. 2003. Linked redox precipitation of sulfur and selenium under anaerobic conditions by sulfate-reducing bacterial biofilms. Appl. Environ. Microbiol. 69:7063-7072.

Jayaweera, G.R. and J.W. Biggar. 1996. Role of redox potential in chemical transformations of selenium in soils. Soil Sci. Soc. Am. J. 60:1056-1063.

Kadlec, R.H. and S. Wallace. 2008. Treatment wetlands. CRC press, FL.

Kulp, T.R. and L.M. Pratt. 2004. Speciation and weathering of selenium in upper cretaceous chalk and shale from south dakota and wyoming, USA. Geochim. Cosmochim. Acta 68:3687-3701.

Lin, Z. and N. Terry. 2003. Selenium removal by constructed wetlands: Quantitative importance of biological volatilization in the treatment of selenium-laden agricultural drainage water. Environ. Sci. Technol. 37:606-615.

Lindsay, W.L. 1979. Chemical equilibria in soils. Wiley, NY.

Lombi, E. and J. Susini. 2009. Synchrotron-based techniques for plant and soil science: Opportunities, challenges and future perspectives. Plant Soil 320:1-35.

Lombi, E., M. De Jonge, E. Donner, C. Ryan and D. Paterson. 2011. Trends in hard X-ray fluorescence mapping: Environmental applications in the age of fast detectors. Analytical and Bioanalytical Chemistry 400:1637-1644.

Masscheleyn, P.H. and W.H. Patrick. 1993. Biogeochemical processes affecting selenium cycling in wetlands. Environmental Toxicology and Chemistry 12:2235-2243.

Masscheleyn, P.H., R.D. Delaune and W. Patrick. 1991. Arsenic and selenium chemistry as affected by sediment redox potential and pH. J. Environ. Qual. 20:522-527.

Masscheleyn, P.H., R.D. Delaune and W.H. Patrick Jr. 1990. Transformations of selenium as affected by sediment oxidation-reduction potential and pH. Environ. Sci. Technol. 24:91-96.

Mooney, F.D. and C. Murray-Gulde. 2008. Constructed treatment wetlands for flue gas desulfurization waters: Full-scale design, construction issues, and performance. Environmental Geosciences 15:131-141.

Myneni, S., T.K. Tokunaga and G. Brown. 1997. Abiotic selenium redox transformations in the presence of fe (II, III) oxides. Science 278:1106-1109.

Nable, R.O., G.S. Bañuelos and J.G. Paull. 1997. Boron toxicity. Plant Soil 193:181-198.

Nakamaru, Y.M. and J. Altansuvd. 2014. Speciation and bioavailability of selenium and antimony in non-flooded and wetland soils: A review. Chemosphere 111:366-371.

Oram, L.L., D.G. Strawn, M.A. Marcus, S.C. Fakra and G. Möller. 2008. Macro-and microscale investigation of selenium speciation in blackfoot river, idaho sediments. Environ. Sci. Technol. 42:6830-6836.

Ozsvath, D.L. 2009. Fluoride and environmental health: A review. Reviews in Environmental Science and Bio/Technology 8:59-79.

Peak, D. 2006. Adsorption mechanisms of selenium oxyanions at the aluminum oxide/water interface. J. Colloid Interface Sci. 303:337-345.

Peak, D., U. Saha and P. Huang. 2006. Selenite adsorption mechanisms on pure and coated montmorillonite: An EXAFS and XANES spectroscopic study. Soil Sci. Soc. Am. J. 70:192-203.

Peak, D., G.W. Luther and D.L. Sparks. 2003. ATR-FTIR spectroscopic studies of boric acid adsorption on hydrous ferric oxide. Geochim. Cosmochim. Acta 67:2551-2560.

Pickering, I.J., G.E. Brown and T.K. Tokunaga. 1995. Quantitative speciation of selenium in soils using X-ray absorption spectroscopy. Environ. Sci. Technol. 29:2456-2459.

Ponnamperuma, F. 1972. The chemistry of submerged soils. Academic Press NY and London, .

Premarathna, H.L., M.J. McLaughlin, J.K. Kirby, G.M. Hettiarachchi, D. Beak, S. Stacey and D.J. Chittleborough. 2010. Potential availability of fertilizer selenium in field capacity and submerged soils. Soil Sci. Soc. Am. J. 74:1589-1596.

Rahman, K.Z., A. Wiessner, P. Kuschk, M. van Afferden, J. Mattusch and R.A. Müller. 2011. Fate and distribution of arsenic in laboratory-scale subsurface horizontal-flow constructed wetlands treating an artificial wastewater. Ecol. Eng. 37:1214-1224.

Ravel, á. and M. Newville. 2005. ATHENA, ARTEMIS, HEPHAESTUS: Data analysis for X-ray absorption spectroscopy using IFEFFIT. Journal of Synchrotron Radiation 12:537-541.

Refait, P., L. Simon and J.R. Génin. 2000. Reduction of SeO_4^{2-} anions and anoxic formation of iron (II)-iron (III) hydroxy-selenate green rust. Environ. Sci. Technol. 34:819-825.

Sahrawat, K. 2005. Fertility and organic matter in submerged rice soils. Curr. Sci. 88:735-739.

Skaggs, T.H., G.V. Wilson, P.J. Shouse and F.J. Leij. 2002. 6.4 solute transport: Experimental methods. p. 1381-1402. *In* Dane, Jacob H. Topp, Clarke G. (ed.) Methods of soil analysis: Part 4 physical methods. SSSA Book Series 5.4 ed. Soil Science Society of America, .

Srivastava, R.K., W. Jozewicz and C. Singer. 2001. SO_2 scrubbing technologies: A review. Environ. Prog. 20:219-228.

Su, C. and D.L. Suarez. 2000. Selenate and selenite sorption on iron oxides an infrared and electrophoretic study. Soil Sci. Soc. Am. J. 64:101-111.

Sundberg-Jones, S.E. and S.M. Hassan. 2007. Sediment-associated elements in a constructed wetland treatment system: Distribution, characterization, and toxicity. Bioremediation, Biodiversity and Bioavailability 1:41-55.

Talley, M.K. 2012. Analysis of a pilot-scale constructed wetland treatment system for flue gas desulfurization wastewater. M.S. Thesis. Kansas State University, KS.

Tang, Y., C.J. Werth, R.A. Sanford, R. Singh, K. Michelson, M. Nobu, W. Liu and A.J. Valocchi. 2015. Immobilization of selenite via two parallel pathways during in situ bioremediation. Environ. Sci. Technol. 49:4543-4550.

Tate, M. 2005. Kansas water quality standards and supporting documents. Kansas Department of Health and Environment, Topeka, Kansas.

Taylor, M.R., E.S. Rubin and D.A. Hounshell. 2005. Control of SO_2 emissions from power plants: A case of induced technological innovation in the US. Technological Forecasting and Social Change 72:697-718.

Turner, B.D., P. Binning and S. Stipp. 2005. Fluoride removal by calcite: Evidence for fluorite precipitation and surface adsorption. Environ. Sci. Technol. 39:9561-9568.

Wright, M.T., D.R. Parker and C. Amrhein. 2003. Critical evaluation of the ability of sequential extraction procedures to quantify discrete forms of selenium in sediments and soils. Environ. Sci. Technol. 37:4709-4716.

Wylie, R., R. Baker, W. Kennedy, M. Riffe, B. Heimbigner and T. Pickett. 2008. Duke energy carolina LLC's strategy and initial experience of FGD waste water treatment systems. *In* Duke energy carolina LLC's strategy and initial experience of FGD waste water treatment systems. San Antonio, Texas. October 2008.

Ye, Z., Z. Lin, S. Whiting, M. De Souza and N. Terry. 2003. Possible use of constructed wetland to remove selenocyanate, arsenic, and boron from electric utility wastewater. Chemosphere 52:1571-1579.

Ye, Z., S. Whiting, J. Qian, C. Lytle, Z. Lin and N. Terry. 2001. Trace element removal from coal ash leachate by a 10-year-old constructed wetland. J. Environ. Qual. 30:1710-1719.

Yeh, T. 2008. Removal of metals in constructed wetlands: Review. Pract. Periodical Hazard. , Toxic, Radioact. Waste Manage. 12:96-101.

Zhang, Y. and J.N. Moore. 1997. Reduction potential of selenate in wetland sediment. J. Environ. Qual. 26:910-916.

Zhang, Y. and J.N. Moore. 1996. Selenium fractionation and speciation in a wetland system. Environ. Sci. Technol. 30:2613-2619.

Zhang, Y., J.N. Moore and W.T. Frankenberger. 1999. Speciation of soluble selenium in agricultural drainage waters and aqueous soil-sediment extracts using hydride generation atomic absorption spectrometry. Environ. Sci. Technol. 33:1652-1656.

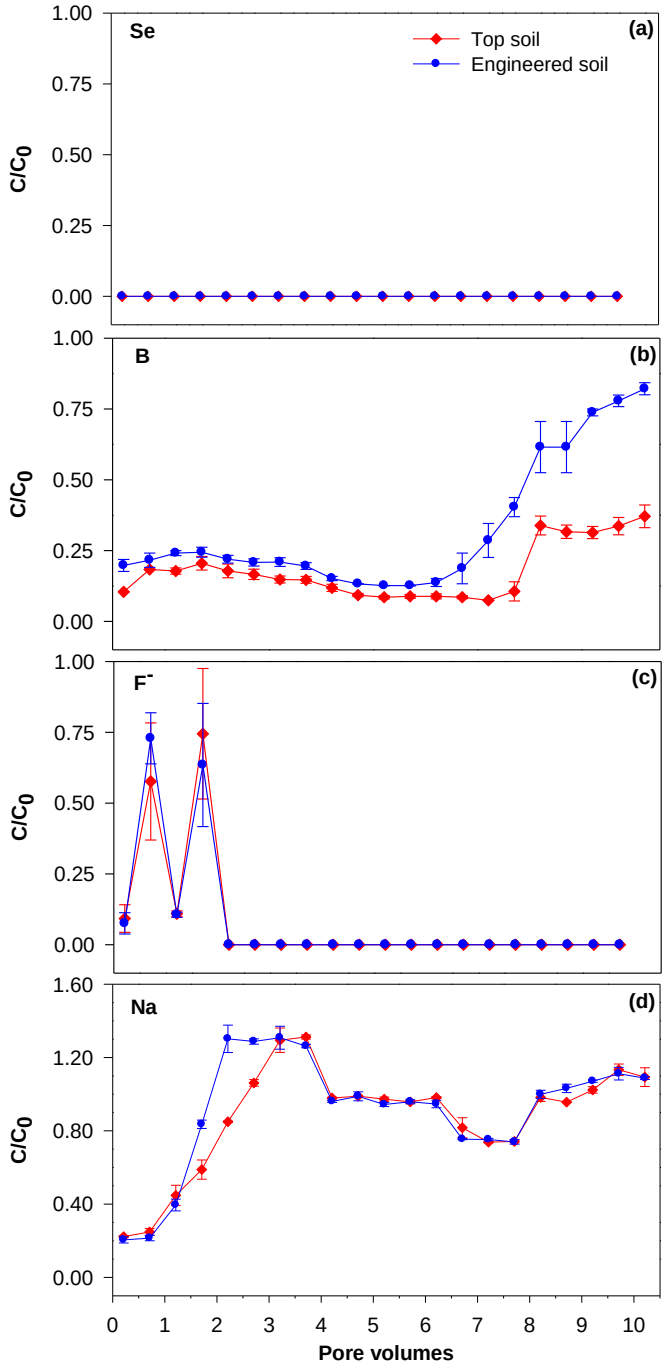

Figure 3.1 Breakthrough curves; (a) selenium (Se), (b) boron (B), (c) fluoride (F^-), and (d) sodium (Na) after 100 days of feeding with FGD wastewater. Here, C is the effluent concentration and C_0 is the influent concentration of constituents.

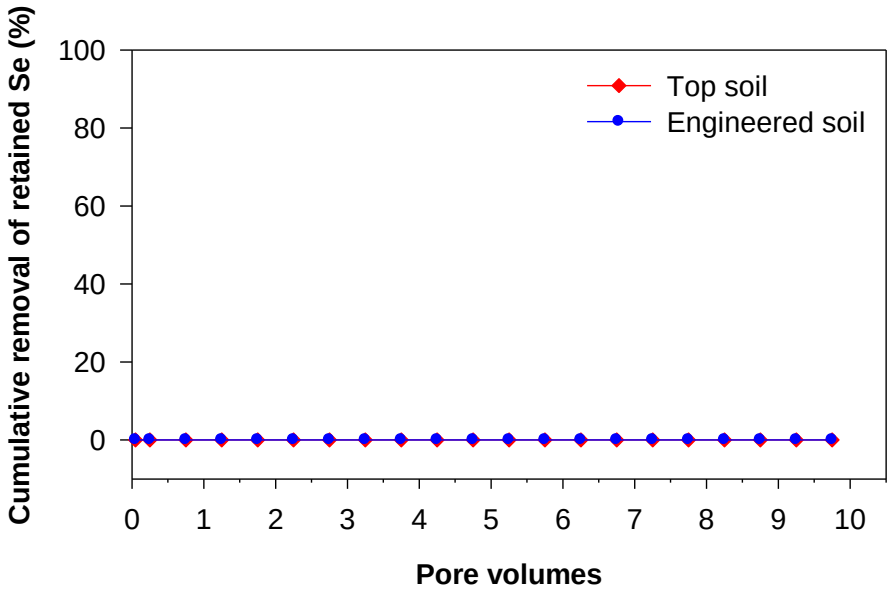

Figure 3.2 Cumulative removal of initially-retained Se from the topsoil, and engineered soil columns by flushing with the raw water for an additional 100 days.

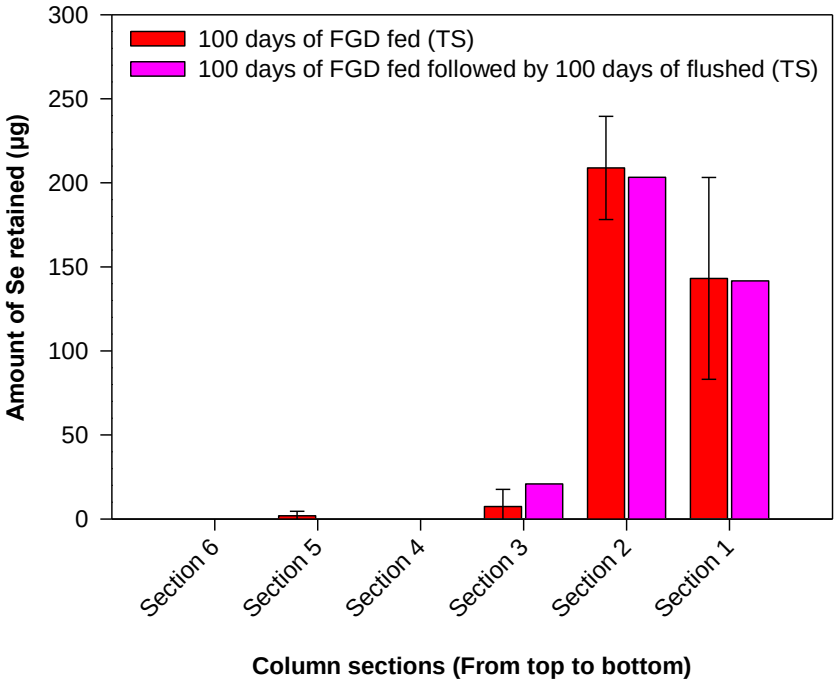

Figure 3.3 Distribution of Se of FGD wastewater in the topsoil (TS) columns for 100 days of FGD fed and, 100 days of FGD fed followed by 100 days of flushed. Error bars represent standard error of two columns.

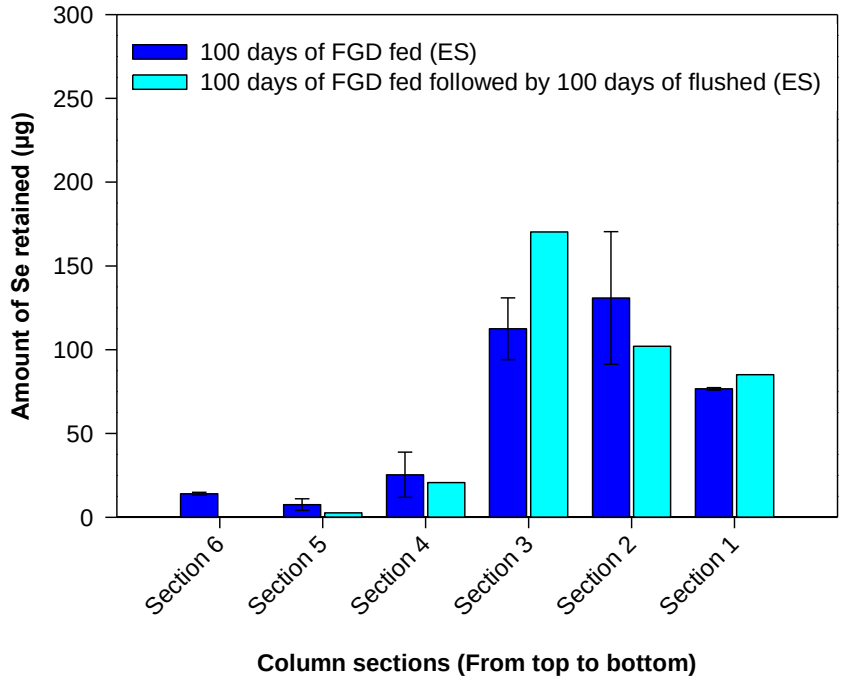

Figure 3.4 Distribution of Se of FGD wastewater in the engineered soil (ES) columns for 100 days of FGD fed and, 100 days of FGD fed followed by 100 days of flushed. Error bars represent standard error of two columns.

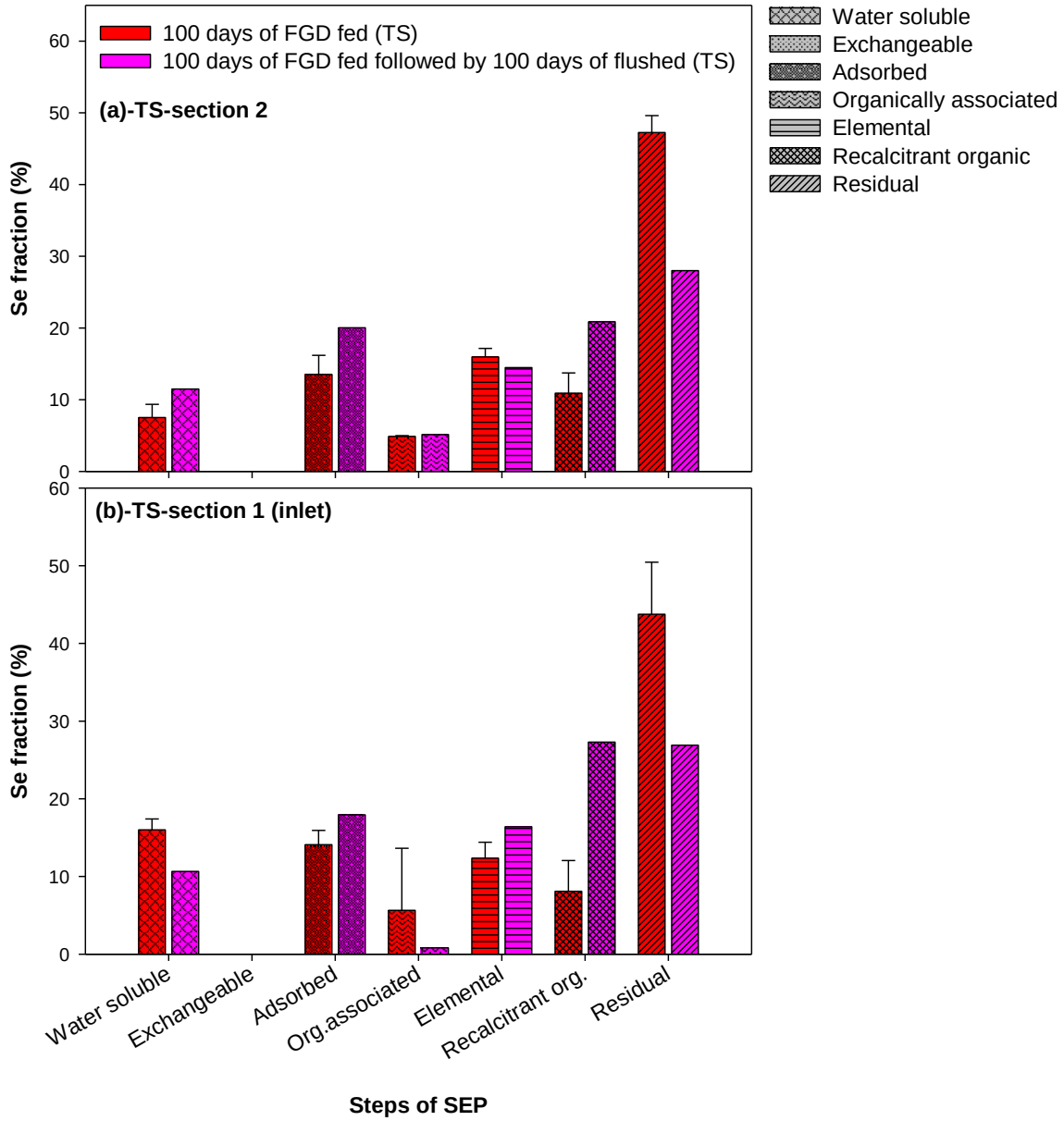

Figure 3.5 Fractionation of accumulated Se of the 100 days of FGD fed, and the 100 days of FGD fed followed by 100 days of flushed topsoil (TS) columns; (a) TS-section 2, and (b) TS-section 1 (inlet). Error bars represent standard error of two columns.

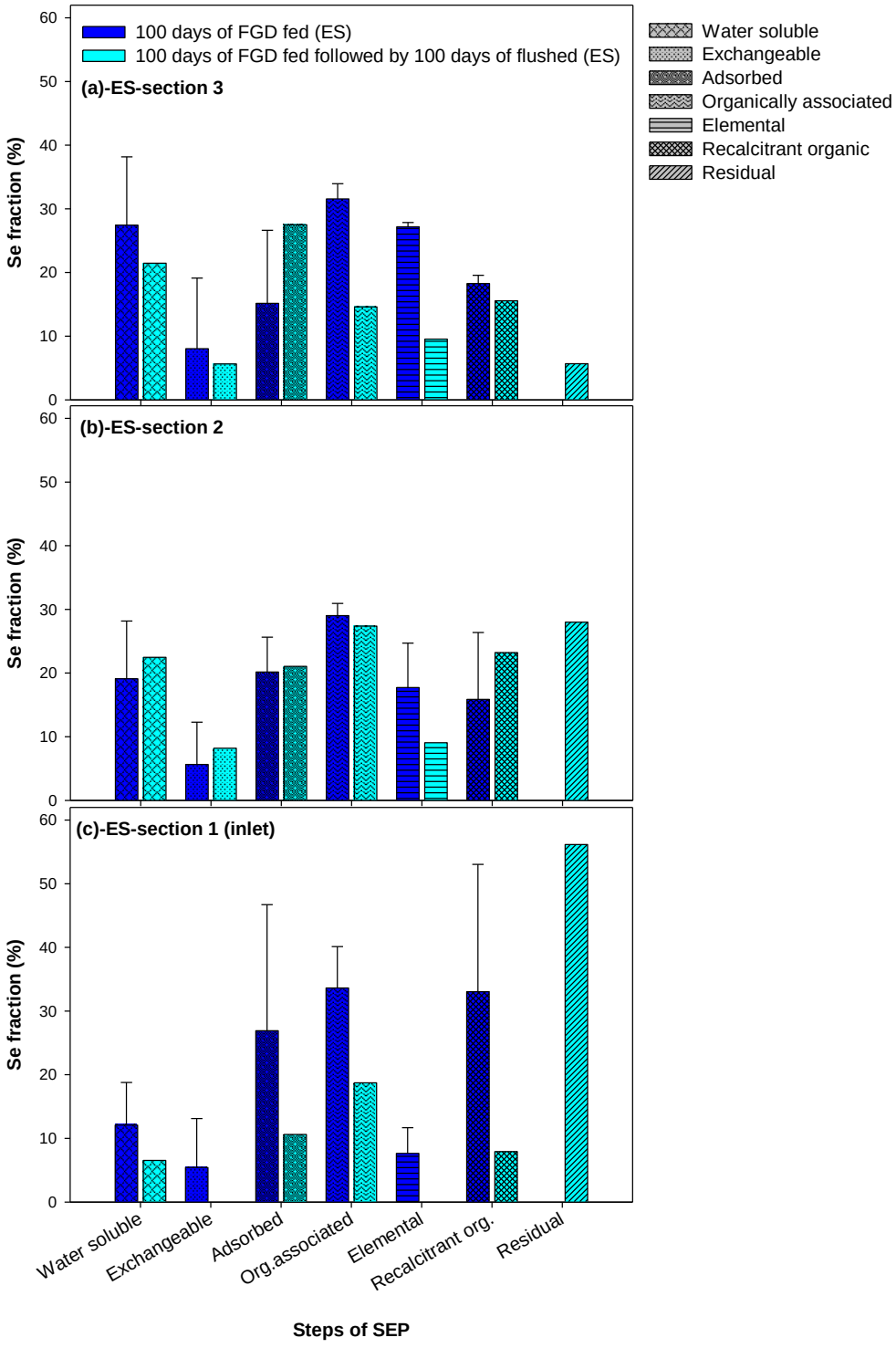

Figure 3.6 Fractionation of accumulated Se of the 100 days of FGD fed, and the 100 days of FGD fed followed by 100 days of flushed engineered soil (ES) columns; (a) ES-section 3, (b) ES-section 2, and (c) ES-section 1(inlet). Error bars represent standard error of two columns.

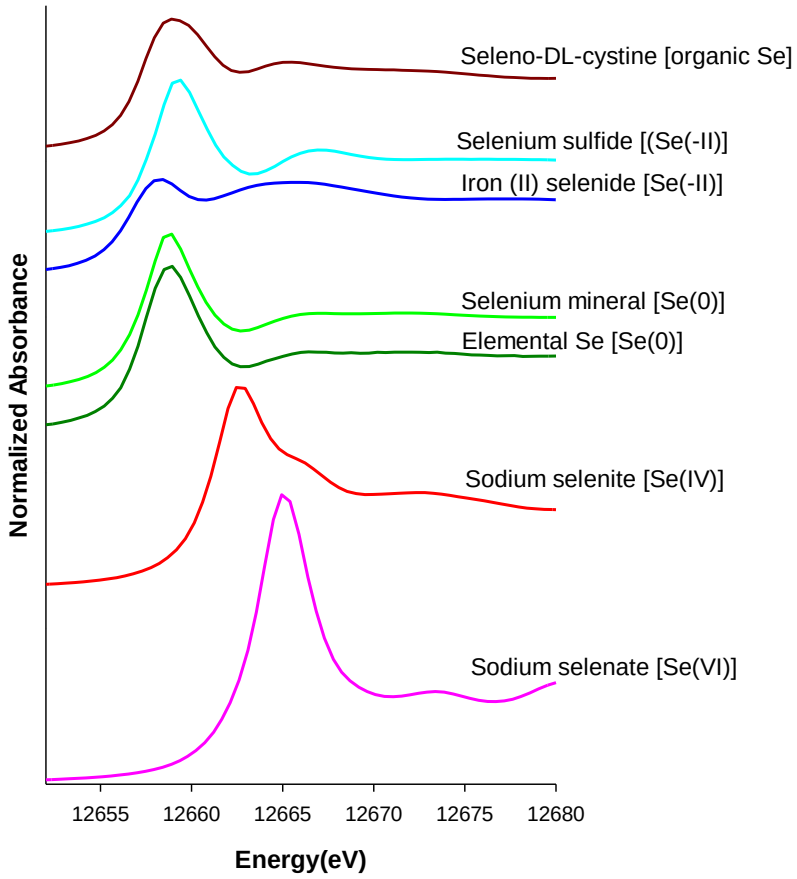

Figure 3.7 Selenium XANES spectra of standards used for linear combination fitting (LCF) analysis.

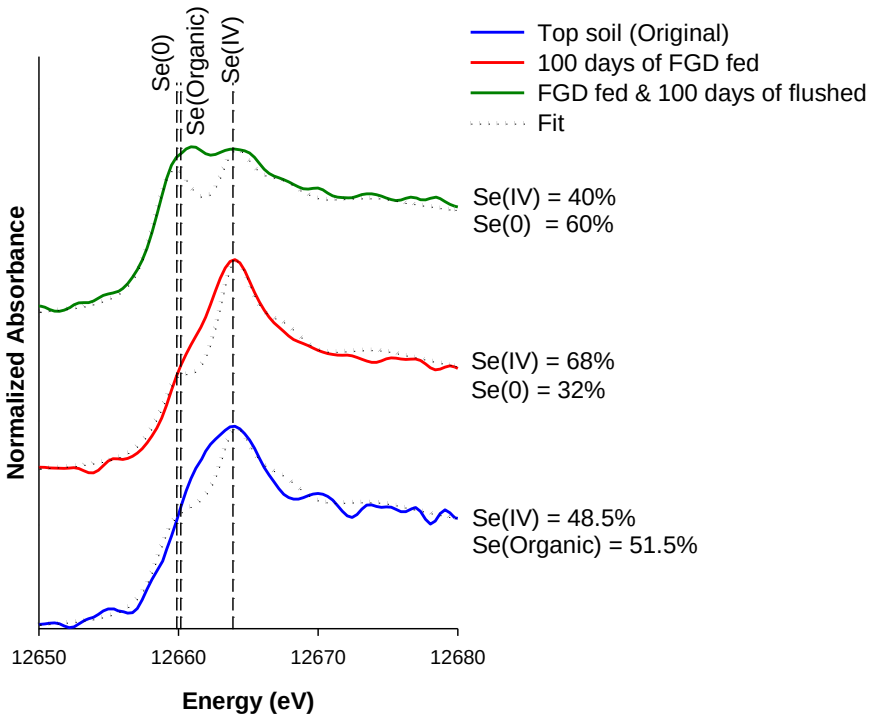

Figure 3.8 Selenium bulk-XANES collected for the topsoil (original), 100 days of FGD fed, and 100 days of FGD fed fallowed by 100 days of flushed soil. Solid lines represent the normalized spectra and the dotted lines represent the best fits by LCF. Vertical short-dashed lines to represent white line energies of Se(IV) (12664.0 eV), organic-Se (12660.1 eV), and Se(0) (12659.9 eV).

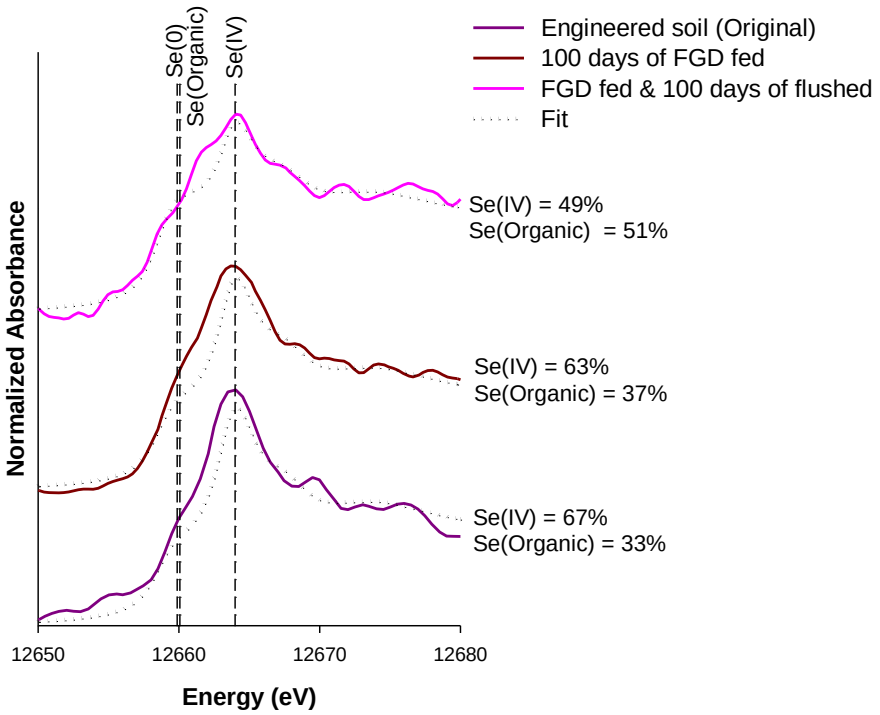

Figure 3.9 Selenium bulk-XANES collected for the engineered soil (original), 100 days of FGD fed, and 100 days of FGD fed fallowed by 100 days of flushed. Solid lines represent the normalized spectra and the dotted lines represent the best fits obtained by LCF. Vertical short-dashed lines to represent white line energies of Se(IV) (12664.0 eV), organic-Se (12660.1 eV), and Se(0) (12659.9 eV).

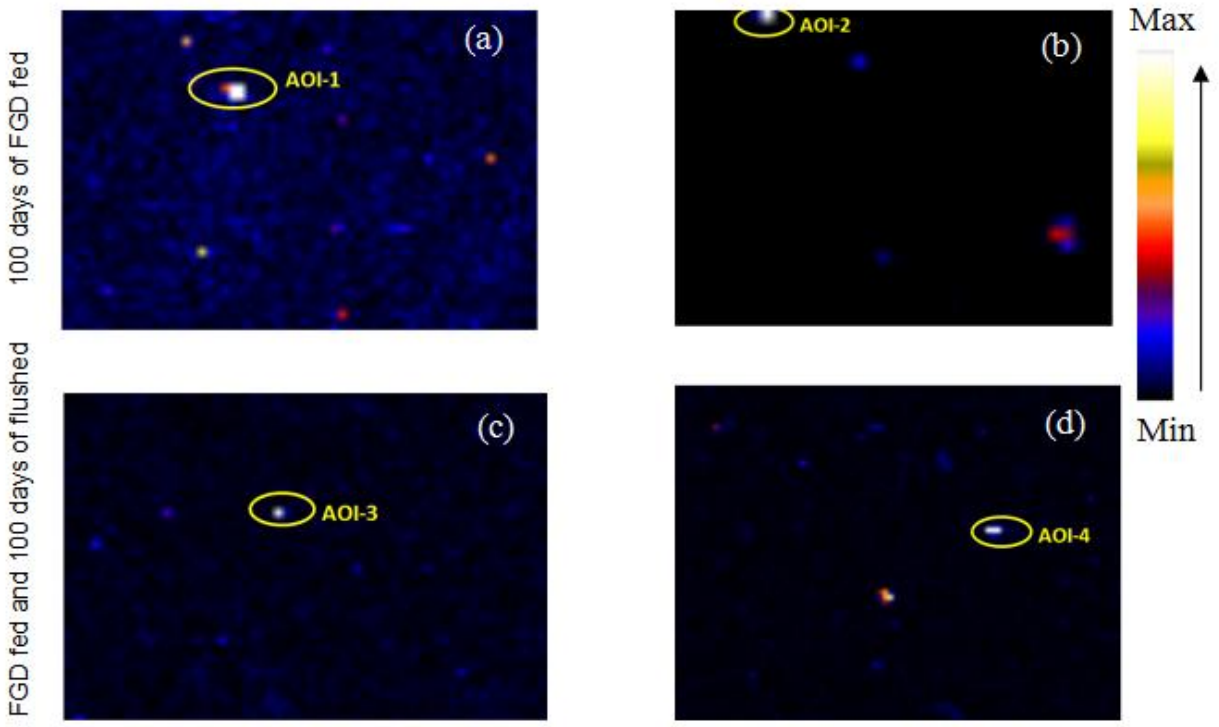

Figure 3.10 Selenium micro-XRF coarse maps for the topsoil of 100 days of FGD fed (a and b), and the 100 days of FGD fed fallowed by 100 days of flushed (c and d). Area of Interest (AOI) on coarse maps of each sample was used to generate micro-XRF sub maps.

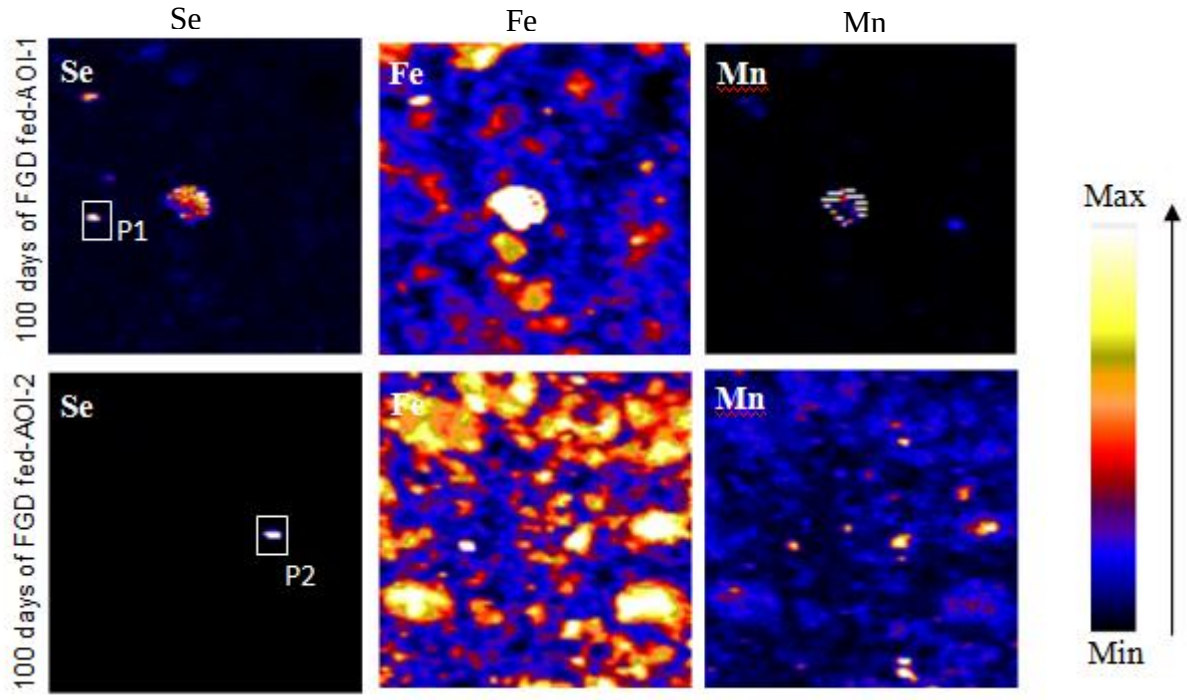

Figure 3.11 Micro-XRF maps showing the elemental distribution of selenium (Se), iron (Fe), and manganese (Mn) generated from the areas of interest, AOI-1 and AOI-2, on the 100 days of FGD fed topsoil. P1 and P2 are Se hotspots used for micro-XANES.

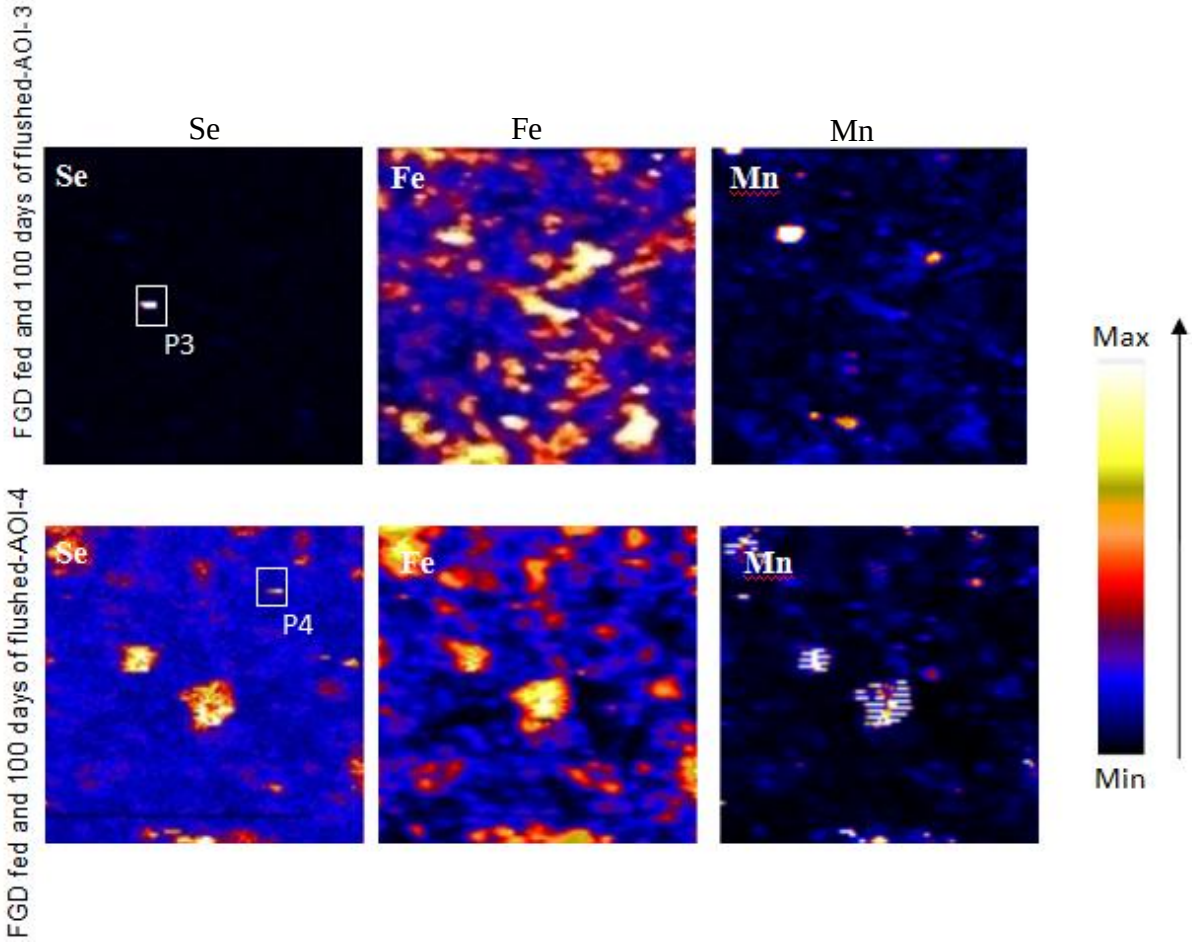

Figure 3.12 Micro-XRF maps showing the elemental distribution of selenium (Se), iron (Fe), and manganese (Mn) generated from the areas of interest, AOI-3 and AOI-4, on the 100 days of FGD fed followed by 100 days of flushed topsoil. P3 and P4 are Se hotspots used for micro-XANES.

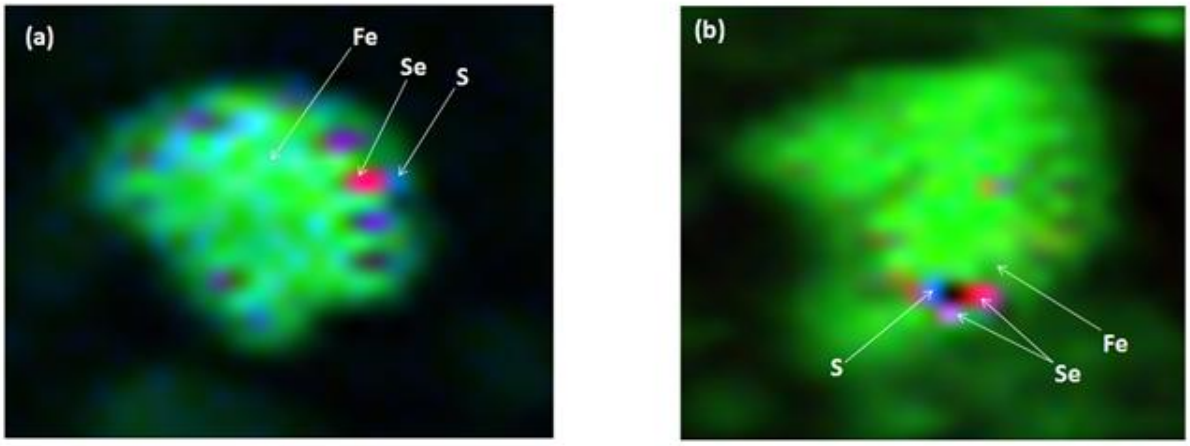

Figure 3.13 Selected sections from a micro-XRF map showing the relationship between selenium (Se), iron (Fe), and sulfur (S); (a) 100 days of FGD fed, (b) 100 days of FGD fed followed by 100 days of flushed topsoil.

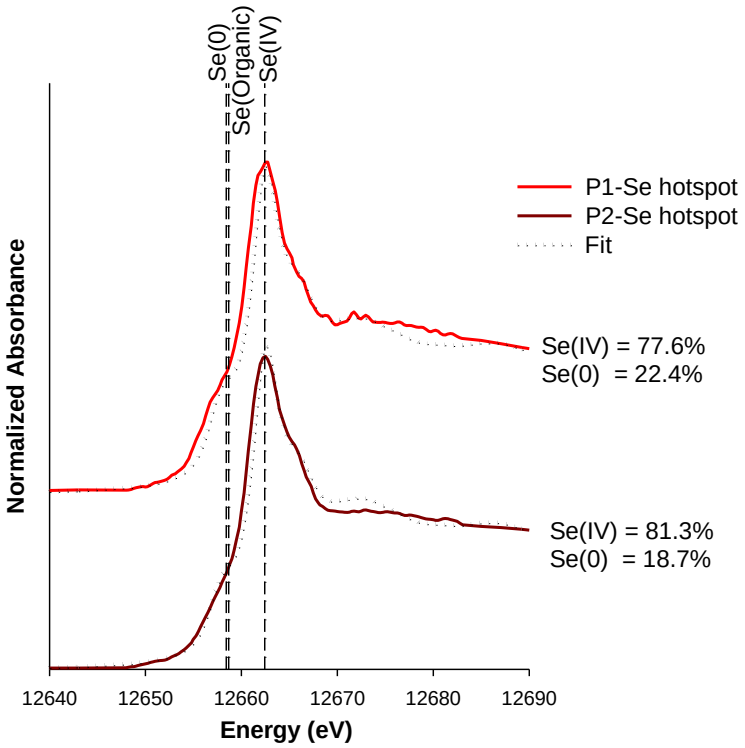

Figure 3.14 Selenium micro-XANES collected for the hotspots (P1 and P2) of 100 days of FGD fed topsoil. Solid lines represent the normalized spectra, and the dotted lines represent the best fits by LCF.

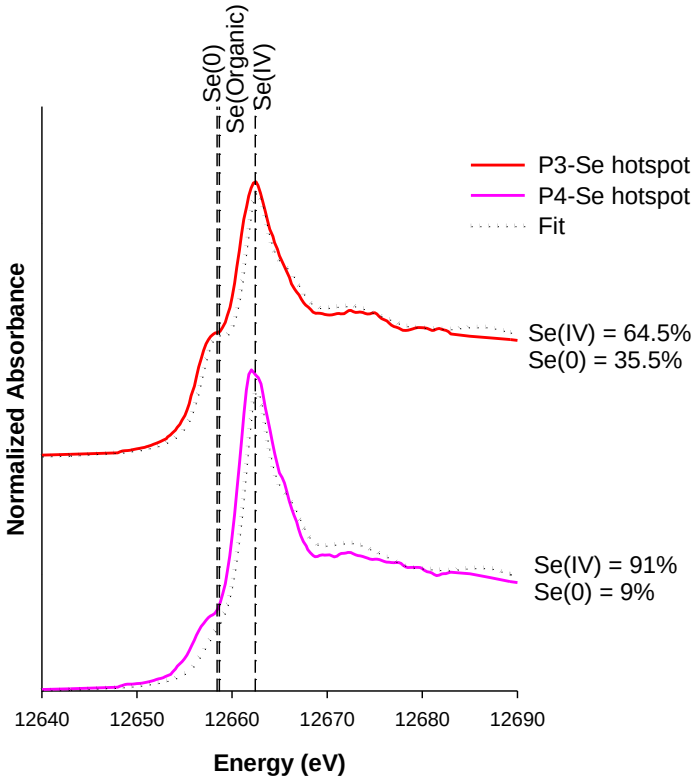

Figure 3.15 Selenium micro-XANES collected for the hotspots (P3 and P4) of 100 days of FGD fed followed by 100 days of flushed topsoil. Solid lines represent the normalized spectra, and the dotted lines represent the best fits by LCF.

Table 3.1 Total element concentrations and soil parameters of topsoil and engineered soil

Total element concentrations and soil parameters	Topsoil	Engineered soil
Se, mg/kg	0.40	0.32
As, mg/kg	5.8	4.6
B, mg/kg	104.2	80.0
S, mg/kg	295.6	591.2
Mn, mg/kg	569.4	336.1
Fe, %	2.2	1.5
pH (1:5 soil:water)	7.1	6.8
OM[#], %	5.1	3.1
CEC[¶], $cmol_c/kg$	31.4	22.4
Sand, silt, and clay, %	7.7, 50.5, 41.8	43.2, 30.7, 26.1

Organic matter

¶ Cation exchange capacity

Table 3.2 Concentrations of constituents of the FGD wastewater and the raw water collected in May, 2011.

Constituents	FGD wastewater*	Raw water
As, µg/L	3.1	2.7
Hg, µg/L	8.2	2.3
Se, µg/L	255.3	1.8
Mg, mg/L	868.0	20.6
B, mg/L	6.4	1.4
K, mg/L	133.0	9.0
Ca, mg/L	672.4	91.1
Na, mg/L	904.4	70.0
Total-S, mg/L	1175.7	49.6
Mn, mg/L	5.1	< D.L.
Fe, mg/L	0.03	0.01
SO_4^{2-}, mg/L	3828.1	122.3
SO_4^{2-}-S, mg/L	1276.0	40.8
F^-, mg/L	20.5	1.5
Cl^-, mg/L	902.4	64.0
NO_3^-, mg/L	330.4	11.6
PO_4^{3-}, mg/L	60.0	20.1
EC¶, ds/m	8.08	-
pH	8.43	8.65
Total solids, mg/L	6915.0	602.5
Total dissolved solids, mg/L	6735.0	552.5
Total suspended solids, mg/L	180.0	50.0

¶ Electrical conductivity

* The FGD wastewater is the water after treatments to remove some of the sulfur and other compounds. It is the wastewater used to conduct this experiment. The 1:1 mixture of FGD wastewater:raw water was used as the influent for the soil columns.

Table 3.3 Comparison of removal efficiencies of FGD wastewater constituents by the soil columns (after flushing with the raw water), and the pilot-scale CWTS.

Constituents	Soil columns		Pilot-scale CWTS
	Topsoil	Engineered soil	
	Removal efficiencies (%)		
Se	100	100	80
B	19	15	17
F^-	78	67	72
Cl^-	-11	-14	-3
SO_4^{2-}	2.73	-11	-17

Table 3.4 Selenium (%) associated with each operationally defined fraction as quantified by sequential extraction procedure (SEP) in topsoil column. Se fractionation (%) was calculated by subtracting the original concentration of Se in each fraction from the Se extracted after completion of the experiment (100 days of FGD fed and FGD fed fallowed by 100 days flushed). The difference was then divided by the total Se accumulated from FGD wastewater in each section. The Se (%) from FGD wastewater in each section was calculated by dividing the total accumulated Se in each section by the total Se accumulated from FGD wastewater within the whole column.

Soil	§ Step 1	Step 2	Step 3	Step 4	Step 5	Step 6	Step 7	Se from FGD wastewater
				Selenium (%)				
Topsoil (original)	-	28.8±5.8	29.5±8.1	55.5±2.8	7.6±2.5	21.5±4.8	-	0
				100 days of FGD fed-TS¶				
Section 2	7.5±1.8	-	13.5±2.7	5.0±0.1	16.0±1.2	11.0±2.8	47.3±2.4	58.4±11.7
Section 1 (inlet)	16.0±1.4	-	14.1 ±1.8	5.7±8.0	12.4±2.1	8.1±4.0	43.8±6.7	39.4±14.6
				100 days of FGD fed followed by 100 days of flushed-TS				
Section 2	11.5	-	20.0	5.1	14.5	20.9	28.0	55.6
Section 1 (inlet)	10.7	-	17.9	0.8	16.4	27.3	26.9	38.7

§Step 1, Water soluble Se; Step 2, Exchangeable Se; Step 3, Adsorbed Se; Step 4, Organically associated Se; Step 5, Elemental Se; Step 6, Recalcitrant organic Se; Step 7, Residual Se = $[100 - \sum_1^6 extracted\ Se\ (\%)]$. Selenium fraction < 5% is not included in the results.

¶ All results are in averaged and standard error of two soil columns.

Table 3.5 Selenium (%) associated with each operationally defined fraction as quantified by sequential extraction procedure (SEP) in engineered soil column. Se fractionation (%) was calculated by subtracting the original concentration of Se in each fraction from the Se extracted after completion of the experiment (100 days of FGD fed and FGD fed fallowed by 100 days flushed). The difference was then divided by the total Se accumulated from FGD wastewater in each section. The Se (%) from FGD wastewater in each section was calculated by dividing the total accumulated Se in each section by the total Se accumulated from FGD wastewater within the whole column.

Soil	Step 1	Step 2	Step 3	Step 4	Step 5	Step 6	Step 7	Se from FGD wastewater
	Selenium (%)							
Engineered soil (original)	6.1±0.2	46.6±1.3	25.2±0.6	13.1±1.8	9.3±1.2	27.7±0.2	-	0
100 days of FGD fed-ES¶								
Section 3	27.5±10.7	8.0±11.1	15.2±11.5	31.6±2.4	27.2±0.7	18.3±1.3	-	30.7±6.0
Section 2	19.1±9.1	5.6±6.6	20.2±5.5	29.0±1.9	17.7±7.0	15.9±10.5	-	35.5±9.7
Section 1 (inlet)	12.1 ±6.7	5.4±7.7	27±19.8	33.6±6.5	7.6±4.0	33.1±20.0	-	21.0±0.4
100 days of FGD fed followed by 100 days of flushed-ES								
Section 3	21.5	5.6	27.5	14.6	9.5	15.6	5.7	44.7
Section 2	22.5	8.2	21.1	27.4	9.1	23.2	-	26.8
Section 1 (inlet)	6.5	-	10.6	18.7	-	7.9	56.2	22.3

§Step 1, Water soluble Se; Step 2, Exchangeable Se; Step 3, Adsorbed Se; Step 4, Organically associated Se; Step 5, Elemental Se; Step 6, Recalcitrant organic Se; Step 7, Residual Se = $[100 - \sum_1^6 extracted\ Se\ (\%)]$. Selenium fraction < 5% is not included in the results.

¶ All results are in averaged and standard error of two soil columns

Table 3.6 Selenium K-edge energies for standards

Se reference standards	Oxidation state	Edge energy (eV)
Sodium selenate	Se(VI)	12666.7
Sodium selenite	Se(IV)	12663.4
Elemental Se	Se(0)	12659.1
Se mineral	Se(0)	12658.2
Seleno-DL-cystine	Organic-Se	12658.7
Iron selenide	Se(-II)	12657.8
Selenium sulphide	Se(-II)	12658.7

Table 3.7 Percentages of Se species of accumulated Se determined by linear combination fitting of bulk- and micro-XANES spectra

Sample	Se(IV)	Se(0)	Organic-Se	R-factor¶	Red. χ^2†
Se bulk-XANES					
Topsoil (original)	48.5	-	51.5	0.01	0.011
100 days of FGD fed-TS	68	32	-	0.01	0.008
100 days of FGD fed followed by 100 days of flushed-TS	40	60	-	0.01	0.010
Engineered soil (original)	67	-	33	0.02	0.019
100 days of FGD fed-ES	63	-	37	0.01	0.016
100 days of FGD fed followed by 100 days of flushed-ES	49	-	51	0.01	0.008
Se micro-XANES for 100 days of FGD fed-TS					
P1	77.6	22.4	-	0.008	0.011
P2	81.3	18.7	-	0.004	0.005
Se micro-XANES for100 days of FGD fed followed by 100 days of flushed-TS					
P3	64.5	35.5	-	0.008	0.012
P4	91	9	-	0.02	0.030

¶R-factor: normalized sum of the squared residuals of the linear combination fit.

†$\chi^2 = \sum[(\text{fit-data})/\varepsilon)]^2 / (N_{data}-N_{components})$ is the reduced chi-square statistic. Here ε is the estimated uncertainty in the normalized XANES data (taken as 0.01 for all data). The sum is over N_{data} points (140 data points between E= 12642 and 12692 eV for all data of bulk-XANES, and 145 data points between E= 12641 and 12691 eV for micro-XANES), and $N_{components}$ is the number of components in the fit (2 as indicated in the Table). The total percentage was constrained to be 100% in all fits. Typical uncertainties in the percentages listed for each standard component are 5%.

Chapter 4 - Minimizing arsenic mobility using ferrihydrite in a pilot-scale constructed wetland treatment system designed for flue-gas desulfurization wastewater

Abstract

Constructed wetland treatment systems (CWTSs) are efficient in removing Se from flue-gas desulfurization (FGD) wastewater. Arsenic (As) released from native soil under wetland conditions will create additional complications due to stricter regulations in place for As in water. A laboratory-based soil column experiment mimicking a pilot-scale CWTS was carried out to access the effectiveness of minimizing native soil As mobility in the CWTS using ferrihydrite (Fh) as an amendment, and to understand the underlying mechanisms for native soil As mobility or retention in the CWTS. Soil columns were packed with topsoil, and ferrihydrite (1.0% w/w) amended topsoil. The experiment was conducted for 60 days by feeding with deoxygenated 1:1 mixture of FGD: raw water at a flow rate of 2.84 mL/hour. Two columns were selected for drying and re-wetting experiments. Concentrations of Se and As in the FGD original wastewater were 135 µg/L and 1.2 µg/L, respectively. The Se concentration of collected effluents from the first study was non-detectable (<0.2 µg/L), regardless of the treatment. Some (~4 to 5%) of initially retained Se was mobilized by fluctuating oxidation-reduction conditions in the soil. The As concentration of effluent collected from the non-treated columns increased with time (1.0±1.0 to 27.3±4.0 µg/L). However, As released from the Fh-treated system remained comparatively low (1.1±1.0 to 5.0±0.5 µg/L). Micro-X-ray fluorescence mapping coupled with micro-, and bulk-X-ray absorption near edge structure (XANES) spectroscopy analyses showed a transformation of ferrihydrite to secondary Fe minerals. The proposed mechanism of native soil

As retention in the CWTS treated with ferrihydrite was the sequestration of released As with newly precipitated secondary Fe phases upon the reductive dissolution of ferrihydrite.

Introduction

A constructed wetland treatment system (CWTS) is an economically and environmentally efficient solution to treat trace elements, and other constituents in flue-gas desulfurization (FGD) wastewater. In general, FGD wastewater has elevated concentration of trace elements such as selenium (Se), arsenic (AS), and mercury (Hg) as well as other major constituents. Depending on the coal type used for electricity generation, and treatment methodologies in power plants, the concentrations of constituents could be different from site to site (EPRI, 2006). It has been widely documented that CWTSs are efficient in removing Se and other pollutants from different types of wastewater (Cheng et al., 2002; Dorman et al., 2009; Díaz et al., 2012; Hammer, 1989; Hansen et al., 1998; Kadlec and Wallace, 2008a; Lin and Terry, 2003; Ye et al., 2003), but studies on CWTSs for FGD wastewater treatment are limited (Eggert et al., 2008; Rodgers Jr and Castle, 2008; Wylie et al., 2008). Although the CWTS is effective for polishing Se and Hg from the FGD wastewater, As removal was less efficient as shown by previous studies (Eggert et al., 2008; Rodgers Jr and Castle, 2008). Depending on the redox potential (Eh), pH, and other soil/sediment conditions, the behavior of As is contradictory to that of Se (Masscheleyn et al., 1991a), and that could potentially impact the efficacy of the CWTS for As retention.

Arsenic is one of the most toxic metalloids, which influences human health in many countries and regions around the world (Bissen and Frimmel, 2003). The speciation and the biogeochemical behavior of As is controlled by altering pH, and redox potential along with adsorption/desorption and precipitation reactions (Cherry et al., 1979; Sadiq, 1997). The major oxidation states of inorganic As species that predominant in soil solution are As(V) as arsenate

and As(III) as arsenite, and these species mainly exist as oxyanions (Bhattacharya et al., 2007; Smedley and Kinniburgh, 2002). Arsenic(III) is the most abundant species in an anoxic (pe+pH<6) condition while in an oxic condition (pe+pH>10), As(V) is more dominant. Both As(III) and As(V) can be found in suboxic soil solution where pe+pH ranges between 6 and 8 (Sadiq, 1997).

These two species, As(III) and As(V), form complexes with clay minerals, iron (Fe), manganese, and aluminum oxides (Goldberg, 2002; Manning and Goldberg, 1997; Manning et al., 2002). In general, As(V) binds strongly and more or less irreversibly to soil/sediment mineral constituents than As(III). Therefore, As(V) is potentially less mobile and bioavailable (Dixit and Hering, 2003; Goldberg and Johnston, 2001; Manning and Goldberg, 1996). The effectiveness of As(III) and As(V) adsorption on minerals and clay surfaces is strongly correlated with pH, and competitive anions (Dixit and Hering, 2003; Goldberg, 2002; Raven et al., 1998; Sadiq, 1997). Under high pH conditions, As(III) is strongly adsorbed to soil components than As(V) (Manning and Goldberg, 1997; Sadiq, 1997). Arsenic mobility in natural systems is often coupled with Fe and sulfur (S) biogeochemical cycles, most likely due to the precipitation/co-precipitation reactions with poorly crystalline Fe oxy(hydr)oxides, Fe monosulfides, and pyrite (Moore et al., 1988; O'Day et al., 2004; Smedley and Kinniburgh, 2002).

The fate and transport of As in the environment and its toxicity are controlled by the biogeochemical transformations of As associated phases (Kocar et al., 2008; Polizzotto et al., 2005). Microbially-stimulated reductive dissolution of Fe-bearing minerals and subsequent desorption of As is a worldwide culprit (Horneman et al., 2004; Nickson et al., 1998; Nickson et al., 2000; Yamaguchi et al., 2011). Dissolution of As followed by its mobility is promoted by the input of dissolved organic matter (Bauer and Blodau, 2006; Mladenov et al., 2009). The reduced

conditions in the CWTS may enhance the reductive dissolution of As bearing minerals, ultimately mobilizing As through the wetland system. Since the CWTSs are being used to treat FGD wastewater, there is a need for understanding the mechanisms of As mobility and possible treatments to minimize As mobility in the CWTS designed for FGD wastewater treatment.

The biogeochemistry of As is predominantly controlled by adsorption, precipitation reactions with Fe oxy(hydr)oxide soil minerals. Ferrihydrite [$Fe_{10}O_{14}$ $(OH)_2$] is a meta-stable Fe mineral amorphous in nature and has a high surface reactive area (Jambor and Dutrizac, 1998). Ferrihydrite has been extensively studied as a "scavenger" for As removal from contaminated water through the reaction of surface adsorption (Carlson et al., 2002; Lizama et al., 2011; Michel et al., 2007; Mohan and Pittman, 2007; Riveros et al., 2001). Although As mobility is coupled with both S and Fe cycles in anoxic soils, since FGD wastewater is enriched with SO_4^{2-}, there is no need to provide additional S to promote As retention.

The instability of poorly crystalline ferrihydrite and its transformation to crystalline Fe(III) phases has been studied as a function of pH, temperature, and other factors (Cudennec and Lecerf, 2006; Das et al., 2010; Schwertmann and Murad, 1983). The neutral pH favors the formation of hematite while goethite is favored to form at low and high pH (2-5 and 10-14) (Cudennec and Lecerf, 2006). The influence of anions on the transformation rate of ferrihydrite was studied by Baltpurvins et al. (1996). Microbially-assisted reduction results in dissolution and reprecipitation of ferrihydrite to stable mineral phases such as goethite, and magnetite in the presence of Fe(II) (Benner et al., 2002; Berthelin et al., 2006; Hansel et al., 2003; Pedersen et al., 2006). Zachara et al. (2002) reported that dissimilatory metal-reducing bacteria transforms ferrihydrite to crystalline ferric (goethite, hematite, lepidocrocite), ferrous (siderite, vivianite), and mixed valence (magnetite, green rust) Fe solids in anoxic conditions. The primary factor,

which controls the formation of secondary Fe phases is the biogenic Fe(II) flux (Zachara et al., 2002). The ability and the retention capacity of newly formed Fe phases for As sequestration has widely been studied (Kocar et al., 2006; Pedersen et al., 2006; Tufano and Fendorf, 2008). Das et al. (2014) found that As(V) speciation is controlled by its incorporation into hematite via both bidentate-mononuclear and binuclear corner-sharing complexes. Previous studies have found that the reductive transformation of ferrihydrite increases both As(V) and As(III) adsorption (Kocar et al., 2006; Pedersen et al., 2006). It is hypothesized in the current study that secondary transformation of added ferrihydrite enhances sequestration of released As from native soil upon the reductive dissolution of Fe minerals under the wetland conditions.

A laboratory-based continuous flow through soil columns experiment mimicking a pilot-scale CWTS was performed to address two main objectives: to minimize native soil As mobility in the CWTS using ferrihydrite as an amendment, and to understand the underlying mechanisms for native soil As mobility or retention in the non-treated and the ferrihydrite-treated wetland materials using synchrotron-based X-ray spectroscopy techniques.

Materials and Methods

Collection of soil and FGD wastewater

Topsoil (Clime (Fine, mixed, active, mesic Udorthentic Haplustolls)-Sogn (Loamy, mixed, superactive, mesic Lithic Haplustolls) complex silty clay) was collected at 0-10 cm depth from an area nearby Westar Energy's Jeffrey Energy Center (JEC) located at, Pottawatomie County, St. Marys, Kansas (39°17’10”N, 96°07’01”W). Basic soil properties including soil texture, pH, cation exchange capacity (CEC), and organic matter (OM) content were determined (Table 4.1). Soil pH was determined using a 1:5 mixture of soil: Milli-Q water. Organic matter (OM) content of soil was measured by loss on ignition (LOI) method (Combs and Nathan, 1998).

The FGD wastewater and Kansas river water (i.e., raw water) for the study were also collected from JEC on 4th of October, 2011. Determination of concentrations of constituents in both types of water is described in the influent and effluent analysis section.

Synthesis of 2-line ferrihydrite

Two-line ferrihydrite (Fh) was synthesized in the laboratory following the procedure described by (Schwertmann and Cornell, 2000) (see details in supporting information (SI) of Appendix B). The prepared iron-oxide was characterized using an X-ray diffractometer (XRD) (Philips X-Ray diffractometer, Mahwah, NJ) equipped with a theta compensating slit and curved crystal graphite monochromator.

Setting-up of soil column study

The experiments were conducted using flow cells (Soil Measurement Systems LLC., Arizona, USA) that each consisted of an acrylic tube (5.08 cm diameter, 30.5 cm length), and two acrylic end-plate assemblies. Three columns were packed with pre-wetted soil (non-treated) and the other three columns were packed with 1.0% (w/w) of ferrihydrite (Fh) amended soil (Fh-treated). The ferrihydrite was thoroughly mixed with soil prior to wetting. The packing bulk density of both non-treated and Fh-treated soil was 1.0 Mg/m^3. The detailed procedures for packing the soil columns, and feeding with influent solution were described in Chapter 3. After steady-state flow was achieved with the raw water (approximately within ten days), a deoxygenated 1:1 mixture of FGD wastewater and raw water (influent) was introduced, with flow in upward at a rate of 2.84 mL/hour. This influent was constantly delivered for 60 days with the upward flow. Effluent samples were collected every other day from the outlet at top of each column. One pore volume (PV) of these columns equals to 5.5 days. After recording the weight,

and pH effluent samples were immediately filtered and stored as non-acidified or acidified samples at 4 ^{0}C, depending on targeted analyses.

Drying and re-wetting experiment

At the end of the experiment (after 60 days of FGD wastewater feeding), two selected columns, one from non-treated (non-treated-2) and the other from Fh-treated (Fh-treated-2), were used for drying and re-wetting conditions to qualitatively assess the behavioral changes of redox sensitive elements (such as Se and As). About -90 millibar vacuum pressure was applied to drain water from the saturated soil columns. The vacuum pressure did not exceed the bubbling pressure of the nylon membrane placed at the bottom of the soil columns due to the possibility for damaging it by high pressure. This method was not sufficient to dry out the soil. Therefore, the soil columns were further dried at 40 ^{0}C in an oven. At the end of the drying step (after 21 days), the remaining volumetric water content of non-treated-2, and Fh-treated-2 columns was 22.4%, and 20.7%, respectively. Then, the FGD wastewater influent was fed again with the upward flow at the same rate (2.84 mL/hour) for an additional 30 days. Effluent samples were collected everyday and analyzed for Se, and As.

Analysis of influent and effluent

The FGD wastewater, the raw water, and the collected effluent samples were immediately filtered through 0.45 µm syringe filters (Environmental Express Inc., South Carolina, USA), and acidified with 2-3 drops of 6 M HCl. The concentration of As was measured using a graphite furnace atomic absorption spectrometry (GF-AAS) (Varian Inc.) equipped with Zeeman background correction. The concentration of Se of these solutions was measured using an Agilent 7500 series inductively coupled plasma-mass spectrometry equipped with a dynamic reaction cell (ICP-MS-DRC). A Varian 720-ES Inductive couple plasma-optical

emission spectrometry (ICP-OES) was used to determine the total concentrations of other constituents. More detail about the analysis is given in SI of Appendix B.

Soil sampling and analysis

At the end of the flow experiments, the soil columns were cut into six sections (each ~5.08 cm in length). Those sections were numbered 1 through 6 from bottom to top. The soil samples were appropriately prepared and preserved for future analyses as described in Chapter 3. The soil samples from each section were used for the total elemental analyses of As, and Se. The total elemental concentrations of the starting soil material and the soil from column sections was determined by following the USEPA-3051A Microwave assisted method (USEPA, 2007). The total As, and Se concentrations of soil were measured using the GF-AAS with 500 mg/L palladium modifier (see more details in SI of Appendix B). Arsenic was leaching out from the soil columns packed with non-treated soil material (discussed below), over time. Therefore, two steps of a sequential extraction procedure (SEP) were used to determine the mobile As fraction of the original soil (Wenzel et al., 2001). More information about the SEP is given in SI of Appendix B.

Arsenic micro-XRF mapping and micro-XANES analysis

Arsenic micro-XRF mapping followed by micro-XANES was conducted at sector 13 ID-E, GSE CARS (GeoSoilEnviro Consortium of Advanced Radiation Sources) of the Advanced Photon Source (APS) at Argonne National Laboratory (ANL), Argonne, IL. Micro-XRF maps and micro-XANES spectra were collected with a solid-state 13-element solid state Ge detector, and a double-crystal monochromator; Si (111) and Si (311). Appropriate care was taken to minimize beam-induced changes of speciation, by collecting the data at helium environment. The micro-XRF maps were generated at the energy of 12500 eV to locate As rich areas (hotspots) in

the soil. Arsenic hotspots (brightest points) on the micro-XRF maps were selected to collect micro-XANES spectra to get As speciation at microscale. The energy was calibrated at 11873.3 eV using a sodium arsenate standard. Data was processed by following the standard procedures in ATHENA (Ravel and Newville, 2005). The As speciation was determined by linear combination fitting (LCF) analysis in the ATHENA software (see SI of Appendix B for more information).

Arsenic bulk-XANES analysis

For overall As speciation in the collected from non-treated and ferrihydrite-treated columns. The As bulk-XANES data were collected at sector 5 BM-D of DND-CAT of the APS. The detector used for the analysis was Canberra 13-element Ge solid state detector, and it was covered with two aluminum foil layers of a thickness of 50 µm to minimize background fluorescence emissions from Fe, and to improve signal-to-noise ratio (Gräfe et al., 2014). The sample preparation and more detail for As bulk-XANES analysis is provided in SI of Appendix B. The energy was calibrated to As K-edge energy of 11,866.7 eV using an As filter. The sample spectra were collected under a continuous flow of the X-streamTM cryogenic crystal cooler (Rigaku company, Tokyo, Japan). Collected data was analyzed using the ATHENA software. The As standards used for the LCF are listed in SI of Appendix B.

Iron bulk-XANES analysis

Iron speciation of these samples was also analyzed at sector 5-BM-D of the APS. Iron-metal foil was used to calibrate the Fe K-edge energy at 7112 eV. Detector was covered with the two aluminum foil layers of a thickness of 50 µm to minimize background fluorescence. Three XANES spectra per each sample were collected in the fluorescence mode. The XANES spectra of sixteen Fe standards were used for LCF of each sample. Those standards are listed in SI if

Appendix B. Data processing was performed by ATHENA program. Iron speciation was determined by LCF analysis within an energy range of −20 eV below to +30 eV above the edge. For each samples, lowest reduced χ^2 and R-factor were selected as the best combination to reconstruct the sample spectrum with the set of Fe reference standards. Species abundance < 5% was not accounted for LCF results.

Statistical Analysis

Statistical analysis was performed using SAS for Windows version 9.4 (SAS Institute Inc., 2013). The overall design was repeated-measures over time. A one-way analysis of variance (ANOVA) using PROC GLMMIX was performed to analyze the effect of treatments (non-treated and Fh-treated) on the concentration of constituents in effluent samples. Pairwise Bonferroni method was used for pairwise comparison between the treatment means at 5% level of significance (α=0.05).

Results and Discussion

pH of effluent and soil

The behavior of As is significantly dependent upon the pH of the system (Masscheleyn et al., 1991b). The pH of the influent solution was 8.2. Over the experiment period, the pH of the columns effluent remained near neutral (6.8-7.2) for the non-treated and the Fh-treated soil. The pH of the original soil was 6.6. After 60 days of feeding with the FGD influent, the pH of the bottom sections (inlet) increased to ~7.3 whereas that for the top sections was 7.0 (Table S2 in SI). A similar trend was observed for the bottom sections of the Fh-treated system (pH~7.3), but the top sections showed slightly acidic pH (6.7-6.8). Initially addition of alkaline FGD wastewater can greatly influence the pH of the bottom sections. Upon submergence, the reductive dissolution of Fe minerals can increase the soil pH due to the consumption of protons

(Takahashi et al., 2004; Yamaguchi et al., 2011). The decrease of the pH in the Fh-treated soil could most likely be due to the release of Fe(III) during the reductive dissolution of ferrihydrite.

Drying and re-wetting of soil influence the soil pH further, specifically there was a decrease of pH in the top sections of the soil columns. The top sections of the non-treated soil (pH 6.6-6.7), and the Fh-treated soil (pH 6.4-6.6) tended to be slightly acidic. Following completion of re-feeding with the FGD wastewater influent for an additional 30 days, the pH of the bottom sections of both systems was ~7.3. Thus, drying of the soil columns over 21 days affected decrease in the soil pH of the top sections, most likely due to the production of protons during the re-oxidation of dissolved Fe(II) to Fe(III), and concomitantly precipitation of $Fe(OH)_3$ (Ponnamperuma, 1972; Yamaguchi et al., 2011).

Behavior of selenium

The concentration of Se of this batch of FGD wastewater was 135 µg/L (Table 4.2). This was low compared to the FGD wastewater used for previous column study (Chapter 3). Depending on the raw material (coal), and the treatment strategies at the electricity power plant, the concentrations of constituents may also change. However, the concentration of Se was a little more than 3 times higher than Kansas surface water quality standard (20 µg Se/L based on acute criteria) (Tate, 2005), even after 1:1 dilution with raw water. The concentrations of other constituents such as B (8.6 mg/L), F^- (18.0 mg/L), total-S (1334.4 mg/L), SO_4^{2-}-S (1354.1 mg/L) were also elevated relative to the water quality standards.

Breakthroughs curves (BTCs) for targeted constituents were generated to understand their behavior, and how flow rate would impact on the retention capacity of the constituents within the CWTS. In a BTC, the x-axis represents the pore volumes and the y-axis represents the relative effluent solute concentration (C/C_0). The concentration of a constituent of interest in an effluent

solution was denoted as C whereas C_0 was the concentration of that same constituent in the influent FGD wastewater solution. The BTC of Se (Figure 4.1) clearly showed that Se in the effluent water released from both types of the soil columns (non-treated and Fh-treated) over the 60 days was below the detection limit (<0.2 µg/L). Ferrihydrite has been identified as a greater adsorbent for selenite (Parida et al., 1997). However, because the control soil (non-treated) was capable of retaining Se successfully under reduced conditions, we were not able to see any changes in the breakthrough curves. In the previous soil column study as well, we found that Se fed with the FGD wastewater was mainly sequestered as reduced/stable Se forms such as Se(IV), Se(0), and organic Se. Reduction of Se(VI) to a mixture of Se(IV), Se(0), and organic Se was also identified in a CWTS designed for Se contaminated agricultural drainage water (Lin and Terry, 2003). Selenite is more prone for strong inner-sphere complexation with soil oxy(hydr)oxide minerals which could attribute to immobilize Se within the CWTS (Parida et al., 1997; Peak, 2006; Su and Suarez, 2000). Since the reduced Se species are less mobile compared to the oxidized species (Elrashidi et al., 1987; Fernández-Martínez and Charlet, 2009; Masscheleyn et al., 1990), extra addition of ferrihydrite did not result in any observed change s in Se biogeochemical cycling in this small-scale CWTS.

Behavior of arsenic

Compared to Se, the As concentration of the FGD wastewater was low (1.2 µg/L). Although Se showed a strong retention in both non-treated and Fh-treated soil systems, the behavior of As was different to that of Se. Even with a negligible level of As in FGD wastewater influent, the concentrations of As in the effluent samples collected from the non-treated soil columns increased with time (1.0±1.0 to 27.3±3.8 µg/L) (Figure 4.2). The original soil material was not contaminated with As because the total As concentration was 7.3±0.5 mg/kg, which is

the normal As background concentration of a soil. The average surface soil As concentrations of US soils is about 6.4 mg/kg (Smith et al., 2013), and the average As concentration in world soil is about 7.2 mg/kg (McCarty et al., 2011). Thus, the reductive dissolution of native soil (wetland construction material) Fe minerals resulted in releasing As in to soil solution. The phenomenon of ground water contamination with As due to the reductive dissolution of Fe minerals is well documented in previous studies (Berg et al., 2001; Masscheleyn et al., 1991a; Masscheleyn et al., 1991b; Nickson et al., 1998; Nickson et al., 2000; Yamaguchi et al., 2011). A high concentration of SO_4^{2-} in the FGD wastewater (Table 4.2) can also affect As dissolution (Qafoku et al., 1997). Although, this batch of FGD wastewater did not have a detectable concentration of PO_4^{3-}, enhanced solubility of PO_4^{3-} in soils can be expected upon submergence (Savant and Ellis Jr, 1964), which could ultimately compete for specifically and non-specifically bound arsenate sites (Dixit and Hering, 2003). From the first two steps of the SEP performed for the original soil, we found that only 5.2±0.2 % was constituted to the As available fraction. This implies that As in inherent soil material was stable under oxic conditions. Thus, the As dissolution from the native soil can increase with enforced reduced conditions in the CWTS. The cumulative amount of As released from the non-treated soil columns over the 60 days of feeding with the FGD wastewater was 86.6±19.8 µg. The non-treated-2 soil column which was subjected to drying, and re-wetting with the FGD influent for an additional 30 days further released 118.8 µg of As to the soil solution. Interestingly, the concentrations of As in the effluent samples collected from the Fh-treated soil columns (Figure 4.2) remained comparatively low (1.1±0.5 to 5.0±0.5 µg/L), indicating that the ferrihydrite amendment significantly retarded native soil As mobility. The total amount of As came out from the Fh-treated soil columns over the 60 days was 15.8±6.5 µg, and the Fh-treated-2 (drying and re-wetting) soil column released 26.3 µg of As over an

additional 30 days. There was a significant difference between the As concentration of effluent collected from the non-treated and the Fh-treated soils ($p<0.05$).

Behavior of iron

The Fe concentration of the FGD influent was non-detectable (<0.1 mg/L). However, the total dissolved Fe concentration increased with time in both systems (Figure 4.3), suggesting that the reductive dissolution exceeded the re-precipitation of Fe minerals in these systems. Iron released from the non-treated soil increased from non-detectable (<0.1 mg/L) to 34.5±0.9 mg/L whereas the Fe concentration of effluent collected from the Fh-treated soil was non-detectable (<0.1 mg/L) to 72.5 ±3.9 mg/L (Figure 4.3), and this difference was statistically significant ($p<0.05$). The amorphous nature and the high surface area of ferrihydrite is more susceptible to go through reductive dissolution (Benner et al., 2002; Schwertmann, 1991), and this phenomenon can be induced by the presence of dissolved soil organic matter (Mladenov et al., 2009), subsequently releasing As from associated mineral phases.

The increased As and Fe concentrations in the effluent with reduced conditions are in agreement with previous studies (Pedersen et al., 2006; Yamaguchi et al., 2011). The correlation between the total concentrations of Fe and As of effluent samples (Figure 4.4) also explains the differences in As mobilization for the non-treated and the Fh-treated systems. There was a strong and a significant correlation between As and Fe solution concentrations of the non-treated system ($r^2 = 0.80$, $p<0.05$), implying that releasing of native soil As into the soil solution is driven by the dissolution of Fe mineral phases. With the aid of the correlations, previous studies have also suggested that the mechanism of As mobilization is mainly from the reductive dissolution of Fe oxy(hydr)oxides (Kneebone et al., 2002; Masscheleyn et al., 1991b). In contrast, the correlation of As and Fe for the Fh-trated system was weak and non-significant ($r^2 =$

0.20, $p>0.05$), suggesting that the release of As into the solution from the Fh-treated soil was significantly delayed and/or complicated by significant re-precipitation reactions than the release of As.

Behavior of sulfate

There was no significant difference of SO_4^{2-} concentration in the effluent collected from both systems (Figure 4.5), presumably that the high flow rate of the influent solution was not favorable for SO_4^{2-} reduction in the Fh-treated system. In addition, we cannot rule out that effect of high salt concentration in the FGD wastewater, because that can inhibit soil microbial activities, concomitantly hindering the SO_4^{2-} reduction (Rietz and Haynes, 2003). Previous studies have revealed that the efficiency of CWTSs for pollutants removal can be improved by decreasing the hydraulic loading rate and lengthening the hydraulic retention time (HRT) (Ghosh and Gopal, 2010; Kadlec and Wallace, 2008; Marchand et al., 2010). Constructed wetlands designed for Cu, and Zn removal from swine wastewater showed enhanced efficiency with longer HRT (Cortes-Esquivel et al., 2012). In addition, lack of conducive conditions such as abundance of sulfate reducing bacteria (less likely) and organic carbon (more likely) may have also affected the sulfate reduction in the present study.

Behavior of Se and As in drying and re-wetting soils

There was no detectable amount of Se came out with the effluent implied that Se fed with the FGD wastewater accumulated in the soil columns under reduced conditions. However, the effluent samples collected from the soil columns that were subjected to drying and re-wetting showed detectable levels of Se in the effluent samples (Figure 4.6). Furthermore, as the system gets progressively reduced again, Se concentration in the effluent decreased. As a result of drying and rewetting (i.e., changing redox conditions in soils), about 4 to 5 % of initially retained

Se was mobilized. Previous studies have also observed enhanced Se mobility with increasing redox potential (Jayaweera and Biggar, 1996; Masscheleyn et al., 1990). This implies that the fluctuation of the soil redox potential can affect the efficiency of the Se retention in the CWTS. Therefore, maintaining continuous wetting conditions in the CWTS is necessary to enhance the treatment efficiency for Se removal.

At the beginning of re-feeding with the FGD wastewater, the As concentration of effluent solutions collected from drying and re-wetting columns was low. In contrast to the Se behavior, As concentration increased as the system gets progressively reduced (Figure 4.7). However, the As concentration in the effluent released from the Fh-treated column remained comparatively low. Continuous releasing of As from the non-treated soil implies that native soil behaves as a source for releasing As to the soil solution. Although the ferrihydrite substantially helped retaining native soil As, it appeared to be that As concentration of the effluent from the Fh-treated-2 column was also comparatively greater than before (Figure 4.7). This could most likely be due to the perturbation of the system, and the effect of wetting-drying or changing the redox conditions of soils that have been studied before (Beak et al., 2011; Biasioli et al., 2010). Thus, these results emphasize the importance of understanding the potential changes of the behavior of trace elements that could alter with changes in environmental conditions in the CWTS.

Results from soil analysis

Selenium distribution within the soil columns

After 60 days of feeding with the FGD wastewater, Se mainly accumulated in the bottom parts (inlet) of the non-treated soil columns (Figure 4.8). The total amount of Se accumulated from the FGD wastewater in sections 1, and 2 was 56.1±24.8 µg, and 117.6±12.7 µg, respectively. A similar trend was observed in the previous study (Chapter 3), implying that the

mobility of Se was retarded by reduced conditions in the soil. However, Se was slightly moved to the middle and upper sections compared to the previous study. This could possibly be due to the higher flow rate of the FGD influent used in this study.

In the column of 60 days of FGD fed followed by drying and re-wetting, some of initially retained Se further moved to the upper sections. This is in accordance with the solution results that indicated some movement of initially retained Se due to the drying and re-wetting conditions (Figure 4.8). However, Se fed over an additional 30 days mainly accumulated in the section 1(192.7 µg), and section 2 (94.3 µg). This implies that the transformation of Se into stable forms is kinetically rapid. Tokunaga et al. (1997) revealed that the sequential transformation of Se(VI) to Se(IV) and Se(0) occur within 3.8 days upon flooding. A similar trend was observed for the Fh-treated system (Figure 4.9). The Se fed with the FGD wastewater over 60 days mainly accumulated in section 1 (119.3±37.3 µg), and section 2 (82.5±18.5 µg) of the Fh-treated soil columns.

Arsenic distribution within soil columns

After As was released over 60 days of the study period, the total amount of As that remained in the non-treated soil columns was evenly distributed among the column sections (Figure 4.10). There was a slight movement of As within the non-treated-2 soil column which was used for 60 days of FGD feeding followed by drying and re-wetting. This is an indication that continuous release of As from the native soil can transport As from one cell to another within the CWTS. The distribution of remaining As in the Fh-treated soil columns was more or less similar to the non-treated soil (Figure 4.11). However, the remaining As in the Fh-treated-2 soil column (drying and re-wetting) slightly moved to the upper sections. This could most likely

due to the fluctuation of oxidation-reduction conditions in the soil that can affect sequestered/stabilized As in the ferrihydrite.

Spatial distribution of As, Fe, and Mn in the soil

The spatial distribution of As, Fe, and Mn of the non-treated and the Fh-treated soil is depicted in Figure 4.12. In these micro-XRF maps, the bright color (white-yellow) represents the high concentration of an element (hot spots) whereas the dark color (blue-black) represents the low concentration of the element. Arsenic micro-XRF maps of both situations indicated that the As in the soil was heterogeneously distributed within the sample area selected for mapping. On the other hand, several hotspots of Fe compared to As and Mn were scattered throughout the images most likely due to the high concentration of Fe in the soil compared to Mn and As. It should also be noted that the colors are relative, so concentrations between the elements cannot be compared.

The correlation between As and Fe generated for the whole micro-XRF map provides the co-localization of the elements at microscale (Figure 4.13a and Figure 4.13 b). The correlations between As and Fe for both non-treated ($r^2 = 0.56$, $p<0.05$) and Fh-treated ($r^2 = 0.21$, $p<0.05$) soil were weak, although they were statistically significant. Weaker correlation most likely be due to the low concentration of As sparsely distributed within the area of sample chosen for mapping. In this type of situation, As rich areas or sub-maps should be selected to get a better correlation (Figure 4.14). Then, the sub maps showed that the correlations between As and Fe in the non-treated soil ranged between 0.08 and 0.62, and most of these relationships were non-significant ($p>0.05$). In contrast, the correlations of As and Fe for the Fh-treated soil ranged between 0.28 to 0.88, and those were significant ($p<0.05$), except for one point (Figure 4.14). These results indirectly suggest the association between Fe and As in the ferrihydrite treated soil.

The co-precipitation of As with Fe is one of the main driving mechanisms of As removal in CWTSs (Lizama et al., 2011). Previous studies have addressed that As may precipitate on the surface of newly formed Fe mineral phases such as magnetite and hematite (Aredes et al., 2013; Kocar et al., 2006). Kocar et al. (2006) found that incorporation of As into the biotransformed Fe minerals upon the reductive dissolution of ferrihydrite can enhance As sequestration.

Soil arsenic speciation

Arsenic K-edge energy shifts as the oxidation state of As changes from reduced to oxidized forms (Arsenic-sulfide to arsenate) (Figure 4.15). Arsenate and arsenite have distinct K-edge energies at 11873.3 eV and 11869.7 eV, respectively which can easily be identified by their XANES spectra. Therefore, XANES analysis can successfully be used to identify different oxidation states of As even in a heterogeneous and complex system like soil. According to the micro-XANES results of As hotspots (P1-NT, P2-NT, P3-NT, and P4-NT) on the non-treated soil, speciation was dominated by As(V) (Figure 4.16). In this study, As(V)_Gib, As(V)_Goe, As(V)_Hem, and As(V)_Fh represented As(V) adsorbed to gibbsite, goethite, hematite, and ferrihydrite, respectively. Also, As(III)_Fh was to represent As(III) adsorbed to ferrihydrite.

A significant portion of total As in the non-treated soil was As(V) adsorbed to Fe and Al hydroxy minerals including, As(V)_Gib (41.8 %), As(V)_Goe (20.5 to 66.9 %), As(V)_Hem (5.3 to 11.9 %), and As(V)_Fh (26.1 %) (Table 4.3). In addition, As(V) associated solid phases,yukonite-like (48.9%), and pharmacosiderite-like (55.0 %), were also detected in some of these hotspots . Minor amount of As was As(III)_Fh (12.4 to 24.5 %), implying that As(V) was the most dominant species in the non-treated soil columns. Organically-associated As speciation in the hotspots of the non-treated soil was 16.5 to 10.2 %. This was not surprising as this original soil was rich in OM (6.2% of OM). It should be mentioned here that we were essentially looking

at the speciation of remaining or more stable As in the soils So, it is possible that the remaining As in the soil to be dominated by As(V) over reduced species of As. In addition, 60 days of the experimental period might not be long enough to transform all As(V) species into As(III) under the given conditions. Using the As micro-XANES analysis, a previous study has also found As(V) was the main species that dominated in an anoxic soil (Fan et al., 2014).

The LCF results of micro-XANES (Figure 4.17) collected from As hotspots on the Fh-treated soil (P1-FhT, P2-FhT, P3-FhT, and P4-FhT) also observed a similar trend, implying that As(V) was the dominant species. The main As phases that existed in these hotspots were yukonite-like (18.3 to 21.5 %), As(V)_Hem (21.2 to 32.8 %), As(V)_Fh (27.7 to 40.2 %), As(III)_Fh (15.1 to 28.2 %), and organically-associated As (10.5 %) (Table 4.4). In addition, 28.2 % of realgar (As_4S_4/AsS)-like species was detected in the P4-FhT hotspot. This indirectly implies that addition of the ferrihydrite may enhance the sulfate reduction, subsequently forming stable As-S mineral phases (O'Day et al., 2004; Root et al., 2013). Bulk S-XANES analysis (results not shown here) showed a slightly different S speciation in these systems. The oxidized S species of the non-treated and the Fh-treated systems was 93% and 86%, respectively, indicating that oxidized S was dominant in the soil treated with FGD wastewater for 60 days. The reduced S species (elemental S) was 16% in the Fh-treated compared to the non-treated soil which showed only 7%. This implies that, under the given conditions, the addition of ferrihydrite and its reductive dissolution can enhance sulfate reduction to some extent.

The LCF results of As micro-XANES for both non-treated and Fh-treated soil systems (Figure 4.18) showed more hematite, a secondary Fe mineral phase, in the Fh-treated soil columns compared to the non-treated system. Fan et al. (2014) found As (V) sorbed on hematite to be the main As species in the anoxic soil. The total As concentration in soil of their study was

8.1 mg/kg, which was similar to our study. However, they did not explain the reason for forming the hematite in the system. Previous studies indicated that poorly crystalline ferrihydrite and its dissimilatory reductive dissolution tends to transform to thermodynamically stable secondary Fe mineral phases, depending on Fe(II) concentration (Benner et al., 2002; Hansel et al., 2003; Kocar et al., 2006; Pedersen et al., 2006; Zachara et al., 2002). Hematite is formed by dehydration and internal atomic arrangement of solid ferrihydrite at pH between 7 and 8 through topotactic transformation (Cudennec and Lecerf, 2006), and this reaction is catalyzed by Fe(II) (Schwertmann and Murad, 1983). In our study, the pH remained at slightly acidic to near neutral and the high concentration of Fe(II) in the Fh-treated system can promote the hematite formation. Thus, re-adsorption of As(V) to newly formed hematite surfaces can ultimately suppress the mobility of native soil, which could support our hypothesis. Previous studies also revealed that As(V) is incorporated to hematite by both a bidentate-mononuclear complex and a bidentate binuclear corner-sharing complexes (Das et al., 2014; Das et al., 2015; Tufano et al., 2008). The amount of As(V) adsorbed to ferrihydrite was also increased in the Fh-treated soil (Figure 4.18). This suggests that desorbed As upon the reductive dissolution of Fe minerals appeared to be re-adsorbed by the remaining reactive surfaces of the ferrihydrite. Ferrihydrite has strong affinity for both As(V) and As(III). At low As concentration and pH between 5.2 to 7.0, As(V) adsorbs to ferrihydrite more so than As(III) (Raven et al., 1998). In addition, As(V) can remain adsorbed onto the surface of ferrihydrite during ongoing precipitation reactions with Fe (Pedersen et al., 2006).

The As bulk-XANES analysis elucidates the overall As speciation in the soil. The As speciation of the original material was mainly dominated by As(V) phases, including beudantite-like (60.4 %), pharmacosiderite-like (17.7 %), and As(V)_Goe (8.4 %) whereas 13.5 % of

As(III)_Fh was found to be as As(III) species (Figure 4.19). Therefore, we can expect As in the original material is stable under the oxic conditions. Agreeing with the micro-XANES analysis results, the As bulk-XANES speciation also showed that As in both non-treated and Fh-treated soil mainly existed as As(V) (Figure 4.19). Compared to the non-treated soil system, the Fh-treated soil showed enhanced amount of As(V) adsorbed to ferrihydrite. However, As(V)_Hem was not detected by the As bulk-XANES, which could most likely that it was confined to micro sites, and not an abundant species in soils at this stage. The speciation of As(III) adsorbed to ferrihydrite did not change, regardless of the treatment, and it remained around 13 % of the total speciation. This may probably be that specifically or inner-sphere bound As(III) with ferrihydrite in the original soil material resist the transformation and its mobility (Ona-Nguema et al., 2005).

Soil iron speciation

Among the XANES spectra of Fe standards, siderite has a unique post-edge peak appearing around at 7138 eV (Figure 4.20). Also, we can see a pre-edge feature of the XANES spectra (energy at 7117 eV), which is unique to paramagnetic elements like Fe. The bulk-XANES analysis showed that Fe speciation of the original soil was mostly Fe(III) (Figure 4.21andTable 4.6). Although Fe(III) was still predominant, about 17-18 % of $FeSO_4$ was detected in the FGD wastewater treated soil. The high concentration of SO_4^{2-} in the FGD wastewater can form $FeSO_4$ by the reaction of Fe(II) that was released under reduced conditions. The mixed oxidation states of Fe [Fe(II) and Fe(III)] were also found in these two systems, regardless of the treatment. In the Fh-treated soil, about 23 % of hematite was detected which supports the observation that the enhanced amount of As(V) adsorbed to hematite detected by the As micro-XANES.

Conclusions

There was no Se released over the experimental period with or without ferrihydrite treatment suggests that Se fed with the FGD wastewater was strongly retained in the soil under reduced conditions. Some of the Se that was initially retained was mobilized by fluctuating oxidation-reduction conditions in the soil. Under the wetland conditions, reductive dissolution of Fe minerals induced the native soil As mobility. Ferrihydrite amendment was able to suppress overall As release to the effluent. Spatially resolved micro-XRF technique revealed a strong correlation of As and Fe in the ferrihydrite treated soil, indicating that As was associated with Fe. Micro- and bulk- As XANES identified that As(V) was the primary As species in both systems. Further, micro-XANES analysis showed increased the association of As with Fe phases in the ferrihydrite treated soil. Thus, our study showed that secondary transformation of added ferrihydrite enhanced the sequestration of released As from the native soil, upon reductive dissolution of Fe minerals under the wetland conditions. This will also help retaining As if the FGD wastewater had higher concentration of As besides Se. In addition, our findings recommend that maintaining continuous wetting conditions is needed to enhance the treatments efficiency of the CWTS and to avoid remobilization of FGD wastewater constituents.

Acknowledgements

We acknowledge the funding support of this study by Westar Energy, Burns & McDonnell, and Kansas Agricultural Experimental Station. Portion of this work was performed at the DND-CAT located at Sector 5 BM-D, and at Sector 9 BM-B of the Advanced Photon Source (APS). DND-CAT is supported by Northwestern University, E.I. DuPont de Nemours & Co., and The Dow Chemical Company. This research used resources of the APS, a U.S. Department of Energy (DOE) Office of Science User Facility operated for the DOE Office of

Science by Argonne National Laboratory under Contract No. DE-AC02-06CH11357. We like to acknowledge http://xraysweb.lbl.gov/uxas/Databases/Overview.htm for providing XAS database for iron standards.

References

Aredes, S., B. Klein and M. Pawlik. 2013. The removal of arsenic from water using natural iron oxide minerals. J. Clean. Prod. 60:71-76.

Baltpurvins, K.A., R.C. Burns, G.A. Lawrance and A.D. Stuart. 1996. Effect of pH and anion type on the aging of freshly precipitated iron (III) hydroxide sludges. Environ. Sci. Technol. 30:939-944.

Bauer, M. and C. Blodau. 2006. Mobilization of arsenic by dissolved organic matter from iron oxides, soils and sediments. Sci. Total Environ. 354:179-190.

Beak, D.G., J.K. Kirby, G.M. Hettiarachchi, L.A. Wendling, M.J. McLaughlin and R. Khatiwada. 2011. Cobalt distribution and speciation: Effect of aging, intermittent submergence, in situ rice roots. J. Environ. Qual. 40:679-695.

Benner, S.G., C.M. Hansel, B.W. Wielinga, T.M. Barber and S. Fendorf. 2002. Reductive dissolution and biomineralization of iron hydroxide under dynamic flow conditions. Environ. Sci. Technol. 36:1705-1711.

Berg, M., H.C. Tran, T.C. Nguyen, H.V. Pham, R. Schertenleib and W. Giger. 2001. Arsenic contamination of groundwater and drinking water in vietnam: A human health threat. Environ. Sci. Technol. 35:2621-2626.

Berthelin, J., G. Ona-Nguema, S. Stemmler, C. Quantin, M. Abdelmoula and F. Jorand. 2006. Bioreduction of ferric species and biogenesis of green rusts in soils. Comptes Rendus Geoscience 338:447-455.

Bhattacharya, P., A.H. Welch, K.G. Stollenwerk, M.J. McLaughlin, J. Bundschuh and G. Panaullah. 2007. Arsenic in the environment: Biology and chemistry. Sci. Total Environ. 379:109-120.

Biasioli, M., J. Kirby, G. Hettiarachchi, F. Ajmone-Marsan and M. McLaughlin. 2010. Copper lability in soils subjected to intermittent submergence. J. Environ. Qual. 39:2047-2053.

Bissen, M. and F.H. Frimmel. 2003. Arsenic—a review. part I: Occurrence, toxicity, speciation, mobility. Acta Hydrochim. Hydrobiol. 31:9-18.

Carlson, L., J. Bigham, U. Schwertmann, A. Kyek and F. Wagner. 2002. Scavenging of as from acid mine drainage by schwertmannite and ferrihydrite: A comparison with synthetic analogues. Environ. Sci. Technol. 36:1712-1719.

Cherry, J., A. Shaikh, D. Tallman and R. Nicholson. 1979. Arsenic species as an indicator of redox conditions in groundwater. Journal of Hydrology 43:373-392.

Combs, S.M. and M.V. Nathan. 1998. Soil organic matter. p. 53-58. In Recommended chemical soil test procedures for the north central region. Missouri Ag. Exp. Stn. SB 1001, Colombia, MO.

Cortes-Esquivel, J.A, G. Giácoman-Vallejos, I. D. Barceló-Quintal, R. Méndez-Novelo and M. Ponce-Caballero. 2012. Heavy metals removal from swine wastewater using constructed wetlands with horizontal sub-surface flow. Environ. Prot. 3:871–877.

Cudennec, Y. and A. Lecerf. 2006. The transformation of ferrihydrite into goethite or hematite, revisited. Journal of Solid State Chemistry 179:716-722.

Das, S., J. Essilfie-Dughan and M.J. Hendry. 2014. Arsenate partitioning from ferrihydrite to hematite: Spectroscopic evidence. Am. Mineral. 99:749-754.

Das, S., M.J. Hendry and J. Essilfie-Dughan. 2010. Transformation of two-line ferrihydrite to goethite and hematite as a function of pH and temperature. Environ. Sci. Technol. 45:268-275.

Das, S., J. Essilfie-Dughan and M.J. Hendry. 2015. Fate of adsorbed arsenate during phase transformation of ferrihydrite in the presence of gypsum and alkaline conditions. Chem. Geol. 411:69-80.

Dixit, S. and J.G. Hering. 2003. Comparison of arsenic (V) and arsenic (III) sorption onto iron oxide minerals: Implications for arsenic mobility. Environ. Sci. Technol. 37:4182-4189.

Elrashidi, M., D. Adriano, S. Workman and W. Lindsay. 1987. Chemical equilibria of selenium in soils: A theoretical Development1. Soil Sci. 144:141-152.

Fan, J., Y. Wang, C. Liu, L. Wang, K. Yang, D. Zhou, W. Li and D.L. Sparks. 2014. Effect of iron oxide reductive dissolution on the transformation and immobilization of arsenic in soils: New insights from X-ray photoelectron and X-ray absorption spectroscopy. J. Hazard. Mater. 279:212-219.

Fernández-Martínez, A. and L. Charlet. 2009. Selenium environmental cycling and bioavailability: A structural chemist point of view. Reviews in Environmental Science and Bio/Technology 8:81-110.

Ghosh, D. and B. Gopal. 2010. Effect of hydraulic retention time on the treatment of secondary effluent in a subsurface flow constructed wetland. Ecol. Eng. 36:1044-1051.

Goldberg, S. 2002. Competitive adsorption of arsenate and arsenite on oxides and clay minerals. Soil Sci. Soc. Am. J. 66:413-421.

Goldberg, S. and C.T. Johnston. 2001. Mechanisms of arsenic adsorption on amorphous oxides evaluated using macroscopic measurements, vibrational spectroscopy, and surface complexation modeling. J. Colloid Interface Sci. 234:204-216.

Gräfe, M., E. Donner, R.N. Collins and E. Lombi. 2014. Speciation of metal (loid) s in environmental samples by X-ray absorption spectroscopy: A critical review. Anal. Chim. Acta 822:1-22.

Hansel, C.M., S.G. Benner, J. Neiss, A. Dohnalkova, R.K. Kukkadapu and S. Fendorf. 2003. Secondary mineralization pathways induced by dissimilatory iron reduction of ferrihydrite under advective flow. Geochim. Cosmochim. Acta 67:2977-2992.

Horneman, A., A. van Geen, D.V. Kent, P. Mathe, Y. Zheng, R. Dhar, S. O'connell, M. Hoque, Z. Aziz and M. Shamsudduha. 2004. Decoupling of As and Fe release to Bangladesh groundwater under reducing conditions. part I: Evidence from sediment profiles. Geochim. Cosmochim. Acta 68:3459-3473.

Jambor, J.L. and J.E. Dutrizac. 1998. Occurrence and constitution of natural and synthetic ferrihydrite, a widespread iron oxyhydroxide. Chem. Rev. 98:2549-2586.

Jayaweera, G.R. and J.W. Biggar. 1996. Role of redox potential in chemical transformations of selenium in soils. Soil Sci. Soc. Am. J. 60:1056-1063.

Kadlec, R.H. and S. Wallace. 2008. Treatment wetlands. CRC press.

Kneebone, P., P. O'Day, N. Jones and J. Hering. 2002. Deposition and fate of arsenic in iron-and arsenic-enriched reservoir sediments. Environ. Sci. Technol. 36:381-386.

Kocar, B.D., M.J. Herbel, K.J. Tufano and S. Fendorf. 2006. Contrasting effects of dissimilatory iron (III) and arsenic (V) reduction on arsenic retention and transport. Environ. Sci. Technol. 40:6715-6721.

Kocar, B.D., M.L. Polizzotto, S.G. Benner, S.C. Ying, M. Ung, K. Ouch, S. Samreth, B. Suy, K. Phan and M. Sampson. 2008. Integrated biogeochemical and hydrologic processes driving arsenic release from shallow sediments to groundwaters of the Mekong delta. Appl. Geochem. 23:3059-3071.

Lin, Z. and N. Terry. 2003. Selenium removal by constructed wetlands: Quantitative importance of biological volatilization in the treatment of selenium-laden agricultural drainage water. Environ. Sci. Technol. 37:606-615.

Lizama, K., T.D. Fletcher and G. Sun. 2011. Removal processes for arsenic in constructed wetlands. Chemosphere 84:1032-1043.

Manning, B.A. and S. Goldberg. 1997. Adsorption and stability of arsenic (III) at the clay mineral-water interface. Environ. Sci. Technol. 31:2005-2011.

Manning, B.A. and S. Goldberg. 1996. Modeling competitive adsorption of arsenate with phosphate and molybdate on oxide minerals. Soil Sci. Soc. Am. J. 60:121-131.

Manning, B.A., S.E. Fendorf, B. Bostick and D.L. Suarez. 2002. Arsenic (III) oxidation and arsenic (V) adsorption reactions on synthetic birnessite. Environ. Sci. Technol. 36:976-981.

Marchand, L., M. Mench, D. Jacob and M. Otte. 2010. Metal and metalloid removal in constructed wetlands, with emphasis on the importance of plants and standardized measurements: A review. Environmental Pollution 158:3447-3461.

Masscheleyn, P.H., R.D. Delaune and W. Patrick. 1991a. Arsenic and selenium chemistry as affected by sediment redox potential and pH. J. Environ. Qual. 20:522-527.

Masscheleyn, P.H., R.D. Delaune and W.H. Patrick Jr. 1991b. Effect of redox potential and pH on arsenic speciation and solubility in a contaminated soil. Environ. Sci. Technol. 25:1414-1419.

Masscheleyn, P.H., R.D. Delaune and W.H. Patrick Jr. 1990. Transformations of selenium as affected by sediment oxidation-reduction potential and pH. Environ. Sci. Technol. 24:91-96.

McCarty, K.M., H.T. Hanh and K. Kim. 2011. Arsenic geochemistry and human health in South East Asia. Rev. Environ. Health 26:71-78.

Michel, F.M., L. Ehm, S.M. Antao, P.L. Lee, P.J. Chupas, G. Liu, D.R. Strongin, M.A. Schoonen, B.L. Phillips and J.B. Parise. 2007. The structure of ferrihydrite, a nanocrystalline material. Science 316:1726-1729.

Mladenov, N., Y. Zheng, M.P. Miller, D.R. Nemergut, T. Legg, B. Simone, C. Hageman, M.M. Rahman, K.M. Ahmed and D.M. McKnight. 2009. Dissolved organic matter sources and consequences for iron and arsenic mobilization in Bangladesh aquifers. Environ. Sci. Technol. 44:123-128.

Mohan, D. and C.U. Pittman. 2007. Arsenic removal from water/wastewater using adsorbents—a critical review. J. Hazard. Mater. 142:1-53.

Moore, J.N., W.H. Ficklin and C. Johns. 1988. Partitioning of arsenic and metals in reducing sulfidic sediments. Environ. Sci. Technol. 22:432-437.

Newville, M. 2013. Larch: An analysis package for XAFS and related spectroscopies. p. 012007. In Larch: An analysis package for XAFS and related spectroscopies. Journal of physics: Conference series. IOP Publishing .

Nickson, R., J. McArthur, W. Burgess, K.M. Ahmed, P. Ravenscroft and M. Rahmann. 1998. Arsenic poisoning of Bangladesh groundwater. Nature 395:338-338.

Nickson, R., J. McArthur, P. Ravenscroft, W. Burgess and K. Ahmed. 2000. Mechanism of arsenic release to groundwater, Bangladesh and west Bengal. Appl. Geochem. 15:403-413.

O'Day, P.A., D. Vlassopoulos, R. Root and N. Rivera. 2004. The influence of sulfur and iron on dissolved arsenic concentrations in the shallow subsurface under changing redox conditions. Proc. Natl. Acad. Sci. U. S. A. 101:13703-13708.

Ona-Nguema, G., G. Morin, F. Juillot, G. Calas and G.E. Brown. 2005. EXAFS analysis of arsenite adsorption onto two-line ferrihydrite, hematite, goethite, and lepidocrocite. Environ. Sci. Technol. 39:9147-9155.

Parida, K., B. Gorai, N. Das and S. Rao. 1997. Studies on ferric oxide hydroxides: III. adsorption of selenite (SeO_2^{-3}) on different forms of iron oxyhydroxides. J. Colloid Interface Sci. 185:355-362.

Peak, D. 2006. Adsorption mechanisms of selenium oxyanions at the aluminum oxide/water interface. J. Colloid Interface Sci. 303:337-345.

Pedersen, H.D., D. Postma and R. Jakobsen. 2006. Release of arsenic associated with the reduction and transformation of iron oxides. Geochim. Cosmochim. Acta 70:4116-4129.

Polizzotto, M.L., C.F. Harvey, S.R. Sutton and S. Fendorf. 2005. Processes conducive to the release and transport of arsenic into aquifers of Bangladesh. Proc. Natl. Acad. Sci. U. S. A. 102:18819-18823.

Ponnamperuma, F. 1972. The chemistry of submerged soils. Adv. Agron. 24:29-96.

Qafoku, N.P., U. Kukier, M.E. Sumner, W.P. Miller and D.E. Radcliffe. 1997. Sulfate and phosphate displacement of arsenic from fly ash amended soil.

Ravel, á. and M. Newville. 2005. ATHENA, ARTEMIS, HEPHAESTUS: Data analysis for X-ray absorption spectroscopy using IFEFFIT. Journal of Synchrotron Radiation 12:537-541.

Raven, K.P., A. Jain and R.H. Loeppert. 1998. Arsenite and arsenate adsorption on ferrihydrite: Kinetics, equilibrium, and adsorption envelopes. Environ. Sci. Technol. 32:344-349.

Rietz, D. and R. Haynes. 2003. Effects of irrigation-induced salinity and sodicity on soil microbial activity. Soil Biol. Biochem. 35:845-854.

Riveros, P., J. Dutrizac and P. Spencer. 2001. Arsenic disposal practices in the metallurgical industry. Can. Metall. Q. 40:395-420.

Root, R.A., S. Fathordoobadi, F. Alday, W. Ela and J. Chorover. 2013. Microscale speciation of arsenic and iron in ferric-based sorbents subjected to simulated landfill conditions. Environ. Sci. Technol. 47:12992-13000.

Saalfield, S.L. and B.C. Bostick. 2009. Changes in iron, sulfur, and arsenic speciation associated with bacterial sulfate reduction in ferrihydrite-rich systems. Environ. Sci. Technol. 43:8787-8793.

Sadiq, M. 1997. Arsenic chemistry in soils: An overview of thermodynamic predictions and field observations. Water Air Soil Pollut. 93:117-136.

SAS Institute Inc. 2013. SAS software. 9.4. Cary, NC, USA.

Savant, N.K. and R. Ellis Jr. 1964. Changes in redox potential and phosphorus availability in submerged soil. Soil Sci. 98:388-394.

Schwertmann, U. and E. Murad. 1983. Effect of pH on the formation of goethite and hematite from ferrihydrite. Clays Clay Miner. 31:277-284.

Schwertmann, U. and R.M. Cornell. 2000. Iron oxides in the laboratory: Preparation and characterization. Wiley-VCH, Federal Republic of Germany.

Schwertmann, U. 1991. Solubility and dissolution of iron oxides. Plant Soil 130:1-25.

Smedley, P. and D. Kinniburgh. 2002. A review of the source, behaviour and distribution of arsenic in natural waters. Appl. Geochem. 17:517-568.

Smith, D.B., W.F. Cannon, L.G. Woodruff, F. Solano, J.E. Kilburn and D.L. Fey. 2013. Geochemical and mineralogical data for soils of the conterminous united states. US Geological Survey Data Series 801:19.

Su, C. and D.L. Suarez. 2000. Selenate and selenite sorption on iron oxides an infrared and electrophoretic study. Soil Sci. Soc. Am. J. 64:101-111.

Takahashi, Y., R. Minamikawa, K.H. Hattori, K. Kurishima, N. Kihou and K. Yuita. 2004. Arsenic behavior in paddy fields during the cycle of flooded and non-flooded periods. Environ. Sci. Technol. 38:1038-1044.

Tate, M. 2005. Kansas water quality standards and supporting documents. Kansas Department of Health and Environment, Topeka, Kansas.

Tokunaga, T.K., G.E. Brown, I.J. Pickering, S.R. Sutton and S. Bajt. 1997. Selenium redox reactions and transport between ponded waters and sediments. Environ. Sci. Technol. 31:1419-1425.

Tufano, K.J. and S. Fendorf. 2008. Confounding impacts of iron reduction on arsenic retention. Environ. Sci. Technol. 42:4777-4783.

Tufano, K.J., C. Reyes, C.W. Saltikov and S. Fendorf. 2008. Reductive processes controlling arsenic retention: Revealing the relative importance of iron and arsenic reduction. Environ. Sci. Technol. 42:8283-8289.

USEPA. 2007. Method 3051A: Microwave assisted acid digestion of sediments, sludges, soils, and oils. Test methods http://www3.epa.gov/epawaste/hazard/testmethods/sw846/pdfs/3051a.pdf (accessed on 10th of December, 2011).

Wenzel, W.W., N. Kirchbaumer, T. Prohaska, G. Stingeder, E. Lombi and D.C. Adriano. 2001. Arsenic fractionation in soils using an improved sequential extraction procedure. Anal. Chim. Acta 436:309-323.

Yamaguchi, N., T. Nakamura, D. Dong, Y. Takahashi, S. Amachi and T. Makino. 2011. Arsenic release from flooded paddy soils is influenced by speciation, Eh, pH, and iron dissolution. Chemosphere 83:925-932.

Zachara, J.M., R.K. Kukkadapu, J.K. Fredrickson, Y.A. Gorby and S.C. Smith. 2002. Biomineralization of poorly crystalline fe (III) oxides by dissimilatory metal reducing bacteria (DMRB). Geomicrobiol. J. 19:179-207.

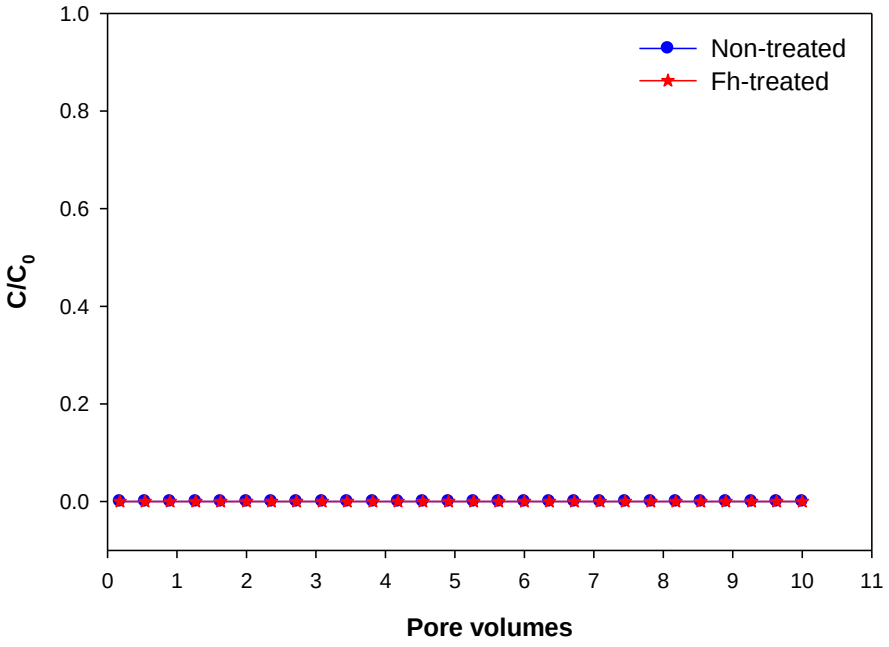

Figure 4.1 Breakthrough curves of selenium for the non-treated and the ferrihydrite (Fh)-treated soil columns.

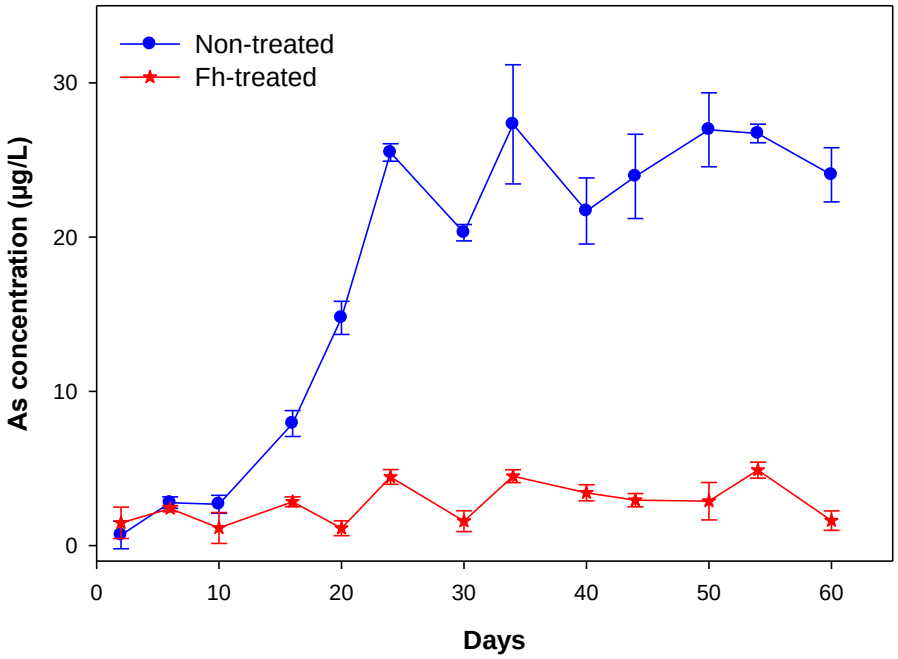

Figure 4.2 Arsenic concentrations of effluent samples collected from the non-treated and the ferrihydrite (Fh)-treated soil columns.

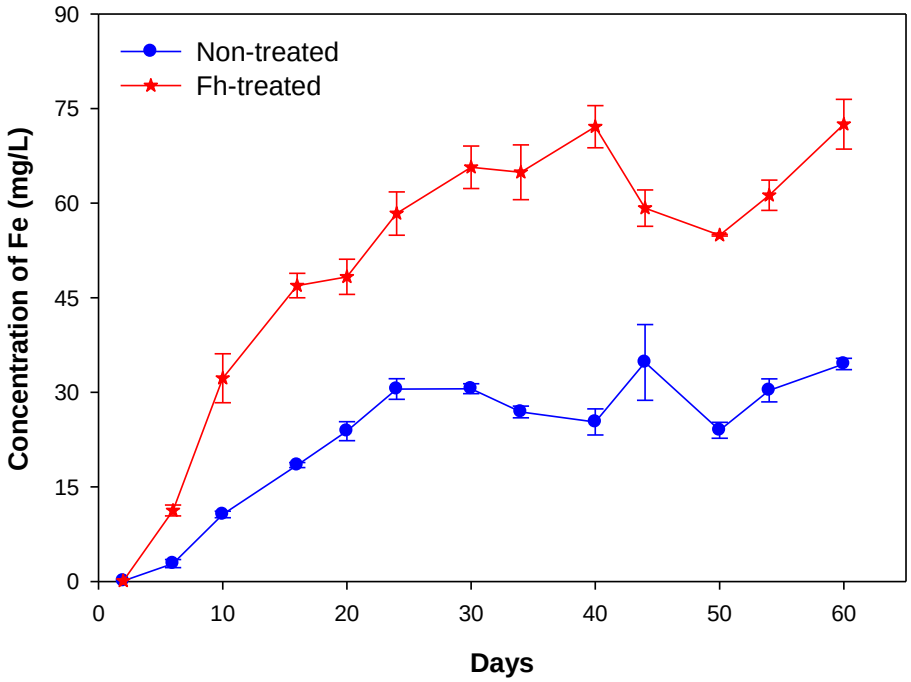

Figure 4.3 Total dissolved iron (Fe) concentration of effluent samples collected from the non-treated and the ferrihydrite (Fh)-treated soil columns.

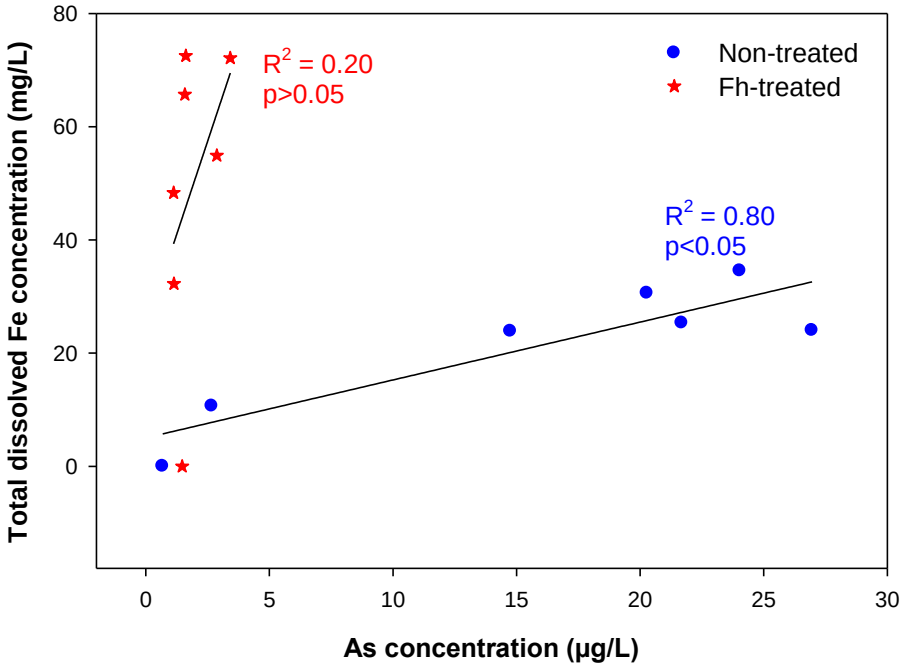

Figure 4.4 Relationship of As vs Fe of effluent samples collected from the non-treated and ferrihydrite (Fh)-treated soil columns.

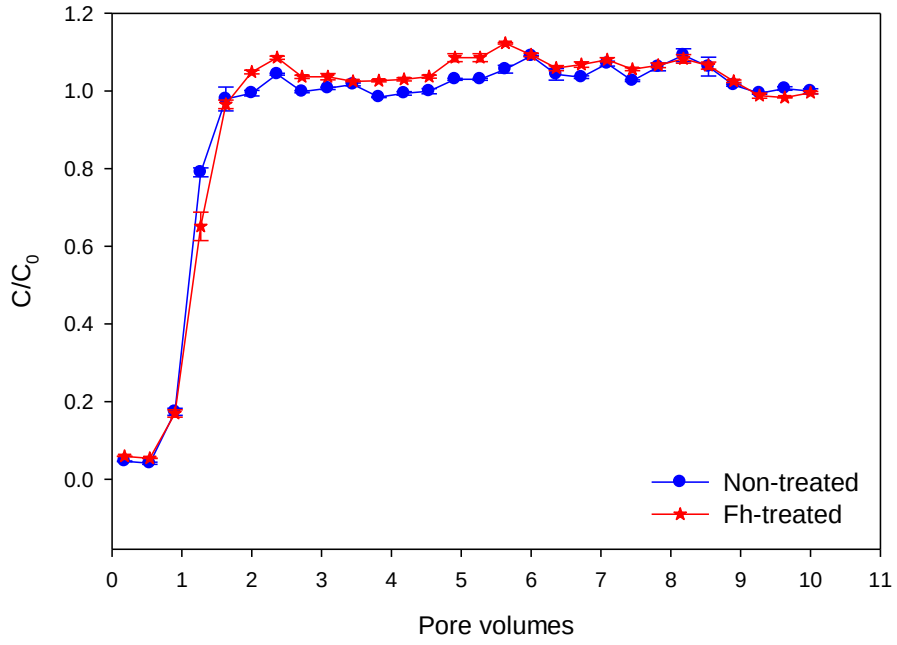

Figure 4.5 Breakthrough curves of sulfate-sulfur (SO_4^{2-}-S) for the non-treated and the ferrihydrite (Fh)-treated soil columns.

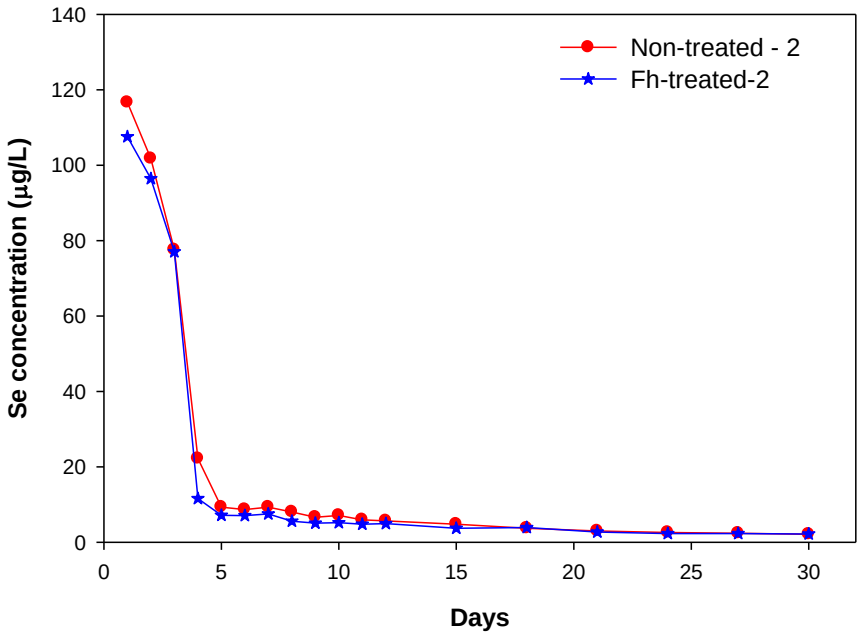

Figure 4.6 Selenium concentration of effluent samples collected after 60 days of feeding with the FGD wastewater followed by drying and re-wetting with the FGD wastewater for an additional 30 days of the non-treated-2 and the ferrihydrite (Fh)-treated-2 columns.

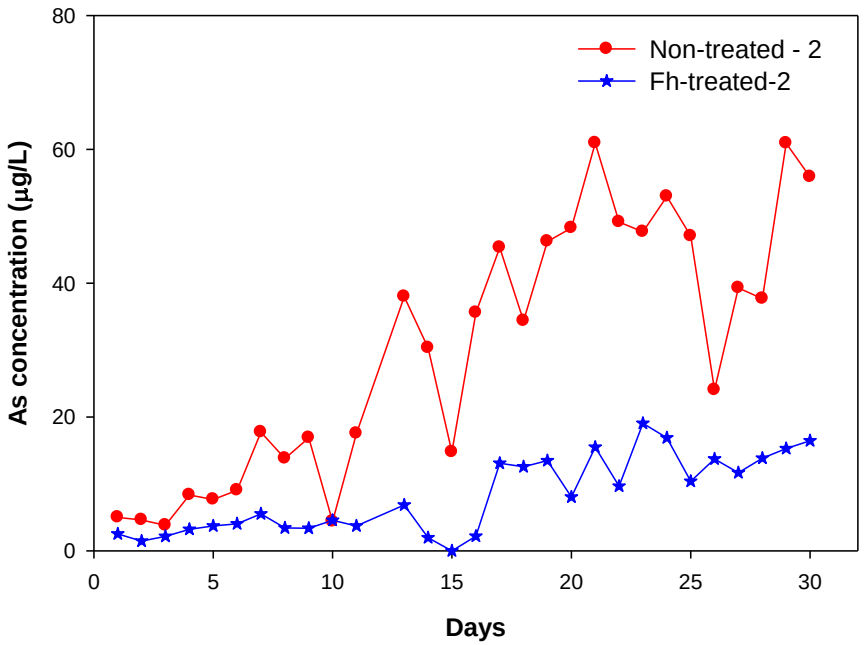

Figure 4.7 Arsenic concentration of effluent samples collected after 60 days of feeding with the FGD wastewater followed by drying and re-wetting with the FGD wastewater for an additional 30 days of the non-treated-2 and the ferrihydrite (Fh)-treated-2 columns.

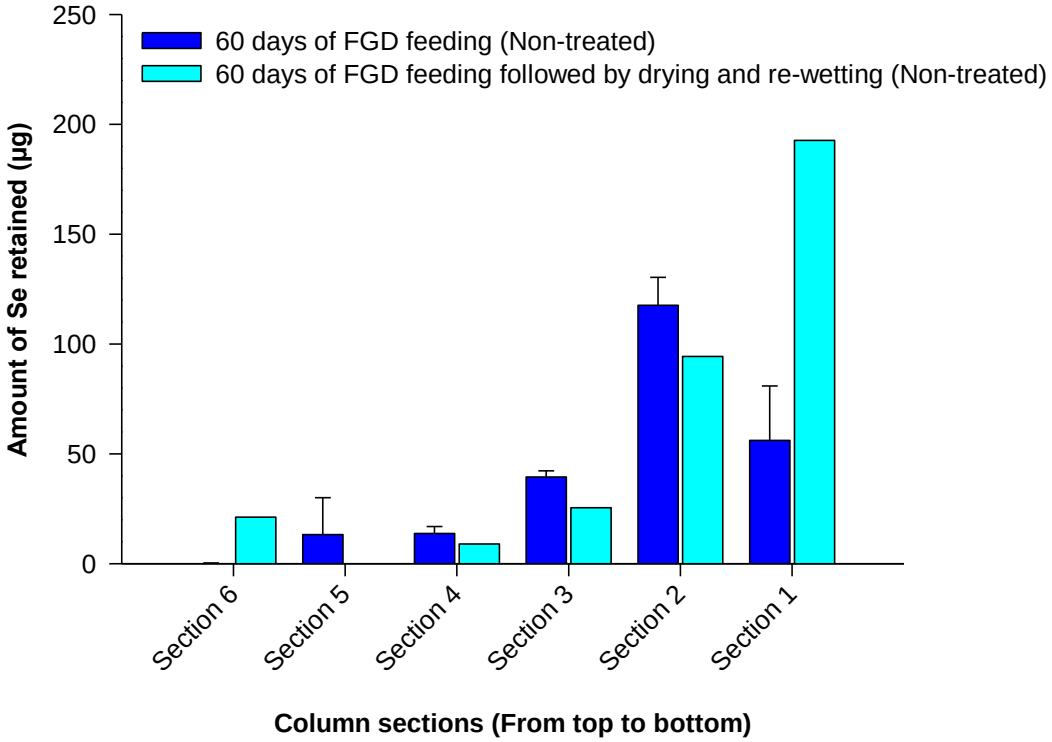

Figure 4.8 Distribution of Se in soil columns after feeding of the FGD wastewater in non-treated soil columns for 60 days and 60 days of the FGD feeding followed by drying and re-wetting with the FGD wastewater for 30 additional days.

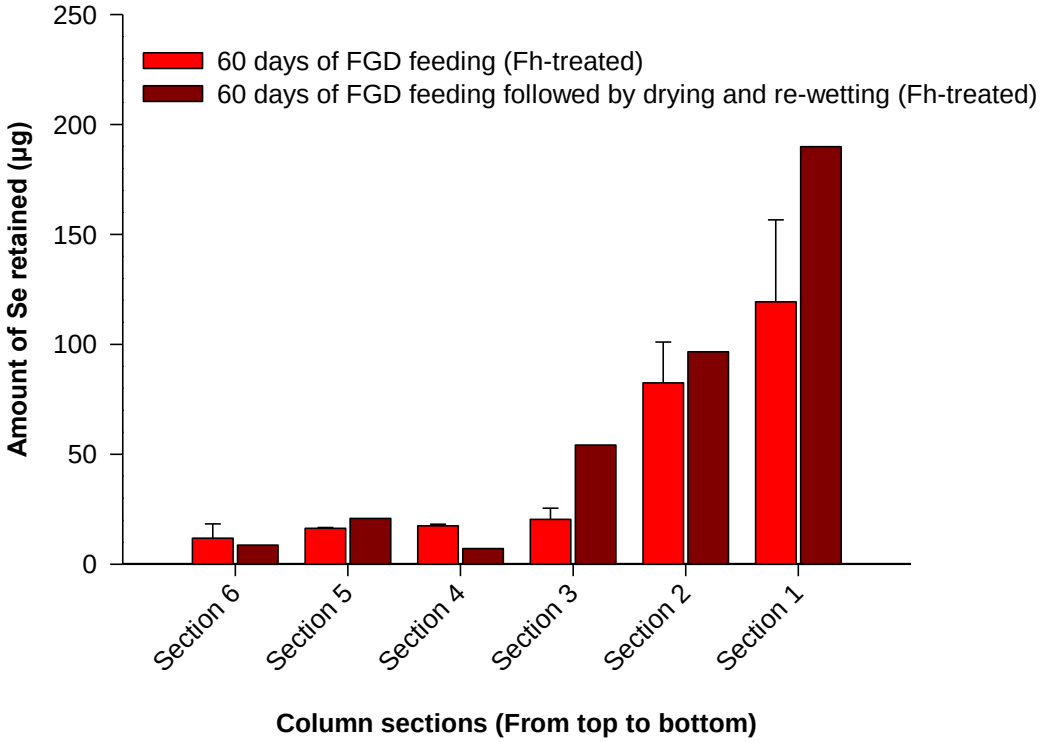

Figure 4.9 Distribution of Se in soil columns after feeding of the FGD wastewater in the ferrihydrite (Fh)-treated soil columns for 60 days and 60 days of the FGD feeding followed by drying and re-wetting with the FGD wastewater for 30 additional days.

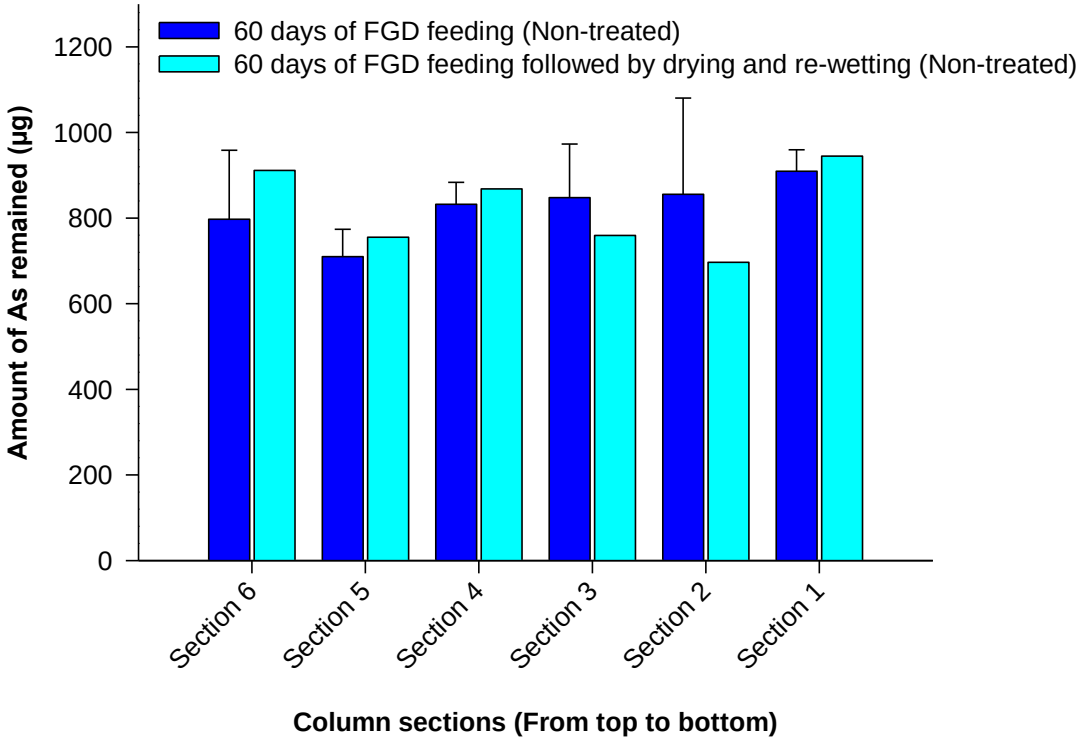

Figure 4.10 Distribution of remaining As in the non-treated soil columns after 60 days of the FGD wastewater feeding followed by drying and re-wetting with the FGD wastewater feeding for 30 additional days.

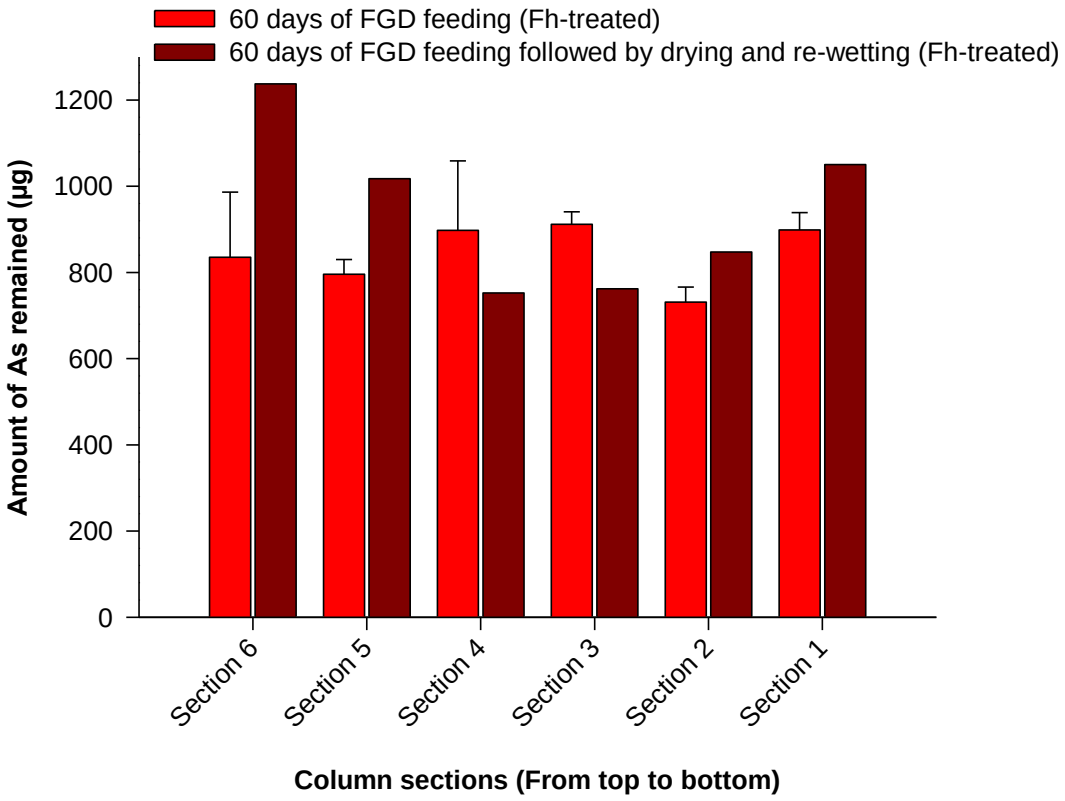

Figure 4.11 Distribution of remaining As in the ferrihydrite (Fh)-treated soil columns after 60 days of the FGD wastewater feeding followed by drying and re-wetting with the FGD wastewater feeding for 30 additional days.

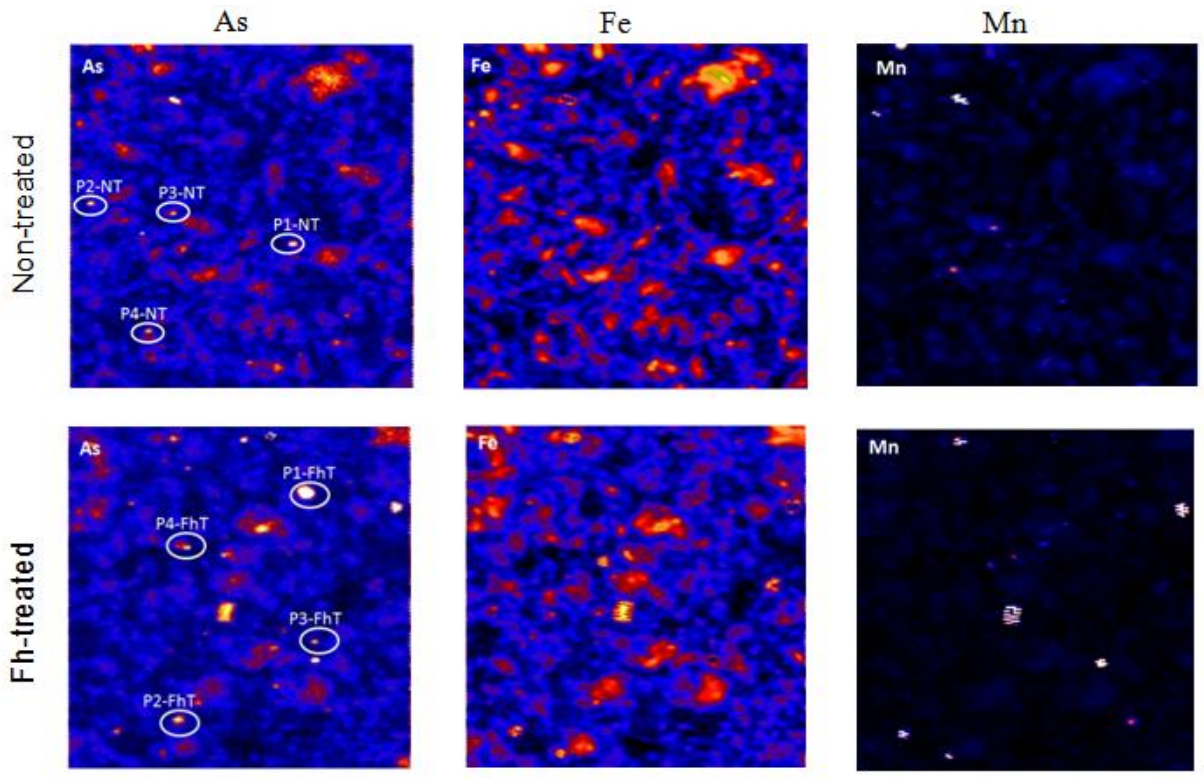

Figure 4.12 Micro-XRF maps showing the elemental distribution of arsenic (As), iron (Fe), and manganese (Mn) generated on the non-treated and the ferrihydrite (Fh)-treated soils. P1-NT, P2-NT, P3-NT and P4-NT are the As hotspots on non-treated soil and P1-FhT, P2-FhT, P3-FhT and P4-FhT are As hotspots on Fh-treated soil used for micro-XANES analysis.

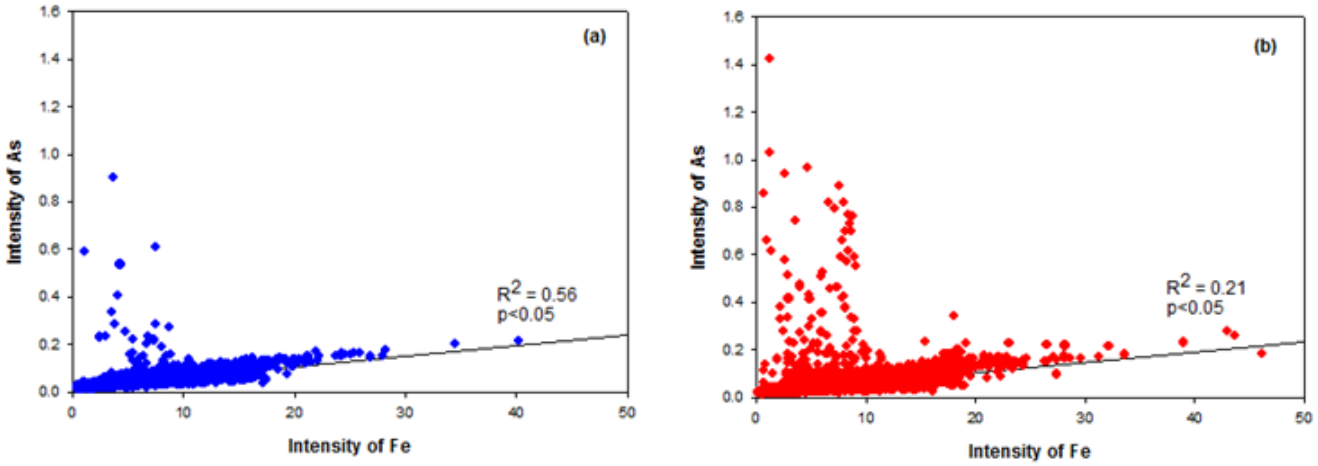

Figure 4.13 Correlation of arsenic (As) and iron (Fe) generated from the whole micro-XRF maps; (a) non-treated soil (b) Ferrihydrite (Fh)-treated soil.

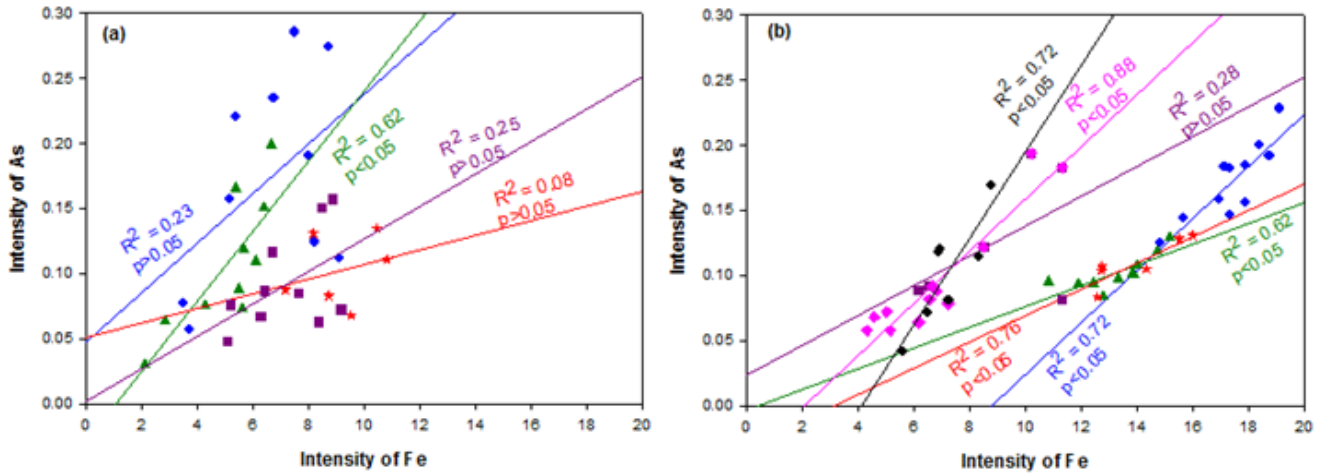

Figure 4.14 Correlation of arsenic (As) and iron (Fe) generated As rich areas; (a) non-treated soil (b) Ferrihydrite (Fh)-treated soil.

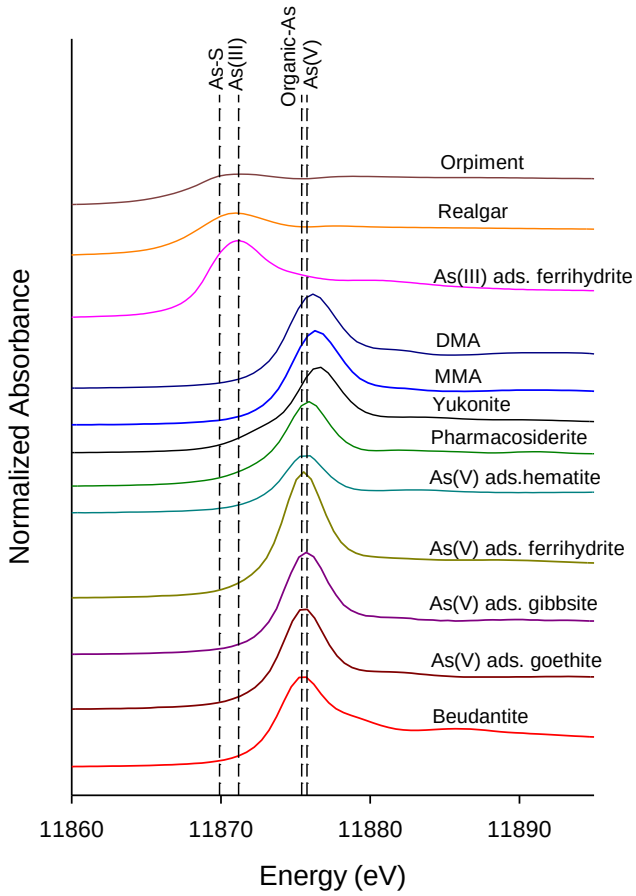

Figure 4.15 Arsenic K-edge XANES spectra of the standards used for linear combination fitting (LCF) analysis. Vertical short-dashed lines are to represent white line energy of As(V) (11875.8 eV), organic-As (11875.4 eV), As(III) (11871.2 eV), and As-sulfide (11870.0 eV).

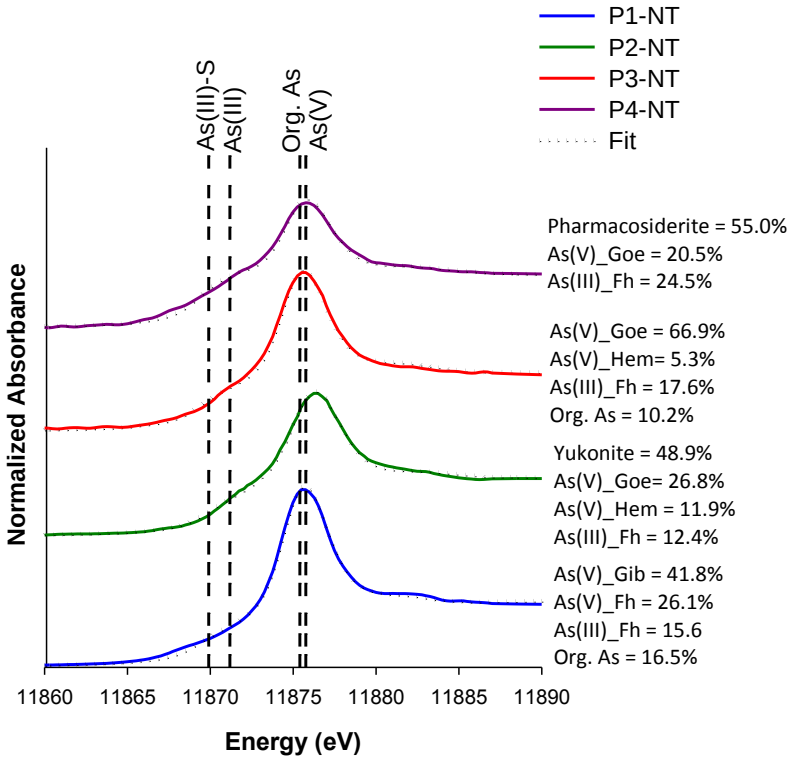

Figure 4.16 Arsenic K-edge XANES spectra of hotspots (P1-NT, P2-NT, P3-NT, and P4-NT) and linear combination fitting (LCF) results of the non-treated soil. Dotted lines are showing the fit from LCF and vertical short-dashed lines are to represent white line energy of As(V) (11875.8 eV), organic-As (11875.4 eV), As(III) (11871.2 eV), and As-sulfide (11870.0 eV).

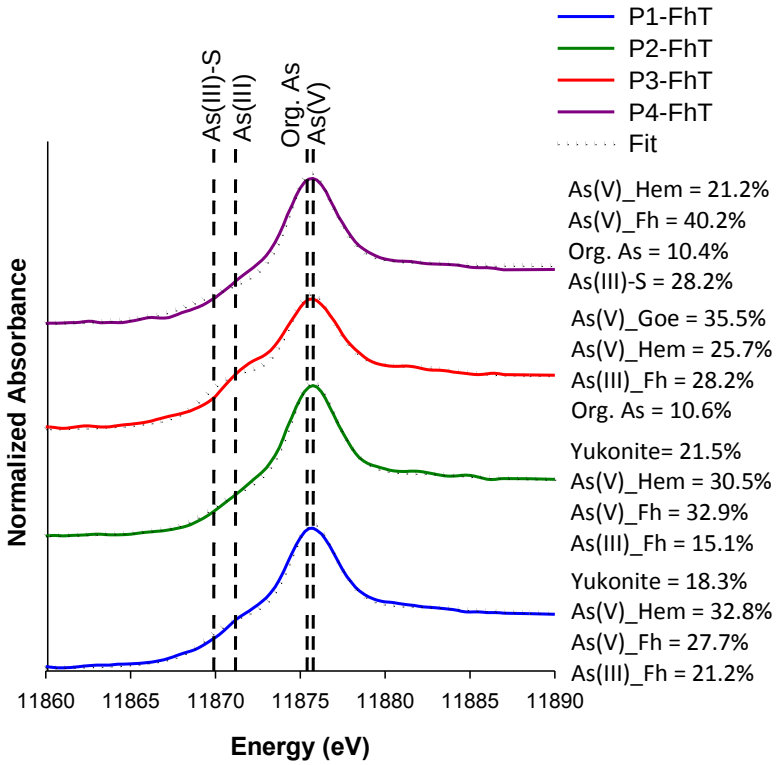

Figure 4.17 Arsenic K-edge XANES spectra of hotspots (P1-FhT, P2-FhT, P3-FhT, and P4-FhT) and linear combination fitting (LCF) results of the ferrihydrite (Fh)-treated soil. Dotted lines are showing the fit from LCF and vertical short-dashed lines are to represent white line energy of As(V) (11875.8 eV), organic-As (11875.4 eV), As(III) (11871.2 eV), and As-sulfide (11,870.0 eV).

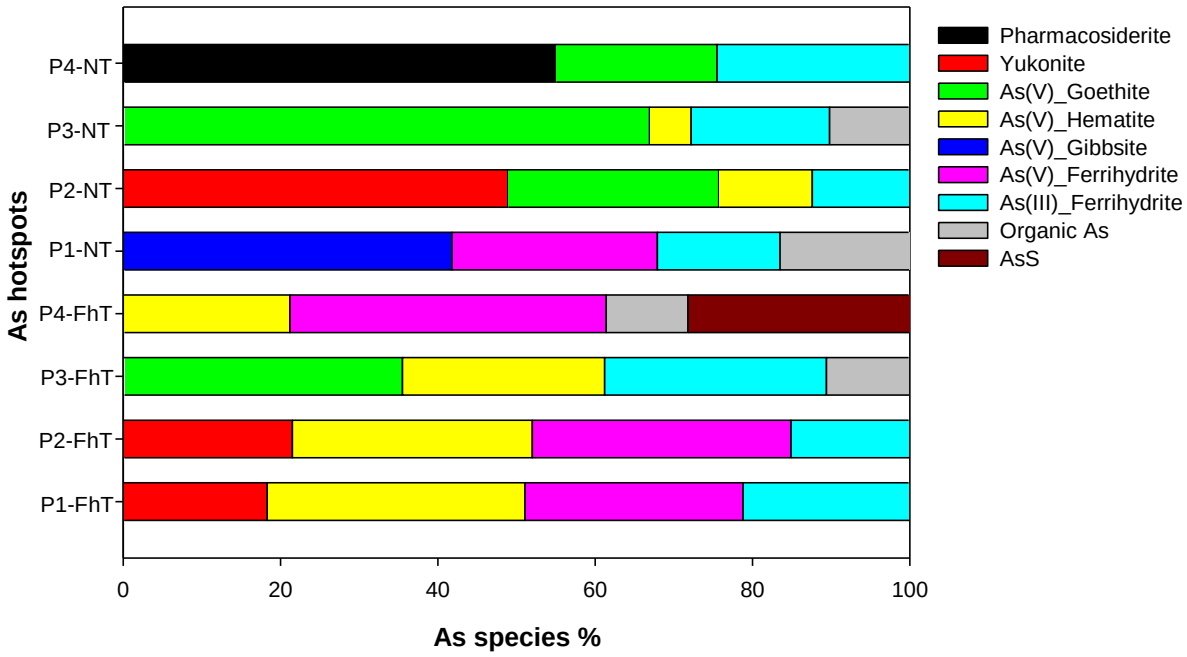

Figure 4.18 Summary of micro As-XANES linear combination fitting results (LCF) for As hotspots (P1-NT, P2-NT, P3-NT, and P4-NT) on the non-treated soil and P1-FhT, P2-FhT, P3-FhT, and P4-FhT hotspots on the ferrihydrite(Fh)-treated soil.

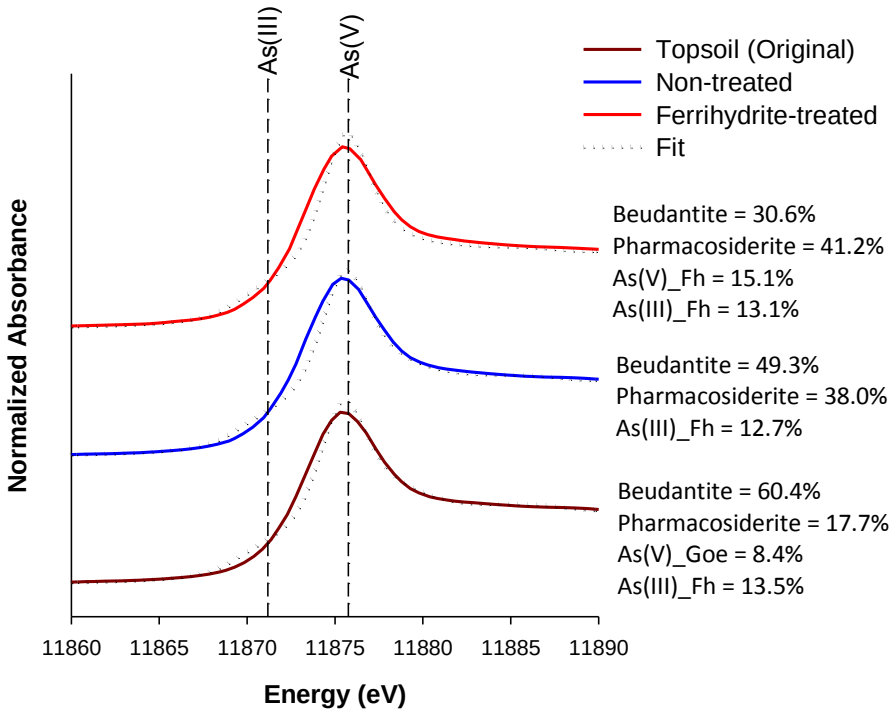

Figure 4.19 Arsenic K-edge bulk-XANES spectra and linear combination fitting (LCF) results of the non-treated and the ferrihydrite (Fh)-treated soils. Dotted lines are showing the fit from LCF and vertical short-dashed lines are to represent white line energy of As(V) (11875.8 eV), and As(III) (11871.2 eV) species.

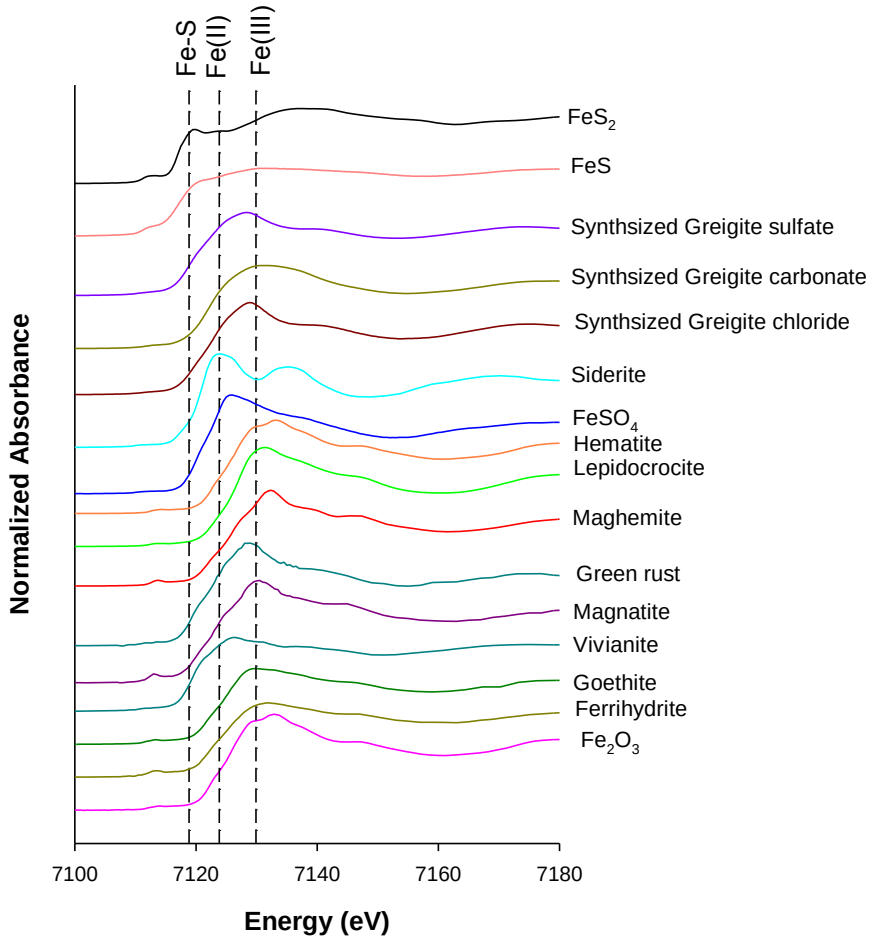

Figure 4.20 K-edge XANES spectra of the iron standards used for linear combination fitting (LCF) analysis. Vertical short-dashed lines are to represent white line energy of Fe(III) (7129.9 eV), Fe(II) (7123.8 eV), and Fe-sulfur (7118.9 eV).

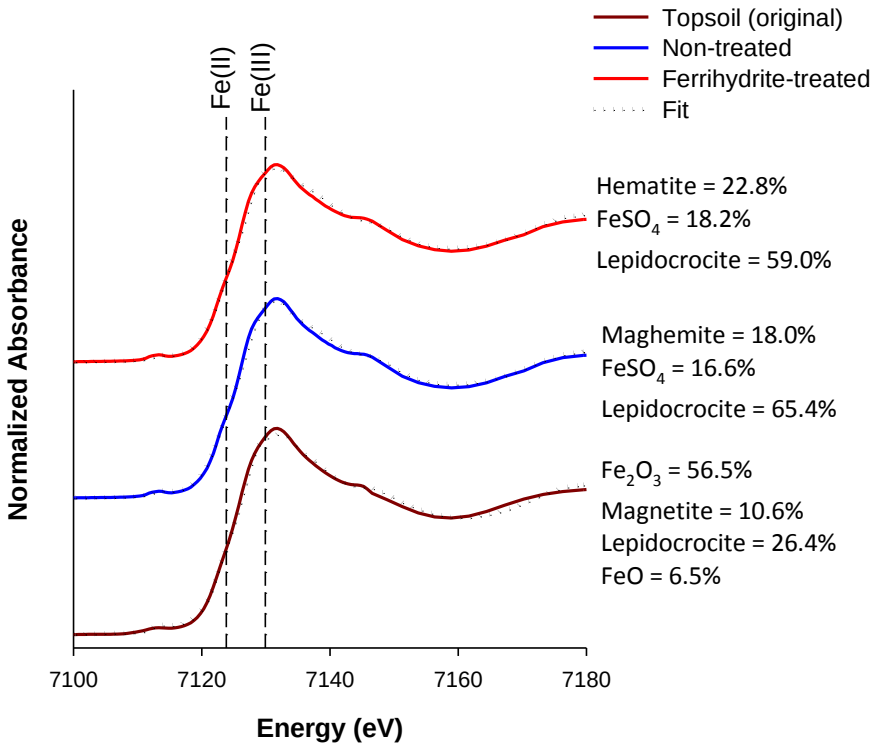

Figure 4.21 Iron K-edge bulk-XANES spectra and linear combination fitting (LCF) results of the non-treated and the ferrihydrite (Fh)-treated soil. Dotted lines are showing the fit from LCF and vertical short-dashed lines are white line energy of Fe(III) (7129.9 eV), and Fe(II) (7123.8 eV).

Table 4.1 Total element concentration and soil parameters of topsoil original material

Total element concentration and soil parameters	Topsoil
Se, mg/kg	0.5
As, mg/kg	7.3
S, mg/kg	507.0
Mn, mg/kg	521.0
Fe, %	1.5
Al, %	1.8
pH (1:5 soil:water)	6.6
OM[#], %	6.2
CEC[¶], $cmol_+/kg$	31.8
Sand, silt, and clay, %	4.3, 49.1, 46.6

Organic matter

¶ Cation exchange capacity

Table 4.2 Concentrations of constituents of the FGD wastewater and the raw water collected from the Jeffery Jeffrey Energy Center (JEC), St. Marys, KS on 4th of October, 2011.

Constituents	FGD wastewater*	Raw water
As, µg/L	1.2	2.0
Se, µg/L	135	1.0
Mg, mg/L	553.6	16.4
B, mg/L	8.6	1.4
K, mg/L	215.6	11.5
Ca, mg/L	653.8	67.8
Na, mg/L	706.0	46.5
Fe, mg/L	<0.1	<0.1
Total-S, mg/L	1334.4	32.0
SO_4^{2-}, mg/L	4062.3	105.0
SO_4^{2-}-S, mg/L	1354.1	35.0
F^-, mg/L	18.0	< 0.1
Cl^-, mg/L	1010.0	54.1
NO_3^-, mg/L	146.6	18.0
EC†, ds/m	5.3	-
pH¶	8.2	-

¶pH of 1:1 mixture of FGD wastewater:raw water

† EC-Electrical conductivity of 1:1 mixture of FGD wastewater:raw water

* The FGD wastewater is the water after treatments to remove some of the sulfur and other compounds. It is the wastewater used to conduct this experiment. The 1:1 mixture of FGD wastewater:raw water was used as the influent for the soil columns.

Table 4.3 Arsenic speciation of the hotspots on non-treated soil determined by linear combination fitting (LCF) of As micro-XANES analysis.

As hot spots	§1	2	3	4	5	6	7	8	9	10	R-factor¶	Red. χ^2†
						As micro-XANES of non-treated soil (%)						
P1-NT	-	-	-	41.8	-	-	26.1	16.5	15.6	-	0.0005	0.001
P2-NT	-	-	48.9	-	26.8	11.9	-	-	12.4	-	0.0081	0.001
P3-NT	-	-	-	-	66.9	5.3	-	10.2	17.6	-	0.0011	0.002
P4-NT	-	55.0	-	-	20.5	-	-	-	24.5	-	0.0020	0.002

§1, Beudantite; 2, Pharmacosiderite; 3, Yukonite; 4, As(V) adsorbed to gibbsite; 5, As(V) adsorbed to goethite; 6, As(V) adsorbed to hematite; 7, As(V) adsorbed to ferrihydrite; 8, As(organic); 9, As(III) adsorbed to ferrihydrite; 10, As(III)-S

¶R-factor: normalized sum of the squared residuals of the linear combination fit.

†$\chi^2 = \sum[(\text{fit-data})/\varepsilon)\ ]^2 /(N_{data}-N_{components})$ is the reduced chi-square statistic. Here ε is the estimated uncertainty in the normalized XANES data (taken as 0.01 for all data). The sum is over N_{data} points (133 data points between E=11854 and 11904 eV for all data), and $N_{components}$ is the number of components in the fit (3 or 4 as indicated in the Table). The total percentage was constrained to be 100% in all fits. Typical uncertainties in the percentages listed for each standard component are 5%.

Table 4.4 Arsenic speciation of the hotspots on ferrihydrite (Fh)-treated soil determined by linear combination fitting (LCF) of As micro-XANES analysis

As hot spots	§1	2	3	4	5	6	7	8	9	10	R-factor¶	Red. χ^2†
As micro-XANES of ferrihydrite-treated soil (%)												
P1-FhT	-	-	18.3	-	-	32.8	27.7	-	21.2	-	0.0012	0.002
P2-FhT	-	-	21.5	-	-	30.5	32.9	-	15.1	-	0.0010	0.001
P3-FhT	-	-	-	-	35.5	25.7	-	10.6	28.2	-	0.0030	0.004
P4-FhT	-	-	-	-	-	21.2	40.2	10.4	-	28.2	0.0028	0.004

§1, Beudantite; 2, Pharmacosiderite; 3, Yukonite; 4, As(V) adsorbed to gibbsite; 5, As(V) adsorbed to goethite; 6, As(V) adsorbed to hematite; 7, As(V) adsorbed to ferrihydrite; 8, As(organic); 9, As(III) adsorbed to ferrihydrite; 10, As(III)-S

¶R-factor: normalized sum of the squared residuals of the linear combination fit.

†$\chi^2 = \sum[(\text{fit-data})/\varepsilon)\ ]^2 /(N_{data}-N_{components})$ is the reduced chi-square statistic. Here ε is the estimated uncertainty in the normalized XANES data (taken as 0.01 for all data). The sum is over N_{data} points (133 data points between E=11854 and 11904 eV for all data), and $N_{components}$ is the number of components in the fit (4 as indicated in the Table). The total percentage was constrained to be 100% in all fits. Typical uncertainties in the percentages listed for each standard component are 5%.

Table 4.5 Arsenic speciation of the top soil (original), non-treated and ferrihydrite (Fh)-treated soils determined by linear combination fitting (LCF) of As bulk-XANES analysis

Sample	§1	2	3	4	5	6	7	8	9	10	R-factor¶	Red. χ^2†
	As bulk-XANES species											
Top soil (original)	60.4	17.7	-	-	8.4	-	-	-	13.5	-	0.0040	0.005
Non-treated	49.3	38.0	-	-	-	-	-	-	12.7	-	0.0055	0.008
Fh-treated	30.6	41.2	-	-	-	-	15.1	-	13.1	-	0.0063	0.010

§1, Beudantite; 2, Pharmacosiderite; 3, Yukonite; 4, As(V) adsorbed to gibbsite; 5, As(V) adsorbed to goethite; 6, As(V) adsorbed to hematite; 7, As(V) adsorbed to ferrihydrite; 8, As(organic); 9, As(III) adsorbed to ferrihydrite; 10, As(III)-S

¶R-factor: normalized sum of the squared residuals of the linear combination fit.

†$\chi^2 = \sum[(\text{fit-data})/\varepsilon)\ ]^2 /(N_{data}-N_{components})$ is the reduced chi-square statistic. Here ε is the estimated uncertainty in the normalized XANES data (taken as 0.01 for all data). The sum is over N_{data} points (99 data points between E=11852 and 11902 eV for all data), and $N_{components}$ is the number of components in the fit (4 as indicated in the Table). The total percentage was constrained to be 100% in all fits. Typical uncertainties in the percentages listed for each standard component are 5%.

Table 4.6 Iron speciation of the top soil (original), non-treated and ferrihydrite (Fh)-treated soils determined by linear combination fitting (LCF) of Fe bulk-XANES analysis

Sample	Fe_2O_3	Magnetite	Maghemite	Hematite	Lepidocrocite	FeO	$FeSO_4$	R-factor¶	Red. χ^2†
					Fe bulk-XANES species				
Top soil (original)	56.5	10.6	-	-	26.4	6.5	-	0.0004	0.0004
Non-treated	-	-	18.0	-	65.4	-	16.6	0.0006	0.0005
Fh-treated	-	-	-	22.8	59.0	-	22.8	0.0005	0.0004

¶ R-factor: normalized sum of the squared residuals of the linear combination fit.

†$\chi^2 = \sum[(\text{fit-data})/\varepsilon)]^2 / (N_{data}-N_{components})$ is the reduced chi-square statistic. Here ε is the estimated uncertainty in the normalized XANES data (taken as 0.01 for all data). The sum is over N_{data} points (84 data points between E=7105 and 7155 eV for all data), and $N_{components}$ is the number of components in the fit (3 or 4 as indicated in the Table). The total percentage was constrained to be 100% in all fits. Typical uncertainties in the percentages listed for each standard component are 5%.

Chapter 5 - Understanding of the retention of trace elements by sulfate reduction in a pilot-scale constructed wetland treatment system designed for flue-gas desulfurization wastewater

Abstract

Generally, flue-gas desulfurization (FGD) wastewater fails to comply with surface water quality standards. Our previous work showed that constructed wetland treatment systems (CWTSs) are effective in removing selenium from FGD wastewater, but less effective for arsenic (As), and sulfur (S). A laboratory-based soil column experiment mimicking a pilot-scale CWTS was carried out to assess the effect of flow rate and soil treatments (ferrihydrite, and labile organic carbon (OC)) on S and As retention by the CWTS, and to gather mechanistic information of interrelationships between S, As, and Fe cycling in the CWTS. Soil columns were packed with topsoil inoculated with 0.5% (w/w) of soil slurry. Deoxygenated 1:1 mixture of FGD wastewater:raw water was used as the influent. It was delivered to the saturated soil columns for 60 days with an upward constant flow at X (1.42 mL/hr), and 2X rates. Based on the results from this study, a long-term study (365 days) was also performed with X, and 1/2 X rates. Effluents were analyzed for constituents of concern. At the end of these experiments, the soil from the sectioned columns were used for bulk S, As, and Fe X-ray absorption near edge structure (XANES) spectroscopy analysis. The results indicated that the slow flow rate with labile OC was conducive for the S retention. The As concentration of the effluent collected from these columns also decreased with time. The bulk S-, As-, and Fe-XANES revealed that the long submergence period formed reduced S [S(0), and S(-2)], realgar-like (AsS), and greigite-like stable phases.

These results indicated that the slow flow rates could have a significant impact on the long-term sequestration of trace elements (such as As) in the CWTS.

Introduction

The capability of constructed wetland treatment systems (CWTSs) to purify flue-gas desulfurization (FGD) wastewater is being considered as an economically and environmentally effective adaptation. Within the function of the FGD system, lime or limestone scrubbers react with sulfur dioxide of the flue-gas and form calcium sulfate, improving the quality of the flue-gas emissions (Srivastava and Jozewicz, 2001; Srivastava et al., 2001). In general, FGD wastewater is enriched with trace elements as well as elevated levels of sulfate (SO_4^{2-}) as a result of the dewatering process of the FGD system (EPRI, 2006). Because of high concentrations of constituents including SO_4^{2-}, FGD wastewater fails to meet water quality parameters. Typically, FGD wastewater has total SO_4^{2-} concentration about 10 g/L and dissolved SO_4^{2-} concentration about 3 g/L. The FGD wastewater is supersaturated with respect to gypsum (EPRI, 2006). The SO_4^{2-} concentration in domestic wastewater is between 20 and 500 mg/L compared to several thousands of milligrams per liter of industrial wastewater (Lens et al., 1998).

Sulfate reduction induced by microbial activities, and concomitant metal sulfide formation is one of the main mechanisms for the retention of trace elements in acid-mine drainage, and metal-contaminated wastewaters (Dvorak et al., 1992; Lewis, 2010; Sheoran and Sheoran, 2006). The physical, chemical, and biological processes in CWTSs provide the capability of removing trace elements, and other constituents from contaminated waters (Vymazal, 2010; Yeh, 2008). Low oxidation-reduction potential of the wetlands, typically ranged between -300 mV and +700 mV, favors the bacterial reduction of sulfate. The reduction of sulfate to sulfide in waterlogged soils occurs at the redox potential between +100 mV and -

250 mV, and pH at 6.5 to 8.5 (Connell and Patrick, 1968). Upon flooding soils, first oxygen concentration decreases followed by nitrate, oxidized manganese, and ferric ion compounds. Under anoxic environments, and when there is no sufficient substrate for microbial activities, microbes look for alternative sources and reduce SO_4^{2-} to sulfide.

Dissimilatory SO_4^{2-} reduction is mediated by sulfate reducing bacteria (SRB) which acts as an electron donor during the anaerobic oxidation of inorganic or organic substrate such as H_2, CO_2, lactate, and acetate (Stein et al., 2007). Organic carbon is an energy source for the activities of microorganisms, and affects in decreasing the redox potential in soils (Rahman et al., 2011). A typical reaction for the reduction of SO_4^{2-} in the presence of lactate (an electron donor) is:

$$SO_4^{2-} + 2\ lactate \rightarrow 2\ acetate + H_2S + 2HCO_3^-$$

Then, at high concentration of dissolved metals (M^{n+}) in soil solution tend to precipitate as stable metal sulfide phases (Benner et al., 1999; Stein et al., 2007). Previous studies have revealed that the microbially-mediated SO_4^{2-} reduction is one of the main mechanisms that involves in trace metals sequestration in the environment through chemical stabilization (Buddhawong et al., 2005; White et al., 1997).

$$H_2S + M^{n+} \rightarrow M_2S_n + 2H^+$$

In addition, Fe(II) produced by dissimilatory Fe reducing bacteria, and subsequent reaction with sulfide forms biogenic ferrous sulfides such as Fe monosulfides (FeS), greigite, and pyrite (FeS_2) (Kwon et al., 2014; Neal et al., 2001; Saalfield and Bostick, 2009).

The microbially-mediated SO_4^{2-} reduction followed by stable metal sulfide formation is a vital mechanism for As sequestration in soils (Borch et al., 2009; Kaksonen and Puhakka, 2007; Saalfield and Bostick, 2009). The fate and transport of As in soils/sediments is controlled by the coupling of S, and Fe biogeochemical cycling. Under reducing environments, and in the presence

of S and Fe, As tends to form insoluble sulfide compounds such as orpiment, realgar, and arsenopyrite (Buddhawong et al., 2005; O'Day et al., 2004) in addition to co-precipitation reactions with Fe sulfides (Bostick and Fendorf, 2003; Burton et al., 2014; Schwindaman et al., 2014).

Influent flow rate of FGD wastewater may have a significant effect on the removal of constituents by the CWTS. Hydraulic residence time (HRT), and hydraulic loading rate (HLR) determine the performance efficiency of the CWTS (Kadlec and Wallace, 2008; Marchand et al., 2010; USEPA, 1995). With high HLR and short HRT, adsorption sites become saturated, and there is inefficient capacity for adsorption, precipitation, and biotic reactions. The long HRT favors biotic reactions and SO_4^{2-} reduction, because prolonged submergence will transfer more electrons from the degradation of solid substrates (organic matter) to the aqueous phase. Previous studies have revealed that slow flow rate significantly enhances SO_4^{2-} reduction and sulfide formation due to decrease in redox potential (Stark et al., 1995). Additionally, wastewater with high salt concentration can influence microbial activities by exertion of osmotic pressure on their metabolism (Bassin et al., 2011; Oren, 2011). Besides the effect of salinity, and sodicity on soil physical properties, the microbially-mediated processes are inhibited by salt-affected soil most likely due to the decrease of enzyme activities, soil aggregation, and stabilization (Kaksonen and Puhakka, 2007; Rietz and Haynes, 2003).

The CWTSs are an effective option to remove trace elements such as selenium (Se), and mercury (Hg) from FGD wastewater, but less effective for As (Eggert et al., 2008; Rodgers Jr and Castle, 2008). A series of continuous flow-through experiments that carried out to assess the performance of a pilot-scale CWTS designed for FGD wastewater also showed similar results. According to our previous studies, addition of ferrihydrite to construction wetland material was

able to minimize As mobility that was primarily caused by reductive dissolution of native soil. The efficiency of the removal of S or the sulfate reduction in the CWTS was weak as revealed by our previous studies. Since SO_4^{2-} is a common, and enriched constituent in FGD wastewater, transformation of SO_4^{2-} to sulfide can have a significant impact on the efficiency of the CWTS. Therefore, it is hypothesized here that reduction of SO_4^{2-} can be induced by the presence of SRB, and labile OC, thereby enhancing the retention of S, and trace elements (such as As) in the CWTS designed for FGD wastewater. We further hypothesize that the secondary transformation of added ferrihydrite can enhance the sequestration of released As by the reductive dissolution of native soil.

A laboratory-based continuous flow-through soil column experiment mimicking a pilot-scale CWTS at Jeffery Energy Center (JEC), St. Mary, KS was carried out assess the effect of flow rate and soil treatments (ferrihydrite, and labile OC) on S and As retention by the CWTS, and to gather mechanistic information of interrelationships between S, As, and Fe cycling in the CWTS using synchrotron-based X-ray absorption near edge structure (XANES) spectroscopy analysis.

Materials and Methods

Soil and FGD wastewater collection

Topsoil (Clime (Fine, mixed, active, mesic Udorthentic Haplustolls)-Sogn (Loamy, mixed, superactive, mesic Lithic Haplustolls) complex silty clay) was collected at 0-10 cm depth from an area nearby Westar Energy's Jeffrey Energy Center (JEC) located at, Pottawatomie County, St. Marys, Kansas (39°17’10”N, 96°07’01”W). The topsoil (TS) material was analyzed for basic soil properties such as soil texture, soil pH, cation exchange capacity (CEC), and organic matter (OM) content using established methodologies (Table 5.1) described in previous

studies (Chapter 3, and Chapter 4). Flue-gas desulfurization wastewater and Kansas river water (i.e., raw water) were also collected from the JEC on 27th of February, 2012. The concentrations of constituents of 1:1 mixture of FGD wastewater: raw water was determined (Table 5.2) by following the detailed steps given in Chapter 3, and Chapter 4.

Packing of soil columns and FGD wastewater feeding

Soil columns were packed using topsoil according to the wet packing procedure described in Chapter 3. There were twelve soil columns used for this study. The soil was inoculated with 0.5% (dry weight basis) of soil slurry (Ivan, Kennebec, and Kahola silt loams) collected from North Agronomy farm closer to the creek at Kansas State University, Manhattan, KS. The main purpose of inoculating the soil with the soil slurry was to enhance microbial activities in the soil columns. Karna (2014) confirmed the presence of SRB in this soil slurry. About 1% (w/w) of 2-line ferrihydrite (Fh) was also used as a treatment. The ferrihydrite was thoroughly mixed with the soil prior to wetting step.

There were two influent flow rates used for this study; 1.42 mL/hour (X rate) and 2.84 mL/hour (2X rate). Similar to the previous column studies, deoxygenated 1:1 mixture of FGD wastewater: raw water was the influent. Sodium lactate (labile OC substrate) was added to the influent solution to promote microbial activities further. For X rate, and 2X rate columns, 48 mM, and 24 mM of sodium lactate was respectively mixed with one liter of the diluted FGD wastewater in order to provide same amount of OC to all soil columns. In this study, there were two treatments for X flow rate, and four treatments for 2X flow rate. Each treatment consisted of two replicates. Treatment composition/amendments are as follows:

1.42 mL/hour (X rate)

1. TS (control X)

2. TS + OC + Fh (X)

2.84 mL/hour (2X rate)

1. TS (control 2X)

2. TS + OC (2X)

3. TS + Fh (2X)

4. TS + OC + Fh (2X)

After the columns were packed with the inoculated soil, they were slowly saturated with raw water (see Chapter 3 for more detail). Once columns were saturated and achieved steady-state condition (approximately within 10 days), the influent solution was continuously delivered to the soil columns with flow in upward direction. Effluent samples were collected every other day, and their weight was recorded. The effluent samples were immediately filtered and stored as non-acidified or acidified samples at 4 ^{0}C depending on the targeted analysis.

Analysis of influent and effluent

The FGD wastewater (influent), and the column effluent samples that had been filtered through 0.45 µm syringe filters (Environmental Express Inc., South Carolina, USA), and acidified with 2 to 3 drops of 6 M HCl were used for dissolved elemental analysis. A graphite furnace atomic absorption spectrometry (GF-AAS) (Varian Inc.) equipped with Zeeman. In this analysis, palladium modifier (500 mg/L) was used to enhance the As absorbance signal. The concentrations of other major constituents of the solutions were measured using a Varian 720-ES Inductive couple plasma-optical emission spectrometry (ICP-OES). The samples that were unacidified, and filtered through 0.2 µm syringe filters (Environmental Express Inc., South Carolina, USA) were analyzed by an ion chromatograph (ICS-1000, Dionex Corporation) to determine the concentrations of anions, including SO_4^{2-}. A blank, a sample of NIST 1643e

"Trace Elements in Water" SRM, and randomly selected spiked samples were used for quality assurance/quality control assessment. The recoveries were in the range of 94% to 98% for the NIST sample, and those were for the spiked samples ranged from 91% to 114%.

Long-term soil column study

Based on the results of above study (discussed below), a long-term experiment (365 days long) was carried out. In this study as well, the soil was inoculated with 0.5% (dry weight basis) of soil slurry collected from the North Agronomy farm at Kansas State University. The flow rates of the influent for this experiment were 0.71 mL/hour (1/2 X rate), and 1.42 mL/hour (X rate). There were two replicates for each flow rate. For 1/2X rate, and X rate columns, 96 mM, and 48 mM of sodium lactate was respectively mixed with one liter of the influent. The column study with X-flow rate [TS+OC (X)] was terminated after 191 days due to clogging issues encountered in those columns. The 1/2 X rate columns [TS+OC (1/2X)] were continued for 365 days. At the end of these studies, columns were cut into six sections (more detail in Chapter 3). Appropriately preserved soil samples from bottom sections of the columns were used for bulk-XANES analysis of S, As, and Fe.

Soil preparation and S bulk-XANES analysis

The synchrotron-based X-ray absorption spectroscopy analysis was performed at the Advanced Photon Source (APS), Argonne National laboratory (ANL), Argonne, IL. The soil samples that were stored in a freezer at -20 ^{0}C were transported to the APS using an air-tight container (Oxoid AnaeroJar, 2.5 L) with an AnaeroGen sachet. At the APS, samples were stored in a freezer until the analysis was performed. The sample preparation was carried out in a N_2 filled glove box located at the beamline. First, a small amount (~ 0.1-0.2 g) of a sample was finely ground with an agate mortar and pestle. The effect of grinding influences the quality of S-

XANES spectra (Bolin, 2010). In the glove box, the ground soil was used to prepare pellets with a diameter of 4 mm using a quick press kit with 4mm die set (International Crystal Laboratories, Garfield, NJ). Until the analysis was performed, the prepared samples were stored in the glove box to avoid air exposure.

The S K-edge bulk-XANES data were collected at Sector 9 BM-B at the APS. This beamline is equipped with Si (111) monochromator. The beam size used for our study was 300 µm x 300 µm. Energy was calibrated using the absorption edge of sodium thiosulfate standard by setting the energy at 2469.2 eV. A prepared sample was attached onto a S-free tape, which was centered on a piece of Teflon holder, and finally it was fixed on to an aluminum sample holder (Figure C.1). The sample compartment, and flight path were in the helium environment to eliminate air absorption. The samples were mounted at 45^0 angle with respect to the X-ray beam. The data were collected in fluorescence mode using a 4-element Vortex Si drift detector. Four to six scans per sample were collected within energy between 2435 to 2600 eV. The step size was 2.0 eV in pre edge region (2435 to 2465 eV), 0.125 eV in XANES region (2465 to 2510 eV), and 0.5 k weight in post edge region (2510 to 2600 eV) with integration time of 5 seconds per point. A set of ten S standard compounds was used for this study. The S-XANES spectra of all these standards were also collected at the Sector 9 BM-B. Those standards were calcium sulfate ($CaSO_4$), ferrous sulfate ($FeSO_4$), sodium sulfite anhydrous (Na_2SO_3), sodium methanesulfonate (CH_3SO_3Na), L-methionine, L-cysteine, DL-methionine sulfoxide, elemental S, pyrite (FeS_2), and iron sulfide (FeS). The data processing was done following the standard procedures of ATHENA software version 0.9.20 (Ravel and Newville, 2005).

The normalized spectra were analyzed using Gaussian peak fitting with the 0.9.20 version of the ATHENA in the energy range of 2462 to 2492 eV. The S-XANES spectra were fitted

using a series of Gaussian peaks which represent the s →p transitions, and arctangent step functions which represent the transition of ejected photoelectrons to the continuum (Prietzel et al., 2003; Prietzel et al., 2011; Prietzel et al., 2009; Xia et al., 1998). The first, and the second arctangent function represent the edge step of reduced (2469.4 eV), and the oxidized S species (2477.4 eV), respectively (Prietzel et al., 2003; Xia et al., 1998). The positions of the Gaussians were selected based on the white-line energy (energy at which the first inflection point of the first derivative) positions of the S standards. In the analysis, the positions, and widths of the all Gaussians and the arctangent functions were kept as fixed, while the peak heights were allowed to vary with the fits. The area of the S white-line peak is proportional to the oxidation state of the X-ray-absorbing S atom (Xia et al., 1998). Thus, the peak area should increase as the oxidation state increases. A strong correlation between the white-line peak energy, and the oxidation state of the S standards was observed (Figure C.2). It was in agreement with previous studies (Prietzel et al., 2003; Xia et al., 1998). Various species of S in the soil samples were identified by comparing the respective white-line peak energy of the standards (Table 5.3). The fractions of different S species are not directly proportional to the relative areas of each Gaussian peak (Manceau and Nagy, 2012). Therefore, the areas of the Gaussian peaks obtained from the fitting were subsequently corrected using the calibration curve of absorption cross-section area as described in Xia et al. (1998). The adjusted peak area was the calculated peak area divided by absorption constants taken from the calibration curve. The respective proportions of the various S species were calculated by comparing the corrected area under the peak of interest with the sum of all areas in the energy range between 2462 and 2492 eV.

Arsenic, and iron bulk-XANES analysis

The sample preparation for both As, and Fe bulk-XANES analysis was similar to the procedure described in Chapter 4. The data analysis was performed using linear combination fitting (LCF) method in ATHENA version 0.8.056 (Ravel and Newville, 2005). Arsenic standards used for LCF include dimethylarsenate (DMA), monomethylarsenate (MMA), orpimant (As_2S_3), realgar (As_4S_4), As(V) adsorbed to gibbsite, As(V) adsorbed to goethite, As(V) adsorbed to ferrihydrite, As(V) adsorbed to hematite, pharmacosiderite [$KFe_4^{3+}(AsO_4)_3(OH)_4 \cdot$ 6-7H_2O], and beudantite [$PbFe^{3+}_3(AsO_4)(SO_4)(OH)_6$], yukonite [$Ca_7Fe^{3+}_{11}(AsO_4)_9O_{10} \bullet 24.3(H_2O)$], and As(III) adsorbed to ferrihydrite, sodium arsenate, and sodium arsenite. A set of Fe standards included siderite ($FeCO_3$), vivianite [$Fe_3(PO_4)_2.8H_2O$], magnetite (Fe_3O_4), ferrihydrite [$Fe_{10}O_{14}(OH)_2$], goethite (α-FeOOH), green rust, Fe(III) oxide (Fe_2O_3), Fe(II) oxide (FeO), iron sulfate ($FeSO_4$), maghemite (1/2γ-Fe_2O_3) , lepidocrocite (γ-FeOOH), hematite (1/2α-Fe_2O_3), Fe(II) sulfide (FeS) and pyrite (FeS_2). In addition, synthesized-greigite,-chloride,-sulfate, and -carbonate were obtained from XAS databases (http://xraysweb.lbl.gov/uxas/Databases/Overview.htm). The species abundance <5% was not accounted for LCF results.

Statistical analysis

Statistical analysis was performed using SAS for Windows version 9.4 (SAS Institute Inc., 2013). The overall design was repeated-measures over time. A one-way analysis of variance (ANOVA) using PROC MIXED was performed to analyze the effect of treatments on the concentrations of constituents in the effluent samples. Pairwise Bonferroni method was used for pairwise comparison between the treatment means at 5% level of significance (α=0.05).

Results and Discussion

Treatment effects on S behavior

The breakthrough curves (BTCs) developed in the experiment for SO_4^{2-}-S was used to understand how the behavior of SO_4^{2-} altered with the soil treatments, and the influent flow rate. In the BTCs, the x-axis represents the pore volumes (PVs), and the y-axis represents the relative effluent concentration of SO_4^{2-} (C/C_0). The concentration SO_4^{2-} in the effluent solution was denoted by C whereas C_0 was the concentration of SO_4^{2-} in the influent FGD wastewater solution. One pore volume for the 2X flow rate (2.84 mL/hour) soil columns was equal to 5.5 days, and that for 1X rate (1.42 mL/hour) columns was 11 days.

For the 2X rate soil columns, breakthrough of SO_4^{2-}-S occurred early (around at 1.5 PVs) in the control (TS inoculated with soil slurry) (Figure 5.1). This could imply that the retention of SO_4^{2-} in the soil was weak or minimal under given conditions. Also, the behavior of SO_4^{2-}-S in the columns treated with sodium lactate (labile OC source) was more or less similar to the TS (control 2X) soil columns (Figure 5.1). The reason could most likely be that faster flow rate of the FGD influent did not provide sufficient time for the biogenic SO_4^{2-} reduction (Stark et al., 1995). In addition, the FGD wastewater is enriched with substantial amount of salts, total dissolved solids, and other constituents which may also create non-conducive and/or non-favorable environment for SRB (Kaksonen and Puhakka, 2007; Oren, 2011). The relative concentration of SO_4^{2-}-S was greater than one after 1.5 pore volumes of both systems. Leaching of SO_4^{2-} bound to exchangeable sites of soil particles can affect the effluent concentration exceeding the influent concentration. Once exchangeable SO_4^{2-} completely leached out, the relative concentration of SO_4^{2-}-S reached the level closer to one, after 6 PVs in both soil columns. Non-specifically bound sulfate ions can easily exchange by similar ions because they

are held only by electrostatic charges in the diffuse double layer. They are not held as tightly as specifically adsorbed ions to metal oxides in the Helmholtz layer (Edwards, 1998). The enhanced SO_4^{2-} mobility can also be due to the fact that depolymerization of a large organic matrix into smaller organic moieties by enzyme activities in the soil (i.e., mineralization of organic S to inorganic S) (Edwards, 1998).

The addition the ferrihydrite to the soil did not enhance SO_4^{2-} reduction (Figure 5.2a). The patterns of the BTC for the ferrihydrite added columns were more or less similar to that of the control (2X). Previous studies have revealed that SO_4^{2-} reduction is delayed if an anoxic sediment is abundant with Fe(III) oxy(hydr)oxide (Chapelle and Lovley, 1992; Lovley and Phillips, 1987). The behavior of SO_4^{2-} -S in the TS+Fh+OC (2X) was similar to the TS (control 2X) as depicted in Figure 5.2b. There was a slight increment of SO_4^{2-} retention in the TS+Fh+OC (2X) columns towards the end of the study (Figure 5.2b), but it was not statistically significant. As stated in previous studies, after Fe(III) is depleted from reductive dissolution, increased Fe(II) concentration in solution can favor SO_4^{2-} reduction (Chapelle and Lovley, 1992; Ponnamperuma, 1972). However, high flow rate used in this study may not have provided sufficient conditions to see significant difference between the two treatments. Thus, hydraulic residence time, and loading rate are important parameters that assess the performance efficiency of a CWTS (Kadlec and Wallace, 2008; Marchand et al., 2010; USEPA, 1995).

The columns fed with the FGD wastewater at the slow flow rate [TS (control X)] showed significantly enhanced ($p<0.05$) SO_4^{2-} reduction compared to the control with the high flow rate [(TS (control 2X)] (Figure 5.3). This indicates that the slow flow rate helped retaining S in the FGD wastewater. Neculita et al. (2008) evaluated the long-term performance efficiency of a sulfate reducing passive bioreactor using two HRTs (7.3 days and 10 days). They found that the

higher HRT produced better effluent because longer residence time was able to enhance the quality of physiochemical parameters such as pH, alkalinity, SO_4^{2-}, and metals removal. In the reactor that was conducted at 10 days HRT, sulfide associated with Fe, and metals were detected using X-ray dispersion and X-diffraction methods (Neculita et al., 2008). Drury (2000) presented a mathematical model for sulfate reduction in wetlands. That study predicted that the rate of sulfate reduction depends on several factors including temperature, biodegradability of the organic substrate, and HRT. Stark et al. (1995) found that low flow rate of a wetland mesocosm experiment significantly influenced lowering the redox potential, and enhancing the SO_4^{2-} reduction.

In the present study, the slow flow rate columns treated with ferrihydrite, and labile OC [TS+Fh+OC (X)] appeared to increase S retention significantly ($p<0.05$), compared to the control [TS (control X)] (Figure 5.4). The ferrihydrite only treatment at the 2X flow rate did not affect SO_4^{2-} reduction. Our previous study as well observed similar results (Chapter 4). This suggests that the addition of labile OC along with the slow flow rate of the FGD wastewater can significantly enhance the S retention in the CWTS. It has been widely documented that organic carbon drives the mechanism of microbially-mediated sulfate reduction (Borch et al., 2009; Edwards, 1998; Stein et al., 2007). In addition, organic carbon can increase the reduction of Fe(III) by promoting the activities of Fe reducing bacteria, which could also enhance the sulfate reduction (Chapelle and Lovley, 1992; Lovley and Phillips, 1987).

The pH of the aqueous medium is a critical factor that determines the metal/metalloid-sulfide precipitation in a CWTS (Dorman et al., 2009). In the present study, the pH of effluent samples remained between 6.5 and 7.1. The soil pH of the original material was 6.6. After feeding with the FGD wastewater, the pH of top sections of the columns was near neutral (6.8 to

7.1) whereas that of bottom sections was 7.3 to 7.6. There was a slightly alkaline pH at the bottom section (inlet) of soil columns compared to the top section. Initially, the addition of FGD wastewater with alkaline pH can significantly influence the pH of the bottom sections. Upon submergence, reductive dissolution processes can increase the soil pH due to the consumption of protons, and subsequent release of trace elements (such as As) from binding sites.

Treatment effect behavior on native soil As

The As concentration in the 1:1 mixture of FGD wastewater and raw water was negligible (1.1 µg/L) (Table 5.2). However, the As concentration of effluents collected from the soil columns increased with time, suggesting that reductive dissolution of Fe minerals of native soil released As into soil solution. This is in accordance with the results observed in Chapter 4. Previous studies have also observed that CWTSs are less effective for As retention due to the effect of reductive dissolution (Eggert et al., 2008; Rodgers Jr and Castle, 2008). The dissolved As concentration of effluents collected from the TS (control 2X), and the control treated with sodium lactate [TS+OC (2X)] is depicted in Figure 5.5. The As concentration in the effluent of both sets of columns increased with time (until 2.5 PVs), and then decreased during the latter part of the experiment. It is also clear from the figure that As leaching from the OC treated soil columns was significantly (7.3 ±0.5 to 55.3±2.3µg/L) greater than that from the control soil [TS control (2X)] columns (8.3 ±0.6 to 45.6±1.3µg/L). The cumulative amount of As released from the TS (control 2X) was 98.4 ±1.2 µg whereas that from the TS+OC (2X) was 110.2±0.3 µg. This implies that the addition of OC led to increase the activity of Fe reducing bacteria, thereby promoting the reductive dissolution of As associated Fe minerals in the soil. Previous studies have reported that the reductive dissolution of As from Fe oxy(hydr)oxide minerals is

biologically driven by the presence of dissolved OC (Islam et al., 2004; Kocar et al., 2008; Nickson et al., 1998; Polizzotto et al., 2005; Yamaguchi et al., 2011).

The concentration of As in the effluent collected from the non-treated soil columns (2X rate) of previous study (Chapter 4) was in the range of 1.0±1.0 to 27.3±3.8 µg/L. It was significantly low compared to the As concentration of effluent from TS (control 2X) of this study (8.3 ±0.6 to 45.6±1.3µg/L). This implies that the soil inoculated with the soil slurry positively influenced the reductive dissolution of native soil under wetland conditions, most likely due to the enhancement of microbial activities. The concentrations of As of effluent collected from the ferrihydrite treated columns [TS+Fh (2X)] were significantly low (2.4±0.4 to 8.8 ±0.8 µg/L), compared to the TS (control 2X) soil columns (8.3±0.6 to 45.6±1.7 µg/L) as shown in Figure 5.6. Similar results were observed in the previous study (Chapter 4). The cumulative amount of As released from the TS (control 2X) was 98.4 ±1.2 µg and that of from TS+Fh (2X) was 13.2±0.5 µg over 60 days of the study period. There results confirm that the amendment of native soil (constructed wetland material) with ferrihydrite plays a significant role in slowing down the native soil As mobility in the CWTS. This will also help to enhance the effectiveness of the CWTS for As removal, if the FGD wastewater had elevated levels of As in it. There was no significant difference for As retention in both TS+Fh (2X) and TS+Fh+OC (2X) soil columns (Figure 5.7). Although the dissolution of As associated Fe minerals is accelerated by the labile OC, the sequestration of released As onto newly formed Fe phases upon the reductive dissolution of the ferrihydrite can retard As mobility in the native soil (Benner et al., 2002; Hansel et al., 2003; Kocar et al., 2006; Tufano et al., 2008). This mechanism was confirmed in the previous study (Chapter 4).

The effect of influent flow rate on the dissolution of As is important to ascertain its behavior in the CWTS because these wetlands can be operated at different flow rates (Figure 5.8). The concentration of As in the effluent collected from the slow flow rate [TS (control X)] columns (8.5±0.3 to 58.5±8.8 µg/L) was significantly greater than that from the fast flow rate [TS (control 2X] columns (8.3±0.6 to 45.6±1.7 µg/L). This could most likely be due to the reason that slow flow rate, and long residence time can increase microbial activities as well as decrease in soil redox potential (McGeehan and Naylor, 1994; Stark et al., 1995). Also, changes in redox potential can have a significant impact on the As mobility (Masscheleyn et al., 1991; Smedley and Kinniburgh, 2002). However, this difference tended to decrease with time because as the soil gets further reduced, the As dissolution is controlled by precipitation/co-precipitation reactions in conjunction with Fe and S cycling (Fan et al., 2014; Smedley and Kinniburgh, 2002). Over the study period, the cumulative amount of As released by the TS (control X) columns was 72.0±6.3 µg while that of by the TS (control 2X) was 98.4±6.3 µg. The volume of effluent collected from the TS (control 2X) columns was as doubled as the TS (control X) columns. Hence, the cumulative amount of As released from TS (control 2X) was greater than that from the TS (control X), although the concentration differences showed the opposite trend. The As concentration of effluent collected from the TS+Fh+OC (X) columns remained significantly low (2.7±0.03 to 12.3±0.4 µg/L) compared to that of TS (control X) (Figure 5.9). The addition of ferrihydrite was able to minimize the As mobility in the native soil, regardless of the flow rate.

Behavior of S and As in the long-term study with slower flow rates

In this study, breakthrough curves were developed for total-S instead of SO_4^{2-}-S to understand how the behavior of S alters with the flow rate. The results from the short-term study

showed that the behavior of SO_4^{2-}-S was similar to that of total-S (Figure C.3). One pore volume of the X rate (1.42 mL/hour) columns was 11 days, and that of the 1/2 X rate (0.71 mL/hour) columns was 22 days. The total number of pore volumes performed for X rate, and 1/2 X rate columns were 17.4 (191 days) and 16.6 (365 days), respectively.

After 191 days of feeding with the FGD wastewater, the pH of the soil in bottom sections (inlet) was 8.0 to 8.2 whereas that of in top sections was 7.6 to 7.9. The pH of the columns that were fed with the FGD wastewater for 365 days was 8.3 to 8.5 (bottom sections), and that for top sections was 8.1 to 8.3. The pH of the soil collected from the long-term study was alkaline compared to the short-term studies. The increase in soil pH is most likely due to the accumulation of alkali salt over time (Essington, 2004).

The BTCs (Figure 5.10) clearly showed that the total-S concentrations of effluent came out from TS+OC (1/2X) columns was significantly ($p<0.05$) lower than that of the TS+OC (X) columns. Although the total-S concentration of column effluent increased with time, the S retention in the TS+OC (1/2X) columns was still striking. The mass balance calculation revealed that 47.5% of the total S fed with the FGD wastewater was retained by the TS+OC (X) columns whereas 62.3% of the total S was retained by the TS+OC (1/2X) columns. This shows that the slow flow rates intensified the S retention. The decrease in S retention over time suggested that even if the S retention was via biogenic reduction of sulfate, there would be a maximum limit that the soil can retain S. As the soil pores get filled over time by newly formed precipitates, biological processes are expected to slowdown. In addition, high loading of salts in the FGD wastewater can retard microbial activities in the soil columns over time. Previous studies have found that wastewater with high salt concentration can affect the microbial activities most likely due to the exertion of osmotic pressure on their metabolism (Bassin et al., 2011; Oren, 2011).

Similar to the previous studies, the As concentration of effluent samples was high (Figure 5.11) although the As concentration in the influent was negligible (1.1 µg/L). During the first half of the experiment (0 to 6.8 PVs), As concentration of effluents collected from the TS+OC (1/2X) columns was significantly ($p<0.05$) greater (4.1±1.0 to 86.8±2.3 µg/L) than that of from the TS+OC (X) columns (3.8±0.5 to 54.6±5.6 µg/L). The cumulative amount of As released during this period (0 to 6.8 PVs) was 146.1±2.3 µg, and 105.0±1.0 µg for the 1/2X rate, and the X rate soil columns, respectively. During the latter part of the study (~7.3 to 17.0 PV), the As concentration of the effluent from the TS+OC (X) was 56.0±3.0 to 13.6±3.0 µg/L. It was for the TS+OC (1/2X) columns was 60.25±8.6 to 9.0±0.6 µg/L. When the soil system established reduced conditions over time, the As concentration of effluent from the TS+OC (1/2X) columns decreased. During this period (~7.3 to 17.0 PV), the cumulative amount of As released from the X rate columns was 128.5±8.0 µg while that of from the 1/2X rate columns was 78.6±12.5 µg. The increase of As retention during the latter part of the study most likely be due to the establishment of As cycling couple with the biogeochemical cycles of Fe, and S in the CWTS (Lizama et al., 2011).

Effect of flow rate on S-XANES speciation

The S bulk-XANES spectra of the S standards (Figure 5.12) clearly show white-line energy shifts with changing oxidation state from -2 to +6. The white-line energy increases from 2468.3 to 2480.0 eV as the oxidation state increases (Table 5.3). Because of distinct peak separation depending on the white-line peak energy, the S-XANES analysis has widely been employed to identify, and measure S species in well-aerated as well as in wetland soils (Hashimoto and Yamaguchi, 2013; Prietzel et al., 2003; Prietzel et al., 2009; Xia et al., 1998). Due to the complexity of S speciation in soils/sediments, Gaussian peak fitting analysis has been

suggested from previous studies to identify different S species (Manceau and Nagy, 2012; Xia et al., 1998). An example of the S-XANES analysis that was performed with Gaussian peak fitting on the soil collected from the TS+OC (1/2 X) soil columns is shown in Figure 5.13. The consistent features in the XANES spectra allowed one to deconvolute, and to fit the experimental spectra using a series of Gaussian curves, and two arctangent functions (Figure 5.13). Previous studies have recommended to identify S speciation as distinctly categorized groups such as oxidized S, intermediate S, and reduced S (Hashimoto and Yamaguchi, 2013; Prietzel et al., 2003; Prietzel et al., 2009). Therefore, in the present study, different S standards were categorized into these three main groups, depending on the white-line energy. Those were oxidized S (peak energy > 2478 eV), intermediate S (peak energy 2473 eV-2478 eV), and reduced S (peak energy < 2473). The group of oxidized S species included inorganic sulfate [S(+6)], and sulfonate [S(+5)] compounds whereas sulfite [S(+3.68)], and DL-Methionine sulfoxide [S(+2)] were included as the intermediate S category. Iron sulfide [S(-2)], pyrite [S(-1)], elemental S [S(0)], L-Cysteine [S(+0.5)], and L-Methionine [S(+0.5)] references represented reduced S species.

According to the peak fitting analysis of the soil obtained from the long-term study, we were able to see the S speciation that altered with the submergence period (Figure 5.14). All our samples showed two distinct resonance-peak ranges. First peak was oxidized S, and the second peak was reduced S while the intermediate S species in which the peak energy ranges from 2473 to 2478 eV were generally shown as less abundant (Figure 5.14). The S-XANES analysis showed that S in the original soil material (Figure 5.15a) mainly existed as oxidized S (67.7%), and reduced S (32.2%), indicating that oxidized S was dominant in the starting material. An organic S (L-Cysteine) was also identified by the S bulk-XANES. This can be incorporated with

organic matter (6.2%) in the original soil (Table 5.4). The S speciation of the soil collected from the TS+OC (X) columns (Figure 5.15b) was oxidized S (23.7%), and reduced S (74.6%) (Table 5.4). The intermediate S species were detected as 1.7% which can be negligible (note that anything < 5% cannot be accounted with certainty). The elemental S was the predominant S species found in the reduced S group. This implies that as submergence progressed S from the FGD wastewater tended to be sequestered as stable/reduced species.

Compared to the 191 days of submergence of TS+OC (X) columns, the TS+OC (1/2X) columns which were under 365 days of submergence was dominated by reduced S species (Figure 5.15c). The speciation of oxidized S, intermediate S, and reduced S in this system was 12.2%, 5.4%, and 82.4%, respectively (Table 5.4). Among the reduced S species, sulfide/FeS (46.2%) was the main species that existed in the TS+OC (1/2X) soil columns. This indicates that long submergence period reduced the system (and S) further, helping to retain more S from the FGD wastewater as stable sulfide phases. The sulfide produced by SRB during the oxidation of labile OC can react with the dissolved Fe(II) ion in the solution, produced under reductive dissolution of Fe oxy(hydr)oxide phases, and forms insoluble monosulfide or FeS (Smith and Melville, 2004). While the soil columns were being cut, a "rotten egg" smell came from the TS+OC (1/2X) soil columns. Further, the soil collected from these columns was black in color (Figure C.4). These observations also indirectly suggested the monosulfide formation in the long-term submerged soil. Prietzel et al. (2009) found that the S in wetland soil is mainly present as reduced inorganic (monosulfide, pyrite), elemental S, and reduced organic S. Under reducing soil conditions, the formation of sulfide and subsequent precipitation/co-precipitation reactions are important for trace elements immobilization (Borch et al., 2009; Buddhawong et al., 2005; Dorman et al., 2009; Kröpfelová et al., 2009; Saalfield and Bostick, 2009 ; Schwindaman et al.,

2014). According to the results of the short-term study (60 days submergence), we found that the presence of labile OC significantly increased the S retention in the slow flow rate [TS+Fh+OC (X)] columns (Figure 5.4). The bulk-XANES also showed that OC added columns had a greater amount of reduced/stable S species (68%) compared to the TS (control X) (31.3%) or the no OC added systems (Figure 5.15 a,b and Table 5.4).

Arsenic bulk-XANES speciation

The As K-edge bulk- XANES spectroscopic analysis was used to identify the solid-state As species. The normalized As-XANES spectra, and the LCF results of the original soil, TS+OC (X) (191 days of submergence), and TS+OC (1/2X) (365 days of submergence) are shown in Figure 5.16. Here As(III)_Fh and As(V)_Fh represent As(III), and As(V) adsorbed to ferrihydrite, respectively. The sodium arsenate, and sodium arsenite represent As(V), and As(III) solid species, respectively. The As speciation of the original soil was dominated by As(V). According to the XANES spectra of the soil samples collected from the soil columns (Figure 5.16), the absorption maximum for both samples was near 11875.8 eV which confirmed that As was predominantly present in the As(V) oxidation state, although it was expected to see some enhancement of the reduced As species in the TS+OC (1/2X) (more reduced system). The As(V) (68.3%), As(V)_Fh (9.0%), and As(III)_Fh (22.7%) were found in the TS+OC (X) soil (Table 5.5). Similar results observed in the previous column studies which can confirm that retained As (after desorbed by reductive dissolution) primarily existed as more stable As(V). The As species found in the TS+OC (1/2X) soil was As(V) (32.6%), As(V)_Fh (18.6%), As(III) (34.1%), and realgar-like (14.7%). These results indicate that the slow flow rate of the influent and long submergence help to minimize the As mobility most likely due to the formation of realgar-like stable sulfide phases. Previous studies have depicted that the solubility of As(III) is controlled by

the sulfide solid phases such as orpiment, realgar, and FeAsS-like minerals that are more prone to be formed under highly reducing soil conditions (Bostick and Fendorf, 2003 ; Moore et al., 1988; Sadiq, 1997; Smedley and Kinniburgh, 2002).

Iron bulk-XANES speciation

The LCF results of the Fe K-edge bulk- XANES spectra (Figure 5.17) revealed that the major Fe species in the original soil were Fe_2O_3 (56.5%), magnetite (10.6%), lepidocrocite (26.4%), and FeO (6.5%) (Table 5.6). The soil which was under 191 of submergence [TS+OC (X)] had Fe species of hematite (34.8%), green crust (20.7%), and lepidocrocite (44.5%) while the Fe speciation of the TS+OC (1/2X) columns (submerged for 365 days) existed lepidocrocite (73.2%), and greigite_Cl (26.8%). Regardless of the submergence period, Fe(III) was the dominant species in both soil columns. Since we are essentially looking at the speciation of the remaining portion, it is possible that the majority of the remaining Fe is present as Fe(III) species. However, the Fe-XANES analysis detected greigite-like (~27%) species in the TS+OC (1/2X) soil, indicating a biogenic Fe-S formation with the pro-long submergence. The greigite (Fe_3S_4) is known to be formed by bacterial activities in blackish sulfide-rich sediment (Stanjek et al., 1994). Thermodynamically greigite is an intermediate of the formation of pyrite. In our study, a secondary Fe mineral phase, green rust, was detected in the TS+OC (X) soil (Table 5.6). Green rust is a mixed valence Fe [Fe(II) and Fe(III)] mineral that can be formed under reduced conditions of hydromorphic soil (Berthelin et al., 2006; Randall et al., 2001), also by the reductive dissolution of Fe(III) oxy(hydr)oxides (Benner et al., 2002). Because of greater reactivity, green rust can control the mobility of trace elements such as Se, and As (Myneni et al., 1997; Randall et al., 2001).

Conclusions

It is clear from the current study that the flow rate had a significant effect on S retention in the CWTS designed for FGD wastewater. The slow flow rate with labile OC (sodium lactate) enhanced S retention, further implying that longer residence time provided conducive conditions for sulfate reduction. The ferrihydrite-amended soil columns showed a limited release of As upon the reductive dissolution of native soil, regardless of the flow rate. This further supports the results from the previous column study (Chapter 4). The bulk S-XANES analysis indicated that slow flow rate and prolonged submergence period favored the formation of reduced/stable S species, mainly S(0), and S(-2). Data obtained from this study showed that realgar-like stable As-S phases formed in the sulfide enriched soil system, which can ultimately retard the mobility of native soil As in the CWTS. The main mechanism here suggested that transformation of sulfate in FGD wastewater to reduced/stable sulfides could have a significant impact on S retention and long-term sequestration of trace elements (such as As) in the CWTS.

Acknowledgements

We acknowledge the funding support of this study by Westar Energy, Burns & McDonnell, Kansas Agricultural Experimental Station, and KSU Electrical Power Affiliate Program. Portion of this work was performed at the DND-CAT located at Sector 5 BM-D, and at Sector 9 BM-B of the Advanced Photon Source (APS). The DND-CAT is supported by Northwestern University, E.I. DuPont de Nemours & Co., and The Dow Chemical Company. This research used resources of the APS, a U.S. Department of Energy (DOE) Office of Science User Facility operated for the DOE Office of Science by Argonne National Laboratory under Contract No. DE-AC02-06CH11357. We also acknowledge Adam T. Marshall from University of Florida who worked under the program of research experience for undergraduates supported

by the National Science Foundation under Grant No. EPS-0903806 in 2013. We also acknowledge http://xraysweb.lbl.gov/uxas/Databases/Overview.htm for providing XAS database for some of iron standards.

References

Bassin, J.P., M. Pronk, G. Muyzer, R. Kleerebezem, M. Dezotti and M.C. van Loosdrecht. 2011. Effect of elevated salt concentrations on the aerobic granular sludge process: Linking microbial activity with microbial community structure. Appl. Environ. Microbiol. 77:7942-7953.

Benner, S., D.W. Blowes, W.D. Gould, R.B. Herbert and C.J. Ptacek. 1999. Geochemistry of a permeable reactive barrier for metals and acid mine drainage. Environ. Sci. Technol. 33:2793-2799.

Benner, S.G., C.M. Hansel, B.W. Wielinga, T.M. Barber and S. Fendorf. 2002. Reductive dissolution and biomineralization of iron hydroxide under dynamic flow conditions. Environ. Sci. Technol. 36:1705-1711.

Berthelin, J., G. Ona-Nguema, S. Stemmler, C. Quantin, M. Abdelmoula and F. Jorand. 2006. Bioreduction of ferric species and biogenesis of green rusts in soils. Comptes Rendus Geoscience 338:447-455.

Bolin, T.B. 2010. Direct determination of pyrite content in argonne premium coals by the use of sulfur X-ray near edge absorption spectroscopy (S-XANES). Energy Fuels 24:5479-5482.

Borch, T., R. Kretzschmar, A. Kappler, P.V. Cappellen, M. Ginder-Vogel, A. Voegelin and K. Campbell. 2009. Biogeochemical redox processes and their impact on contaminant dynamics. Environ. Sci. Technol. 44:15-23.

Bostick, B.C. and S. Fendorf. 2003. Arsenite sorption on troilite (FeS) and pyrite (FeS 2). Geochim. Cosmochim. Acta 67:909-921.

Buddhawong, S., P. Kuschk, J. Mattusch, A. Wiessner and U. Stottmeister. 2005. Removal of arsenic and zinc using different laboratory model wetland systems. Engineering in Life Sciences 5:247-252.

Burton, E.D., S.G. Johnston and B.D. Kocar. 2014. Arsenic mobility during flooding of contaminated soil: The effect of microbial sulfate reduction. Environ. Sci. Technol. 48:13660-13667.

Chapelle, F.H. and D.R. Lovley. 1992. Competitive exclusion of sulfate reduction by Fe (lll)-reducing bacteria: A mechanism for producing discrete zones of high-iron ground water. Groundwater 30:29-36.

Connell, W.E. and W.H. Patrick Jr. 1968. Sulfate reduction in soil: Effects of redox potential and pH. Science 159:86-87.

Dorman, L., J.W. Castle and J.H. Rodgers Jr. 2009. Performance of a pilot-scale constructed wetland system for treating simulated ash basin water. Chemosphere 75:939-947.

Drury, W.J. 2000. Modeling of sulfate reduction in anaerobic solid substrate bioreactors for mine drainage treatment. Mine Water and the Environment 19:19-29.

Dvorak, D.H., R.S. Hedin, H.M. Edenborn and P.E. McIntire. 1992. Treatment of metal-contaminated water using bacterial sulfate reduction: Results from pilot-scale reactors. Biotechnol. Bioeng. 40:609-616.

Edwards, P.J. 1998. Sulfur cycling, retention, and mobility in soils: A review. Rep. NE-250. US Department of Agriculture, Forest Service, Northeastern Research Station, .

Eggert, D.A., J.H. Rodgers Jr, G.M. Huddleston and C.E. Hensman. 2008. Performance of pilot-scale constructed wetland treatment systems for flue gas desulfurization waters. Environmental Geosciences 15:115-129.

EPRI. 2006. Guidance for assessing wastewater impacts of FGD scrubbers. Technical manual. Rep. 1013313. Electric Power Research Institute, Palo Alto, CA.

Essington, M.E. 2004. Soil and water chemistry: An integrative approach. CRC press, Boca Raton, FL.

Fan, J., Y. Wang, C. Liu, L. Wang, K. Yang, D. Zhou, W. Li and D.L. Sparks. 2014. Effect of iron oxide reductive dissolution on the transformation and immobilization of arsenic in soils: New insights from X-ray photoelectron and X-ray absorption spectroscopy. J. Hazard. Mater. 279:212-219.

Hansel, C.M., S.G. Benner, J. Neiss, A. Dohnalkova, R.K. Kukkadapu and S. Fendorf. 2003. Secondary mineralization pathways induced by dissimilatory iron reduction of ferrihydrite under advective flow. Geochim. Cosmochim. Acta 67:2977-2992.

Hashimoto, Y. and N. Yamaguchi. 2013. Chemical speciation of cadmium and sulfur K-edge XANES spectroscopy in flooded paddy soils amended with zerovalent iron. Soil Sci. Soc. Am. J. 77:1189-1198.

Islam, F.S., A.G. Gault, C. Boothman, D.A. Polya, J.M. Charnock, D. Chatterjee and J.R. Lloyd. 2004. Role of metal-reducing bacteria in arsenic release from Bengal delta sediments. Nature 430:68-71.

Kadlec, R.H. and S. Wallace. 2008. Treatment wetlands. CRC press. Florida, USA.

Kaksonen, A. and J. Puhakka. 2007. Sulfate reduction based bioprocesses for the treatment of acid mine drainage and the recovery of metals. Engineering in Life Sciences 7:541-564.

Karna, R.R. 2014. Mechanistic understanding of biogeochemical transformations of trace elements in contaminated minewaste materials under reduced conditions. Ph.D Dissertation. Kansas State University, Manhattan, KS.

Kocar, B.D., M.J. Herbel, K.J. Tufano and S. Fendorf. 2006. Contrasting effects of dissimilatory iron (III) and arsenic (V) reduction on arsenic retention and transport. Environ. Sci. Technol. 40:6715-6721.

Kocar, B.D., M.L. Polizzotto, S.G. Benner, S.C. Ying, M. Ung, K. Ouch, S. Samreth, B. Suy, K. Phan and M. Sampson. 2008. Integrated biogeochemical and hydrologic processes driving arsenic release from shallow sediments to groundwaters of the mekong delta. Appl. Geochem. 23:3059-3071.

Kröpfelová, L., J. Vymazal, J. Švehla and J. Štíchová. 2009. Removal of trace elements in three horizontal sub-surface flow constructed wetlands in the Czech republic. Environmental Pollution 157:1186-1194.

Kwon, M.J., M.I. Boyanov, D.A. Antonopoulos, J.M. Brulc, E.R. Johnston, K.A. Skinner, K.M. Kemner and E.J. O'Loughlin. 2014. Effects of dissimilatory sulfate reduction on Fe III (hydr) oxide reduction and microbial community development. Geochim. Cosmochim. Acta 129:177-190.

Lens, P., A. Visser, A. Janssen, L.H. Pol and G. Lettinga. 1998. Biotechnological treatment of sulfate-rich wastewaters. Crit. Rev. Environ. Sci. Technol. 28:41-88.

Lewis, A.E. 2010. Review of metal sulphide precipitation. Hydrometallurgy 104:222-234.

Lizama, K., T.D. Fletcher and G. Sun. 2011. Removal processes for arsenic in constructed wetlands. Chemosphere 84:1032-1043.

Lovley, D.R. and E.J. Phillips. 1987. Competitive mechanisms for inhibition of sulfate reduction and methane production in the zone of ferric iron reduction in sediments. Appl. Environ. Microbiol. 53:2636-2641.

Manceau, A. and K.L. Nagy. 2012. Quantitative analysis of sulfur functional groups in natural organic matter by XANES spectroscopy. Geochim. Cosmochim. Acta 99:206-223.

Marchand, L., M. Mench, D. Jacob and M. Otte. 2010. Metal and metalloid removal in constructed wetlands, with emphasis on the importance of plants and standardized measurements: A review. Environmental Pollution 158:3447-3461.

Masscheleyn, P.H., R.D. Delaune and W.H. Patrick Jr. 1991. Effect of redox potential and pH on arsenic speciation and solubility in a contaminated soil. Environ. Sci. Technol. 25:1414-1419.

McGeehan, S. and D. Naylor. 1994. Sorption and redox transformation of arsenite and arsenate in two flooded soils. Soil Sci. Soc. Am. J. 58:337-342.

Moore, J.N., W.H. Ficklin and C. Johns. 1988. Partitioning of arsenic and metals in reducing sulfidic sediments. Environ. Sci. Technol. 22:432-437.

Myneni, S., T.K. Tokunaga and G. Brown. 1997. Abiotic selenium redox transformations in the presence of fe (II, III) oxides. Science 278:1106-1109.

Neal, A.L., S. Techkarnjanaruk, A. Dohnalkova, D. McCready, B.M. Peyton and G.G. Geesey. 2001. Iron sulfides and sulfur species produced at hematite surfaces in the presence of sulfate-reducing bacteria. Geochim. Cosmochim. Acta 65:223-235.

Neculita, C., G.J. Zagury and B. Bussière. 2008. Effectiveness of sulfate-reducing passive bioreactors for treating highly contaminated acid mine drainage: I. effect of hydraulic retention time. Appl. Geochem. 23:3442-3451.

Nickson, R., J. McArthur, W. Burgess, K.M. Ahmed, P. Ravenscroft and M. Rahmann. 1998. Arsenic poisoning of Bangladesh groundwater. Nature 395:338-338.

O'Day, P.A., D. Vlassopoulos, R. Root and N. Rivera. 2004. The influence of sulfur and iron on dissolved arsenic concentrations in the shallow subsurface under changing redox conditions. Proc. Natl. Acad. Sci. U. S. A. 101:13703-13708.

Oren, A. 2011. Thermodynamic limits to microbial life at high salt concentrations. Environ. Microbiol. 13:1908-1923.

Polizzotto, M.L., C.F. Harvey, S.R. Sutton and S. Fendorf. 2005. Processes conducive to the release and transport of arsenic into aquifers of Bangladesh. Proc. Natl. Acad. Sci. U. S. A. 102:18819-18823.

Ponnamperuma, F. 1972. The chemistry of submerged soils. Adv. Agron. 24:29-96.

Prietzel, J., J. Thieme, U. Neuhäusler, J. Susini and I. Kögel-Knabner. 2003. Speciation of sulphur in soils and soil particles by X-ray spectromicroscopy. Eur. J. Soil Sci. 54:423-433.

Prietzel, J., A. Botzaki, N. Tyufekchieva, M. Brettholle, J. Thieme and W. Klysubun. 2011. Sulfur speciation in soil by S K-edge XANES spectroscopy: Comparison of spectral deconvolution and linear combination fitting. Environ. Sci. Technol. 45:2878-2886.

Prietzel, J., J. Thieme, N. Tyufekchieva, D. Paterson, I. McNulty and I. Kögel-Knabner. 2009. Sulfur speciation in well-aerated and wetland soils in a forested catchment assessed by sulfur K-edge X-ray absorption near-edge spectroscopy (XANES). Journal of Plant Nutrition and Soil Science 172:393-403.

Randall, S.R., D.M. Sherman and K.V. Ragnarsdottir. 2001. Sorption of as (V) on green rust ($Fe_4(II)Fe_2(III)(OH)12\ SO_4 \cdot\ 3H_2O$) and lepidocrocite (γ-FeOOH): Surface complexes from EXAFS spectroscopy. Geochim. Cosmochim. Acta 65:1015-1023.

Ravel, á. and M. Newville. 2005. ATHENA, ARTEMIS, HEPHAESTUS: Data analysis for X-ray absorption spectroscopy using IFEFFIT. Journal of Synchrotron Radiation 12:537-541.

Rietz, D. and R. Haynes. 2003. Effects of irrigation-induced salinity and sodicity on soil microbial activity. Soil Biol. Biochem. 35:845-854.

Rodgers Jr, J.H. and J.W. Castle. 2008. Constructed wetland systems for efficient and effective treatment of contaminated waters for reuse. Environmental Geosciences 15:1-8.

Saalfield, S.L. and B.C. Bostick. 2009. Changes in iron, sulfur, and arsenic speciation associated with bacterial sulfate reduction in ferrihydrite-rich systems. Environ. Sci. Technol. 43:8787-8793.

Sadiq, M. 1997. Arsenic chemistry in soils: An overview of thermodynamic predictions and field observations. Water Air Soil Pollut. 93:117-136.

SAS Institute Inc. 2013. SAS software. 9.4. Cary, NC, USA.

Schwindaman, J.P., J.W. Castle and J.H. Rodgers. 2014. Fate and distribution of arsenic in a process-designed pilot-scale constructed wetland treatment system. Ecol. Eng. 68:251-259.

Sheoran, A. and V. Sheoran. 2006. Heavy metal removal mechanism of acid mine drainage in wetlands: A critical review. Minerals Eng 19:105-116.

Smedley, P. and D. Kinniburgh. 2002. A review of the source, behaviour and distribution of arsenic in natural waters. Appl. Geochem. 17:517-568.

Smith, J. and M.D. Melville. 2004. Iron monosulfide formation and oxidation in drain-bottom sediments of an acid sulfate soil environment. Appl. Geochem. 19:1837-1853.

Srivastava, R.K. and W. Jozewicz. 2001. Flue gas desulfurization: The state of the art. J. Air Waste Manage. Assoc. 51:1676-1688.

Srivastava, R.K., W. Jozewicz and C. Singer. 2001. SO_2 scrubbing technologies: A review. Environ. Prog. 20:219-228.

Stanjek, H., J. Fassbinder, H. Vali, H. Wägele and W. Graf. 1994. Evidence of biogenic greigite (ferrimagnetic Fe_3S_4) in soil. Eur. J. Soil Sci. 45:97-104.

Stark, L.R., W.R. Wenerick, F.M. Williams and P.J. Wuest. 1995. The effects of pH, flow rate, and carbon supplementation on manganese retention in mesocosm wetlands. J. Environ. Qual. 24:816-826.

Stein, O.R., D.J. Borden-Stewart, P.B. Hook and W.L. Jones. 2007. Seasonal influence on sulfate reduction and zinc sequestration in subsurface treatment wetlands. Water Res. 41:3440-3448.

Tufano, K.J., C. Reyes, C.W. Saltikov and S. Fendorf. 2008. Reductive processes controlling arsenic retention: Revealing the relative importance of iron and arsenic reduction. Environ. Sci. Technol. 42:8283-8289.

USEPA. 1995. A handbook of constructed wetlands, vol 1. Environment Protection Agency, Washington, DC.

Vymazal, J. 2010. Constructed wetlands for wastewater treatment. Water 2:530-549.

White, C., J.A. Sayer and G.M. Gadd. 1997. Microbial solubilization and immobilization of toxic metals: Key biogeochemical processes for treatment of contamination. FEMS Microbiol. Rev. 20:503-516.

Xia, K., F. Weesner, W. Bleam, P. Helmke, P. Bloom and U. Skyllberg. 1998. XANES studies of oxidation states of sulfur in aquatic and soil humic substances. Soil Sci. Soc. Am. J. 62:1240-1246.

Yamaguchi, N., T. Nakamura, D. Dong, Y. Takahashi, S. Amachi and T. Makino. 2011. Arsenic release from flooded paddy soils is influenced by speciation, eh, pH, and iron dissolution. Chemosphere 83:925-932.

Yeh, T. 2008. Removal of metals in constructed wetlands: Review. Pract. Periodical Hazard. , Toxic, Radioact. Waste Manage. 12:96-101.

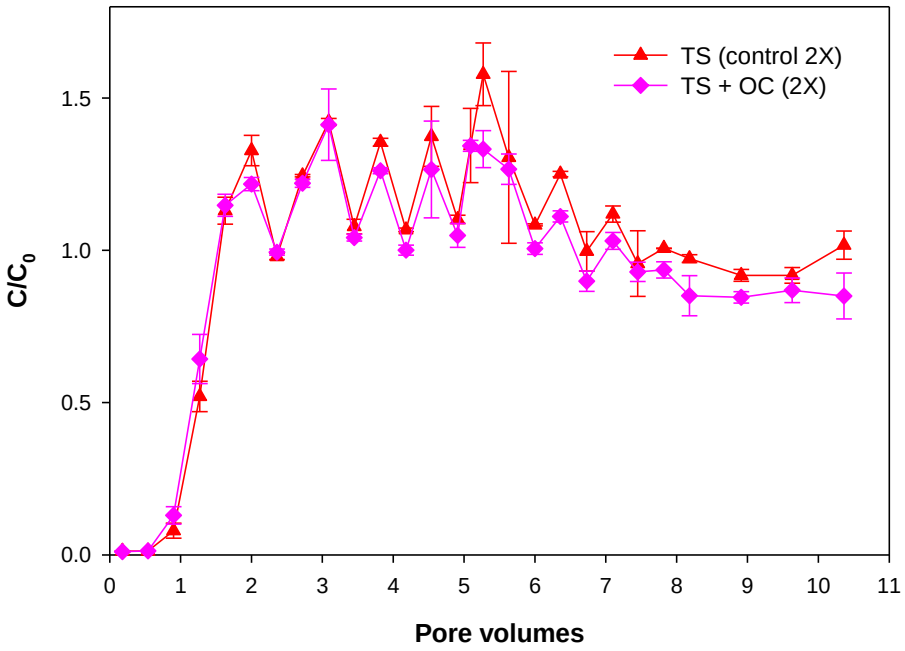

Figure 5.1 Breakthrough curves of Sulfate-S (SO_4^{2-}-S) of the TS control, and the control treated with organic carbon (OC) for 2X rate soil columns. One pore volume of 2X rate columns is 5.5 days. C is the effluent concentration and C_0 is the influent concentration of SO_4^{2-}-S.

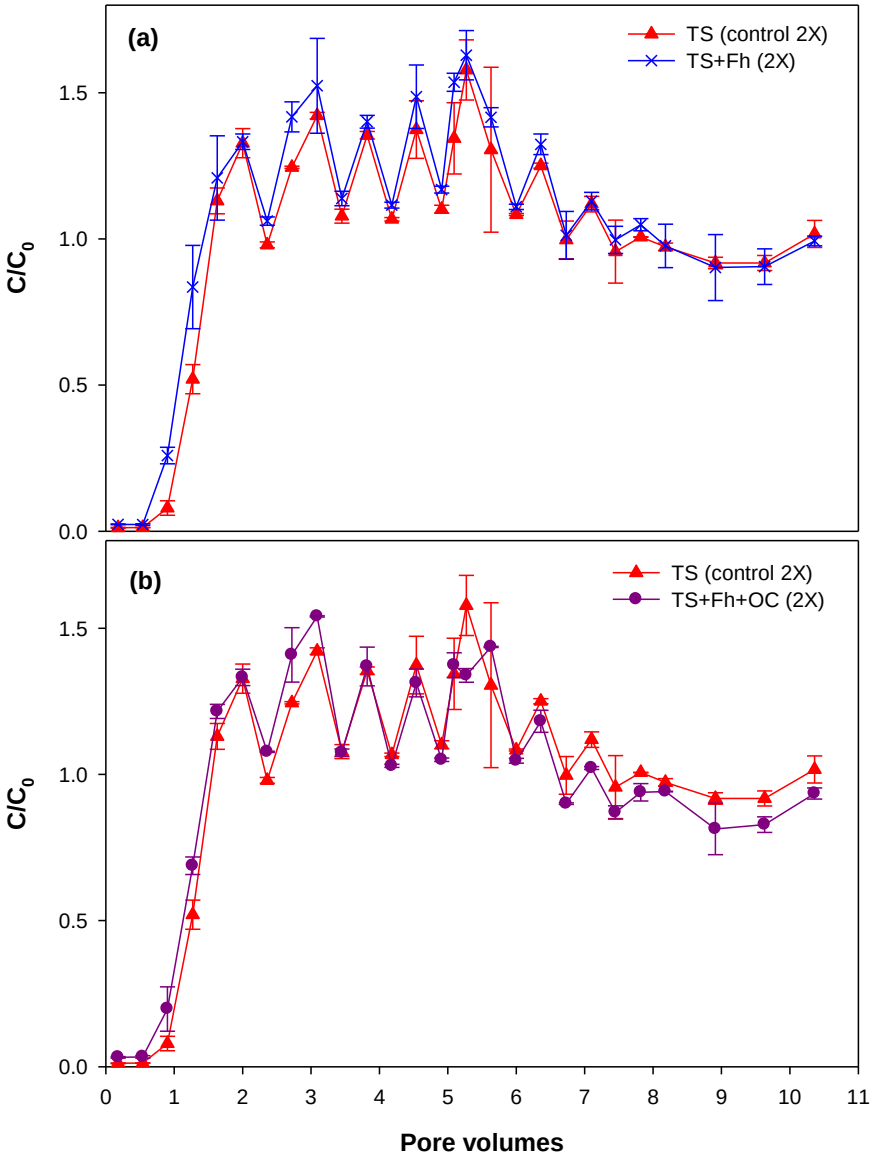

Figure 5.2 Breakthrough curves of Sulfate-S (SO_4^{2-}-S) for the 2X rate soil columns; (a) TS control, and control treated with 1% of ferrihydrite (Fh), (b) TS control, and control treated with 1% ferrihydrite and organic carbon (OC). One pore volume of 2X rate columns is 5.5 days. C is the effluent concentration and C_0 is the influent concentration of SO_4^{2-}-S.

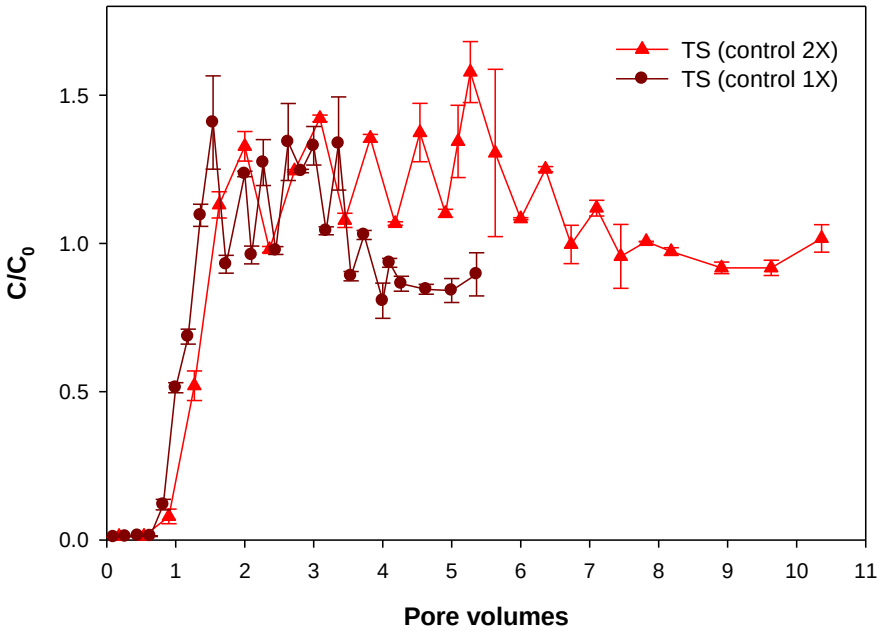

Figure 5.3 Breakthrough curves of Sulfate-S (SO_4^{2-}-S) of control (TS & inoculum) for 2X and, 1X rate soil columns. One pore volume of 2X rate columns is 5.5 days and that of 1X rate columns is 11 days. C is the effluent concentration and C_0 is the influent concentration of SO_4^{2-}-S.

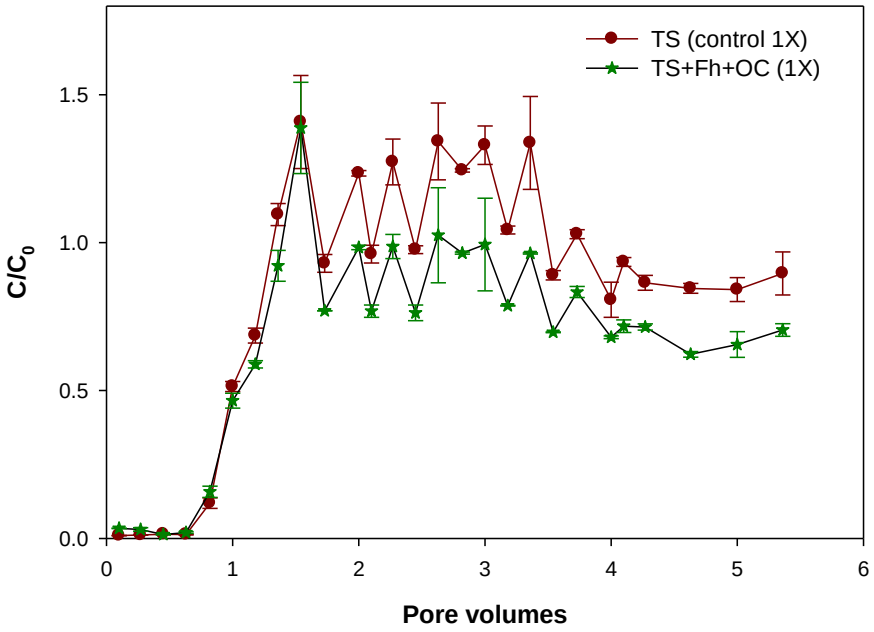

Figure 5.4 Breakthrough curves of Sulfate-S (SO_4^{2-}-S) of the control (TS & inoculum) and the control treated with 1% of ferrihydrite (Fh), and organic carbon (OC) for the 1X rate soil columns.

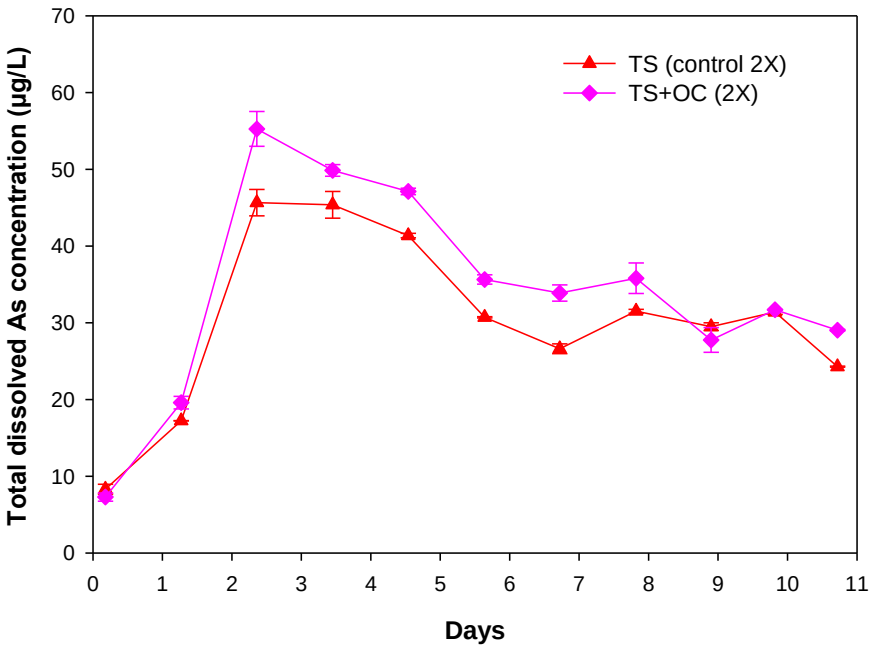

Figure 5.5 Arsenic concentration of column effluent samples collected from the control (TS & inoculum) and the control treated with organic carbon (OC) 2X rate columns.

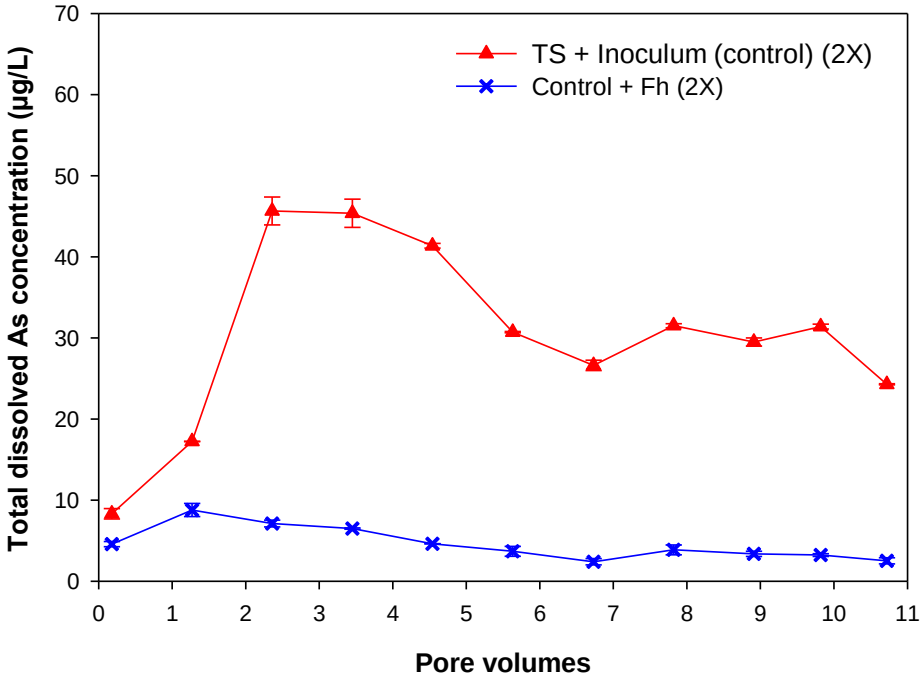

Figure 5.6 Arsenic concentration of column effluent samples collected from the control (TS & inoculum) and the control treated with 1% of ferrihydrite (Fh) 2X rate columns.

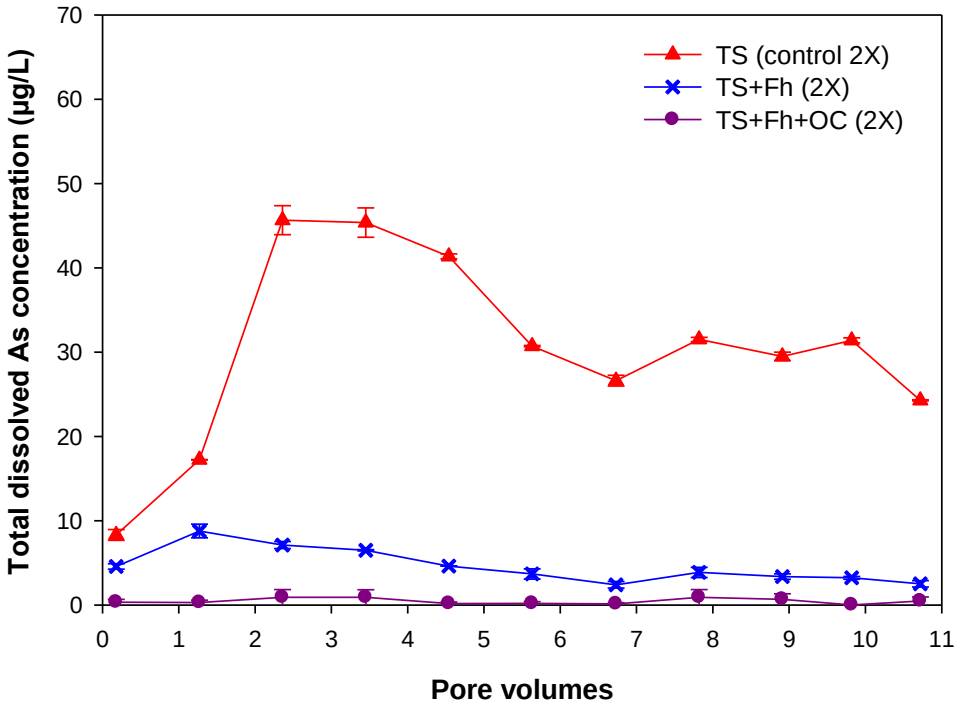

Figure 5.7 Arsenic concentration of columns effluent samples collected from the control (TS & inoculum), control treated with 1% of ferrihydrite (Fh), and control treated with both ferrihydrite and organic carbon 2X rate columns.

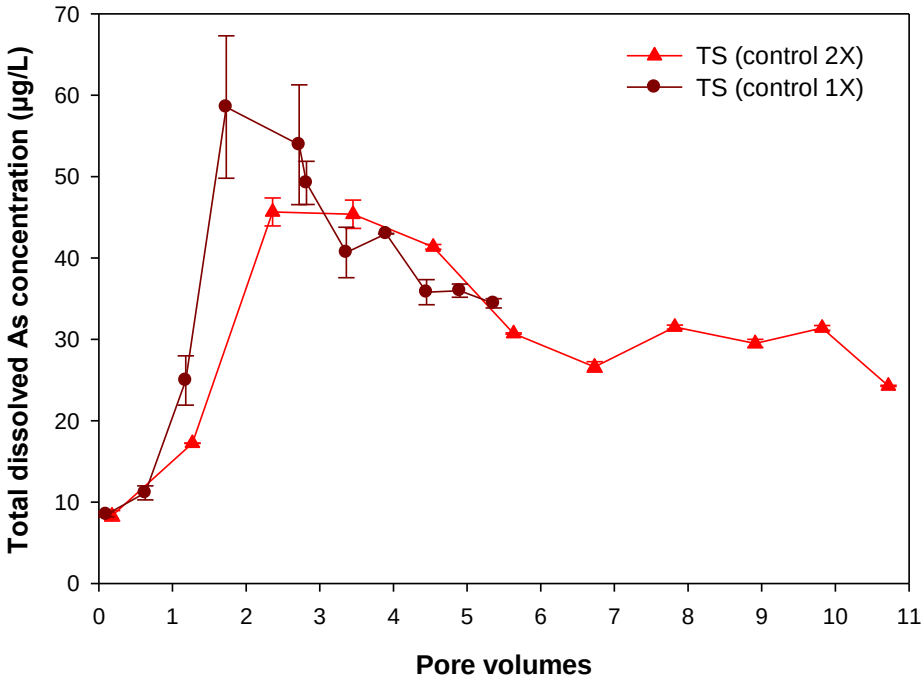

Figure 5.8 Arsenic concentration of column effluents collected from the control (TS & inoculum) 2X and the control (1X) rate soil columns. One pore volume of 2X rate columns is 5.5 days and that of 1X rate columns is 11 days.

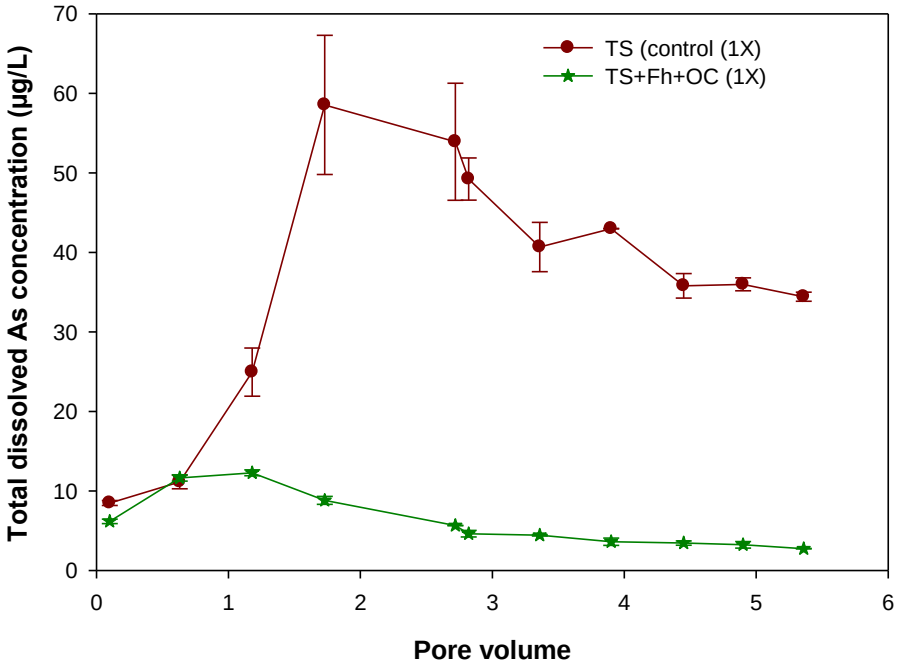

Figure 5.9Arsenic concentration of column effluent samples collected from the control (TS & inoculum), and the control treated with both ferrihydrite and organic carbon 1X rate columns.

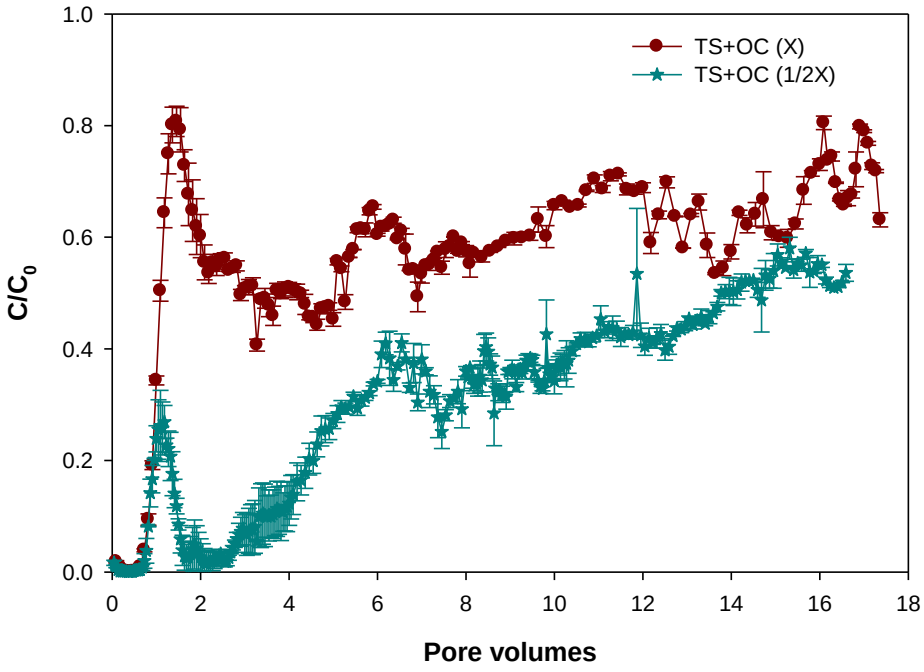

Figure 5.10 Breakthrough curves of total-S of effluent collected from the top soil (TS)+organic carbon (OC) for X and 1/2 X rates. One pore volume of X rate columns was 11 days and that of 1/2 X rate columns was 22 days. C is the effluent concentration and C_0 is the influent concentration of total-S.

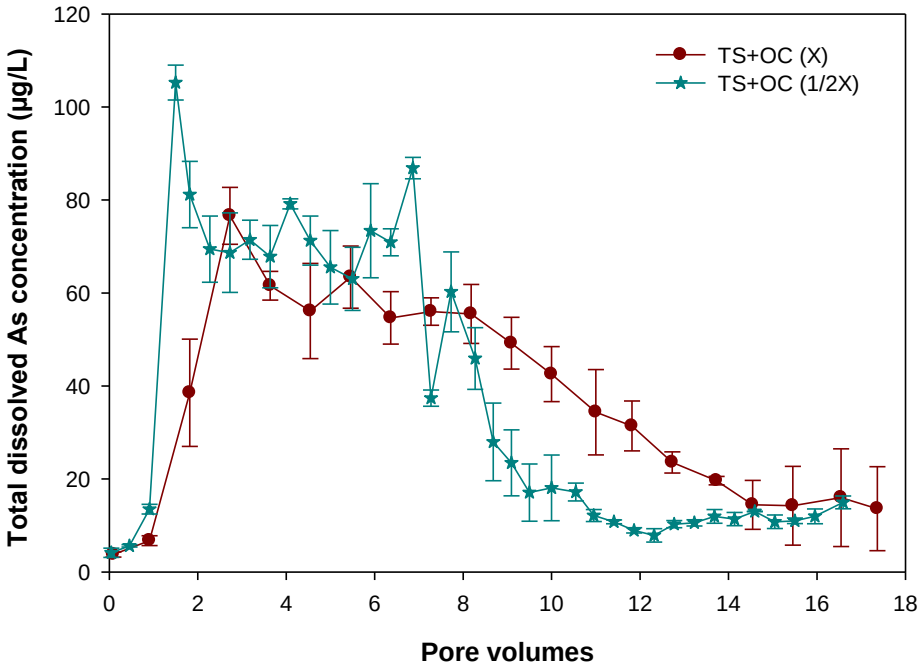

Figure 5.11Arsenic concentration of effluent samples collected from the top soil (TS)+organic carbon (OC) for X and 1/2 X rates.

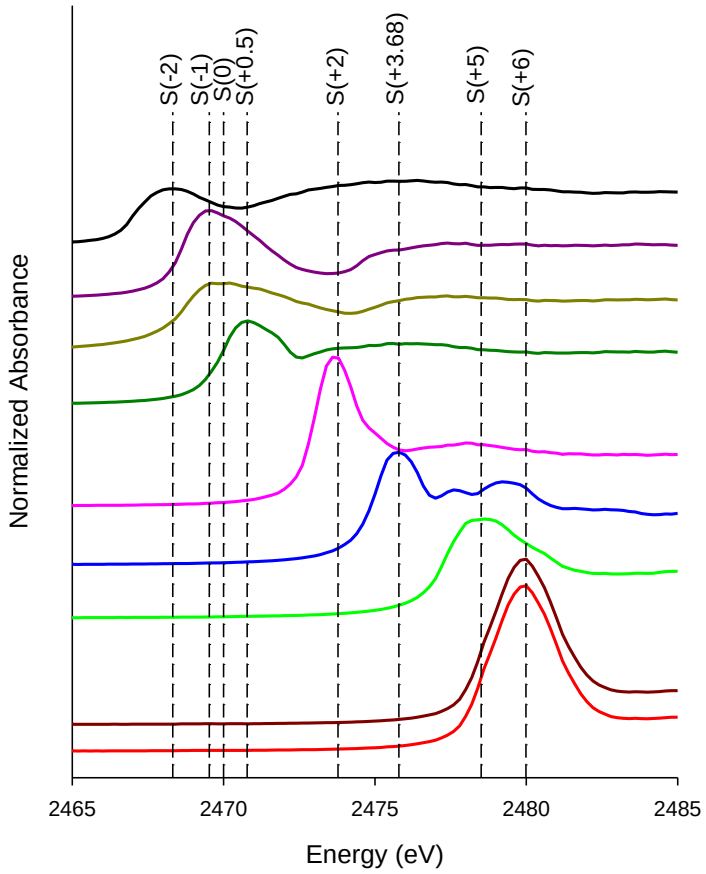

Figure 5.12 Normalized S K-edge XANES spectra for the selected references. Vertical short-dashed lines represent the white line energy of S(+6) (2480.0 eV), S(+5) (2478.5 eV), S(+3.68) (2475.8 eV), S(+2) (2473.8 eV), S(+0.5) (2471.0 eV), S(0) (2470.0 eV), S(-I) (2469.5 eV), and S(-II) (2468.3 eV).

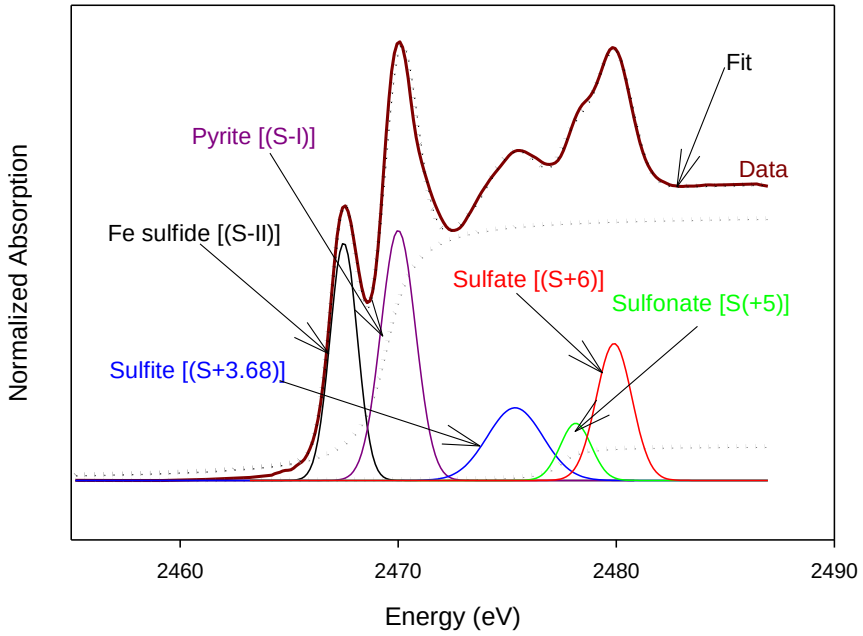

Figure 5.13 An example of major sulfur components obtained by the Gaussian peak fitting analysis on the soil fed at 1/2 X flow rate FGD wastewater. Submergence time was 365 days. Two dotted lines (in gray) represent the two arctangent functions (2469.45 eV and 2477.45 eV).

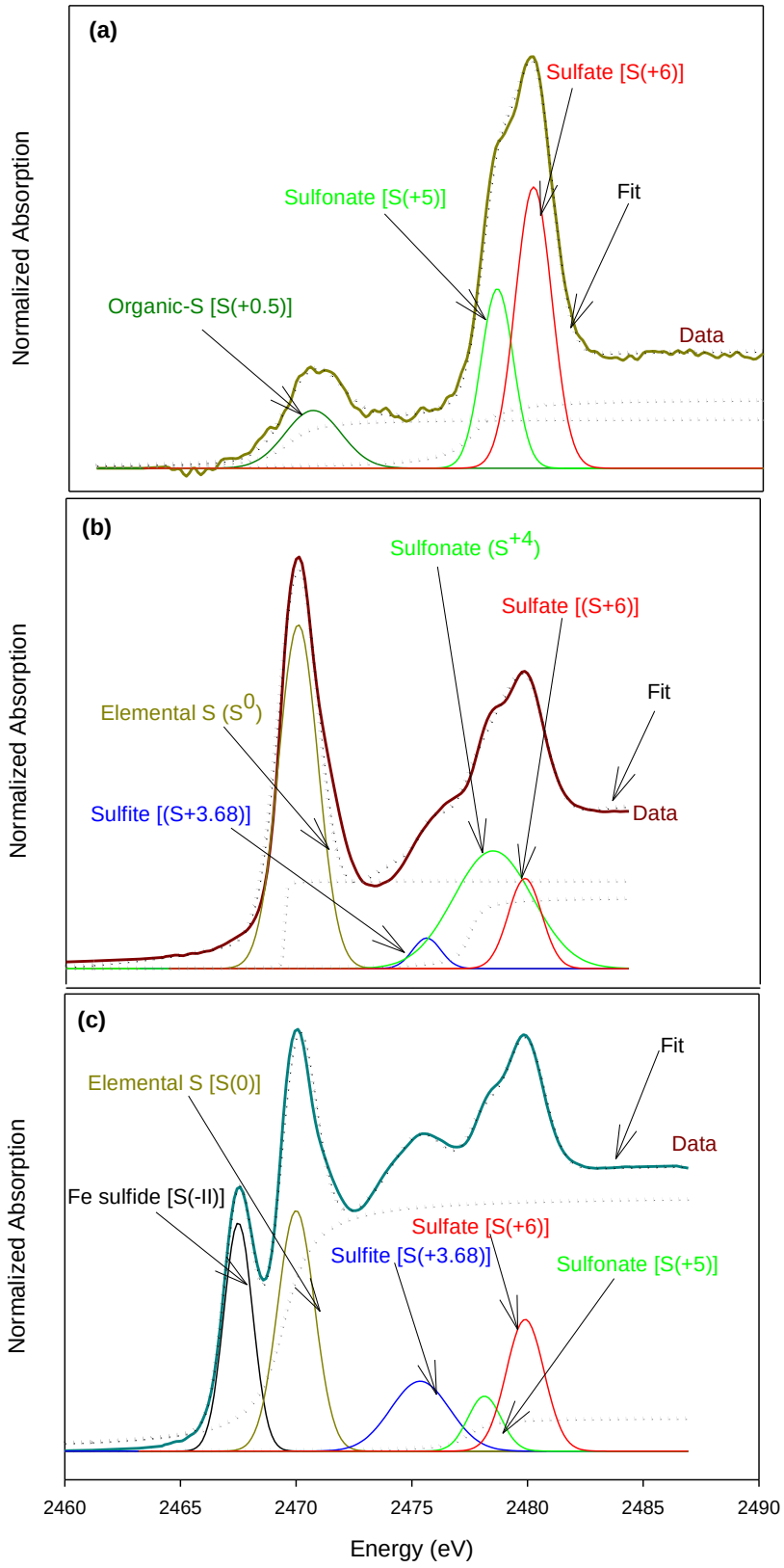

Figure 5.14 Normalized bulk-K-edge S-XANES spectra with several Gaussians and two arctangent curves for (a) topsoil (original), (b) X rate, and (c) 1/2 X rate soils. The rate X represents 1.42 mL/hour and 1/2 X is 0.71 mL/hour that FGD wastewater fed into soil columns. Medium flow rate (X) rate soil was under 191 days submergence, and the slowest rate (1/2 X) soil was under 365 days of submergence. Data, fit and two arctangent functions are represented by solid lines, dotted lines in black, and dotted lines in gray, respectively.

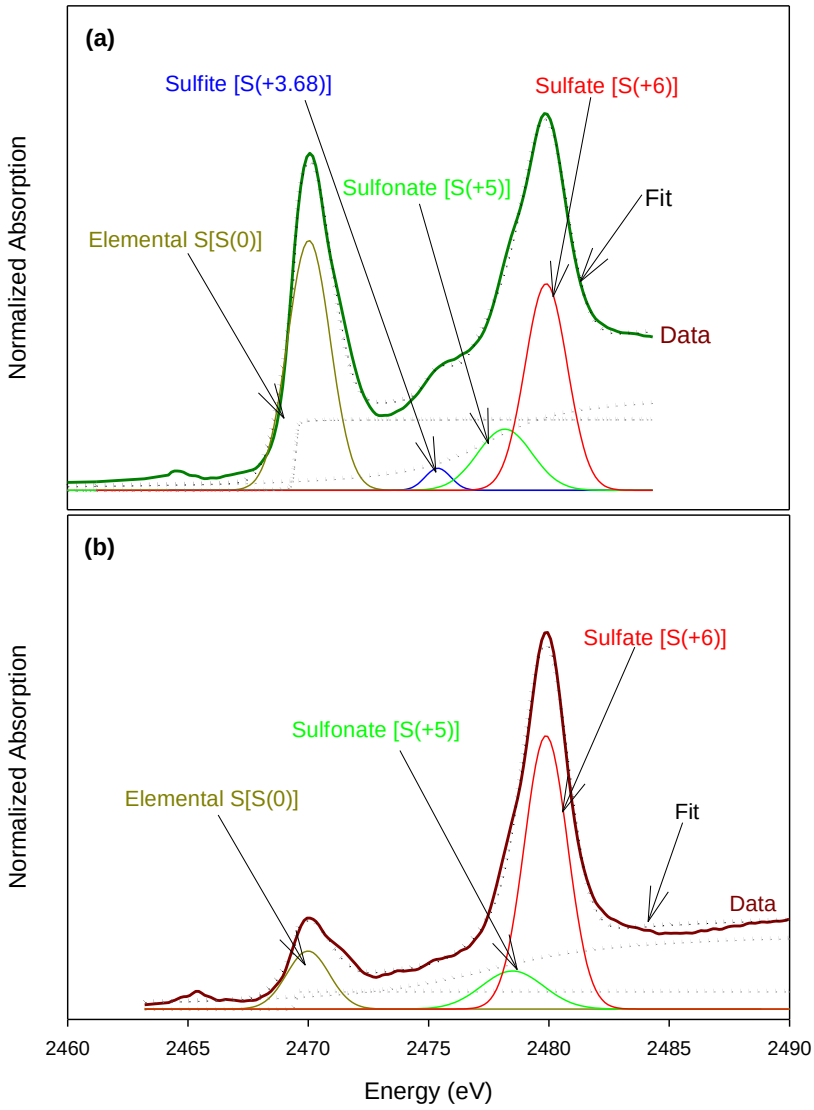

Figure 5.15 Normalized bulk-K-edge S-XANES spectra with several Gaussians and two arctangent curves for (a) control (TS & inoculum), and (b) control treated with both ferrihydrite (Fh) and organic carbon. Both soil samples were under 60 days of submergence with X rate FGD wastewater. Data, fit and two arctangent functions are represented by solid lines, dotted lines in black, and dotted lines in gray, respectively.

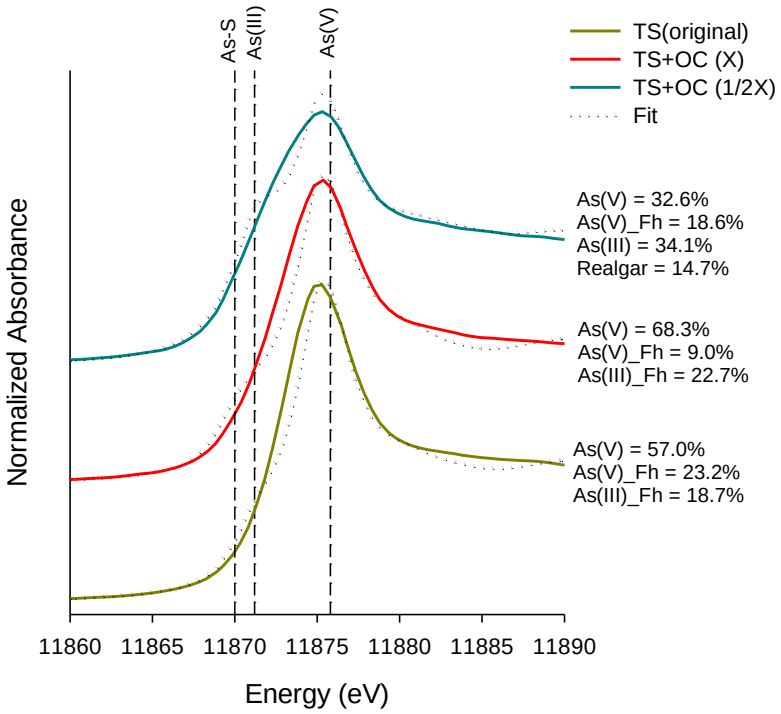

Figure 5.16 Arsenic bulk-XANES collected for the topsoil (TS) (original), TS+OC (X), and TS+OC (1/2 X) soils. The rate X represents flow rate of FGD wastewater fed into the soil columns. TS+OC (X) soil was under 191 days submergence, and the TS+OC (1/2 X) soil was under 365 days of submergence. Dotted lines represent the fit of linear combination fitting (LCF) and vertical short-dash lines to represent white-line peak energy of As(V) (11875.8 eV), As(III) (11871.2 eV), and As-S (11870.0 eV).

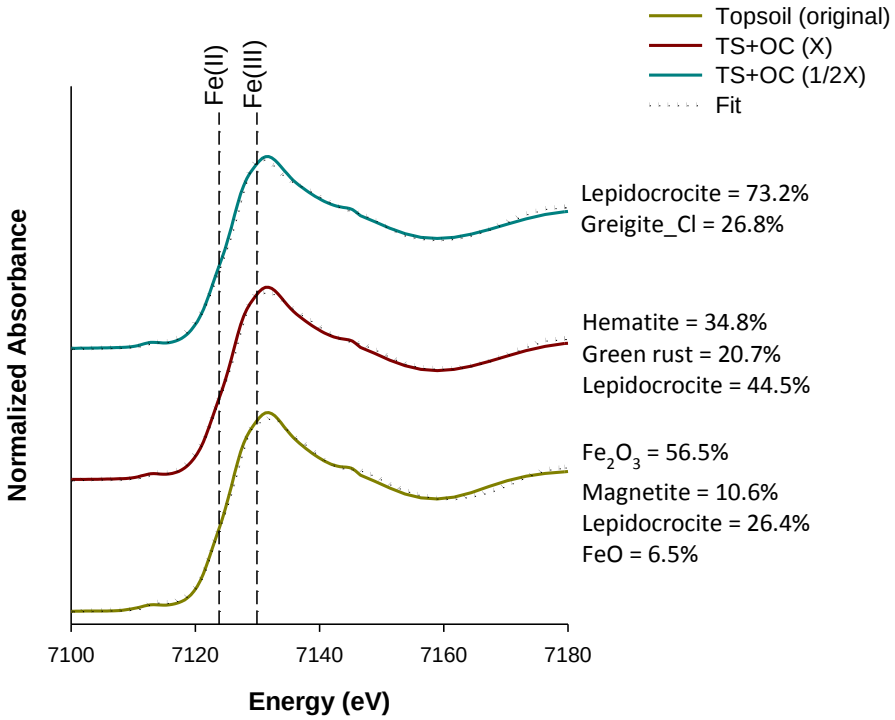

Figure 5.17 Iron bulk-XANES collected for the topsoil (TS) (original), TS+OC (X), and TS+OC (1/2 X) soils. The rate X represents flow rate of FGD wastewater fed into the soil columns. TS+OC (X) soil was under 191 days submergence, and the TS+OC (1/2 X) soil was under 365 days of submergence. Dotted lines represent the fit of linear combination fitting (LCF) and vertical short-dash lines to represent white-line peak energy of Fe(II) (7123.8 eV) and Fe(III) (7129.9 eV).

Table 5.1 Total element concentration and soil parameters of topsoil original material

Total element concentration and soil parameters	Topsoil
Se, mg/kg	0.5
As, mg/kg	7.3
S, mg/kg	507.0
Mn, mg/kg	521.0
Fe, %	1.5
Al, %	1.8
pH (1:5 soil:water)	6.6
OM[#], %	6.2
CEC[¶], $cmol_+/kg$	31.8
Sand, silt, and clay, %	4.3, 49.1, 46.6

Organic matter

¶ Cation exchange capacity

Table 5.2 Concentrations of constituents of 1:1 mixture of FGD wastewater and raw water. These waters were collected from the Jeffery Energy Center (JEC), St. Marys, KS on 27th of February, 2012. The FGD wastewater is the water after treatments to remove some of the sulfur and other compounds. It is the wastewater used to conduct this experiment. The 1:1 mixture of FGD wastewater:raw water was used as the influent for the soil columns.

Constituents	Concentration
As, µg/L	1.1
Se, µg/L	89.0
B, mg/L	4.3
K, mg/L	69.5
Na, mg/L	96.2
Fe, mg/L	<0.1
Total-S, mg/L	794.2
SO_4^{2-}, mg/L	2405.3
SO_4^{2-}-S, mg/L	801.8
F^-, mg/L	15.2
Cl^-, mg/L	623.3
Br^-, mg/L	22.7
NO_3^-, mg/L	129.4
PO_4^{3-}, mg/L	31.3
NO_2^-, mg/L	9.1
EC†, ds/m	5.6
pH	8.2

† Electrical conductivity

Table 5.3 White-line peak energies in S K-edge XANES spectra of different standards.

S compounds	S species	S oxidation state	White-line energy (eV)
Iron sulfide	S^{2-}	-2	2468.3
Pryite	S_2^{2-}	-1	2469.5
Elemental S	S^0	0	2470.0
L-Cysteine	R-SH	+0.5	2470.8
L-Methionine	R-S-R'	+0.5	2471.0
DL-Methionine sulfoxide	R-S=O	+2	2473.8
Sulfite	SO_3^{2-}	+3.68	2475.8
Sulfonate	$R–O–S–(O)_2$	+5	2478.5
Inorganic sulfate	SO_4^{2-}	+6	2480.0

Table 5.4 Percentages of S species of topsoil (TS) (original), X rate (191 days submerged), 1/2 X rate (365 days submerged), TS inoculated with soli slurry (control), and control treated with organic carbon (OC) and ferrihydrite (Fh) soils determined by Gaussian peak fitting of S bulk-XANES analysis. Last two soil samples were under 60 days of submergence with X flow rate.

Soil	[a]Oxidized S (%)		[b]Intermediate S (%)	[c]Reduced S (%)		
	Sulfate [S(+6)]	Sulfonate [S(+5)]	Sulfite [S(+3.68)]	Organic S/Cystiene [S(+0.5)]	Elemental S [S(0)]	Sulfide [S(-2)]
Topsoil (original)	41.6	26.1	-	32.3	-	-
TS+OC (X)	8.2	15.5	1.7	-	74.6	-
TS+OC (1/2X)	7.8	4.4	5.4	-	36.2	46.2
TS (control X)	56.4	12.3	-	-	31.3	-
TS+Fh+OC (X)	21.0	9.0	2.2	-	67.8	

[a]energy range ≥2478 eV and S oxidation states to (+3.68) to (+6), [b]energy range 2473-2478 eV and S oxidation states (+2) to (+3.68), and [c]energy range ≤2473 eV and S oxidation states (+0.5) to (-2).

Table 5.5 Percentages of As species of topsoil (TS) (original), X rate (191 days submerged), and 1/2 X rate (365 days submerged) soils determined by linear combination fitting (LCF) of As bulk-XANES analysis.

Sample	1	2	3	4	5	R-factor¶	Red. χ^2†
	As bulk-XANES speciation (%)						
Top soil (original)	23.2	57.0	-	18.7	-	0.0060	0.008
TS+OC (X)	9.0	68.3	-	22.7	-	0.0053	0.007
TS+OC (1/2X)	18.6	-	34.1	-	14.7	0.0038	0.004

§1, As(V) adsorbed to ferrihydrite; 2, Sodium arsenate [As(V)]; 3, Sodium arsenite [As(III)]; 4, As(III) adsorbed to ferrihydrite; 5, realgar.

¶R-factor: normalized sum of the squared residuals of the linear combination fit.

†$\chi^2 = \sum[(\text{fit-data})/\varepsilon)\ ]^2 /(N_{data}-N_{components})$ is the reduced chi-square statistic. Here ε is the estimated uncertainty in the normalized XANES data (taken as 0.01 for all data). The sum is over N_{data} points (99 data points between E=11852 and 11902 eV for all data), and $N_{components}$ is the number of components in the fit (3 or 4 as indicated in the Table). The total percentage was constrained to be 100% in all fits. Typical uncertainties in the percentages listed for each standard component are 5%.

Table 5.6 Percentages of Fe species top soil (original), X rate, and (c) 1/2 X rate soils. X is the rate of FGD wastewater fed into the soil columns determined by linear combination fitting (LCF) of Fe bulk-XANES analysis. X rate soil was under 191 days submergence, and the slowest rate (1/2 X) soil was under 365 days of submergence.

Sample	Fe_2O_3	Magnetite	Green rust	Lepidocrocite	Hematite	FeO	Greigite_Cl	R-factor¶	Red. χ^2†
	Fe bulk-XANES species								
Top soil (original)	56.5	10.6	-	26.4	-	6.5	-	0.0004	0.0004
TS+OC (X)	-	-	20.7	44.5	34.8	-	-	0.0004	0.0004
TS+OC (1/2X)	-	-	-	73.2	-	-	26.8	0.0006	0.0005

¶ R-factor: normalized sum of the squared residuals of the linear combination fit.

†$\chi^2 = \sum[(\text{fit-data})/\varepsilon)\ ]^2 /(N_{data}-N_{components})$ is the reduced chi-square statistic. Here ε is the estimated uncertainty in the normalized XANES data (taken as 0.01 for all data). The sum is over N_{data} points (84 data points between E=7105 and 7155 eV for all data), and $N_{components}$ is the number of components in the fit (2 or 4 as indicated in the Table). The total percentage was constrained to be 100% in all fits. Typical uncertainties in the percentages listed for each standard component are 5%.

Chapter 6 - Overall conclusions and Recommendations

Sulfur dioxide emission from coal-fired power plants is an environmental concern. Flue-gas desulfurization (FGD) technology is implemented in coal-fired power plants to decrease SO_2 concentration in the flue gas. However, these systems produce wastewater that can cause water pollution due to elevated concentrations of trace elements, and other constituents in it. Constructed wetland treatment system (CWTS) is an economical and environmentally-friendly option to treat FGD wastewater before discharging into surface water bodies or using this wastewater for land application. However, the mechanistic understanding on trace element retention in a CWTS specifically designed for FGD wastewater is lack. In this dissertation, a series of laboratory-based soil column studies mimicking a pilot-scale CWTS was conducted with two main objectives: to understand the transport characteristics and retention capacity of FGD constituents in the CWTS, and to evaluate the effectiveness of soil treatments and influent flow rate on the performance of the CWTS for FGD constituents retention.

The first main objective was addressed through study 1 (Chapter 3) by evaluating the transport characteristics, retention capacity and transformation of selenium (Se) and other FGD constituents in the CWTS, and gathering mechanistic information on Se retention in the CWTS. The key finding from this study showed that Se in the FGD wastewater had more or less irreversible retention in the soil under reduced conditions. Accumulation of Se in the bottom parts (inlet) of the soil columns indicated a limited mobility of Se upon submergence. Results from sequential extraction procedure revealed that Se from the FGD wastewater was mainly sequestered in the columns as stable/residual forms. Data obtained using synchrotron-based X-ray spectroscopy techniques also suggested the mechanism of Se retention in the soil was via transformation of oxidized Se in the FGD wastewater to reduced/stable forms, promoting Se

sequestration through multiple sorption reactions such as adsorption, and precipitation/co-precipitation. Some of the initially-retained Se was mobilized by changing oxidation/reduction conditions in the soil. This suggests that maintaining continuous wetting conditions in the CWTS is needed to avoid remobilization of FGD wastewater constituents.

Study 1 also showed that boron, and fluorine partially retained in the soil whereas sodium, sulfur, and chlorine had a weak retention. The results from the flushing experiment indicated that a significant amount of the initially-retained boron desorbed from the soil. This indirectly implies that boron was weakly adsorbed to the soil, most likely via outer-sphere complexes. In addition, some of the initially-retained fluorine (as calcium fluoride, indicated by Visual MINTEQ) was flushed out by the raw water, presumably due to enhanced solubility of precipitated calcium fluoride upon the introduction of the raw water. Thus, flushing situations in the CWTS (i.e., feeding non-FGD weak salt solutions) can potentially influence mobilization of retained constituents from FGD wastewater. These observations are in agreement with field observations made at the pilot-scale CWTS at Jeffery Energy Center, St. Marys, KS.

Study 2 (Chapter 4), and study 3 (Chapter 5) were performed to assess the second main objective by evaluating the effect of flow rate and soil treatments (i.e., ferrihydrite, and labile organic carbon (OC)) on the retention of FGD wastewater sulfur (S) and the mobility of native soil arsenic (As). This was addressed in conjunction with synchrotron-based X-ray spectroscopy techniques to elucidate the interrelationships between sulfur, arsenic, and iron cycling in the CWTS. Results from the second study depicted that mobilization of native soil As through reductive dissolution influenced the efficiency of the CWTS. Our study revealed that the native soil amended with ferrihydrite minimized As mobility under wetland conditions. Micro X-ray fluorescence mapping coupled with X-ray absorption near edge structure (XANES) spectroscopy

analyses inferred that native soil As mobility was suppressed by ferrihydrite amendment due to the association of released As with newly precipitated Fe phases upon the reductive dissolution of ferrihydrite. Therefore, soil amendments such as ferrihydrite can be used to retard As mobility in the CWTS. This will also help if the FGD wastewater has elevated level of As in addition to Se. Intermittent changes of soil redox conditions influenced the mobility of As associated with newly formed Fe minerals. The results from this study again highlighted the importance of understanding the potential changes of the behavior of the retained trace elements that are affected by changing the environmental conditions in the CWTS.

Considering the results from the soil column studies and the pilot-scale CWTS, which represented real field conditions, removal of S from the FGD wastewater was weak at relatively high flow rates. Breakthrough curves obtained in the third study clearly indicated that slower flow rate of the FGD wastewater influent treated with labile organic carbon was conducive for S retention. This could most prominently be due to the dissimilatory sulfate reduction in the presence of sulfate reducing bacteria. The synchrotron-based bulk-XANES analysis revealed that sulfide-associated As and Fe phases formed in the slow flow rate soil columns. Because of the stability of metal sulfides, the slow flow rate of the FGD wastewater would be the best strategy for long-term sequestration of trace elements (such as As) and promotion of S retention, which would likely enhance the performance efficiency of the CWTS.

Based on this research we recommend using a series of CWTS with reducing conditions treated with organic carbon to remove Se and other trace elements and with oxidizing conditions treated with Fe to remove As in the FGD wastewater or mobilized from native soil (wetland soil material).

In these studies, the FGD wastewater influent was introduced to the soil columns from the bottom. The upward flow through system has the potential to minimize the effect of density and viscosity differences of aqueous solutions on the solute transport, and to prevent the preferential flow through macropores. Future research should investigate whether this flow system is indeed work better for the CWTSs. Similarly, prevention of wastewater movement all the way up to the surface of the vertical flow beds and introducing clean water from the top might be helpful to avoid unnecessary environmental issues that result from accumulated Se in wetland vegetation and animals. However, this also requires further testing in column studies and/or pilot-scale CWTS trials.

Appendix A - Supporting information relevant to Chapter 3

Analysis of influent and effluent

Before analyzing the FGD wastewater and effluent samples on the ICP-MS-DRC, it was highly recommended to digest filtered and acidified effluent further. About 45 mL of aqueous effluent was digested with 3 mL of trace-metal grade concentrated HNO_3 and 2 mL of HCl acids in a microwave digestion unit (MARSXpress, CEM Corporation, Matthews, NC), following the EPA-3015A method(USEPA, 2007). This helped to minimize clogging of the ICP-MS nebulizer from considerable amount of total dissolved solids in the FGD wastewater. Two blanks (acidified Milli-Q water only) and two replicates of NIST 1643e "Trace Elements in Water" SRM were analyzed as quality assurance/quality control (QA/QC) assessment. The recovery percentage was in the range of 83-107%. In addition, spiked recoveries were assessed by adding known amounts of a multi-element standard to randomly selected effluent samples. Recoveries for the spiked samples were found to be 84-103%.

The unacidified samples were filtered through 0.2 µm syringe filters (Environmental Express Inc., South Carolina, USA) and analyzed using an ion chromatograph (ICS-1000, Dionex Corporation) to determine the concentrations of anions. To protect the guard column and analytical column of the IC from the salty nature of the FGD wastewater, solutions were filtered through 0.2 µm syringe filters (Environmental Express Inc., South Carolina, USA) before storing at 4 ^{0}C. Appropriate dilutions were made before analysis, and all samples were analyzed in duplicate. Spiked samples and standards of known concentration were run at the middle of the analysis for QA/QC assessment. The recovery of standards was 116-123% and the spiked recoveries were in the range of 97-115%.

Total elemental analysis of soil

The total elemental concentration in the soil was determined using a 30% H_2O_2 and aqua regia digestion procedure (Premarathna et al., 2010). First, air-dried samples were finely ground with an agate mortar and pestle. Then, 0.5 g of soil was added to a digestion tube and predigested with 0.5 mL of hydrogen peroxide (H_2O_2) for 10 min at room temperature followed by adding another 2.5 mL of H_2O_2. Pre-treated samples were allowed to react overnight at room temperature. The tubes were heated on a digestion block at 90°C until the volume was reduced to ~1 mL. After the tubes were cool, the soils were digested using 5 mL of aqua regia [1:3 (v/v) HNO_3/HCl] following the soil digestion procedure (75°C for 30 min, 100°C for 30 min, 110°C for 30 min, and 140°C until the acid volume decreased to ~1 mL). The final volume was then made up to 20 mL using 0.1% HNO_3. All samples were digested in duplicate. In each batch of digestion, two blanks and two samples of standard reference soil material (NIST 2711a - Montana soil) were included as a QA/QC control. Finally, the digested solution was filtered through a Whatman no. 42 filter paper. Prior to analyze on the ICP-MS-DRC, digested filtrates were further filtered through 0.20µm to protect the instrument by entering finer solid particles to the system. The recovery of NIST 2711a was about 81% and the spiked recoveries were in the range of 95-101%.

Sample preparation for Se bulk-XANES analysis

Soil sample preparation was done inside a glove box filled with N_2 gas. A small amount of a frozen soil sample (0.2-0.5 g) was gently ground with an agate mortar and pestle. Then, it was packed in a sample holder made from 2 mm-thick piece of Plexiglas with a slit of ~ 19 mm x 6.5 mm: H x W. Both sides and edges of the sample holder were sealed with a layer of Kapton tape (Cole Parmer, US), which allowed penetration of high energy X-ray beam. Prepared

samples were transferred to the Advanced Photon Source (APS), Argonne National laboratory (ANL), Argonne, IL using an air-tight container (Oxoid AnaeroJar, 2.5 L). The samples were stored in a freezer until the analysis was performed.

References

Premarathna, H.L., M.J. McLaughlin, J.K. Kirby, G.M. Hettiarachchi, D. Beak, S. Stacey and D.J. Chittleborough. 2010. Potential availability of fertilizer selenium in field capacity and submerged soils. Soil Sci. Soc. Am. J. 74:1589-1596.

USEPA. 2007. Method 3015A: Microwave assisted acid digestion of aqueous samples and extracts. Test methods. http://www.epa.gov/epawaste/hazard/testmethods/sw846/pdfs/3015a.pdf (accessed on 10th of May, 2012).

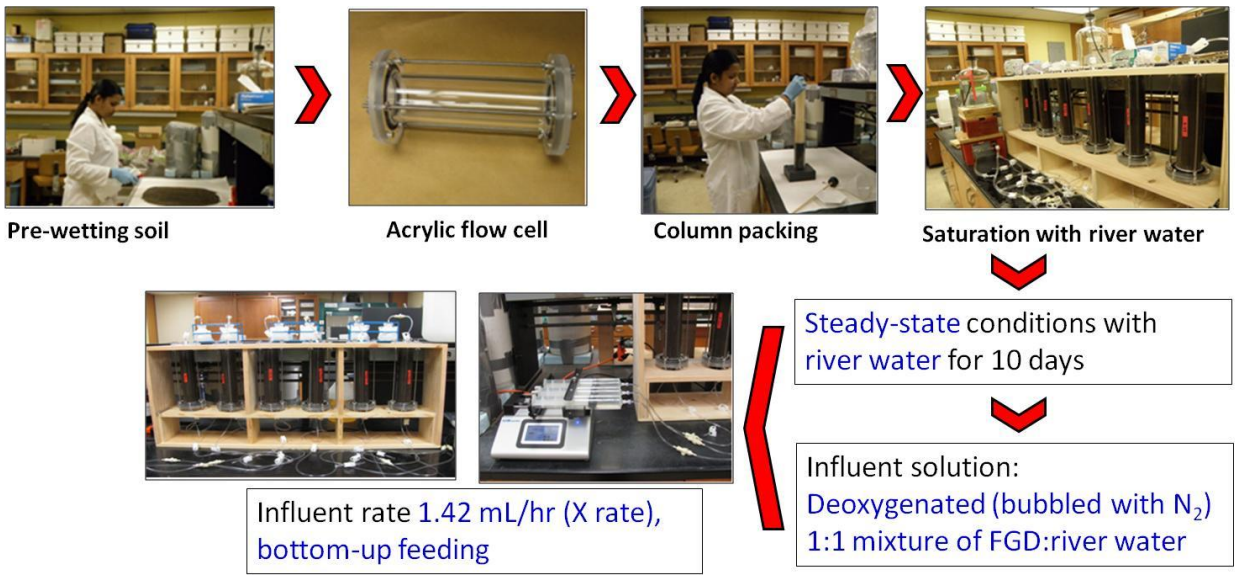

Figure A.1 Diagram showing the systematically followed soil column packing procedure, saturation, and feeding with FGD wastewater solution.

Figure A.2 Laboratory-based soil column experiment setup.

Figure A.3 Effluents collection from top of the soil columns

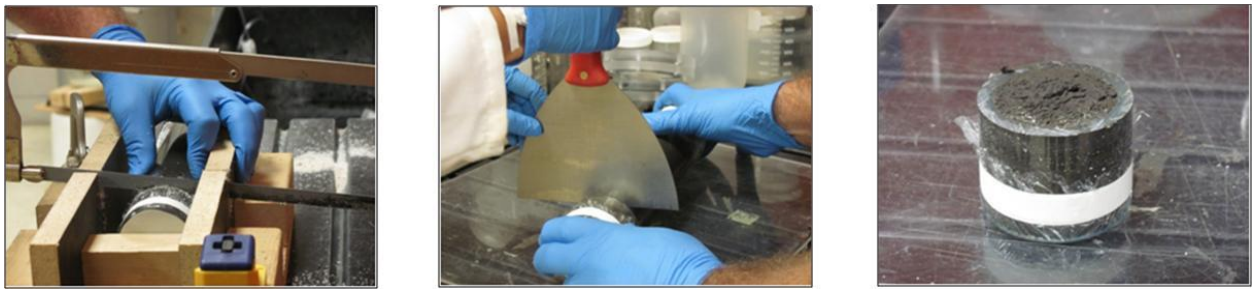

Figure A.4 Soil column cutting in the laboratory

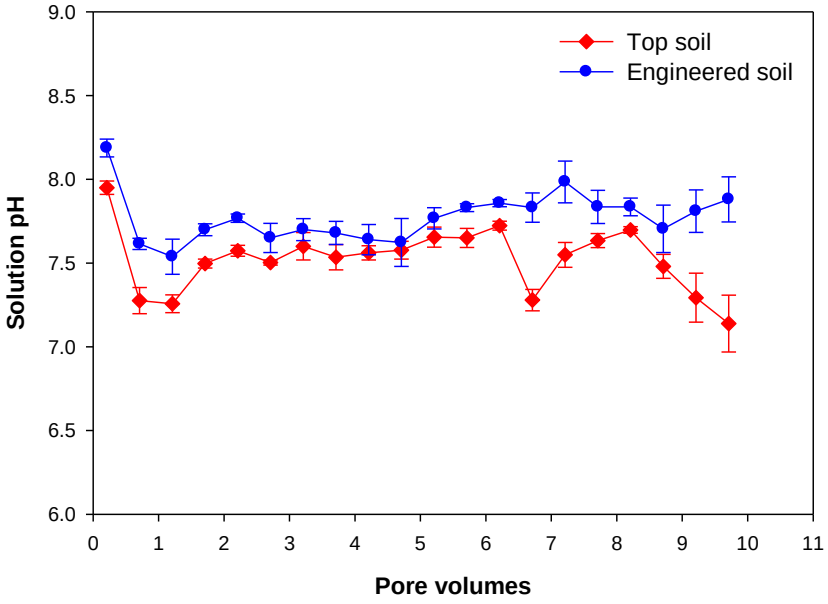

Figure A.5 The solution pH of effluent samples collected from the topsoil and the engineered soil columns over 100 days of feeding with the FGD wastewater.

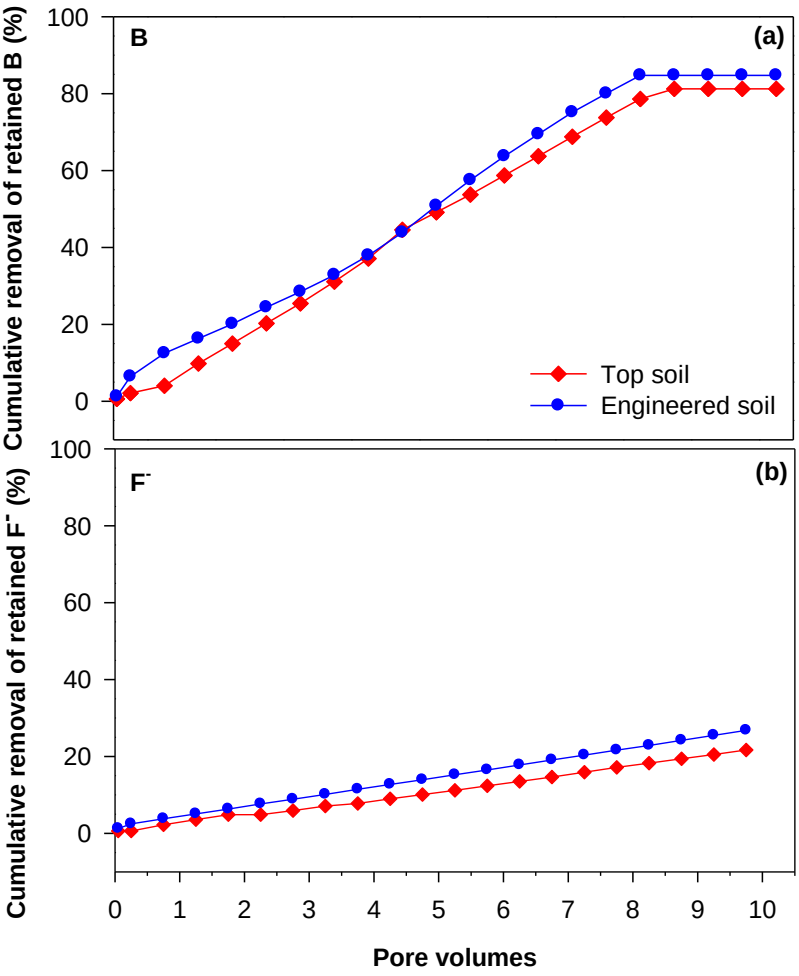

Figure A.6 The cumulative removal (%) of retained boron (B), and fluoride (F^-) in the topsoil and the engineered soil columns by flushing with the raw water for an additional 100 days.

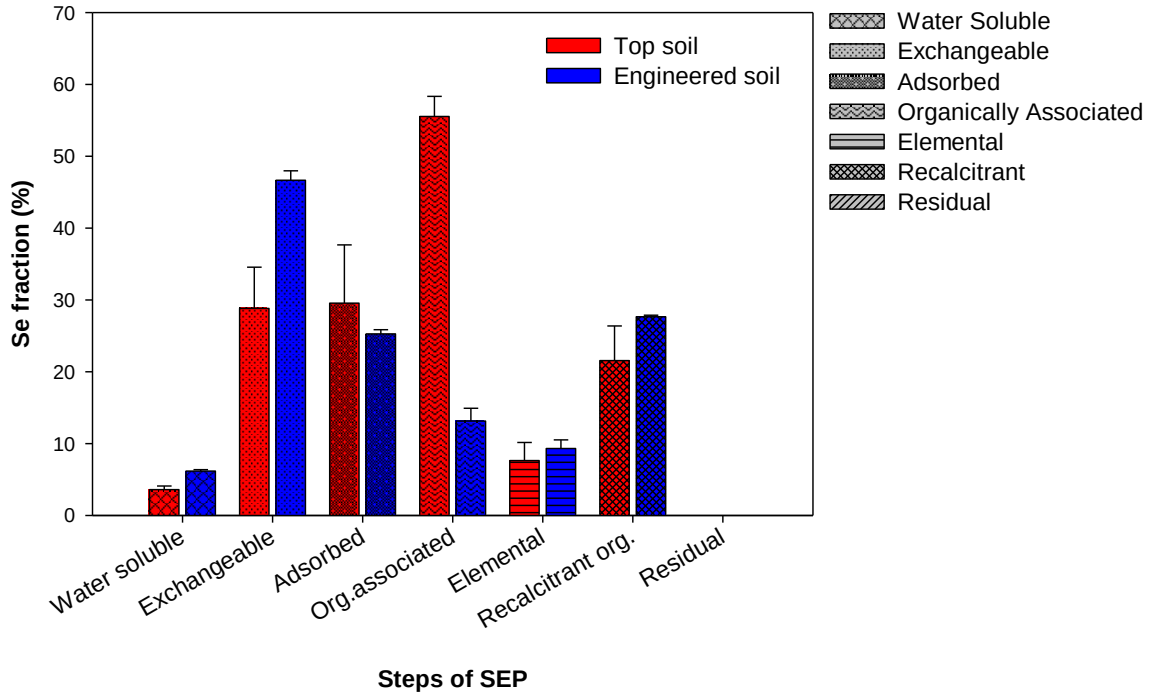

Figure A.7 Fractionation of Se for the topsoil and the engineered soil original materials. Error bars represents standard errors (n=2)

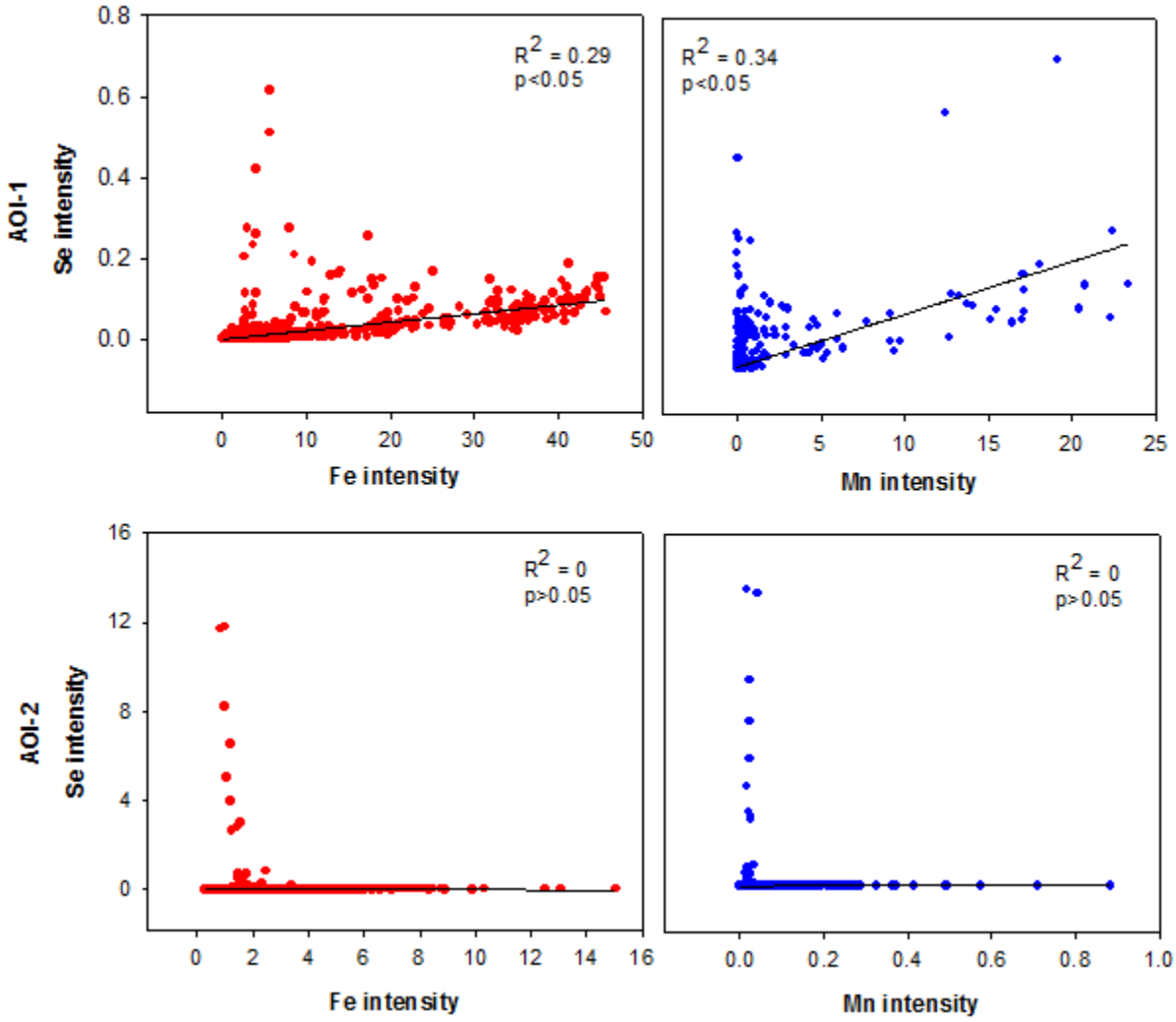

Figure A.8 Correlations plots for fluorescence intensities of Se, Fe, and Mn elemental maps of AOI-1 and AOI-2 in the 100 days of FGD fed topsoil. Each point on the graph represents a pixel in Figure 3.11.

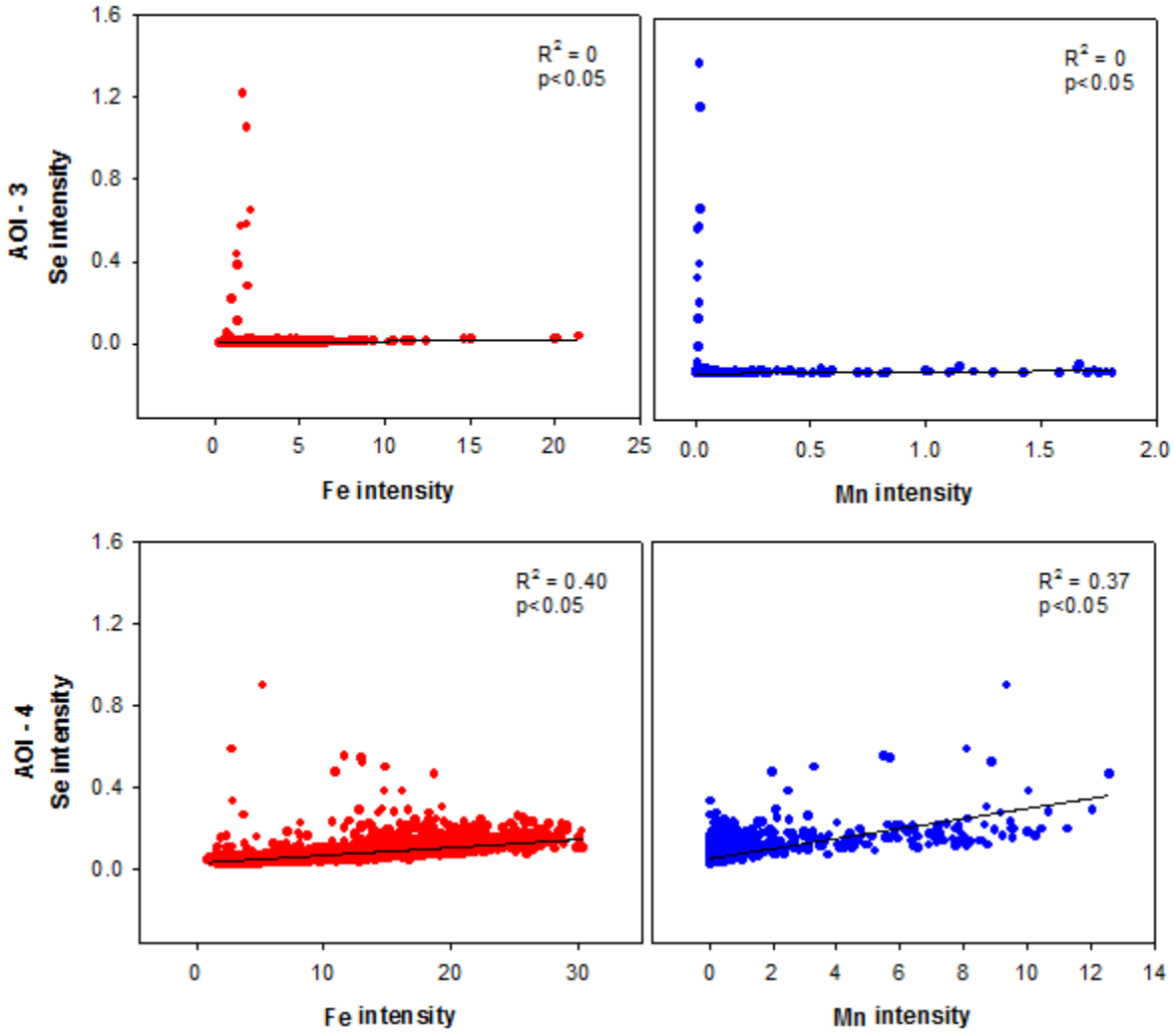

Figure A.9 Correlations plots for fluorescence intensities of Se, Fe, and Mn elemental maps of AOI-3 and AOI-4 in the 100 days of FGD fed followed by 100 days of flushed topsoil. Each point on the graph represents a pixel in Figure 3.12.

Table 6.1 Summary for the sequential extraction procedure

Step	Selenium phases	Extraction
1	Water soluble	25 mL Milli-Q water, shaken for 1 h[*], centrifuged[¶], rinsed with 5 mL of Milli-Q water[#], filtered[†]
2	Exchangeable	25 mL of 0. 25 M KCl, shaken for 2 h[*], centrifuged[¶], rinsed with 5 mL of 0.25 M KCl[#], filtered[†]
3	Adsorbed	25 mL of 0.1 M K_2HPO_4 at pH 8.0, shaken for 2 h[*], centrifuged[¶], repeated the first step, rinsed with 5 mL of 0.25 M KCl[#], filtered[†]
4	Organically associated	25 mL of 0.1 M NaOH, shaken for 4 h[*], centrifuged[¶], rinsed with 5 mL of 0.25 M KCl[#], filtered[†]
5	Elemental	25 mL of 0.25 M Na_2SO_3 at pH 7.0, sonicated at 20 kHz for 2 min, placed in an ultrasonic bath for 4 h, centrifuged[¶], rinsed twice with 5 mL of 0.25 M Na_2SO_3 at pH 7.0[#], filtered[†]
6	Recalcitrant organic forms	25 mL of 5% NaOCl at pH 9.5, shaken for 30 min at 90 ^0C[*], centrifuged[¶], rinsed with 5 mL of 0.25 M KCl[#], filtered[†]
7	Residual	Residual Se = $[\mathbf{100} - \sum_1^6 \boldsymbol{extracted\ Se}\ (\%)]$

* on reciprocal shaker at 130 rounds per minute

¶ centrifuged for 15 min at 10, 000 g

shaken for 2 min and centrifuged for 15 min at 10, 000 g

†filtered through Whatman no. 42 filter paper followed by 0.2 µm before analyzing on ICP-MS

Table 6.2 Average FGD Wastewater Concentrations of Westar Energy's Jeffery Energy Center in 2010.

Metals	*Average FGD Wastewater Dissolved Concentration	*Average FGD Wastewater Total Concentration
	mg/L	mg/L
Aluminum	0.3	0.2
Antimony#	12.5	14.1
Arsenic#	13.3	14.5
Barium#	7.8	7.8
Beryllium#	2.8	2.8
Boron	7.4	7.5
Cadmium#	2.5	2.8
Calcium	573.0	576.8
Chloride	-	1233.1
Chromium	0.1	0.1
Cobalt#	3.4	3.4
Copper#	15.7	16.8
Fluoride	-	32.4
Iron	1.2	1.3
Lead#	8.0	1.1
Magnesium	979.2	989.1
Manganese	7.0	7.0
Mercury#	0.4	0.8
Molybdenum#	76.8	77.5
Nickel#	14.1	15.6
Potassium	132.5	134.1
Selenium	0.3	0.3
Silver#	2.6	2.8
Sodium	1094.5	1108.7
Sulfate	-	5063.8
Thallium#	5.1	6.0
Tin#	15.0	16.5
Vanadium#	13.8	15.3
Zinc#	45.0	50.4

#Concentrations in µg/L

*The average concentration listed is based on the laboratory reported concentrations. In cases where the constituent concentration was reported by the laboratory to be a non-detect value (U), which is at or below the reporting limit, the reporting limit value was used in the calculated average. Samples were collected between 3/30/2009 and 7/24/2009. A total of 16 samples were collected during this period.

Table 6.3 Soil pH of the topsoil and the engineered soil column sections

Sections	100 days of FGD fed TS	FGD fed & 100 days of flushed TS	100 days of FGD fed ES	FGD fed & 100 days of flushed ES
		Soil pH		
Section 1(top)	7.9	7.8	8.0	8.1
Section 2	7.9	7.9	8.0	8.1
Section 3	7.9	7.9	8.0	8.2
Section 4	8.0	7.9	8.1	8.2
Section 5	8.1	8.0	8.1	8.2
Section 6 (bottom)	8.1	8.0	8.1	8.2

Appendix B - Supporting information relevant to Chapter 4

Synthesis of 2-line ferrihydrite

Two-line ferrihydrite (Fh) was synthesized in the laboratory following the procedure described by (Schwertmann and Cornell, 2000). Briefly, 40 g of $Fe(NO_3)_3$. 9 H_2O was dissolved in 500 ml of Milli-Q water, and about 310-320 mL of 1 M KOH was added to bring the pH around 7-8. Then, the remaining volume of KOH was added carefully to bring the volume up to 1000 mL with constant checking of the pH. The solution mixture was stirred vigorously and centrifuged at 3000 rpm for 10 minutes (5810R Eppendorf, Hamburg, Germany). The separated residue solid was washed few times with Milli-Q water to remove excess electrolyte, and freeze dried (Labconco freeze dryer, Kansas City, MO). The prepared iron-oxide was characterized using an X-ray diffractometer (XRD) (Philips X-Ray diffractometer, Mahwah, NJ) equipped with a theta compensating slit and curved crystal graphite monochromator. X-ray diffraction measurements were taken using Cu K_α radiation and were step scanned at a speed of 2^0 2θ per minute. The energy potential was 35 kV, and the amperage was 20 mA. After confirmation by XRD, synthesized 2-line ferrihydrite was used for the experiment without being aged for a long time because ferrihydrite can be transformed into stable Fe oxide minerals such as goethite, and hematite influencing its crystallinity and reactive surface area (Schwertmann and Cornell, 2000).

Analysis of influent and effluent

The As concentration of water samples was measured using a graphite furnace atomic absorption spectrometry (GF-AAS) (Varian Inc.) equipped with Zeeman background correction. The standard addition method was followed and 500 mg/L palladium (Pd) modifier was used to enhance the As absorbance signal. The concentration of Se of these solutions was measured using an Agilent 7500 series inductively coupled plasma-mass spectrometry equipped with a

dynamic reaction cell (ICP-MS-DRC). Before analyzing the FGD wastewater and effluent samples on the ICP-MS-DRC, it was highly recommended to digest filtered and acidified effluent further. About 45 mL of aqueous effluent was digested with 3 mL of trace-metal grade concentrated HNO_3 and 2 mL of HCl acids in a microwave digestion unit (MARSXpress, CEM Corporation, Matthews, NC), following the EPA-3015A method(USEPA, 2007a). A Varian 720-ES Inductive couple plasma-optical emission spectrometry (ICP-OES) was used to determine the total concentrations of other constituents. A blank (acidified Milli-Q water only), NIST 1643e "Trace Elements in Water" SRM, and randomly spiked samples were analyzed for quality assurance/quality control (QA/QC) assessment to validate the analytical method. The recovery percentage was in the range of 98-104 % for the NIST sample, and it was 91-97 % for the spiked samples. The unacidified water samples were filtered through 0.2 µm syringe filters (Environmental Express Inc., South Carolina, USA), and analyzed using an ion chromatograph (ICS-1000, Dionex Corporation) to measure the concentrations of seven anions. The QA/QC analyses provided the recoveries in between 84-99 %.

Soil analysis

The total elemental concentrations of the starting soil material and the soil from column sections was determined by following the USEPA-3051A Microwave assisted method (USEPA, 2007b). Before the digestion, air-dried soil was finely ground with an agate mortar and pestle. Then, 0.5 g of the soil sample was digested with a 10 mL of trace-metal grade concentrated nitric acid in a microwave digestion unit (MARSXpress, CEM Corporation, Matthews, NC) (Attanayake et al. 2014). A blank (trace-metal grade HNO_3 acid), and standard reference soil (NIST 2711a-Montana II) were included in the digestion for QA/QC prediction. The total concentrations of Fe, Al, Mn, and S were measured using the ICP-OES (Varian 720-ES). This

method provided 92-109% recoveries for the spiked samples. The total As, and Se concentrations of soil were measured using the GF-AAS. The absorbance of As, and Se in the GF-AAS was enhanced by palladium modifier (500 mg/L). A high intensity UltrAA Se lamp was used to enhance the sensitivity and to minimize background noise. The recoveries of the 2711a-Montana soil for As and Se were 116 and 94 %, respectively, and those of the spiked samples were in the range of 87-99 % for As, and 83-102 % for Se.

Therefore, two steps of a sequential extraction procedure (SEP) were used to determine the mobile As fraction of the original soil (Wenzel et al., 2001). Although these extracted fractions are operationally defined and are not clearly associated with specific geochemical phases, they are designed to extract As from non-specifically and specifically bound As fractions.

Step 1: 0.05 M Ammonium sulfate [$(NH_4)_2SO_4$]

Approximately 1g of the soil was placed in a 50 mL centrifuge tube. A 25-mL aliquot of 0.05 M $(NH_4)_2SO_4$ was added to it and sealed carefully. The mixture was shaken for 4 hours. Then, the mixture was centrifuged at 3000 rpm for 10 minutes, and the supernatant was filtered through 0.45 μm nylon syringe filters and acidified with two drops of 2 % nitric acid (trace metal grade), and stored at 4 °C prior to analysis.

Step 2: 0.05 M ammonium phosphate monobasic ($NH_4H_2PO_4$)

A 25 mL of 0.05 M $NH_4H_2PO_4$ were added to each of the residual samples from step 1. Then, the mixture was shaken for 16 hours and centrifugation and filtration procedures were performed as described in step 1. All extractions were performed in duplicate.

Extractable As concentration of the above two steps was determined using the GF-AAS with 500 mg/L Pd modifier. The available As fraction was calculated as a percentage of the total measured concentration of As in the soil.

$$Available\ As\ (\%) = \left(\frac{\sum Extracted\ As\ from\ step\ 1 + Extracted\ As\ from\ step\ 2, \mu g/kg}{Total\ As, \mu g/kg}\right) \times 100$$

X-ray spectroscopy analysis

Arsenic micro-XRF mapping followed by micro-XANES was conducted at sector 13 ID-E, GSE CARS (GeoSoilEnviro Consortium of Advanced Radiation Sources) at the APS. Thirteen-element solid state Ge detector equipped with a double-crystal monochromator; Si (111) and Si (311) was used for micro-XRF maps and micro-XANES spectra collection. Prior to the analysis, soil samples were finely ground using an agate mortar and pestle in a N_2 filled glove box. Then, powdered sample was smeared on a scotch tape, and unattached soil particles were carefully removed from the surface. The prepared thin sections were fully covered with another piece of tape before taking out from the glove box. Appropriate care was taken to minimize beam-induced changes of speciation, by collecting the data at helium environment. The micro-XRF maps were generated over an area of 175 µm x 175 µm at the energy of 12500 eV to locate As rich areas (hotspots) in the soil. The fluorescence maps were analyzed using a software package Larch (Newville, 2013). Arsenic hotspots (brightest points) on the micro-XRF maps were selected to collect micro-XANES spectra to get in depth As speciation. A sodium arsenate standard was used to calibrate the energy at 11873.3 eV for As. Three to four scans of each hotspot were collected with energy range from 11760 eV to 12065 eV. The step size was 2.5 eV on pre edge region (11760 eV-11857 eV), 0.25 eV in XANES region (11857 eV-11887 eV) and 1.5 k weight in post edge region (11887 eV-12065 eV) with integration time of 3 seconds per point. Data processing, aligning, smoothing, normalization and merging of collected scans were

done following the standard procedures in ATHENA (Ravel and Newville, 2005). The As speciation was determined by linear combination fitting (LCF) analysis in the ATHENA program within an energy range of −20 eV below to +30 eV above the edge. The combinatorics that had lowest reduced χ^2 and R-factor were selected as the best fitting. The As standards used for the LCF analysis are listed in As bulk-XANES analysis section.

Arsenic bulk-XANES data were collected at sector 5 BM-D of DND-CAT at the APS for overall As speciation in the non-treated and ferrihydrite-treated soil. The sector 5 BM-D is a bending magnet beam line equipped with Si (111) monochromator. This line consists of an unfocused beam size of 15mm x 5mm and a focus beam size of 15000µm x 500µm, and has an energy range of 4.5 to 25 keV. The detector used for the analysis was Canberra 13-element Ge solid state detector. The detector was covered with two aluminum foil layers of a thickness of 50 µm to reduce background fluorescence emissions from Fe, and to improve signal-to-noise ratio (Gräfe et al., 2014). The soil samples for this analysis were prepared as follows. Soil sample preparation was carried out in a glove box filled with N_2 gas. First, a small amount of a frozen soil sample (0.2-0.5 g) was gently ground with an agate mortar and pestle. Then, the ground soil was packed in a sample holder of a thickness of 2 mm piece of Plexiglas with a slit of ~ 19 mm x 6.5 mm: H x W. The both sides and edges of the sample holder were sealed with a layer of Kapton tape (Cole Parmer, US). The prepared samples were transferred to the APS using an air-tight container (Oxoid AnaeroJar, 2.5 L). The samples were stored in a freezer until the analysis was performed. The prepared samples were mounted on the sample stage facing to the beam at 45^0. The energy was calibrated to As K-edge energy of 11866.7 eV using an As filter. The XANES of As-metal foil was collected simultaneously with every sample spectrum. The sample spectra were collected using the beam size of 2 mm x 10 mm under a continuous flow of the X-

streamTM cryogenic crystal cooler (Rigaku company, Tokyo, Japan). The main purpose of using the cryogenic cooler was to avoid any beam induced changes in speciation. The all XANES spectra of our samples were collected in fluorescence mode. Multiple scans (6 scans per sample) were collected to improve signal-to-noise ratio.

The data processing and the LCF analysis were performed using the ATHENA software as described for micro-XANES. The XANES spectra of twelve As standards were used for the LCF. Those were dimethylarsenate (DMA), monomethylarsenate (MMA), orpimant (As_2S_3), realgar (As_4S_4), As(V) adsorbed to gibbsite, As(V) adsorbed to goethite, As(V) adsorbed to ferrihydrite, As(V) adsorbed to hematite, pharmacosiderite [$KFe_4^{3+}(AsO_4)_3(OH)_4 \cdot$ 6-7H_2O], and beudantite [$PbFe^{3+}_3(AsO_4)(SO_4)(OH)_6$], yukonite [$Ca_7Fe^{3+}_{11}(AsO_4)_9O_{10} \bullet 24.3(H_2O)$], and As(III) adsorbed to ferrihydrite.

The bulk Fe-XANES analyzed was performed at sector 5-BM-D of the APS. The soil samples for this analysis were prepared in the same way as did for As bulk-XANES. The XANES spectra of sixteen Fe standards were used for LCF of each sample, and those standards included siderite ($FeCO_3$), vivianite [$Fe_3(PO_4)_2.8H_2O$], magnetite (Fe_3O_4), ferrihydrite [$Fe_{10}O_{14}(OH)_2$], goethite (α-FeOOH), green rust, Fe(III) oxide (Fe_2O_3), Fe(II) oxide (FeO), iron sulfate ($FeSO_4$), maghemite (1/2γ-Fe_2O_3) , lepidocrocite (γ-FeOOH), hematite (1/2α-Fe_2O_3), Fe(II) sulfide (FeS) and pyrite (FeS_2). In addition, synthesized greigite chloride, sulfate and carbonate were included to the set of Fe standards. These standards were obtained from XAS databases (http://xraysweb.lbl.gov/uxas/Databases/Overview.htm).

References

Attanayake, C.P., G.M. Hettiarachchi, A. Harms, D. Presley, S. Martin and G.M. Pierzynski. 2014. Field evaluations on soil plant transfer of lead from an urban garden soil. J. Environ. Qual. 43:475-487.

Gräfe, M., E. Donner, R.N. Collins and E. Lombi. 2014. Speciation of metal (loid) s in environmental samples by X-ray absorption spectroscopy: A critical review. Anal. Chim. Acta 822:1-22.

USEPA. 2007a. Method 3015A: Microwave assisted acid digestion of aqueous samples and extracts. Test methods. http://www.epa.gov/epawaste/hazard/testmethods/sw846/pdfs/3015a.pdf (accessed on 10th of May, 2012).

USEPA. 2007b. Method 3051A: Microwave assisted acid digestion of sediments, sludges, soils, and oils. Test methods http://www3.epa.gov/epawaste/hazard/testmethods/sw846/pdfs/3051a.pdf (accessed on 10th of December, 2011).

Appendix C - Supporting information relevant to Chapter 5

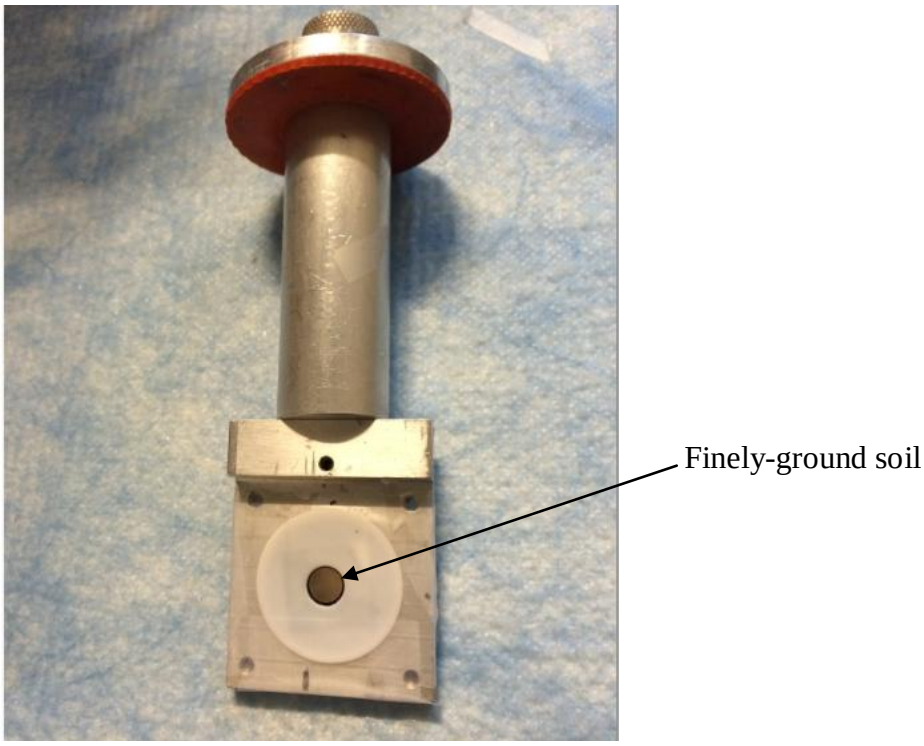

Figure C.1 Finely-ground soil pellet for sulfur bulk-XANES analysis

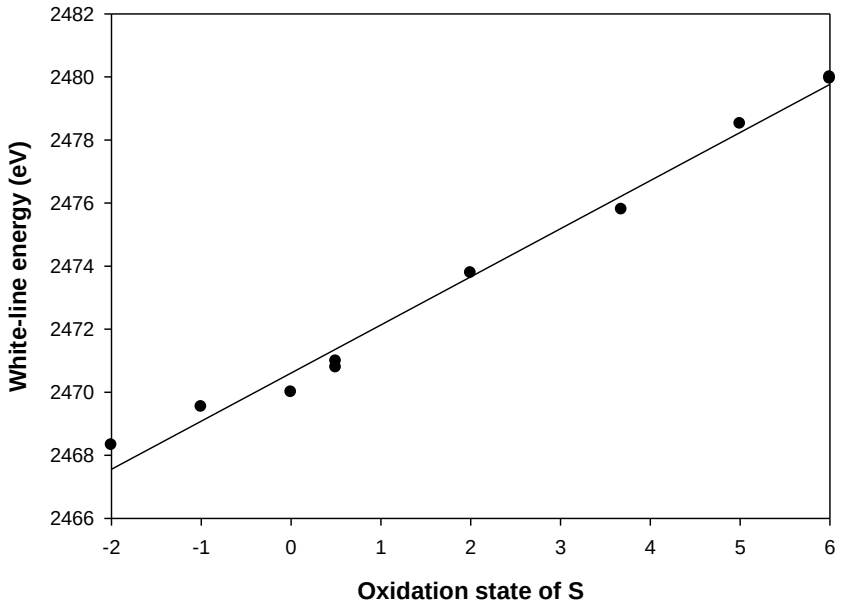

Figure C.2 Correlation between the oxidation state of the S in reference compounds and the white-line energy of their peaks in S-XANES spectra.

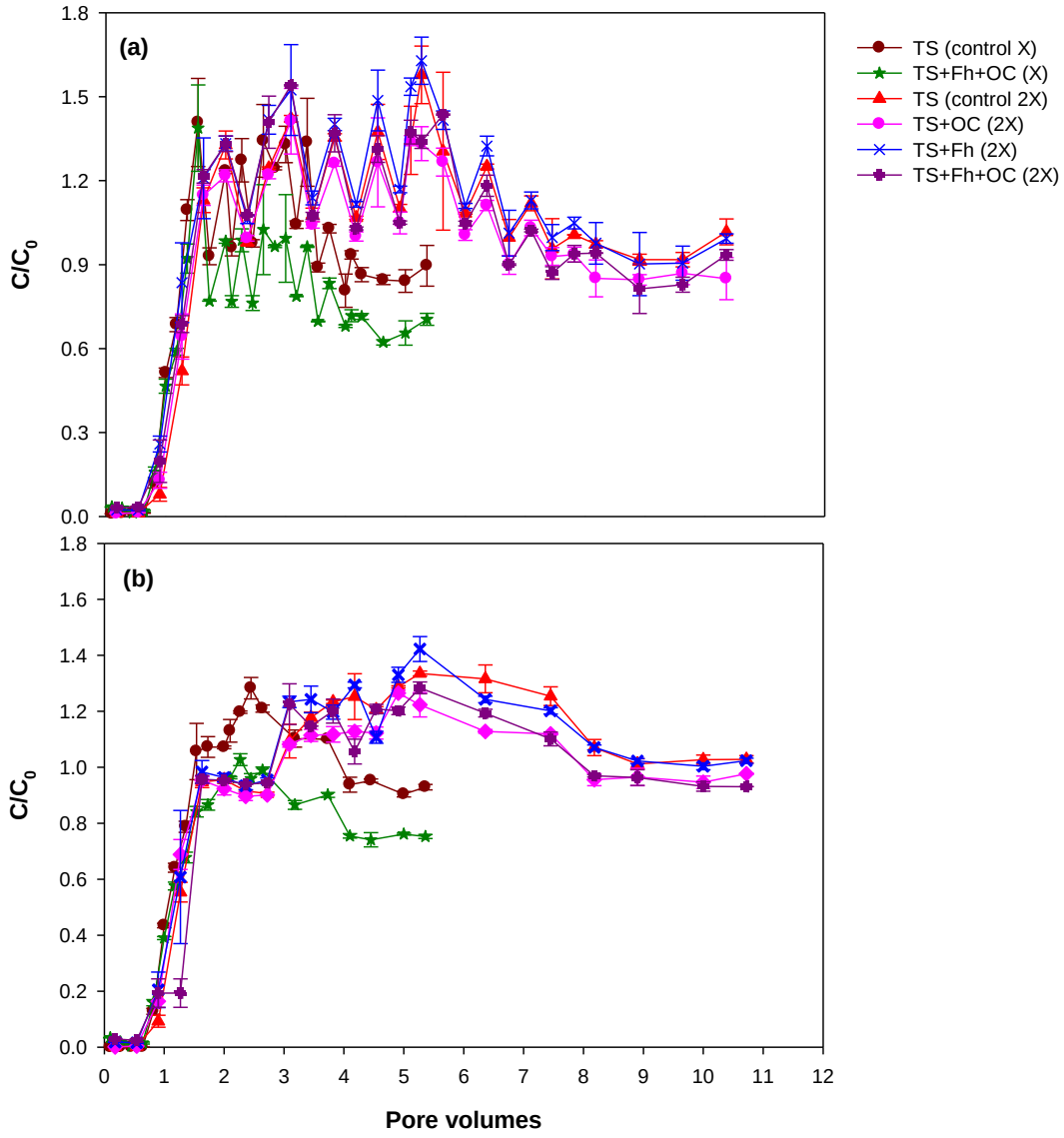

Figure C.3 Breakthrough curves for S; (a) sulfate-S vs pore volumes, (b) total-S vs pore volumes. One pore volume of X rate is 11 days and that of 2X rate is 5.5 days.

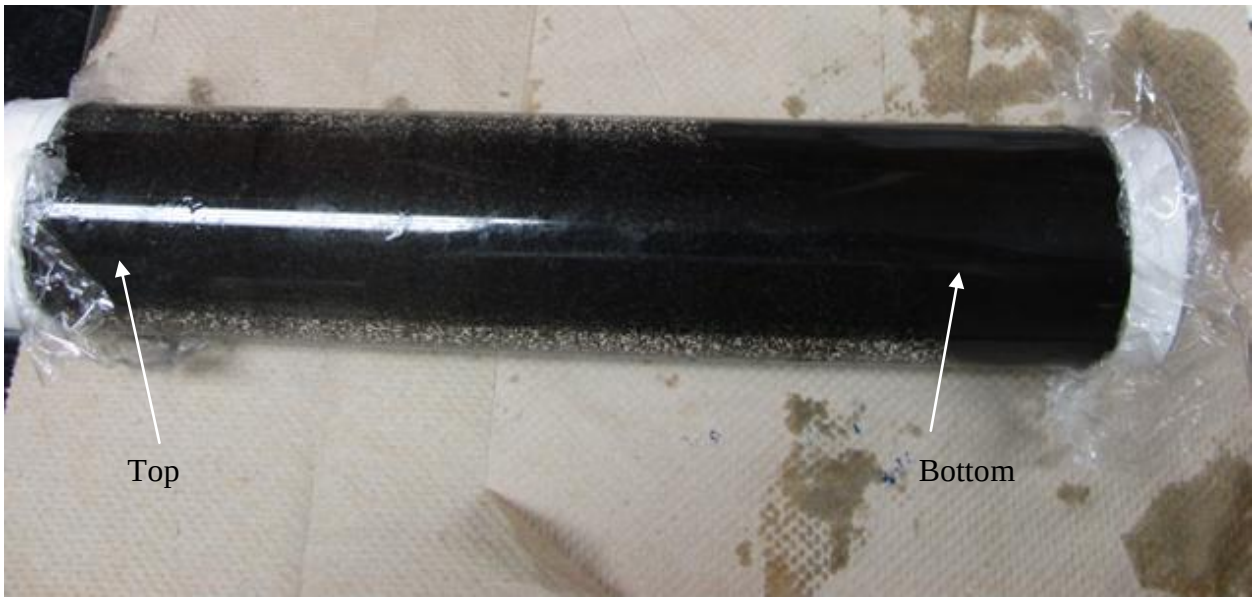

Figure C.4 Black color soil collected from 1/2X rate soil columns after 365 days of feeding with FGD wastewater.